

**DYNAMIC STABILIZATION OF THE LUMBAR SPINE: AN IN VITRO
BIOMECHANICAL INVESTIGATION**

CHRISTINA ANNE NIOSI

B.Sc. University of Alberta, 2002

A THESIS SUBMITTED IN PARTIAL FULFILLMENT OF
THE REQUIREMENTS FOR THE DEGREE OF
MASTER OF APPLIED SCIENCE

in

THE FACULTY OF GRADUATE STUDIES

Department of Mechanical Engineering

THE UNIVERSITY OF BRITISH COLUMBIA

December 2004

© Christina Anne Niosi, 2004

Abstract

The Dynesys, a dynamic posterior stabilization system that provides an alternative to fusion, is designed to preserve intersegmental kinematics and reduce loading at the facet joints. Previous biomechanical investigations have analyzed kinematic behaviour using translations and/or rotations about a primary axis. The objective of this study was to conduct a comprehensive biomechanical evaluation to determine the effect of the Dynesys system on kinematic behaviour and load transfer and to examine the effect of variation in the length of the Dynesys spacer.

Ten cadaveric lumbar spine segments (L2-L5) were subjected to pure moments of ± 7.5 Nm in three loading directions with and without a compressive follower preload of 600 N. The flexibility tests were performed on the specimens under nine different conditions. Intervertebral positions were measured using an optoelectronic camera system, from which range of motion (ROM), neutral zone (NZ), and helical axis of motion (HAM) were calculated. Pressure sensors were placed inside the joint capsules to measure facet contact loads and custom needle pressure transducers were used to measure intradiscal pressures. Statistical significance was determined using repeated measures multivariate analysis of variance (MANOVA) ($p < 0.05$).

The Dynesys resulted in a reduction in ROM to 16%, 30%, 25%, and 88% that of intact ROM in flexion, extension, lateral bending, and axial rotation. The device caused a posterior shift of the HAM in flexion-extension and axial rotation as well as a change in the orientation of the HAM. There was an increase in facet load in flexion with the Dynesys, an initial load created at the facet joints by installation of the system, and the anterior column load in the neutral position and axial rotation was reduced.

In all three loading directions there was an increase in ROM with the long spacer and decrease with the short spacer compared to the standard spacer, with the largest difference seen in axial rotation. The long spacer resulted in a smaller posterior shift in the position of the HAM in axial rotation. Also evident was a reduction in the initial load at the facet joints and a decrease in facet load during flexion and lateral bending.

The Dynesys created compression of the posterior elements and an asymmetric stiffness that both altered the kinematic behaviour and load transfer through the segment, and may have important clinical implications. The Dynesys reduced the large ROM that resulted after injury and allowed a ROM that was similar or greater than that of rigid fixation. However, with the emerging dynamic stabilization systems where motion is preserved, it becomes prudent to consider the complete motion pattern and load transfer through the segment when examining the efficacy of the device.

Table of Contents

Abstract	ii
Table of Contents	iii
List of Figures	vi
List of Tables	x
Acknowledgements	xi
Chapter 1. Introduction	1
1.1 Clinical Importance	1
1.2 Anatomy	2
1.2.1 Vertebrae	3
1.2.2 Intervertebral Discs	5
1.2.3 Ligaments	6
1.2.4 Triple Joint Complex	7
1.3 Current Treatment of Low Back Pain	8
1.4 What is Dynamic Stabilization?	9
1.4.1 The Dynesys System	11
1.4.2 Indications	11
1.5 Biomechanical Testing	12
1.5.1 Specimen Selection	13
1.5.2 Testing Apparatus and Procedure	14
1.5.3 Analysis of Data	16
1.6 New Trends in Biomechanical Testing	19
1.6.1 Existing Dynamic Stabilization Evaluations	19
1.6.2 Follower Preload	21
1.6.3 Additional Kinematic Parameters	22
1.6.4 Load Transfer	25
1.6.5 Results of Dynamic Stabilization Evaluations	30
1.7 Motivation	31
1.8 Objective	32
1.9 Project Scope	32
1.10 Contribution	33
Chapter 2. Methods	35
2.1 Specimen Selection	35
2.2 Test Protocol	35
2.2.1 Explanation of Test Conditions	37
2.2.2 Spine Testing Machine	40
2.2.3 Follower Preload	40
2.3 Data Acquisition	44

Table of Contents

2.3.1	Intervertebral Kinematics	44
2.3.2	Facet Joint Forces	46
2.3.3	Intradiscal Pressures	49
2.4	Kinematic Analysis	51
2.4.1	Intersegmental Motion	51
2.4.2	Calculation of Transformation Matrix	51
2.4.3	Intervertebral Rotation	54
2.4.4	Translation	55
2.4.5	Range of Motion (ROM) and Neutral Zone (NZ)	56
2.4.6	Helical Axis of Motion (HAM)	56
2.4.7	Location of the HAM	60
2.5	Facet Load Analysis	60
2.6	Intradiscal Pressure Analysis	61
2.7	Facet Joint Imaging	62
2.7.1	Specimen Preparation	63
2.7.2	Loading Apparatus	63
2.7.3	Test Conditions	65
2.7.4	Imaging	66
2.7.5	Analysis	66
2.7.6	Validation	68
2.8	Statistical Analysis	68
2.8.1	Kinematic Behaviour	69
2.8.2	Facet Loads	70
2.8.3	Intradiscal Pressures	70
Chapter 3. Results		71
3.1	Kinematic Behaviour	71
3.1.1	Effect of Specimen Condition	71
3.1.2	Effect of Spacer Length	82
3.2	Facet Loads	99
3.2.1	Effect of Specimen Condition	99
3.2.2	Effect of Spacer Length	105
3.3	Intradiscal Pressures	115
3.4	Facet Joint Imaging	121
3.4.1	Contact Area	121
3.4.2	Validation	123
Chapter 4. Discussion		127
4.1	Limitations and Assumptions	129
4.1.1	Clinical Representation	129
4.1.2	Specimen Loading	130
4.1.3	Kinematics	133
4.1.4	Facet Loads	134
4.1.5	Assessment of Facet Contact	136
4.1.6	Statistical Analysis	139
4.2	Comparison with Literature	140

Table of Contents

4.2.1 Kinematic Behaviour in the Literature	140
4.2.2 Facet Loads in the Literature	143
4.2.3 Intradiscal Pressure in the Literature	144
4.3 Facet Loading Patterns	146
4.4 Intradiscal Pressure Patterns	147
4.5 Compression of the Posterior Elements	148
4.5.1 Effect of Spacer Length on Segmental Compression	149
4.6 Asymmetry	150
4.7 Changes in Motion Coupling	151
4.8 Feasibility of Quantifying Contact in Facet Joints Using Imaging	152
4.9 Comparison of Dynesys to Rigid, Intact, and Injured Conditions	153
4.10 Dynesys Spacer Length	154
4.11 Clinical Implications	155
4.12 Goals for Biomechanical Testing	155
Chapter 5. Conclusions	157
5.1 Future Directions	159
5.2 Contributions	159
Bibliography	161
Appendix A. Summary of Results by Specimen	172
Appendix B. Results of Statistical Analysis	177
B.1 Effect of Specimen Condition	178
B.2 Effect of Dynesys Spacer Length	184
Appendix C. HAM Results for Unloaded Position to Max/Min Rotation	186
C.1 Effect of Specimen Condition	187
C.2 Effect of Spacer Length	193

List of Figures

1.1	Regions of the Vertebral Column	3
1.2	Anatomy of a Typical Lumbar Vertebra	4
1.3	Anatomy of a Lumbar Intervertebral Disc	5
1.4	Sagittal Section With Laminectomy Showing the Ligaments of the Lumbar Spine	6
1.5	Sagittal view of Lumbar Triple Joint Complex	7
1.6	Anterior Dynamic Stabilization Devices	10
1.7	Posterior Dynamic Stabilization Devices	11
1.8	Components of the Dynesys System	12
1.9	Explanation of Kinematic Parameters	18
1.10	Schematic of Compressive Follower Preload on the Lumbar Spine	23
1.11	Representation of a Helical Axis of Motion (HAM)	24
1.12	Approximate Locations of the Centre of Rotation in the Intact Lumbar Spine ..	25
1.13	Schematic of Transducer and Method Used for Measuring Intradiscal Pressure within the Intervertebral Disc	26
1.14	Stress Profile Across a Healthy Intervertebral Disc During Axial Compression ..	27
1.15	Strain Gauge Method to Determine Facet Loads	29
1.16	Tekscan Sensors for Direct Force Measurement	30
2.1	Fully Prepared Lumbar Specimen Dissected of Musculature and Potted in Den- tal Stone Mounts	36
2.2	Injury of Spine Ligaments	38
2.3	Three Lengths of Dynesys Polycarbonate Urethane (PCU) Spacers: Short, Standard, and Long	39
2.4	Rigid Fixation System and as Installed at L3-L4	39
2.5	Schematic of the Custom Spine Machine	41
2.6	Follower Load Path	42
2.7	Stainless Steel Follower Load Frame on Vertebra	43
2.8	Application of Compressive Follower Preload	43
2.9	Follower Load Profile	44
2.10	Optoelectronic Camera System Used to Measure the Three-Dimensional Posi- tion of the Markers	45
2.11	Digitization of Points	46
2.12	Tekscan 6900 Quad Thin Film Electroresistive Sensor	47
2.13	Tekscan Sensors Inserted in the Left and Right Facet Joints of L3-L4	48
2.14	Configuration for Conditioning and Calibration of Tekscan Sensors	49
2.15	Intradiscal Custom Needle Pressure Transducer	50
2.16	Radiographs Depicting Placement of Intradiscal Custom Needle Pressure Trans- ducers	50
2.17	Local (Anatomic) Coordinate System Created for Each of the Four Vertebrae ..	52
2.18	Illustration of Vectors used for Marker Transformation Between Initial and Final Marker Distributions	53
2.19	HAM Coordinate System and Penetration Planes	58
2.20	Specimen in Loading Jig	64

List of Figures

2.21	MRI Facet Joint Loading Jig	65
2.22	Schematic of Facet Contact Measurement Techniques	67
2.23	Tekscan Validation of Contact Area Measured Using MRI	68
3.1	Motion vs. Applied Moment of a Typical Specimen in Flexion-Extension	73
3.2	Motion vs. Applied Moment of a Typical Specimen in Lateral Bending	73
3.3	Motion vs. Applied Moment of a Typical Specimen in Axial Rotation	74
3.4	Average ROM in Flexion	75
3.5	Average ROM in Extension	76
3.6	Average ROM in Lateral Bending	76
3.7	Average ROM in Axial Rotation	77
3.8	Average NZ in Flexion-Extension	79
3.9	Average NZ in Lateral Bending	79
3.10	Average NZ in Axial Rotation	80
3.11	Average Position and Orientation of HAM in Flexion-Extension	83
3.12	Average in Position and Orientation of HAM in Lateral Bending	84
3.13	Average Orientation of the HAM in Left and Right Lateral Bending	85
3.14	Average Position and Orientation of HAM in Axial Rotation	86
3.15	Average and Standard Deviation in Position of the HAM in Left and Right Axial Rotation	87
3.16	Average Orientation of the HAM in Left and Right Axial Rotation	87
3.17	Motion vs. Applied Moment of a Typical Specimen in Flexion-Extension for Three Dynesys Spacer Lengths	88
3.18	Motion vs. Applied Moment of a Typical Specimen in Lateral Bending for Three Dynesys Spacer Lengths	88
3.19	Motion vs. Applied Moment of a Typical Specimen in Axial Rotation for Three Dynesys Spacer Lengths	89
3.20	Average ROM in Flexion for Three Spacer Lengths	89
3.21	Average ROM in Extension for Three Spacer Lengths	90
3.22	Average ROM in Lateral Bending for Three Spacer Lengths	90
3.23	Average ROM in Axial Rotation for Three Spacer Lengths	91
3.24	Average NZ in Flexion-Extension for Three Spacer Lengths	92
3.25	Average NZ in Lateral Bending for Three Spacer Lengths	92
3.26	Average NZ in Axial Rotation for Three Spacer Lengths	93
3.27	Average Position and Orientation of HAM in Flexion-Extension (Spacer Length)	96
3.28	Average Position and Orientation of HAM in Axial Rotation (Spacer Length) ..	97
3.29	Average Position and Orientation of HAM in Lateral Bending (Spacer Length) ..	98
3.30	Sample Contact Load vs. Rotation for Left and Right Facet Joints in Flexion- Extension Without a Follower Preload	100
3.31	Sample Contact Load vs. Time in Flexion-Extension Without a Follower Preload for Capsule Condition	101
3.32	Sample Contact Load vs. Rotation for Left and Right Facet Joints in Axial Rotation	102
3.33	Sample Contact Load vs. Time in Axial Rotation Without a Follower Preload for Capsule Condition	103

List of Figures

3.34	Sample Contact Load vs. Time in Flexion-Extension Without a Follower Preload for an Injured Specimen Stabilized with Dynesys	103
3.35	Sample Contact Load vs. Time in Axial Rotation Without a Follower Preload for an Injured Specimen Stabilized with Dynesys	104
3.36	Average Peak Facet Loads in Flexion Without a Follower Preload.....	105
3.37	Average Peak Facet Loads in Flexion With a Follower Preload	106
3.38	Average Peak Facet Loads in Lateral Bending Without a Follower Preload	106
3.39	Average Peak Facet Loads in Lateral Bending With a Follower Preload	107
3.40	Average Peak Facet Loads in Extension Without a Follower Preload	107
3.41	Average Peak Facet Loads in Extension With a Follower Preload	108
3.42	Average Peak Facet Loads in Axial Rotation Without a Follower Preload	108
3.43	Average Peak Facet Loads in Axial Rotation With a Follower Preload	109
3.44	Average Initial Facet Loads Created by Implantation of the Three Different Dynesys Spacers	110
3.45	Average Peak Facet Loads in Flexion Without a Follower Preload (Spacer Length)	110
3.46	Average Peak Facet Loads in Flexion With a Follower Preload (Spacer Length)	111
3.47	Average Peak Facet Loads in Lateral Bending Without a Follower Preload (Spacer Length)	111
3.48	Average Peak Facet Loads in Lateral Bending With a Follower Preload (Spacer Length).....	112
3.49	Average Peak Facet Loads in Extension Without a Follower Preload (Spacer Length).....	112
3.50	Average Peak Facet Loads in Extension With a Follower Preload (Spacer Length)	113
3.51	Average Peak Facet Loads in Axial Rotation Without a Follower Preload (Spacer Length)	113
3.52	Average Peak Facet Loads in Axial Rotation With a Follower Preload (Spacer Length).....	114
3.53	Intradiscal Pressure vs. Applied Moment in Flexion-Extension	117
3.54	Average Intradiscal Pressure in Flexion-Extension	118
3.55	Intradiscal Pressure vs. Applied Moment in Lateral Bending	118
3.56	Average Intradiscal Pressure in Lateral Bending	119
3.57	Intradiscal Pressure vs. Applied Moment in Axial Rotation	120
3.58	Average Intradiscal Pressure in Axial Rotation	120
3.59	MR Image of Specimen in Unloaded State	122
3.60	Segmentation of Cartilage Area in Each Slice to Generate a Volume Within the Joint	123
3.61	Line of Contact Between Cartilage Layers in Each Slice was Identified if the Two Layers Could Not be Distinguished	125
4.1	Motion with Follower Load in Lateral Bending	132
4.2	HAM Validation	134
4.3	Helical Axis of Motion Comparison for Intact Specimen.....	141
4.4	Comparison of Facet Load Pattern in Flexion-Extension	146
4.5	Comparison of Facet Load Pattern in Axial Rotation	147
4.6	Surgical Tensioning Tool for Tightening the Implant	151

List of Figures

C.1	Average HAM in Left and Right Axial Rotation Without Follower Preload	187
C.2	Average HAM in Left and Right Axial Rotation With Follower Preload	188
C.3	Average HAM in Left and Right Lateral Bending Without Follower Preload . . .	189
C.4	Average HAM in Left and Right Lateral Bending With Follower Preload	190
C.5	Average HAM in Flexion and Extension Without Follower Preload	191
C.6	Average HAM in Flexion and Extension With Follower Preload	192
C.7	Average HAM in Left and Right Axial Rotation Without Follower Preload (Spacer Length)	193
C.8	Average HAM in Left and Right Axial Rotation With Follower Preload (Spacer Length)	194
C.9	Average HAM in Left and Right Lateral Bending Without Follower Preload (Spacer Length)	195
C.10	Average HAM in Left and Right Lateral Bending With Follower Preload (Spacer Length)	196
C.11	Average HAM in Flexion and Extension Without Follower Preload (Spacer Length)	197
C.12	Average HAM in Flexion and Extension With Follower Preload (Spacer Length)	198

List of Tables

2.1	Summary of Specimen Gender and Age	36
3.1	Absolute Average Range of Motion Without Follower Load	72
3.2	Absolute Average Range of Motion With Follower Load	72
3.3	Absolute Average Neutral Zone Without Follower Load	78
3.4	Absolute Average Neutral Zone With Follower Load	78
3.5	Absolute ROM Without Follower Load for Three Dynesys Spacer Lengths	82
3.6	Absolute ROM With Follower Load for Three Dynesys Spacer Lengths	85
3.7	Absolute NZ Without Follower Load for Three Spacer Lengths	91
3.8	Absolute NZ With Follower Load for Three Spacer Lengths	93
3.9	Initial Separation Distance Between L3 and L4 Anterior Points with the Three Dynesys Spacer Lengths	94
3.10	Average Facet Contact Load Without and With a Follower Preload	99
3.11	Mean and Standard Deviation of Absolute Intradiscal Pressure at L3-L4	115
3.12	Mean and Standard Deviation of Relative Intradiscal Pressure at L3-L4	116
3.13	Forces and Moments Applied to Specimen for MR Imaging	121
3.14	Summary of Measured Joint Volume	124
3.15	Summary of Measured Contact Area	126
3.16	Comparison of Contact Area Measured Using Tekscan and Imaging	126
4.1	Range of Motion Comparison for Intact Specimen	140
4.2	Range of Motion Comparison with Dynesys System	142
4.3	Comparison of Intact (or Capsule Cut) Facet Loads in Extension, Lateral Bend- ing, and Axial Rotation	144
A.1	Kinematic Summary for Specimens 1-10	173
A.2	Helical Axis of Motion Summary for Specimens 1-10	174
A.3	Facet Load Summary for Specimens 1-10	175
A.4	Intradiscal Pressure Summary for Specimens 1-10	176
B.1	Effect of Specimen Condition on Range of Motion	178
B.2	Effect of Specimen Condition on Range of Motion (continued)	179
B.3	Effect of Specimen Condition on Neutral Zone	180
B.4	Effect of Specimen Condition on Position of Helical Axis of Motion	181
B.5	Effect of Specimen Condition on Orientation of Helical Axis of Motion	182
B.6	Effect of Specimen Condition on Facet Loads	183
B.7	Effect of Dynesys on Intradiscal Pressure	183
B.8	Effect of Dynesys Spacer Length on Range of Motion	184
B.9	Effect of Dynesys Spacer Length on Neutral Zone	184
B.10	Effect of Dynesys Spacer Length on Helical Axis of Motion	185
B.11	Effect of Dynesys Spacer Length on Facet Loads	185

Acknowledgements

I would like to first thank Dr. Tom Oxland for his extraordinary support, guidance, and insight over the past two years. I am thrilled to have had the opportunity to work with such a diverse group of people and to delve into the fascinating nature of the spine. A big thanks to Qingan Zhu and Derek Wilson for their contributions to this project. They were a magnificent pair to work with who always made me laugh even after the longest testing days and from whom I have learned a copious amount. Thank you also to Dr. Ory Keynan for his surgical assistance in this study and enlightenment for my many questions.

I would like to acknowledge the funding and support of the Synos Foundation (Switzerland), Zimmer GmbH (Winterthur, Switzerland), and the Natural Sciences and Engineering Research Council of Canada (NSERC).

I am grateful to my parents who have been instrumental with their constant encouragement, optimism, and faith in me.

There are many others who have helped in some way along this journey including Anthony Choo, Carolyn Greaves, Carolyn Sparrey, Catherine Kinnaird, Simon Sjovold, Juay Seng Tan, Thomas Nydegger, Dr. Peter Crompton, Dr. David Wilson, Chris Van Toen, Hanspeter Frei, Emily McWalter, Doug Bourne, and Chad Larson. Their advice, suggestions, invigoration, friendship, and support is all greatly appreciated. And thanks to Sheryl for her musical motivation.

Chapter 1

Introduction

1.1 Clinical Importance

Low back pain is a significant problem that affects 70–85% of all people at some point in their lifetime [8, 74]. The annual prevalence of low back pain is between 15% and 45%, with point prevalences averaging 30% [8, 90, 137]. In many cases, low back pain can be an extremely debilitating condition, resulting in physical pain, limitations, psychological problems, disability, and significant economic impact on society. Chronic low back pain, defined as pain that persists for longer than three months [35], results in large costs to society, which have been reported to lie between 0.5% and 2% of the gross national product in the United States [15]. Methods to improve the quality of life for chronic low back pain sufferers are desirable to diminish or eliminate pain and disability, as well as to reduce the cost to society.

It has been well established that chronic low back pain is a common condition affecting the general population, but the exact causes of low back pain remain somewhat unknown. A large contributor to the problem of chronic low back pain is of a mechanical nature and coined clinical spinal instability [88]. Although the definition of clinical instability is widely debatable, White and Panjabi [139] use it to describe

the loss of the ability of the spine under physiologic loads to maintain its pattern of displacement so that there is no initial or additional neurological deficit, no major deformity, and no incapacitating pain.

There are many causes of clinical instability, of which a few will be discussed later in this chapter (Section 1.4.2). For the purpose of this study, stability will be used to describe a state

in which the degree and direction of motion are controlled such that abnormal displacement of the spine is reduced to a level of or below that of a healthy spine. In addition, stability will also include the capability of the motion segment to support physiologic loads. Techniques that stabilize the lumbar spine in this context, could therefore improve the degree of low back pain experienced by an individual. Before delving into some of the causes of low back pain, it becomes necessary to highlight the anatomical features of the lumbar spine that are important for clear understanding of treatment options, functions and objectives of specific devices, and their outcomes.

1.2 Anatomy

The spine is an important structure of the body that serves three primary biomechanical functions:

- allows movement between the head, trunk, and pelvis;
- transfers weight and forces between the head, trunk, and pelvis; and
- protects the spinal cord from harmful motions and forces.

The human vertebral column consists of 33 vertebrae in five different regions: seven cervical vertebrae; twelve thoracic vertebrae; five lumbar vertebrae; five fused sacral segments; and four fused coccygeal segments (Figure 1.1). In the frontal plane, the spinal column is usually fairly straight. In the sagittal plane, there are four curves in the normal spine, which provide mechanical advantages like increased flexibility, while still providing stiffness and stability. The primary curves, which develop during the fetal period, are kyphotic (convex posteriorly) in the thoracic and sacral regions. The secondary curves of the cervical and lumbar regions are lordotic (convex anteriorly) and develop after birth. This study focuses strictly on the lumbar spine since that is the area that is most severely affected by back pain.

The spine is a highly complicated system consisting of bones (vertebrae), connected by intervertebral discs and ligaments, and supported and controlled by muscles. Each region of the spine possesses unique characteristics. A description of the vertebrae, intervertebral discs, and

ligaments of the lumbar region follows, including the important biomechanical functions and properties.

1.2.1 Vertebrae

The five lumbar vertebrae are numbered superiorly to inferiorly from L1 through to L5. A vertebra consists of a vertebral body and neural arch, from which the posterior elements arise (Figure 1.2). The anterior portion of each vertebra is the vertebral body and it supports the majority of the load through the spinal column. The vertebral bodies are composed mainly of cancellous bone with a thin cortical shell and are kidney-shaped when viewed from superior.

The neural arch surrounds the neural elements that run through the vertebral column. It consists of two pedicles that project posteriorly from the vertebral body and a lamina that extends from each pedicle towards the midline. The pedicles are thick-walled cylinders, while the lamina is a flat plate fused in the midplane. The architecture of the pedicles enables them to function as weight-bearing components that are strong in compression and bending.

The pedicles are the sole connection between the posterior elements and the vertebral body, and thus are able to transfer the load between the two. The lamina serves to protect the neural components within the vertebral canal, as well as transmitting forces between the posterior elements and the vertebral body. Extending posteriorly from the lamina is the spinous process. This is the bony surface that you can palpate as

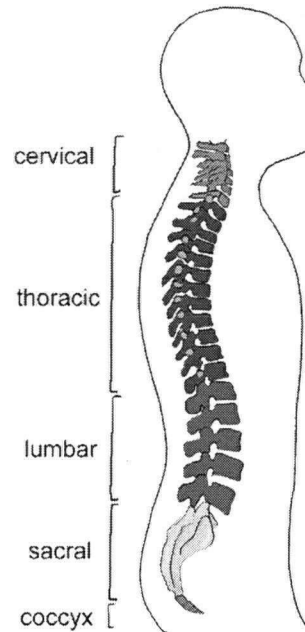


Figure 1.1: *Regions of the vertebral column. Seven cervical vertebrae, twelve thoracic vertebrae, five lumbar vertebrae, five fused sacral segments, and coccyx (four fused coccygeal segments).*

you run your hand down your back. Projecting laterally on each side from the pedicle-lamina junction is a transverse process. The spinous and transverse processes provide points for ligament and muscle attachments and form levers that accentuate the action of the ligaments and muscles.

Each vertebra consists of four articular processes. Two inferior and two superior articular processes are masses of bone that develop inferiorly and superiorly from the lamina. On the medial surface of the right and left superior articular processes and the lateral surface of the right and left inferior articular processes is a smooth area of bone known as the articular facet. The inferior and superior facets of adjacent vertebrae articulate with one another to form the facet joints (also known as zygapophysial joints), whose function will be discussed in further detail in Section 1.2.4.

The space that is surrounded by the neural arch and the posterior aspect of the vertebral body is the vertebral foramen. The series of vertebral foramen at each level collectively form the vertebral canal that runs longitudinally through the spinal column and transmits the spinal cord, nerve roots, and vessels. Superior and inferior notches are present above and below each pedicle. The notches of adjacent vertebrae face each other and form another space, known

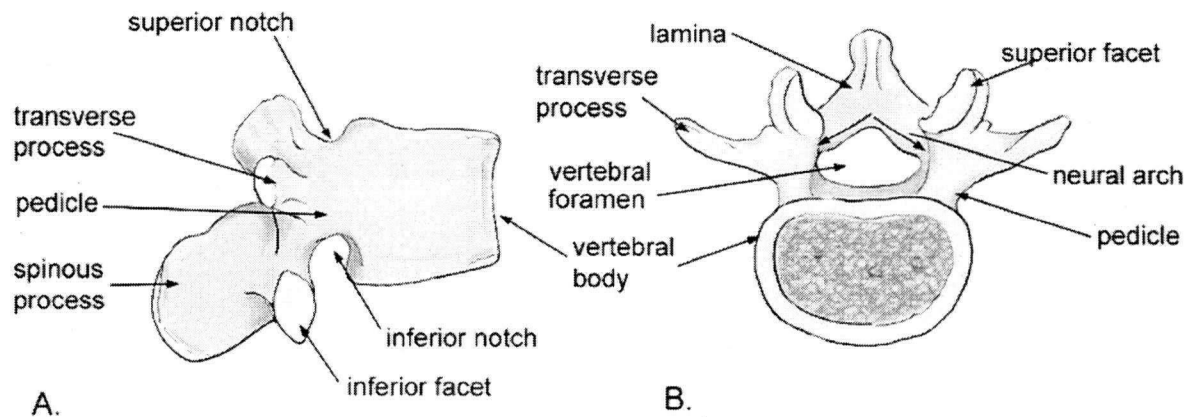


Figure 1.2: Anatomy of a typical lumbar vertebra. Viewed A) laterally from the right and B) from the top. Figure modified from Bogduk, 1997.

as the intervertebral foramen, which provides a passage for the spinal nerve roots and blood vessels.

1.2.2 Intervertebral Discs

The largest avascular structures in the body, the intervertebral discs, lie between adjacent vertebral bodies. The vertebral body and intervertebral disc are separated by cartilaginous endplates composed of hyaline cartilage and fibrocartilage. Intervertebral discs are composed of a fibrous outer ring known as the annulus fibrosus and a gelatinous centre called the nucleus pulposus (Figure 1.3). The annulus fibrosus consists of concentric lamellae of collagen fibres that surround the nucleus pulposus. Within each lamella, the collagen fibres are arranged parallel to one another, but at an angle of 65–70° from the vertical [10]. The angle of inclination alternates with each successive lamella. The nucleus pulposus is composed of a network of fibrous strands that lie in a mucoprotein gel containing various mucopolysaccharides. It is a semi-fluid mass with a water content of 70–90% [139]. The nucleus pulposus is pressurized, analogous to air in a car tire. The principal functions of the intervertebral disc are to enable movement between vertebral bodies and to transmit load between adjacent vertebrae. The disc is a viscoelastic and anisotropic structure, and as such, its mechanical properties and behaviour are time and direction dependent. The disc exhibits a non-linear stiffness and provides greater resistance to

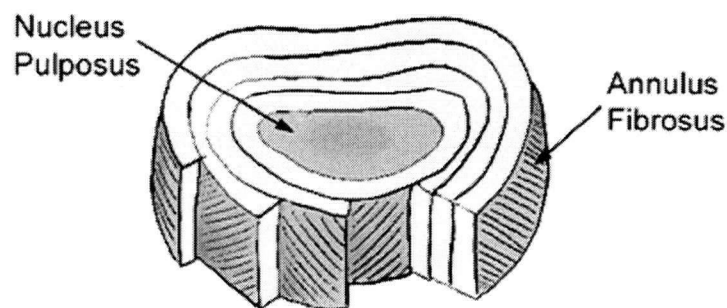


Figure 1.3: *Anatomy of a lumbar intervertebral disc. Figure modified from White and Panjabi, 1990.*

displacement as the load magnitude increases. Therefore the disc allows flexibility at low loads and stability at high loads.

1.2.3 Ligaments

Ligaments primarily resist tensile forces and stabilize the spinal column. While there are many spinal ligaments, only a portion will be highlighted here (Figure 1.4).

The anterior longitudinal ligament is a strong fibrous band that covers and connects the anterolateral aspect of the vertebral bodies and intervertebral discs and helps prevent hyperextension of the column. The posterior longitudinal ligament lies within the vertebral canal along the posterior aspect of the vertebral bodies and discs. It helps prevent hyperflexion of the spinal column and disc herniation.

The ligamentum flavum is short and thick and bilaterally connects the laminae of adjacent vertebrae. This ligament aids in restoring the flexed spine to its extended position. The interspinous

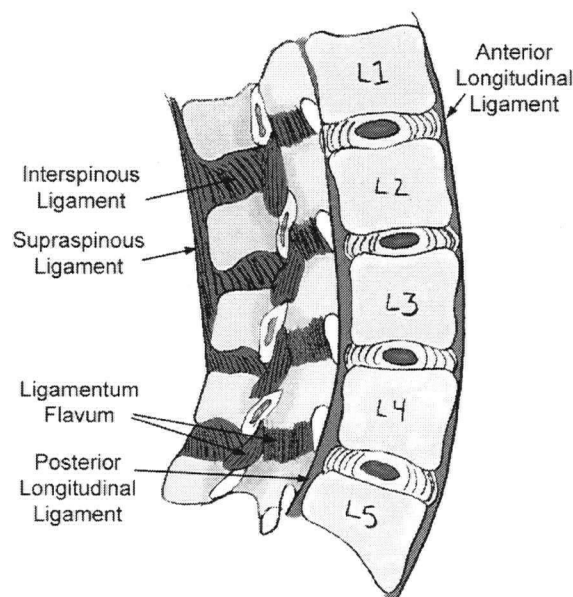


Figure 1.4: *Sagittal section with laminectomy showing the ligaments of the lumbar spine. Figure modified from Bogduk, 1997.*

and supraspinous ligaments are the other two posterior ligaments. Interspinous ligaments are weaker than their strong supraspinous counterparts. Both connect adjacent spinous processes.

1.2.4 Triple Joint Complex

A functional spinal unit or single motion segment is made up of two adjacent vertebrae, one intervertebral disc that lies between them, and the intervening non-muscular soft tissues. Adjacent vertebrae join together by means of a triple joint complex: the two facet joints, posteriorly; and the intervertebral disc, anteriorly (Figure 1.5).

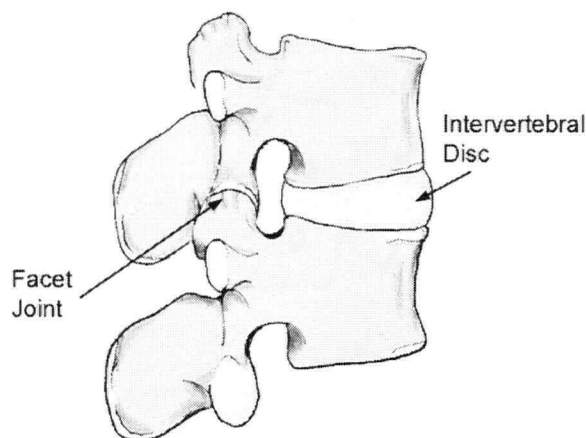


Figure 1.5: *Sagittal view of lumbar triple joint complex. It consists of two adjacent vertebrae and the interlying intervertebral disc. Figure modified from Bogduk, 1997.*

The facet joints are gliding synovial joints and as such, are composed of articular cartilage, capsule, and synovial fluid. The size of the articulating surface of the facets is approximately 16 mm in height and 14 mm in width, with a surface area of about 160 mm² [10, 103]. The size, shape, and inclination of the facets vary with level. Towards the lower levels, the facets are larger and the facet inclination with the sagittal plane decreases [103]. The facet joint articulations are oriented approximately perpendicular to the transverse plane. There is a lot of variation in facet shape among individuals. In some the facet articulation is flat, whereas in others, a varying degree of curvature can be

exhibited from a 'C' to a 'J' shaped superior facet articulating with an appropriately matched curved inferior facet surface [10]. Each facet is covered with cartilage that is an average of 1.5 – 1.9 mm thick in a healthy spine [25]. The thickness is not uniform and varies over the facet surface, with maximum depth typically found near the centre of the facet. The function of

the facet joints is to control motion, mainly by resisting forward displacement and rotation, and to transfer a small portion of the total load through the vertebral column, mainly in extension and axial rotation [4, 68, 127].

The intervertebral disc forms a secondary cartilaginous joint (symphysis) and is the third joint in the triple joint complex. It is designed for strength and weight-bearing functions. The structure and properties, especially the non-linear stiffness, of the disc allow it to be strong enough to sustain large forces, while being deformable to permit the physiologic movements of the spine.

1.3 Current Treatment of Low Back Pain

A wide variety of treatment options exist to address the problem of chronic low back pain. Treatment for chronic low back pain and instability usually first consists of non-operative treatment. This can include bedrest, therapeutic exercise like stretching, flexion-extension exercises, and core strengthening, acupuncture, drug therapy, manipulation, or external bracing. As a last resort, after non-operative treatments have failed, spine surgeons may perform fusion surgery (arthrodesis). The indications for surgical treatment, however, are still controversial [85, 87, 89]. Fusion is considered by some to be the standard and most effective surgical intervention for treatment of chronic low back pain [34]. In 1990, there were 46 500 lumbar fusions, equivalent to 26 per 100 000 adults, performed in the United States [8]. In comparison, there were 21 fusions per 100 000 adults performed in 1990 in Canada [37]. The number of fusions done for low back pain is rapidly increasing. Over an 11 year period, from 1979 to 1990, the number of operations among adults for low-back pain in the United States increased by 55% with the largest increase for fusions (100%) [8]. Although, there are large variations that exist across the country, compared with other developed nations, the surgical rates in the USA are on average 40% higher [8, 17].

Different surgical techniques can be used to achieve fusion depending on various factors including surgeon preference and the predicted source of pain. Posterolateral fusion involves placing

bone over decorticated transverse processes and facet joints and is preferred if pain is believed to stem from the facet joints. Posterior or anterior lumbar interbody fusions (PLIF or ALIF) consist of removal of the disc and insertion of a bone transplant or synthetic implant into the void. This is commonly used when pain appears to be presented in the disc. If the pain comes from both the disc and the posterior elements, a 360° fusion may be performed to provide maximum stability. All of these techniques may be supplemented with internal fixation, which allows for immediate stability, increases the fusion rate, and makes rehabilitation easier. The complication rate increases when internal fixation is used [154].

Fusion of two or more vertebrae results in complete loss of motion at the selected levels. The goals of fusion are to reduce pain and decrease disability [34, 139]. It has been suggested that fusion may actually accelerate degeneration at adjacent levels [29, 64, 119] due to compensation for the eliminated segmental motion. Biomechanical and radiographic studies have shown an increase in forces, motion, and intradiscal pressure in adjacent segments following a lumbar fusion [29]. Pathologically, these changes are often presented as facet joint osteoarthritis and spinal stenosis [64]. For this reason, alternative treatments that aim to maintain some degree of mobility at the indicated level, such as dynamic stabilization, may be advantageous.

1.4 What is Dynamic Stabilization?

Dynamic stabilization is an alternative to fusion for the treatment of degenerative problems in the lumbar spine. Unlike in fusion where the goal is to eliminate motion, dynamic stabilization is a surgical procedure used to provide stability by controlling the motion. Some devices also strive to reduce the loading at the facet joints. These systems can be either anterior or posterior in nature.

Dynamic anterior stabilization is a category made up of artificial discs and prosthetic nuclei. Some examples of these devices include the *Link SB III Charité* total disc prosthesis (Link Inc.), *ProDisc* modular total disc (Spine Solutions Inc.), the *AcroFlex* lumbar disc prosthesis (Depuy-AcroMed Inc.), *PDN* prosthetic disc nucleus (RayMedica Inc.), and polyurethane spirals for

nucleoplasty (Sulzer Medica Inc.) (Figure 1.6). It involves alteration of the anterior portion of

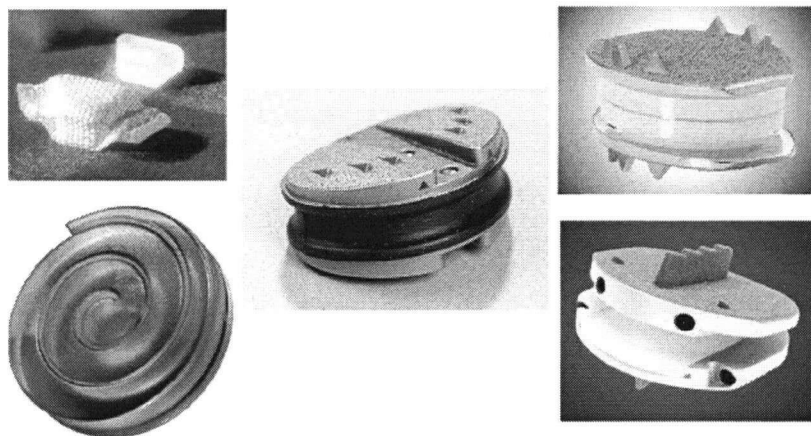


Figure 1.6: Anterior dynamic stabilization devices. From left to right, top to bottom: PDN Prosthetic disc nucleus (RayMedica Inc.), polyurethane spiral (Sulzer Medica Inc.), Acroflex (Depuy-AcroMed Inc.), SB III Charité (Link Inc.), and ProDisc (Spine Solutions Inc.).

the vertebral column. The main concerns of intervertebral disc prostheses are a preservation of disc height, lumbar lordosis, and a partial restoration of local kinematics, to achieve a regional biomechanical compromise between replicating the viscoelasticity and load-bearing behaviour of the disc and simulating the intersegmental motion [65]. Dynamic anterior stabilization will not be discussed in significant detail in this work.

Dynamic posterior stabilization consists of those devices that are geared towards the posterior elements. Examples of these systems are soft system stabilization (*Graf Ligaments*), the *Wallis* system (Spine Next), and the dynamic neutralization system for the spine (*Dynesys*) (Zimmer GmbH) (Figure 1.7). Dynamic posterior stabilization involves implantation of a device into the posterior aspect of the spinal column without disrupting the anterior components (ligaments, soft tissue) and intervertebral disc. The various systems can be classified into four main categories: i) inter-spinous distraction devices; ii) inter-spinous ligament devices; iii) ligaments across pedicle screws; and iv) semi-rigid metallic devices across pedicle screws [123]. The *Dynesys* system was part of the third group and was the focus of this study.

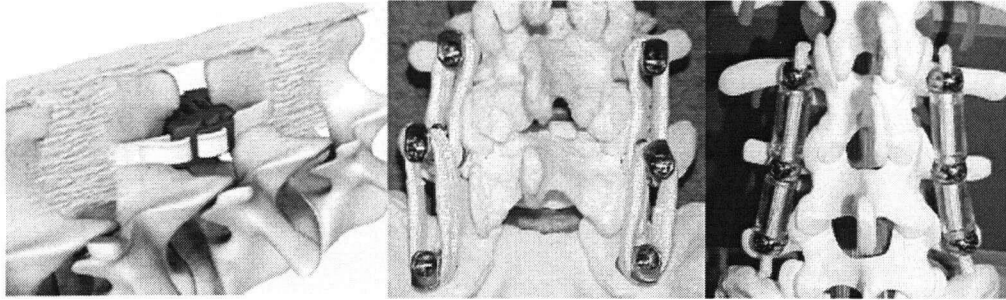


Figure 1.7: *Posterior dynamic stabilization devices. From left to right: Wallis system (Spine Next), Graf Ligaments, and Dynesys system (Zimmer GmbH).*

1.4.1 The Dynesys System

The Dynesys dynamic neutralization system (Zimmer GmbH, Winterthur, Switzerland) is a dynamic posterior stabilization device that is designed to preserve the intersegmental kinematics and reduce the loading at the facet joints. It was created by Dr. Gilles Dubois in France and implanted in a human for the first time in 1994 [27]. The Dynesys is a bilateral device that consists of titanium alloy (TiAl6Nb7) pedicle screws and polycarbonate urethane (PCU) spacers that surround tensioned polyethylene terephthalate (PET) cords (Figure 1.8). The spacers support compressive loads while the tensioned cords stabilize the system and act against tensile loads and flexion moments. It can be utilized as a uni-segmental or multi-segmental system.

The first multi-centre clinical study using the Dynesys was published in 2002 [132]. A total of 83 patients received Dynesys instrumentation for stabilization instead of fusion. The study suggested that the Dynesys was a safe and effective procedure for stabilizing the lumbar spine. The largest complication related to the implant was screw loosening. The mid-term results, in terms of pain and function, were comparable to those of fusion.

1.4.2 Indications

There are many indications that render a spinal column unstable. Causes of instability generally can be classified into several broad categories, including degenerative, traumatic, post-traumatic, congenital, and iatrogenic. The focus in this work was mainly on degenerative

instability.

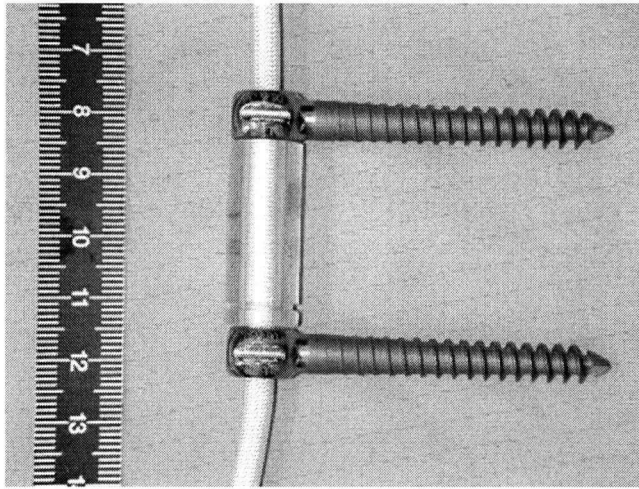


Figure 1.8: *Components of the Dynesys system. Titanium alloy pedicle screws and polycarbonate urethane (PCU) spacers that surround polyethylene terephthalate (PET) cords.*

Indications of low back pain that may make a patient a suitable candidate for the Dynesys system include all forms of degenerative disc disease [92] and conditions requiring lumbar spinal stabilization. Pathological conditions for selection include early stages of degenerative disc disease resulting from spinal stenosis, which is a narrowing of the spinal canal often with impingement of neural elements, and spondylolisthesis, a forward movement of the body of one of the lower lumbar vertebrae on the vertebra below it (grade 1, 25% slippage). Also included are disc bulging, protrusion, and rupture. The Dynesys may also be used in some cases of post traumatic instability [79].

Exclusion criteria include higher grades of spondylolisthesis, isthmic spondylolisthesis, spinal tumours and infections, trauma, vertebral fractures, osteoporosis, and gross degenerative instability [56, 79, 92].

1.5 Biomechanical Testing

The objective of biomechanical testing of spinal implant systems is to confirm that a device accomplishes its functional objectives and to compare the performance of different devices [75]. The biomechanical flexibility, or stability, test is a single part of a comprehensive evaluation of a spinal stabilization system, which additionally includes both strength and fatigue testing [97, 98]. A maximum strength test involves applying a load of increasing magnitude until failure

of the device occurs. This generates a load-displacement curve that provides information on stiffness of the structure, energy absorption, failure mechanism, and failure load. In fatigue testing, a device is loaded cyclically at a magnitude significantly below the failure load until the device fails. This can be done at different loading rates to generate a fatigue curve relating information about the longevity of the device. Both the strength and fatigue tests can be conducted on either the device in isolation or as part of a spinal construct and in each case, the testing is destructive. A flexibility test is non-destructive and for that reason can be used to test a range of loads (magnitude or direction), under a wide variety of conditions. The testing is usually performed on a spinal construct, loads are of a physiologic magnitude, and motion at the site of interest is measured.

The requirements for biomechanical testing of spinal fixation devices have already been fairly well established [1, 97, 98, 144]. The primary goal of fusion is to stabilize a segment by eliminating motion at the particular level, and as such, it seems fundamental that the critical component of an evaluation of the device is a kinematic analysis to investigate to what degree the motion is removed. There has also been some attempt at standardizing the protocol for testing of fixation devices [1, 97, 98, 144] so that comparisons can be performed across studies and conclusions drawn. The important aspects address specimen selection, testing apparatus and procedure, and analysis of data. To some degree, these concepts can also be applied to the evaluation of dynamic devices, but compose only a portion of the necessary biomechanical testing. The goals of dynamic stabilization systems are more complex than those of fixation devices and therefore, a more rigorous investigation must be implemented (further details in Section 1.6).

1.5.1 Specimen Selection

Specimens are excluded from biomechanical studies if there is evidence, radiographic or macroscopic, of injury or tumors. The specimen length has been shown to have a significant effect on segmental motion behaviour [59], and for testing, there should be at least one free segment on either end of the area of interest [59, 144]. The most relevant *in vitro* results, as compared to human *in vivo* behaviour, stem from human cadaveric testing, although due to limited avail-

ability in some instances, testing on other species, is acceptable [141, 144]. The specimens are fresh-frozen between -20 and -30°C , and thawed at room temperature, which has been shown to have negligible effect on the behaviour of the disc and bone [100]. Soft tissue and musculature are carefully dissected and the superior and inferior vertebrae potted to allow attachment to the loading device. One end remains fixed to a base while loads are applied to the other, free, end [97]. Biomechanical testing of injured specimens is common since often the purpose of the fixation device is to stabilize an injured segment. The injury must be reproducible and closely model the *in vivo* injury that is to be simulated [97, 144].

1.5.2 Testing Apparatus and Procedure

Duration of spinal testing should not exceed 20 hours, since exposure to room temperature for a period longer than this can lead to changes in the properties of the specimen [140]. Effort should be exercised to protect the specimen from drying out by conducting tests in a humidity chamber, wrapping the specimen in a moistened wrap, or periodically spraying the specimen with saline.

There are two methods of experimentally testing a construct to determine its biomechanical behaviour. In the stiffness approach, a displacement of a pre-determined magnitude is applied to the free end of the specimen in a particular direction while the resulting forces, moments, and motion are recorded. In contrast, in the flexibility method, a defined load such as a pure moment is applied to the top vertebra, at a constant rate to a pre-determined maximum moment. The motion of each of the segments is recorded. There has been some controversy in the past regarding the advantages and disadvantages of load controlled versus displacement controlled analysis [41, 97, 144]. On the load controlled side, supporters believe that the load controlled method is easier to standardize and allows a constant load to be applied at all levels regardless of the stiffness of the specimen and changes in the specimen condition (ie. injury, stabilization, etc.). Displacement control creates additional complex loads due to the coupling behaviour of the spine and with multi-segmental testing, it becomes a challenging task to determine the resulting loads that are applied to each segment. On the other hand, with displacement control,

translation and rotation can be applied based on motion of the vertebrae, but to specify and apply motion in six degrees of freedom is difficult. The load controlled method has become widely accepted, largely due to the fact that in vivo motion can be reproduced in vitro in most cases and the resulting motion of each vertebra can be easily measured.

A number of requirements for a spinal loading simulator arose based on Wilke's recommendations [144] and the work of others. The loading device should allow unconstrained three-dimensional movement of the specimen. Differences in kinematic behaviour have been observed between constrained and unconstrained testing methods in axial rotation [45]. The magnitude of rotation was found sensitive to the position of the loading axis in a constrained approach. An unconstrained method allowed the specimen to move freely about its helical axis of motion, thereby permitting natural coupling of vertebral motion. Rotations produced in each of the two methods were distinctly different. Arguments supporting constrained testing suggest that loading is more repeatable since the axis of motion remains constant. For in vitro biomechanical studies, however, the condition of the specimen is often altered with implantation of a spinal device or simulation of an injury, for example, which leads to changes in the helical axis of motion of the segment. A constrained approach to testing inhibits migration of the helical axis, thus obviating a portion of the changes in kinematic behaviour that would normally accompany an injury or stabilization. An unconstrained method of load application is therefore more desirable.

The loading apparatus should be able to apply a pure moment in each of the six directions: flexion; extension; right and left lateral bending; and right and left axial rotation. It is important that the loads applied to the specimen be of a constant magnitude along the entire length so that weak points in a construct can be identified [97]. Application of a pure moment to the top vertebra results in a constant bending moment at each cross section along the length of the specimen [97]. The load magnitude suggested for testing in the lumbar spine is ± 7.5 Nm, since this has been shown to replicate motions of physiological magnitude [144]. There are a wide variety of load scenarios that have been applied to cadaveric spines for biomechanical testing. These have included pure moments [14, 26, 61, 104, 120, 151], compressive or shear

forces [33, 70, 82], or eccentric compressive loading [2, 133]. Some researchers argue that complex loading provides a better simulation of in vivo conditions [1]. However, application of shear or eccentric compressive forces generates a non-uniform loading profile through the length of the spine that is undesirable for evaluation of spinal devices [97].

By Wilke's recommendations, the load can be either a continuous or stepwise load applied in the positive and negative directions successively to produce the full cycle of motion [144]. A recent study, however, has shown that stepwise and continuous loading protocols generate differing spinal behaviours [43]. The continuous loading protocol produced significantly smaller rotations (both range of motion and neutral zone), likely because there was cumulative creep of the specimen during the stepwise test which resulted in a larger range of motion. Historically, a stepwise load was used because it was considered to be the most repeatable technique in flexibility testing since loads were generally applied using pulleys and weights. Lately, more advanced actuation systems make continuous loading possible, which better represents in vivo motion.

At least three complete load-unload cycles should be performed, two of which serve to precondition the specimen [97, 98, 144]. It is important to precondition the construct in this manner to minimize the viscoelastic effects of the specimens. The spine itself is viscoelastic, and there may also be settling at the bone-screw interface or of other hardware components.

Because stability testing is non-destructive, a variety of specimen conditions can be evaluated. Where possible, if testing implants, the order should be randomized [144]. In addition, a device commonly used clinically should be included in the testing to provide a relative measure of the efficacy of the newer implant system.

1.5.3 Analysis of Data

The most important measurements when performing an analysis of the stabilizing effect of a spinal fixation device have been the motions at the fusion site. As mentioned previously, the goal of fusion is to eliminate motion, so ideally minimal motion is sought. In addition, motion

at other critical locations may be of interest to analyze the behaviour of the implant or motion at adjacent segments.

Kinematic Behaviour

Movement of the spine is relatively complicated. In response to an applied load, the behaviour of the spine is non-linear and viscoelastic [139]. In other words, the flexibility, defined as the ratio of the displacement produced to the load applied, varies with the magnitude, direction, and rate of the applied load. At small loads the spine deforms quite easily with lesser resistance than at larger loads. The motion of the spine can be divided into two distinct phases: the neutral zone (NZ) and the elastic zone (EZ) (Figure 1.9). The NZ is a measure of the low stiffness behaviour of the spine and is the displacement at low loads from the neutral point, whereas the EZ represents the displacement from the end of the neutral zone to the maximum physiological load [139]. The range of motion (ROM) is the displacement from the neutral point to the maximum load and is the sum of the NZ and EZ.

There are three primary directions of movement for the spine: flexion-extension; lateral bending; and axial rotation. Movement is typically coupled, meaning that motion about a secondary axis will often accompany the primary motion. The degree of coupling depends on intervertebral level, posture, and direction of motion [95]. In a neutral posture, axial torque produced lateral bending, whereas lateral bending caused axial rotation [95, 110]. The strongest coupling pattern is the lateral bending that results from axial rotation [80, 139]. A small degree of coupled flexion was also observed in both lateral bending and axial rotation. There was little coupled motion (less than 1°) seen in flexion-extension, however translation in the sagittal plane was prominent.

The normal range of motion for a lumbar spine segment is between 12° and 17° in flexion-extension, 3° to 8° for lateral bending to one side, and 1° to 2° for axial rotation to one side [139]. In vitro, under a pure moment of 10 Nm, the average NZ was 1.5° in flexion and extension, 1.4° in left and right lateral bending, and 0.5° in left and right axial rotation [151].

In terms of evaluating the stability created by a spinal fixation device, the kinematic parameters

mentioned may all be obtained from the load-displacement curve. The NZ for a specimen subjected to continuous loading is determined based on the difference between the loading and unloading curves at zero applied moment [43] (Figure 1.9). The EZ is the displacement measured from the end of the NZ to the maximum load. ROM is then the sum of the NZ and EZ. Of the three parameters, ROM is the most commonly reported result, followed by NZ. [24, 26, 30, 33, 61, 65, 66, 67, 81, 105, 116, 120, 133, 151].

The three-dimensional motion of the spine encompasses six degrees of freedom, represented for example by three rotations and three translations [97]. For each of these six degrees of freedom, there is a NZ and EZ. Typically, rotation is investigated about the primary axis only. Translation is occasionally reported when quantifying kinematic behaviour of the spine [33, 40, 104, 151], but its occurrence is not as frequent in the literature. The translation between two points can be of interest in answering specific questions regarding the function or behaviour of an implant.

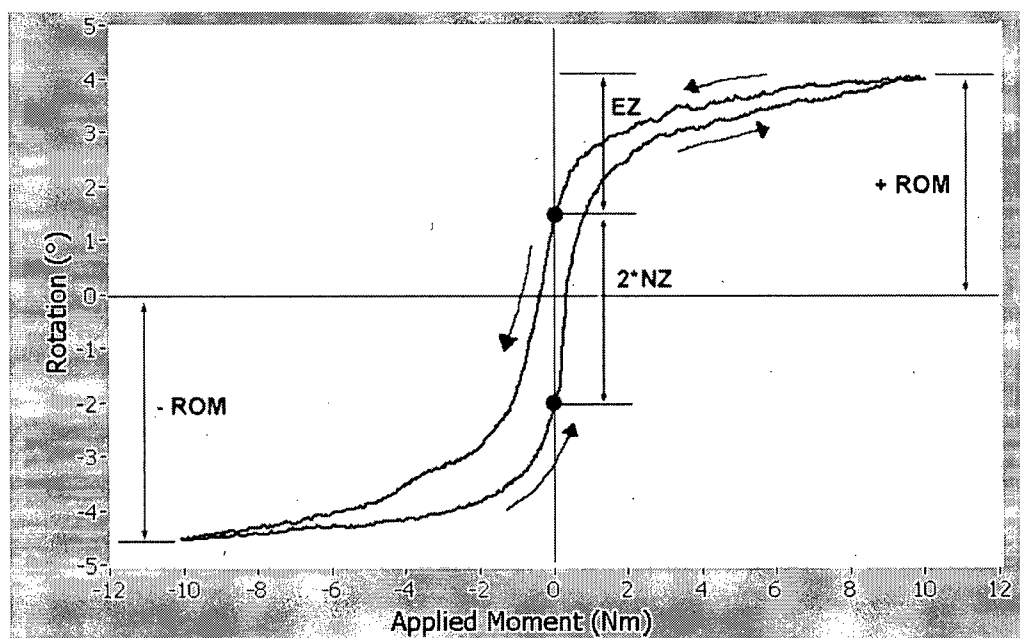


Figure 1.9: Explanation of kinematic parameters. Depicted graphically are the neutral zone (NZ), elastic zone (EZ), and range of motion (ROM) for one full loading cycle (third cycle). ROM is the sum of the NZ and EZ.

1.6 New Trends in Biomechanical Testing

The biomechanical testing to date has been largely concentrated on evaluation of spinal fixation devices, which aim primarily to eliminate segmental motion to provide an appropriate mechanical environment for fusion, and investigation of their effects on ROM and NZ at the level of interest. The standardized biomechanical test protocols that have been developed previously focus on the evaluation of devices of this sort. With the more recent introduction of dynamic or flexible instrumentation for achieving spinal stability, the mechanical objectives have changed. Devices now not only control the rotational motion and attempt to preserve a degree of intersegmental motion, but also modify segmental load transfer through the intervertebral disc, posterior elements, or both. Evaluation of the efficacy of these systems requires additional methods to fully describe the behaviour as well as employment of loading techniques that more closely simulate physiological loading. The protocol for testing of dynamic systems has not been clearly established and previous work in the area appears to overlook important aspects necessary to form a comprehensive biomechanical characterization.

1.6.1 Existing Dynamic Stabilization Evaluations

The existing biomechanical evaluations of dynamic stabilization systems in the literature are fairly sparse, but not entirely unheard of. There are substantially more investigations performed on anterior devices than posterior ones, likely due to the fact that historically anterior devices were introduced earlier and there is a wider variety of anterior devices than posterior devices.

The majority of biomechanical tests of anterior devices were in vitro studies using human cadavers [13, 24, 26, 30, 65, 66, 67], cadaveric sheep [57, 61, 78], or other species [24, 138]. In addition, there were several finite element models created to evaluate the behaviour of an implanted spinal segment [26, 62, 65, 78] and some testing reported on the implant in isolation [13, 61].

There has been a lot of variation in the loading protocol between studies, with no two studies the same. The work was done using either a pure compressive load [13, 26, 57, 78], application

of a moment in flexion-extension, lateral bending, and/or axial rotation [24, 30, 57, 61, 65, 66, 67], or combined compression and rotation [26, 57, 62, 67]. None of these studies were done with a compressive "follower" load, however a few were conducted in the presence of an axial compressive load consistent with that expected in vivo [26, 62, 67].

The evaluated parameters for the anterior devices most commonly consisted of an analysis of the ROM and/or stiffness [24, 26, 30, 57, 61, 65, 66, 67]. One study of the SB Charité disc mentioned the centre of rotation, its important role in kinematic behaviour, and that the SB Charité mimics the natural movement well since the implant is an unconstrained three-dimensional system [66]. A quantitative analysis of the centre of rotation or helical axis of motion appeared to be lacking. In contrast, a few studies looked at very specific parameters like the direction of annular bulging [78], stresses at the bone-implant interface [65], and facet loads [26].

Test protocols for investigation of posterior devices spanned a very wide spectrum. One group created a simplified model to test an elastic stabilization system in flexion [14]. In this case, the internal actions and moments were measured, as well as the stresses and deformations of the intervertebral discs. Construct tests were conducted on polyester braids [63] to evaluate a critical mechanical component of the system. The behaviour of polyester braids was also assessed in vitro [91, 105] and using ultra high molecular weight polyethylene (UHMWPE) models based on ASTM standards [63]. In these studies, the loading was not of a physiological nature. In one of the in vitro studies, facet loads and disc bulge were also recorded. Graf ligaments have undergone a greater deal of biomechanical testing than some of the other posterior systems, including in vitro calculation of the location of a balance point, compressive compliance, ROM, and flexibility [133]. Two studies looking at the Dynesys system [33, 120] were cadaveric investigations that applied a load to the specimen and measured the resulting magnitude of motion (flexibility protocol). The earlier in vitro study by Freudiger et al. [33] employed a unique loading protocol for testing in the sagittal plane. A combination of bending, compressive, and shear loads were simultaneously applied to the spine segments to model the trunk bending under its own weight. The average applied loads were large compared with

other studies. Rotations as well as anterior-posterior and inferior-superior displacements were measured. In a more recent biomechanical evaluation of the Dynesys system [120], cadaveric specimens were loaded with pure moments of 10 Nm in flexion-extension, lateral bending, and axial rotation with no compressive preload. ROM and NZ were measured and compared for intact, injured, stabilized with the Dynesys system, and stabilized with pedicle screw fixation conditions.

The lack of congruity among existing biomechanical evaluations of dynamic stabilization systems reflects the need for a standardized protocol to test these particular devices in a manner that will verify that the system meets its functional goals, adequately stabilizes a segment, and allows for comparisons between different studies and devices. In contrast to rigid fixation systems, the objectives of dynamic stabilization devices are often different from one another and thus may require additional test modules on top of a standard test procedure. Since dynamic stabilization devices modify or attempt to preserve the natural mechanics of the spine, it becomes critical that a biomechanical evaluation of such a device simulates physiological loading conditions [75]. Specifically, this means that a compressive follower preload should be included [109] and that loading should be applied to produce motions similar to those observed in vivo in a healthy spine. It is also important to study the full kinematic behaviour, not simply the magnitude of the motion. Furthermore, investigation into the loading patterns through the posterior elements and anterior column would contribute invaluable information in terms of device functionality.

1.6.2 Follower Preload

Compressive loading has very little effect on the segmental rotation with rigid fixation devices [116], and so while important, the use of compressive preloads was not as critical with evaluation of fusion systems as it is with dynamic stabilization devices. Non-rigid systems can deform under compressive loading, which changes the mechanical behaviour of the device [75], so it becomes prudent to incorporate physiological compressive loads and muscle forces into the loading protocol.

A preload is a “static, continuous, axial compressive load” on the motion segment [55]. The purpose of a follower preload (note that there is a difference between strictly a preload and a follower preload) is to simulate physiologic compressive loading in an in vitro spine study [109]. It has been estimated that compressive loads on the lumbar spine can be as high as 1000 N during standing and walking and can increase to several thousand Newtons (3 – 5 kN [121]) during other activities [84]. Previous studies have incorporated physiologic axial compressive preloads on testing of single motion segments and discovered that compressive preloads increase the bending and shear stiffness of the specimen [55, 102]. When these physiologic conditions were imposed on the whole lumbar spine during in vitro testing, the spine buckled at loads that were much lower than physiologic loads [21, 22]. If a compressive load is applied to the spine along a vertical path, bending moments are created due to the curvature of the spine, which in turn alters the curvature of the specimen. This can lead to buckling of long specimens and damage to the soft tissue or bony structures [21]. During in vitro testing, for the spine to sustain the large compressive loads seen in vivo, the resultant internal compressive load must be tangent to the curve of the spine and pass through the centres of rotation of the vertebrae [109] (Figure 1.10). Caution must be used when devising the methodology for application of a compressive follower preload. Cripton et al. [20] compared the reaction moments and forces resulting at the intervertebral disc and kinematic behaviour for four different preload application techniques on a single motion segment. The degree of constraint on the preload vector was varied. High artefact moments and low shear forces were created in unconstrained preload methods, while constrained preload methods displayed the opposite trend. The results favour the use of a constrained type preload for flexion, extension, and lateral bending and a relatively unconstrained type for axial rotation.

1.6.3 Additional Kinematic Parameters

Previous studies looking at posterior dynamic stabilization have analyzed kinematic behaviour using intersegmental translations and/or rotations about a primary axis. Few studies report more than one degree of freedom per functional spinal unit, even though six degrees of freedom are required to completely describe the motion. A potentially useful technique to fully portray

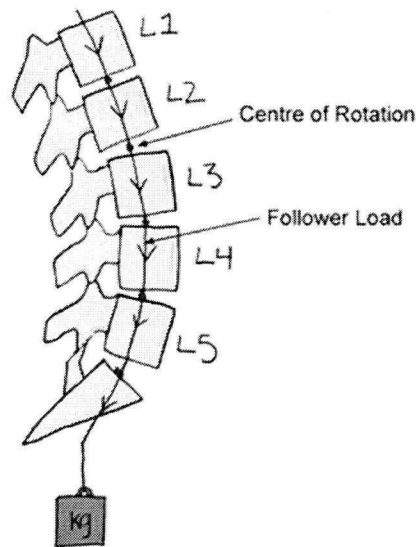


Figure 1.10: Schematic of compressive follower preload on the lumbar spine. The follower preload passes through the centre of rotation of each segment so that at each level, a pure compressive load is applied. Figure modified from Patwardhan et al., 1999.

the six degree of freedom intersegmental movement is the helical axis of motion (HAM). This is important in evaluations of dynamic stabilization systems that attempt to restore not only the ROM, but all other aspects of motion as well, like the direction of motion, centre of rotation, and degree of coupled motion, all of which are described by the HAM.

At any instant, the HAM is the unique axis about which a body rotates and parallel to which it translates [101] (Figure 1.11). It is the three-dimensional equivalent of the two-dimensional centre of rotation. The HAM is specified by six quantities: four that describe the position and orientation of the axis; one defining the amount of rotation about the axis; and one defining the translation along the axis [139]. Typically, the HAM is represented by an orientation in two planes and as a point of intersection with either the sagittal, transverse, or coronal plane. The HAM has been used to specify motion at other joints in the body and the methods are conveyed in detail in the literature [60, 101, 131]. The HAM was utilized to describe kinematics of the lumbar spine in vitro [45, 72, 96, 101] and the canine lumbar spine in vivo [118]. None of

the existing dynamic stabilization investigations included an evaluation of the motion pattern, described by the HAM, as an assessment of kinematic behaviour.

Although there have been differences established in the position and orientation of the HAM, and extent of rotations and translations along the axis at different lumbar vertebral levels [96], a general description of the HAM in the healthy lumbar spine can be discussed. In flexion and extension, the HAM was found to typically intersect the mid-sagittal plane around the centre of the superior endplate of the caudal vertebra [96, 139] (Figure 1.12). The orientation of the HAM was to the left in flexion and to the right in extension. In right lateral bending, the HAM typically intersected the frontal plane in the mid-intervertebral disc to the left of the mid-sagittal plane and was oriented anteriorly, to the left, and slightly cranially. The HAM was similar for left lateral bending, except the axis intersected the frontal plane to the right of the mid-sagittal plane and was oriented posteriorly, to the left, and slightly caudally. In axial rotation, the HAM intersected the transverse plane anterior to the posterior wall of the

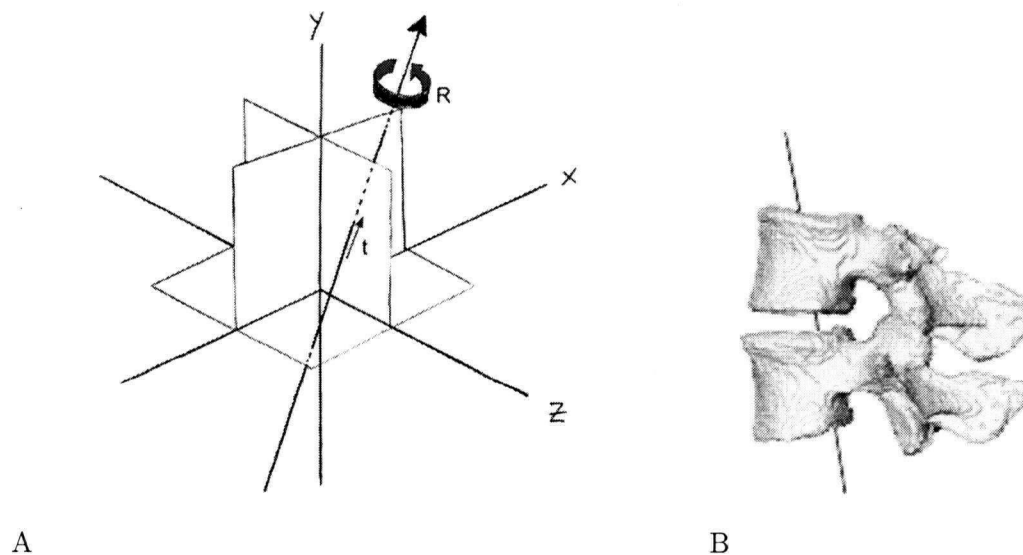


Figure 1.11: Representation of a helical axis of motion (HAM). A) Intersegmental motion can be specified by a single rotation (R) about and translation (t) along the HAM. The HAM is identified by its position and orientation. Figure modified from Panjabi et al., 1981. B) Depiction of HAM between vertebral bodies in left axial rotation. Figure modified from Haberl et al., 2004.

vertebral body and the orientation varied depending on the lumbar level, implying a change in coupling patterns.

To fully evaluate the kinematic behaviour of a non-fusion system, the HAM becomes a key in determining the extent that the system restores normal intersegmental kinematics. In addition, it illustrates the entire three-dimensional motion pattern in a clear and concise manner.

1.6.4 Load Transfer

To thoroughly evaluate the efficacy of non-fusion systems which are intended to alter the load transfer mechanism through vertebrae, it becomes necessary to quantify the loads and load patterns through both the anterior column and posterior elements. This is a large area of investigation that has not been addressed in most previous studies of posterior dynamic stabilization systems.

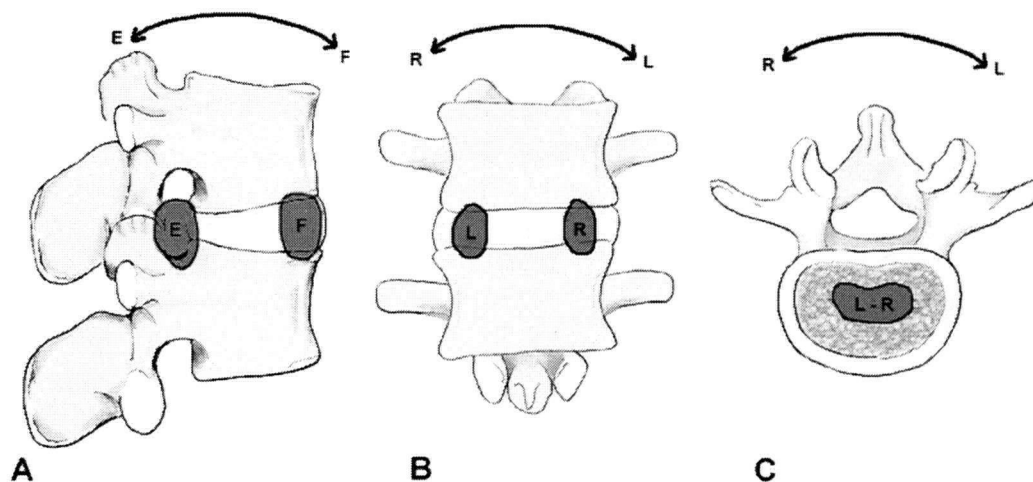


Figure 1.12: Approximate locations of the centre of rotation (COR), the 2-D analog of the 3-D HAM, in the intact lumbar spine. A) flexion-extension (F-E), B) lateral bending, and C) axial rotation. L and R indicate the location of the COR in left and right motions. Figure modified from White and Panjabi, 1990, and Panjabi et al., 1981.

Anterior Column Load

Anterior column loads have been measured for a considerable period of time. In 1959, Nachemson inserted needle pressure transducers into the intervertebral discs to measure the pressures within the cadaveric disc [83] (Figure 1.13). Knowing the surface area of the disc from radiographs and the intradiscal pressure, the total load on the disc could be calculated. This method is well established and is still essentially the same technique that is currently used to measure anterior column loads. It is widely accepted that the majority of a compressive load is transferred through the anterior column [139].

Although a more difficult task, *in vivo* measurements were first conducted by Nachemson and Morris [86] to gain an understanding of the normal loading in the anterior column. Larger pressures and loads were observed in the disc when the subject was sitting, as opposed to in standing or reclining positions. Loads on the discs were examined for different postures of the body [84]. The L3-L4 disc experienced a load of approximately twice body weight in a

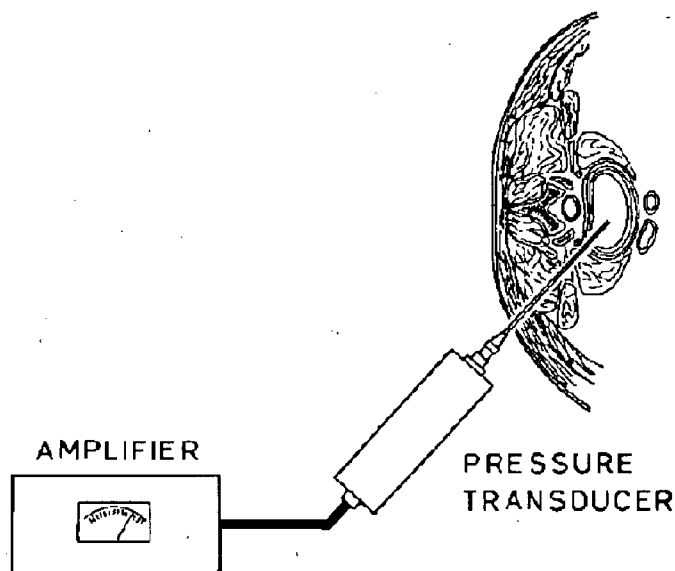


Figure 1.13: Schematic of the transducer and method used for measuring intradiscal pressure within the intervertebral disc. The transducer is inserted into the centre of the disc. Figure modified from Nachemson, 1966.

sitting position and up to four times body weight sitting in a 20° flexed position holding a 20 kg load with the arms. Stress profilometry was used to determine the pressure distributions within the intervertebral disc [6, 76, 77]. The stress distribution in a normal healthy disc under compression was very uniform and isotropic (Figure 1.14). Under eccentric loading, a non-degenerated disc exhibited a similar uniform stress distribution as that witnessed in pure compressive loading [53]. Thus, the stress distribution across the disc was always constant, and lateral bending or flexion simply increased the mean value of the compressive stress, whereas extension decreased it. In another study, the intradiscal pressure increased from that in a neutral position as flexion angle increased and also increased as extension angle increased. The intradiscal pressure magnitude was greater in flexion than in extension [76].

Knowledge of intradiscal pressure has been particularly useful in determining physiological loading conditions for in vitro biomechanical testing and for verifying the loading method that is utilized. In addition, for dynamic stabilization systems, intradiscal pressures provide an indication of the effect the device has on loading behaviour within the spine. The results can be compared to those from an intact specimen.

Facet Loads

The lumbar facet joints provide the other important path through which loads within the spine are transmitted. The facet joints play a critical role in both kinematic behaviour and load transfer through the spinal column. Laboratory tests have shown that the facet joints contribute to the stability of the spine and

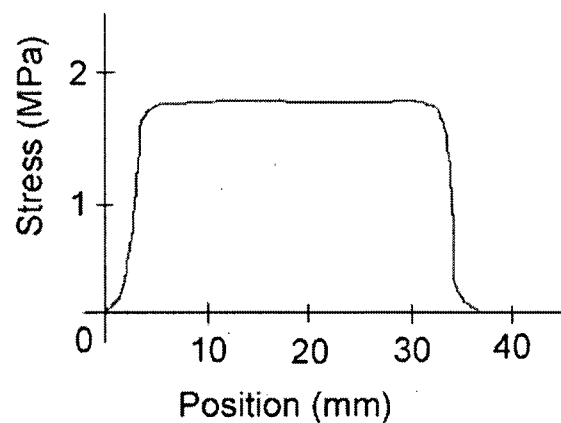


Figure 1.14: *Stress profile across a healthy intervertebral disc during axial compression. The difference between vertical and horizontal stresses was insignificant. Figure modified from McNally et al., 1996.*

that they may restrict motion between vertebrae, specifically in axial rotation, extension, and translation in the antero-posterior direction [152].

Facet loads have been measured in intact loaded cadaver specimens using both indirect and direct techniques. Indirect methods to estimate facet loads have included insertion of pressure transducers [3, 5, 83, 113] or intervertebral load cells [152] into the intervertebral disc to quantify anterior column load. The load in the facet joints was then inferred from the difference between the measured intradiscal load and the total applied axial compressive load. Facet loads have also been measured by placing strain gauges on the superior articular processes [12] (Figure 1.15). This technique was reported to be highly sensitive to the placement and orientation of the gauges [71]. In addition, calibration of the gauges is destructive because the motion segment must be disarticulated. Finite element modeling is another indirect method to study facet loads [26, 125, 126, 127, 129]. Models are typically verified with in vitro experiments and are then utilized to replicate numerous conditions, while rotation, displacement, strain, stress, contact area, forces, and other parameters can be recorded. Difficulties arise in replicating loading conditions and constraints, and modeling the material properties of different structures of the spinal column.

Direct measurement of facet loads using pressure sensitive film is invasive, in that the joint capsule must first be sectioned in order to accommodate insertion of the film. Fuji Prescale Film has been inserted into the joint space to statically measure facet loads in pure and eccentric compressive loading [28, 52, 68, 118]. This method is limited to measuring the peak force only and does not provide a dynamic loading profile.

Based upon previous studies, the magnitude of the facet loads was found to range between 3 and 25% of a total axial compressive load in a neutral position and was largely dependent on posture [58]. Facet loads increased in magnitude with disc space narrowing and as extension increased [68].

There is a lot of variability in results of facet load measurement in the literature. Questions still surround the contact mechanism that occurs within the facet joints. Some groups quantified

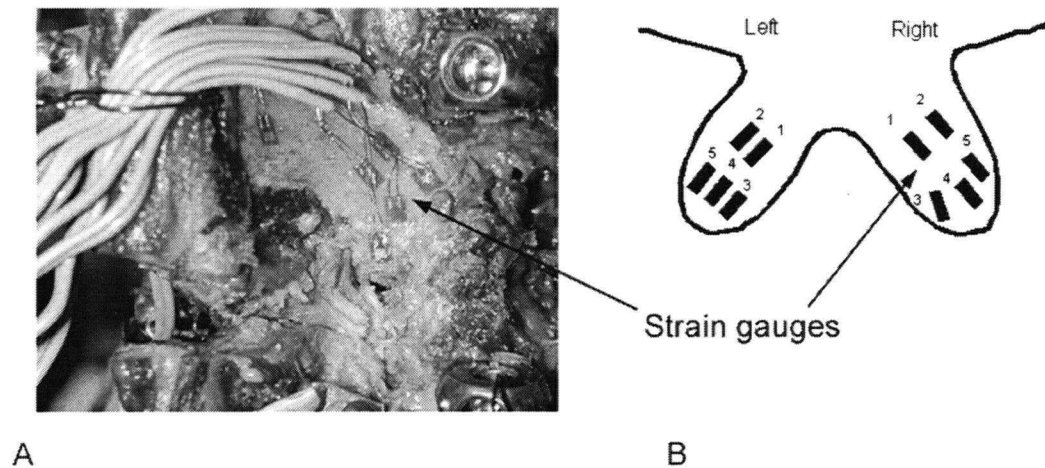


Figure 1.15: *Strain gauge method to determine facet loads. A) photograph showing strain gauge placement on the right L3 inferior facet surface. B) schematic illustrating bilateral strain gauge placement on inferior facet surfaces.*

contact area using Fuji film [68] and movement of the contact location under different loading directions was qualitatively examined in some studies as well [125, 128]. A sound understanding of the contact area patterns within the facet joints would provide a useful stepping stone towards fully understanding the contact mechanism in these joints.

Recently, the accuracy and repeatability of thin film electroresistive pressure sensors (I-scan, Tekscan Inc. South Boston, MA, USA) (Figure 1.16) have been assessed for measurement of contact pressure in the facet joints [146], in a similar fashion to previous work assessing the validity of measurements in the patellofemoral joint [145] and tibiofemoral joint [51]. These sensors measure force distribution dynamically over a grid of sensing elements. The accuracy for facet load measurement was $18\% \pm 9\%$, $35\% \pm 7\%$, and $50\% \pm 9\%$ for compressive forces of 100 N, 50 N, and 25 N, respectively [146]. In the knee, the accuracy and repeatability were found comparable to that of Fuji Prescale Film, but the Tekscan sensor is advantageous for its dynamic capabilities, electronic data acquisition, and ease of use.

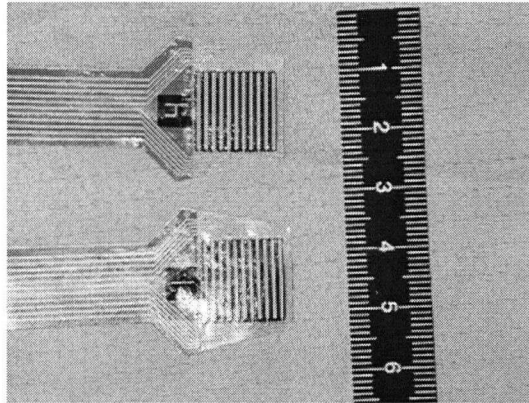


Figure 1.16: *Tekscan sensors for direct force measurement. Sensor is inserted within the joint between the two articulating surfaces.*

1.6.5 Results of Dynamic Stabilization Evaluations

Focusing on the Dynesys dynamic posterior stabilization system specifically, there are two biomechanical evaluations in the literature. Freudiger et al. applied a combination of loads to produce motion in the sagittal plane [33]. The average applied loads were large compared with other studies, with an average of 18.3 Nm moment, 2296 N compression, and 458 N anterior shear load in flexion and 12.5 Nm moment, 667 N compression, and 74 N posterior shear load in extension. The study found that the Dynesys system reduced rotations and horizontal translations, but increased vertical translations compared to the intact spine. In a more recent biomechanical evaluation of the Dynesys system, cadaveric specimens were loaded with pure moments of 10 Nm in flexion-extension, lateral bending, and axial rotation with no axial preload [120]. The Dynesys produced greater intersegmental motion than pedicle fixation in all three loading directions. In extension, ROM was similar to that of the intact spine, but in flexion the Dynesys created a similar stiffness to that of pedicle fixation. In lateral bending and axial rotation, the Dynesys allowed greater intersegmental motion than pedicle fixation, but in lateral bending was still much stiffer than the intact spine. The Dynesys and pedicle fixation both reduced the NZ in lateral bending and flexion to a level below that of the intact spine.

In general, both of these studies observed that the Dynesys system increased the stiffness of the specimen. However, the functional objectives of the Dynesys are to preserve intersegmental kinematics and reduce the loading at the facet joints. Implantation of a posterior device will affect not only the magnitude of rotations, but also the direction of rotation as given by the HAM. It also remains unclear how the Dynesys system affects the loading at the facet joints. Neither of the existing biomechanical studies addressed changes in the pattern of motion or facet joint contact loads.

Presumably, the length of the Dynesys spacer is an important parameter that directly influences both intersegmental motion and loading since it determines the segmental position. This includes disc height, facet joint position, and tension of the ligaments. The previous studies have not evaluated the effects of variation in spacer length.

1.7 Motivation

This study was motivated by a desire to understand the biomechanical behaviour of dynamic posterior stabilization. Primarily of interest was the Dynesys system due to its increasing clinical prevalence and lack of important biomechanical data. None of the previous studies have examined the effect of the Dynesys on the complete kinematic behaviour of the spine, including the HAM. There has also been no indication as to the effect that the Dynesys system has on load transfer through the spine, despite the fact that one objective of the device is to reduce the loading at the facet joints. These are all critical areas to explore in order to gain a more complete understanding of the biomechanical behaviour of the Dynesys system to determine its efficacy in the treatment of lumbar spinal instability.

The methodology behind this study will be useful in helping to determine an acceptable standardized protocol for testing of dynamic stabilization systems so that all critical aspects are evaluated and results of studies are comparable with one another.

Due to the high variability surrounding the facet joint contact loads, this study was also inspired by an avidity to evaluate the contact mechanism within the facet joints in an attempt to gain

a clearer picture as to the precise function of the facets. This is important for the evaluation of spinal implants and may eventually be useful clinically as an indicator or guide for treatments of chronic low back pain.

1.8 Objective

The primary objective of this study was to conduct a three-dimensional investigation of the Dynesys system to determine the effect of dynamic posterior stabilization on the biomechanical behaviour of the lumbar spine.

This was accomplished with the specific goals to:

- determine the effect on kinematic behaviour at the implanted level;
- determine the effect on load transfer through the implanted level;
- determine the effect of the length of the Dynesys spacer on the kinematic behaviour at the implanted level;
- determine the effect of the length of the Dynesys spacer on the load transfer through the implanted level; and
- explore the feasibility of a new technique to quantify the contact area in the facet joints of the lumbar spine.

1.9 Project Scope

This study focused on the biomechanical changes created by dynamic posterior stabilization of the lumbar spine. The project was limited to investigation with a single device, the Dynesys, at the L3-L4 level. The study incorporated testing of ten specimens under nine different conditions, including three Dynesys spacer lengths to evaluate the contribution of the length of the spacer on kinematic behaviour and load transfer through the implanted level.

Flexibility testing was conducted solely at one constant rate of load application. This neglects the viscoelastic behaviour of the spine and therefore was only an evaluation of the elastic spine.

A pure moment was applied and the custom spine testing machine allowed the specimen to move in an unconstrained three-dimensional fashion. The magnitude of the applied moment was ± 7.5 Nm and was applied in all three primary directions of loading (flexion-extension, lateral bending, and axial rotation). It was deemed an adequate load to generate motions of physiologic magnitude.

Testing was done with and without a compressive follower preload of 600 N. A follower preload was used to generate physiologic compressive loading in this *in vitro* spine study. Biomechanical testing with a follower preload is being performed more frequently, but only within the last decade. In this study, flexibility tests were conducted without a follower preload as well to provide a basis for comparison with some of the work that has been done by other groups and with historical data.

The focus of this study was limited to kinematic behaviour and load transfer solely at the segment of interest, and did not take into consideration effects at adjacent levels. The evaluation included intersegmental range of motion, neutral zone, translation, helical axis of motion, intradiscal pressures, and facet contact loads.

1.10 Contribution

This study was part of a large evaluation conducted in our lab and hence the involvement of other individuals in many aspects of the work must be acknowledged. The group consisted of myself, Qingan Zhu, and Derek Wilson, with myself acting as the project leader. In addition, the assistance of spine surgeon Dr. Ory Keynan is also recognized.

It is important to clarify what my exact role was in this project and to highlight our individual contributions. The three main investigators were all involved in the experimental design, establishment of the testing protocol, *in vitro* testing, and data acquisition. Qingan and myself prepared the specimens for testing.

Derek primarily was responsible for the Tekscan sensors, including their preparation, acquiring force measurements using the sensors, and processing of the facet loads. He also designed and

Chapter 1. Introduction

carried out a study to evaluate the validity of using Tekscan sensors to measure facet loads.

Qingan's main focus was on using strain gauges to measure facet loads (not included in this thesis). I assisted with the measurement, but Qingan was solely responsible for processing and analyzing the strain gauge data. He also was responsible for processing the HAM.

My role, specifically, in this project focused on processing and analysis of the ROM, NZ, translations, and intradiscal pressures. I conducted the analysis of the HAM and facet loads as determined using the Tekscan. All aspects of the facet joint imaging exploratory study, from the proposal, experimental design, construction of the loading device, specimen preparation, coordination of scans, and processing and analysis of the data were my responsibility.

Chapter 2

Methods

2.1 Specimen Selection

Ten fresh-frozen cadaveric lumbar spine specimens from L2–L5 were tested. The specimens were selected based upon lack of radiographic evidence of fractures to the spinal column or the presence of bony diseases. The age of the specimens ranged from 70 to 88 years, with a mean age of 77 years (Table 2.1). There were six males, three females, and one unknown gender.

The spines were prepared by dissecting the musculature while preserving the remaining soft tissue, most importantly the facet joint capsules. For fixation in the spine testing machine, the L2 and L5 vertebrae were embedded in dental stone mounts. Steel wires wrapped around the pedicles and screws that were partially inserted into the vertebral bodies of L2 and L5 were incorporated into the dental stone to obtain additional mechanical advantage. To standardize orientation of the specimens, the potting was done such that the L3–L4 disc space remained horizontal since that was the level of interest (Figure 2.1).

2.2 Test Protocol

Three-dimensional flexibility tests were conducted on each of the specimens under nine different conditions:

- i) Intact
- ii) Intact with Dynesys (standard spacer length)
- iii) Sectioned facet joint capsules

Table 2.1: Summary of Specimen Gender and Age

Specimen	Age	Gender
H1092	75	F
H1062	87	M
H1113	76	M
H1107	81	M
H1005	70	M
H1094	77	M
H1109	88	?
H1106	74	M
H1112	71	F
H1111	73	F
Average	77	

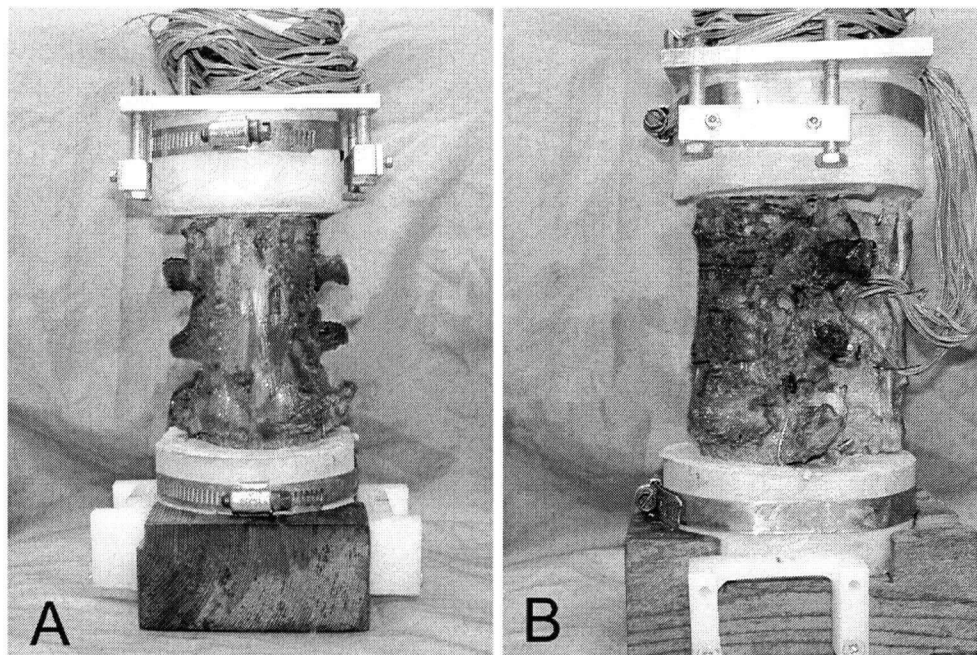


Figure 2.1: Fully prepared lumbar specimen dissected of musculature and potted in dental stone mounts. A) Anterior view. B) Lateral view.

- iv) Injury (nucleotomy and sectioned posterior ligaments)
- v) Injury with Dynesys (standard spacer length)
- vi) Injury with Dynesys (long spacer length)
- vii) Injury with Dynesys (short spacer length)
- viii) Injury with rigid fixation
- ix) Post test (implants removed)

The testing order of conditions v) through viii) was randomized using a Latin Squares randomization to eliminate variability due to test sequence.

2.2.1 Explanation of Test Conditions

The ten specimens were subjected to flexibility testing under the conditions highlighted at the beginning of Section 2.2. In the intact condition, all ligaments and intervertebral discs of the specimen remained unaltered. The standard length Dynesys system was then installed at L3-L4 of the intact specimen. Injury of the specimens was performed by a spine surgeon in two stages. The first stage involved sectioning of the facet joint capsules at L3-L4, which was required for insertion of thin film sensors into the facet joint. The second stage of the injury was a severe injury that was created to simulate instability in the specimen [32]. It involved sectioning of the posterior ligaments (supraspinous and interspinous), as well as cutting through the ligamentum flavum to perform a posterolateral nucleotomy with removal of as much nuclear material as possible (Figure 2.2). The injured specimen was stabilized with three Dynesys spacer lengths.

The Dynesys (Zimmer GmbH, Winterthur, Switzerland) was installed using the manufacturer's recommended operative procedure. Two sizes of pedicle screws were utilized, 6.0 x 45 mm and 6.4 x 50 mm, of which the appropriate size was determined by a spine surgeon. The pedicle screws were inserted into the L3 and L4 pedicles and cemented in place using polymethylmethacrylate (PMMA) to prevent loosening at the bone-screw interface. The PCU spacer was cut to a length that just fit between the pedicle screws as was determined by a spine surgeon

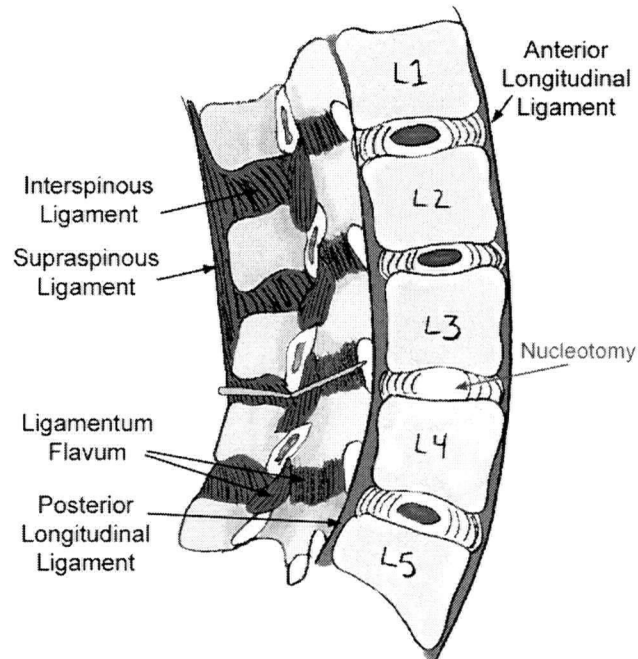


Figure 2.2: *Injury of spine ligaments. Sagittal section of the lumbar spine with laminectomy, showing the major ligaments. The injury involved sectioning of the facet joint capsules and sectioning of the interspinous and supraspinous ligaments, as well as the ligamentum flavum (sectioning represented by lines through ligament) and a posterolateral nucleotomy at L3-L4. Figure modified from Bogduk, 1997.*

so that a neutral position of the spine was maintained. The average standard spacer length was 25.9 ± 5.6 mm and 25.2 ± 5.3 mm for the left and right sides, respectively. Spacer lengths that were 2 mm longer and 2 mm shorter than this standard length were also investigated (Figure 2.3). The material properties of the spacer are temperature dependent. The spacers were therefore manufactured with a modified stiffness to eliminate material property differences that would occur because of testing in an environment other than that of body temperature. There was 300 N of preload applied to the tensioned cord during implantation. The order of implantation was alternated between the left and right sides.

The rigid fixation system was also supplied by Zimmer GmbH (Winterthur, Switzerland) and was a rigid rod and interconnect that was adapted for use with the Dynesys pedicle screws.

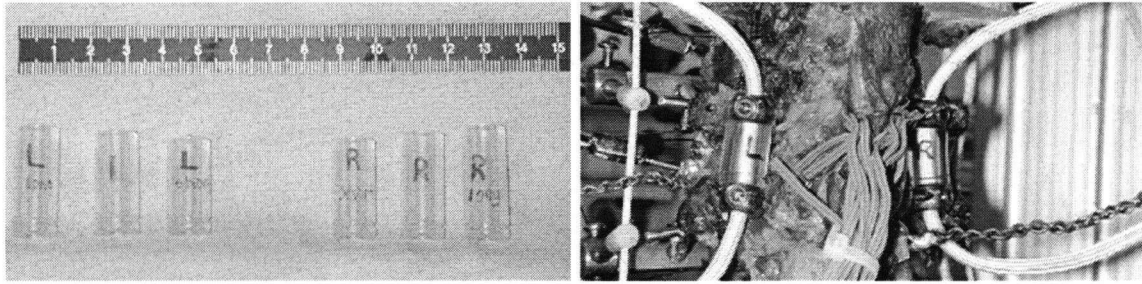


Figure 2.3: Three lengths of Dynesys polycarbonate urethane (PCU) spacers: short, standard, and long. Length differs by 2 mm between each case. Also shown on the right is the Dynesys system implanted at L3-L4, viewed posteriorly.

Transition pieces were fit to the Dynesys pedicle screws to place the rod in a more lateral position. Clinically, the placement of the rod should be more medial, but in this case, lateral placement was used so as not to interfere with the thin film sensors (Figure 2.4). This was expected to have a negligible effect on the stiffness of the construct.

A post test was performed as the very last test condition, in which all implants were removed. This situation was a replication of test condition iv, the injury, and as such was compared to ensure that the specimen did not experience significant degradation over the course of testing.

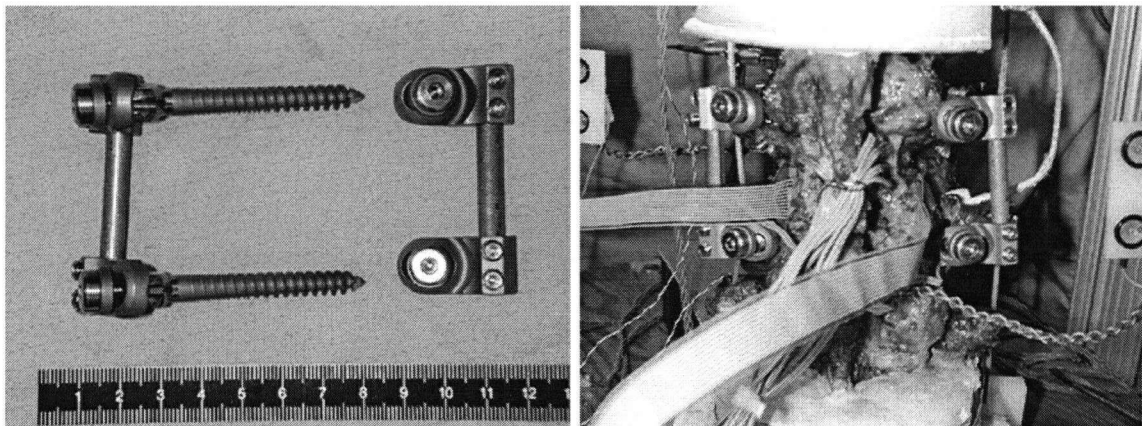


Figure 2.4: Rigid fixation system and as installed at L3-L4.

2.2.2 Spine Testing Machine

A custom spine testing machine was used to apply a continuous pure moment of ± 7.5 Nm to the top vertebra while the specimen was allowed to move in an unconstrained three-dimensional fashion [43]. The spine testing machine was built out of modular aluminum extrusions and was driven by a servo motor and planetary reduction gearbox, which was connected to an articulating arm (Figure 2.5). The arm applied the moment to the specimen and included two universal joints and a ball spline which allowed linear translation of the arm during application of the moment. A load cell was attached between the articulating arm and an aluminum fixture at the superior aspect of the specimen to measure the torque. The inferior vertebra was rigidly attached to the frame of the spine machine. The motor and articulating arm could be placed in three different positions to apply a moment about the three axes of motion: flexion-extension, lateral bending, and axial rotation. The weight of the articulating arm, fixture, and superior dental stone mount was balanced with a counterweight. A second counterweight was attached via a threaded rod in the aluminum fixture block to balance the static moment created by the weight of the arm.

The servo motor was controlled by a motion control card and LabVIEW programming (National Instruments, Austin, Texas, USA). Operation of the spine machine could be done either in a torque or angular controlled fashion. For this study, the spine machine was operated in torque control mode. The specimen was rotated at a rate of approximately $1.3^\circ/\text{second}$ to a maximum applied moment of ± 7.5 Nm in all three primary directions of loading, namely flexion-extension, lateral bending, and axial rotation. The load was applied for three completely reversed loading cycles. The first two cycles were merely conditioning the specimen and all measurements for analyses were based on the third load cycle, unless otherwise noted.

2.2.3 Follower Preload

All tests were conducted with and without the presence of a compressive follower preload of 600 N based on a method described by Patwardhan et al. [109]. (Figure 2.6). The magnitude of the follower preload was chosen as 600 N since this falls within the range of loads that the lumbar

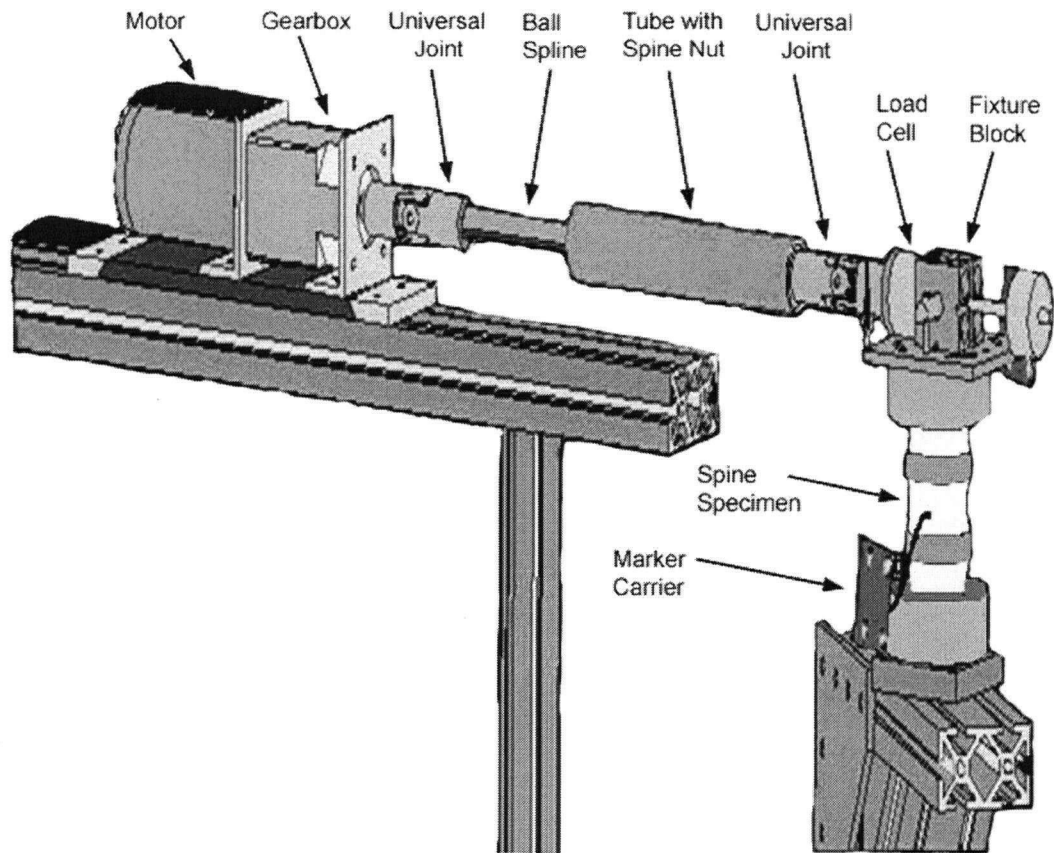


Figure 2.5: Schematic of the custom spine machine. A pure moment was applied to the top vertebra while the specimen was allowed to move in an unconstrained, three-dimensional fashion. Figure modified from Goertzen et al., 2004.

spine is subjected to, as was determined in vivo based on intervertebral disc pressures [84, 142]. It was shown that load on the spine segments varies depending upon posture, physical activity, and mass of the individual. A 70 kg subject, for instance, experienced a 250 N compressive force in the L3–L4 disc when lying supine and a force of nearly 2000 N when sitting in a slightly flexed position [84]. These values are fairly consistent in the literature [142].

Custom stainless steel frames were attached non-invasively to each of the L3 and L4 vertebral bodies. The follower load frames were attached bilaterally at the pedicles and supported by the anterior aspect of the body (Figure 2.7). The path of the follower preload was optimized

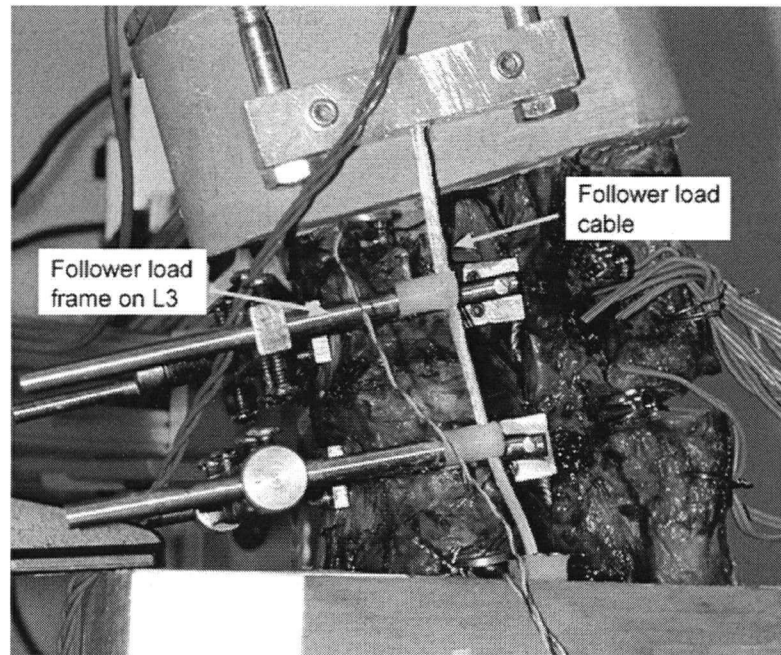


Figure 2.6: *Follower load path. Looking laterally from the left at specimen under a flexion moment.*

in the neutral position to minimize rotation in the mid-sagittal plane upon application of the preload. The follower preload should be applied at the centre of rotation of each segment [109]. The path of the applied compressive load was fine-tuned by adjusting the components of the frames to alter the anterior-posterior position of the cable at each level. The follower load was applied from beneath the specimen using a 1 kN servohydraulic linear actuator (A591-5, Instron, Canton, MA, USA) (Figure 2.8). The load was applied using three pre-conditioning cycles at 0.1 Hz with a magnitude of 80% (480 N) of the maximum load while the specimen was in a neutral position to minimize the viscoelastic effects of the specimen. Immediately following the pre-conditioning cycles, 100% (600 N) of the compressive load was applied at a rate of 193 N/s and held through the duration of the flexibility test. After the flexibility test was completed, the compressive load was released (Figure 2.9).

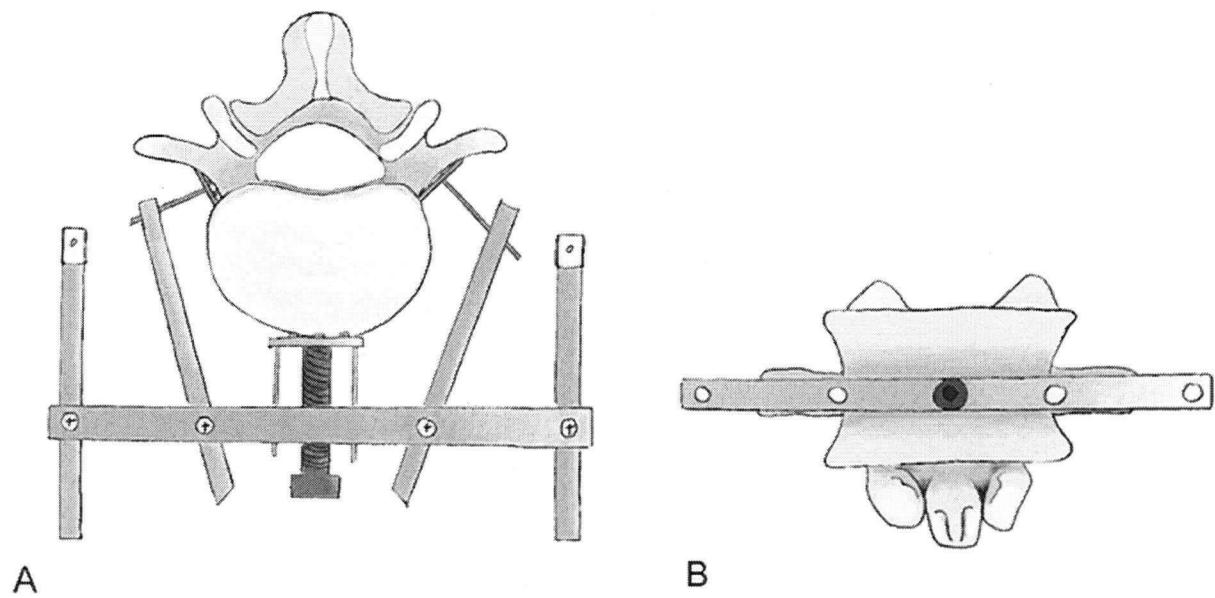


Figure 2.7: *Stainless steel follower load frame on vertebra. Viewed A) superiorly and B) anteriorly.*

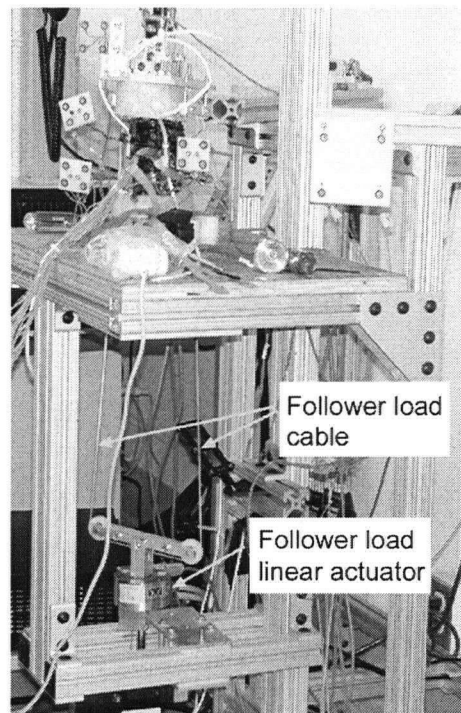


Figure 2.8: *Application of compressive follower preload. A servo-hydraulic linear actuator was used to apply the load from below the specimen.*

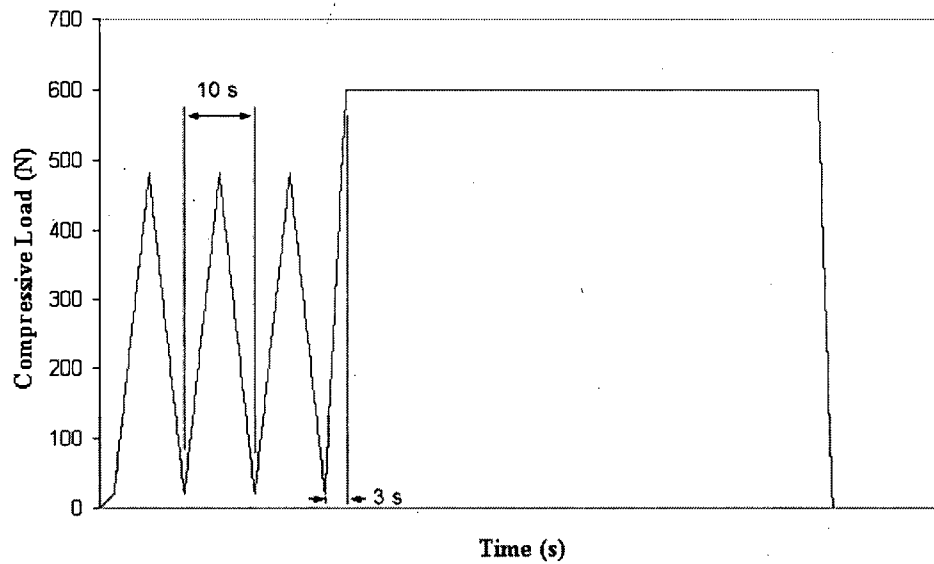


Figure 2.9: *Follower load profile. Compressive preload vs. time curve for application of follower preload. The load was applied using three preconditioning cycles at 80% of the load, ramped up to 100% of the load, held for the duration of the flexibility test, and then ramped down.*

2.3 Data Acquisition

During flexibility tests, a wide variety of information was recorded. The data collected can be separated into three general categories:

1. Intervertebral kinematics
2. Facet joint forces
3. Intradiscal pressures

2.3.1 Intervertebral Kinematics

The position of each vertebra was monitored by rigidly attaching four non-collinear infrared light emitting diodes (LED) to each vertebra. An optoelectronic camera system (Optotrak 3020, Northern Digital, Waterloo, Ontario, Canada) was used to measure the three-dimensional coordinates of the markers (Figure 2.10). The frequency of data collection was 20 Hz and

the optoelectronic camera system measures three-dimensional position of each LED to within 0.10 mm in plane and 0.15 mm out of plane. To determine the position of a body in three-dimensional space, the coordinates of at least three non-collinear points on that body are required [136]. As described previously, the movement between two rigid bodies with six degrees of freedom can be fully described by three rotations and three translations or by a unique axis of motion about which the body rotates and parallel to which it translates. In either case, a transformation matrix, consisting of a rotation and translation component, representing the motion between two vertebrae is required and will be described in detail in Section 2.4. The accuracy of the rotational measurement was within 0.1° [50].

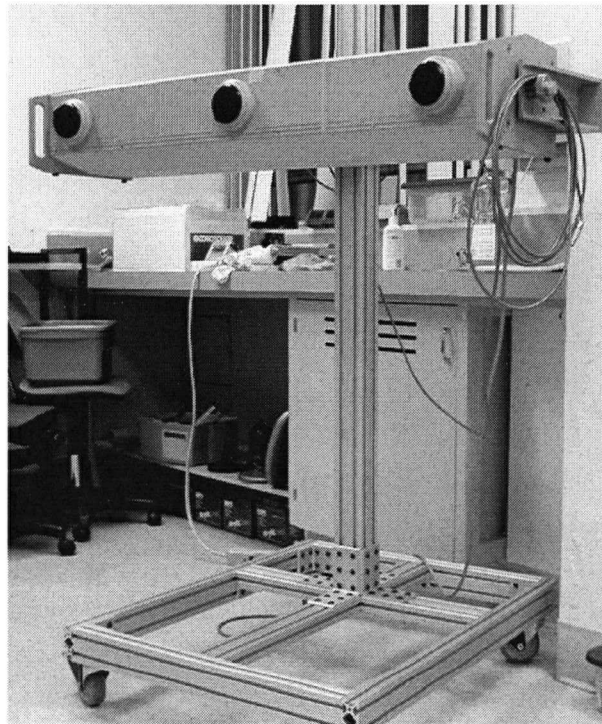


Figure 2.10: *Optoelectronic camera system (Optotrak 3020, Northern Digital, Waterloo, Ontario, Canada) used to measure the three-dimensional position of the markers.*

Six points were digitized for each vertebral body for anatomical reference and for use in the kinematic analysis (Figure 2.11). These points were at the

1. anterior aspect of the vertebral body just superior to the junction between the body and

- the follower load frame,
2. left follower load eyelet,
 3. left pedicle-superior vertebral body junction,
 4. tip of the spinous process,
 5. right pedicle-superior vertebral body junction, and
 6. right follower load eyelet.

2.3.2 Facet Joint Forces

Facet loads were measured directly using thin film electroresistive sensors (Tekscan 6900 Quad sensor) and I-Scan software (Tekscan Inc., South Boston, MA, USA). The sensors are thin flexible printed circuits with 121 individual sensing elements that are located in rows and columns. The sensor behaves like a variable resistor in an electrical circuit, with a high resistance when unloaded [135]. The output voltage is converted to a digital value between 0 and 255.

The sensors were an invasive method of dynamic facet load measurement, and as such, were inserted within the sectioned facet joint capsule. Forces within the facet joints were measured

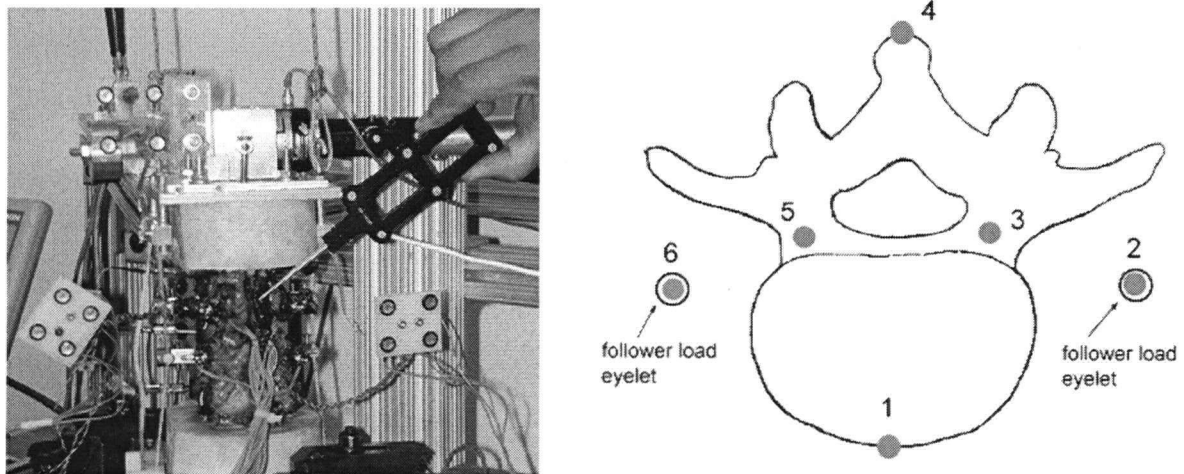


Figure 2.11: *Digitization of points.* A calibrated probe (as shown on the left) was used to digitize six points for each vertebral body as shown in the superior view on the right.

and recorded for all remaining test conditions succeeding capsule sectioning (test conditions iii through ix). The frequency of data collection was 5 Hz. The sensor consisted of four independent fingers each with a sensing matrix size of 14 mm \times 14 mm and a maximum range of 7.6 MPa (Figure 2.12). One finger of the sensor was inserted into each of the left and right facet joints (Figure 2.13). To reduce shear forces experienced by the sensor, the sensor was coated with surgical lubricant prior to insertion and was not rigidly attached to the facet surface. The sensors were supported externally by wires to reduce the likelihood of extrusion from the joint during flexibility tests.

Conditioning and calibration of the sensors followed manufacturer recommendations and method-

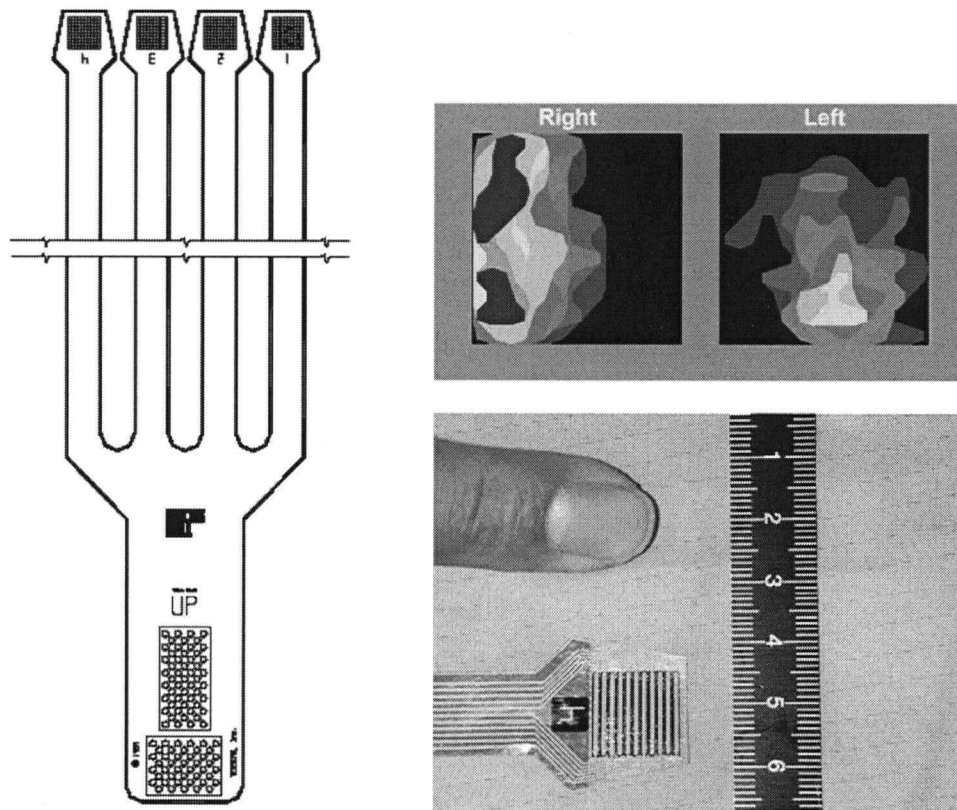


Figure 2.12: Tekscan 6900 Quad thin film electroresistive sensor. Sensor consists of four independent sensing fingers, of which one finger was inserted into each of the left and right facet joints. Also shown is a sample of Tekscan force maps that were generated.

ology presented in previous studies [51, 145, 146]. The expected maximum load, based on previous work in our lab using strain gauges, was predicted to be approximately 100 N. The sensors were conditioned prior to initial use by uniformly loading the sensor between two layers of 3.2 mm thick lubricated rubber covering machined aluminum plates in a materials testing machine (Instron DynaMight 8841, Canton, MA, USA) (Figure 2.14).

The sensor was placed between lubricated rubber surfaces to better approximate the material-sensor interface that would be found within the facet joints due to the articular cartilage. The surface compliance of mating surfaces does affect the sensor response [135]. A notch was etched on the aluminum piece to seat a ceramic ball through which the load was transmitted. The sensors were loaded to 120% of the expected maximum load (120 N) for five loading cycles. The load was ramped up over five seconds, held for five seconds, and ramped down for five seconds with a one minute relaxation time between cycles.

The sensors were calibrated linearly using a similar loading protocol as in the conditioning phase by loading each sensor to 80% of the expected maximum load (80 N). The I-scan software performed a linear interpolation between zero and the known calibration load. The load was applied so that all sensing elements were loaded, while avoiding saturation of the elements. The sensors were calibrated after each test condition and a new sensor was used for each specimen to minimize the effect of sensor deterioration.

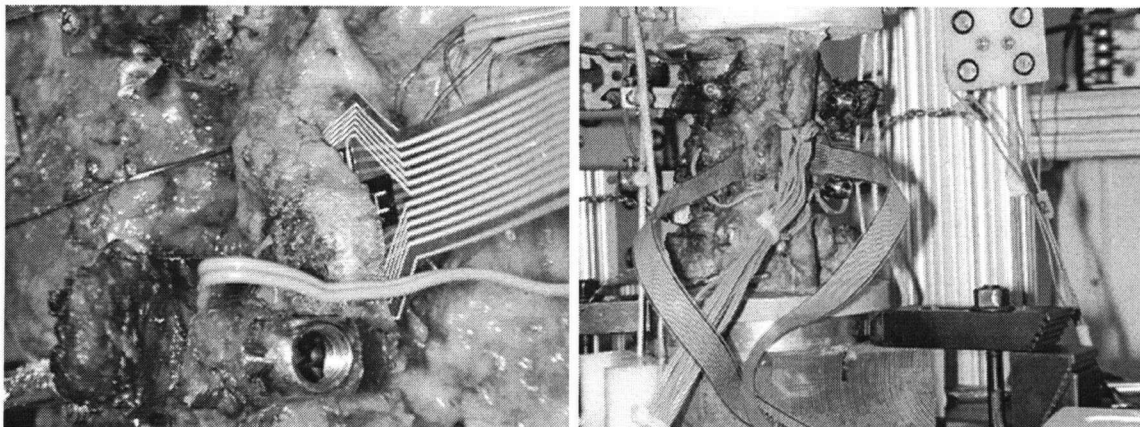


Figure 2.13: *Tekscan sensors inserted in the left and right facet joints of L3-L4.*

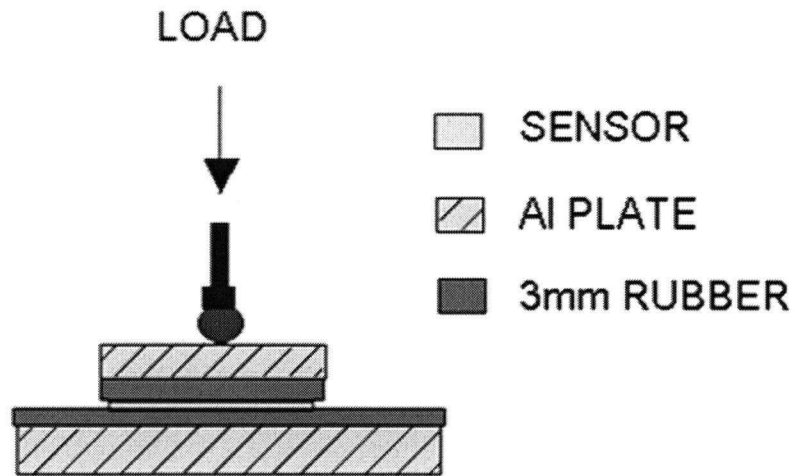


Figure 2.14: Configuration for conditioning and calibration of Tekscan sensors. Figure modified from Wilson et al., 2004.

Forces in the facet joints during the implantation procedure of the Dynesys were also recorded to learn how the device distributes the preload (resulting from implantation) across the two sides of the specimen.

2.3.3 Intradiscal Pressures

Intradiscal pressures were monitored at the three intervertebral levels as an indication of anterior column loading. Custom needle pressure transducers with implanted strain gauges (2.1 mm diameter) were inserted into the centre of each disc (Robert A. Denton Inc., Rochester Hills, MI, USA) (Figure 2.15). The sensitive part of the transducer was oriented superiorly and the transducer was calibrated for pressure measurements. Anterior-posterior (AP) and lateral x-rays were taken of the specimen to ensure correct placement of the pressure transducers (Figure 2.16). The pressure transducer in the L3–L4 disc space was only present for the first three tests (test conditions i through iii) and was removed for the fourth case and subsequent test conditions since a nucleotomy was performed as part of the injury.

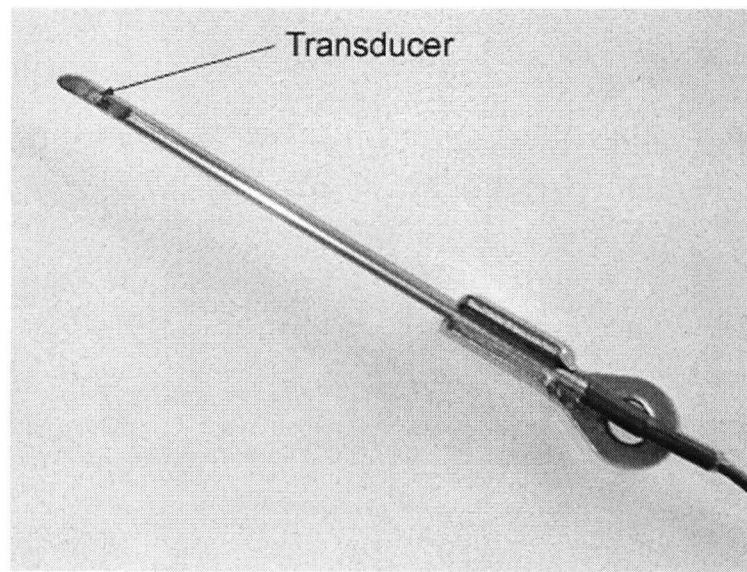


Figure 2.15: *Intradiscal custom needle pressure transducer.*

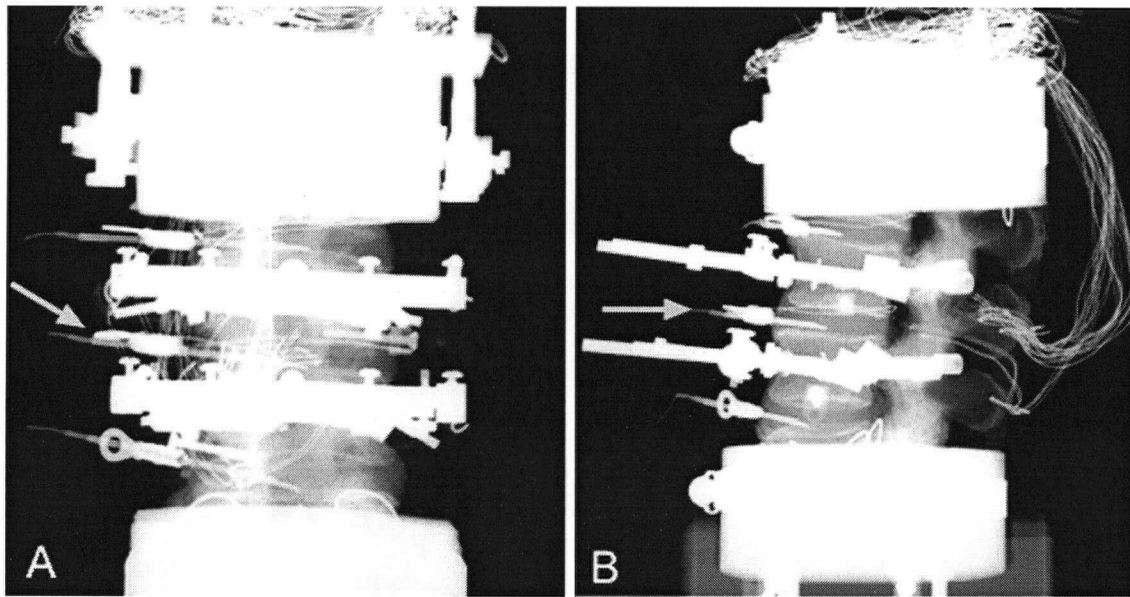


Figure 2.16: *Radiographs depicting placement of intradiscal custom needle pressure transducers. A) anterior-posterior and B) lateral directions. Arrows highlight pressure transducers at L3-L4.*

2.4 Kinematic Analysis

2.4.1 Intersegmental Motion

The first step in determining intersegmental motion between two vertebrae based on three-dimensional position data was to define a global coordinate system. This was essentially pre-defined within the internal parameters of the optoelectronic camera system. All raw positions of the markers were acquired in the global coordinate system. Local coordinate systems were created for each vertebra as follows. A marker carrier with four LEDs on the base of the spine machine defined a general specimen coordinate system. Initially, a local xy -plane was established such that it aligned with the coronal plane of the general specimen coordinate system. This was a right-handed, Cartesian coordinate system with its origin located at the anterior aspect of the vertebral body, based on digitization. Local coordinate systems for all four vertebral bodies had their x -axes pointing laterally to the right sides of the specimen, y -axes directed superiorly, and z -axes pointing posteriorly (Figure 2.17). The orientation of all four local coordinate systems was identical, the only difference being the location of the origin.

2.4.2 Calculation of Transformation Matrix

The intersegmental rotations and translations were derived using a routine previously developed in LabVIEW (Kin2000) based on an algorithm by Veldpaus et al. [136]. The procedure uses the initial and final coordinates of four markers, weighted equally, to estimate the translation vector and rotation matrix that characterizes the motion between two rigid bodies using a least squares method. The best approximations of the rotation matrix, R , and translation vector, t , are the matrix H and vector r that minimize the least squares function $f(r, H)$ defined as

$$f(r, H) = \frac{1}{m} \sum_{i=1}^m \left[(\mathbf{p}_i - \mathbf{a} - \mathbf{r} - H(\mathbf{a}_i - \mathbf{a}))^T (\mathbf{p}_i - \mathbf{a} - \mathbf{r} - H(\mathbf{a}_i - \mathbf{a})) \right] \quad (2.1)$$

where m is the number of markers (four in this study), \mathbf{a}_i and \mathbf{p}_i indicate the initial and final position of marker i , and \mathbf{a} and \mathbf{p} are vectors for the centres of the marker distribution in the

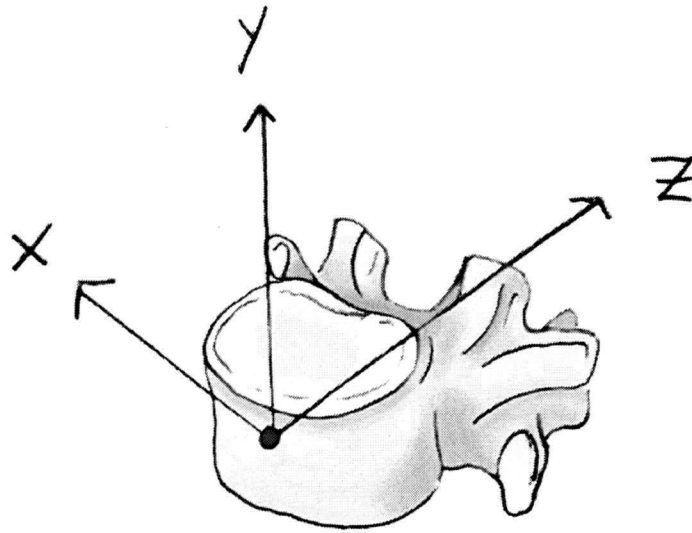


Figure 2.17: Local (anatomic) coordinate system created for each of the four vertebrae. The origin of the coordinate system was located on the anterior aspect of the vertebral body, as identified during digitization. Figure modified from White and Panjabi, 1990.

initial and final positions (Figure 2.18), respectively, and are given by

$$\mathbf{x} = \frac{1}{m} \sum_{i=1}^m \mathbf{x}_i \quad (2.2)$$

The vector $\mathbf{p}_i - \mathbf{a} - \mathbf{r} - H(\mathbf{a}_i - \mathbf{a})$ represents the difference between the measured and fitted vectors of \mathbf{p}_i at the final position.

The rotation matrix, R , is determined using polar decomposition [16] to decompose a matrix, G , given by

$$G = \frac{1}{m} \sum_{i=1}^m [(\mathbf{p}_i - \mathbf{p})(\mathbf{a}_i - \mathbf{a})^T] \quad (2.3)$$

The polar decomposition method states that a 3×3 matrix, G , can be written as the product of a 3×3 rotation matrix, R , and a symmetrical 3×3 matrix, B , as

$$G = RB \quad (2.4)$$

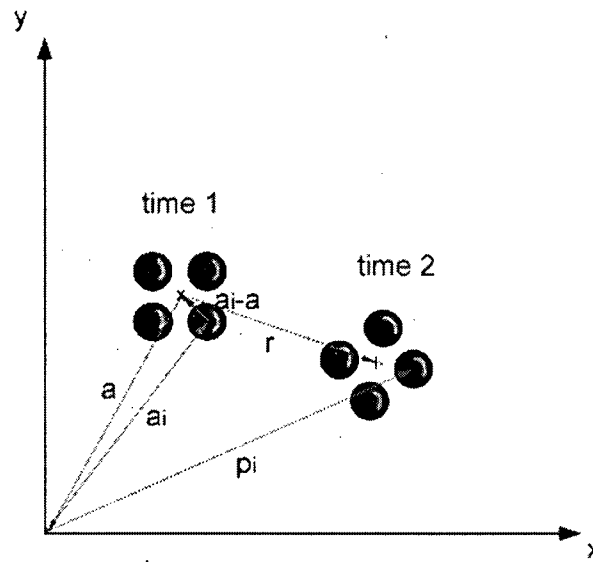


Figure 2.18: Illustration of vectors used for marker transformation between initial and final marker distributions.

In addition, the rotation matrix is used to calculate the translation, t , of the centre of the marker distribution. A transformation matrix (4×4) can then be constructed that describes the motion of a single marker carrier between two points in time in the global coordinate system.

$$T_{C, M1} = \begin{bmatrix} R_{3 \times 3} & t_{3 \times 1} \\ 0 & 1 \end{bmatrix} \quad (2.5)$$

where the subscripts on T represent the transformation matrix of the marker distribution for body 1 in the camera (global) reference frame.

The goal is to describe motion between two bodies over time. Computation of intersegmental motion requires construction of an additional transformation matrix by multiplying individual matrices of bodies 1 and 2 (Equation 2.5) together.

$$T_{M1, M2} = T_{M1, C} \cdot T_{C, M2} \quad (2.6)$$

Information that is more useful is the intersegmental motion between two bodies in anatomical

(local) coordinate frames

$$T_{A1_A2} = T_{A1_M1} \cdot T_{M1_M2} \cdot T_{M2_A2} \quad (2.7)$$

where $A1$ and $A2$ are the anatomical coordinate systems of body 1 and body 2.

To produce Equation 2.7, the individual transformations between the marker distribution and anatomical coordinate system of each body are necessary. This arises from the digitized points and marker coordinates taken from a static (or initial) position.

$$T_{M1_A1} \text{ and } T_{M2_A2}$$

Since the marker coordinates are measured in the camera (global) system, these transformations are equivalent to

$$T_{C_A1} \text{ and } T_{C_A2}$$

The rotation portion of the transformation matrices T_{C_n} , where n is $A1$ or $A2$, is produced using three orthonormal vectors that define the coordinate system (Equation 2.8). The translation vector is the vector defining the origin of the local coordinate system. In this study, the local coordinate system was defined as described in Section 2.4.1.

$$T_{C_A1} = \begin{bmatrix} x_{3 \times 1} & y_{3 \times 1} & z_{3 \times 1} & t_{3 \times 1} \\ 0 & 0 & 0 & 1 \end{bmatrix} \quad (2.8)$$

2.4.3 Intervertebral Rotation

The rotation component of the transformation matrix, as calculated using Equation 2.7, provides a redundant description of frame orientation. It is characterized by nine elements that are not independent, but related by six constraints because of the orthogonality [122]. It is sufficient to describe the orientation of a rigid body in space using three independent parameters, which are termed Euler angles. The order of the sequence of the three rotations is significant, as is working in a fixed or current frame. In a current frame, each subsequent rotation in the sequence is about the previously manipulated axis, whereas in a fixed frame representation,

the succeeding rotations are about the original, non-moving, axes. If the axis of the third rotation is not the same as the axis of the first rotation, the angles are usually termed Cardan or Bryant angles, but in literature the term Euler angles tends to include these as well [148]. In determining kinematic behaviour of the spine, it has been widely accepted to rotate around the x -axis, followed by the y -axis, and finally about the z -axis in a fixed frame [101]. The rotation matrix can be written as

$$R_{xyz} = \begin{bmatrix} \cos y \cos z & \sin x \sin y \cos z - \cos x \sin z & \cos x \sin y \cos z + \sin x \sin z \\ \cos y \sin z & \sin x \sin y \sin z + \cos x \cos z & \cos x \sin y \sin z - \sin x \cos z \\ -\sin y & \sin x \cos y & \cos x \cos y \end{bmatrix} \quad (2.9)$$

The Euler angles are then solved by

$$\begin{aligned} \sin y &= -R_{31} \\ \sin x &= R_{32} / \cos y \\ \sin z &= R_{21} / \cos y \end{aligned} \quad (2.10)$$

The Euler angles were used to determine parameters that quantitatively describe the kinematic behaviour of the specimens, including range of motion and neutral zone. The same rotation matrix was also utilized to calculate the helical axis of motion.

2.4.4 Translation

The origins of the anatomical coordinate systems were located at the anterior points on the vertebral bodies (Figure 2.17). The translation vectors, as extracted from the fourth column of the transformation matrices for L3-L4, described the distance separating the origins of the anatomical coordinate systems of L3 and L4 (Equation 2.7). The x , y , z , and total separation distances between the anterior points of L3 and L4 were determined at the applied moment that corresponded to the calculated neutral point of the third loading cycle for the short, standard, and long spacers. Theoretically, the initial separation distance created by implantation of one set of spacers should be the same for the three different loading directions and two preload conditions. Therefore, a single value for each of the x , y , z , and total separation distances was produced for each specimen by averaging those results for the six loading combinations. This

separation distance was used as an indication of the degree of compression or distraction of the anterior annulus that was created by each of the different Dynesys spacer lengths in the neutral position.

2.4.5 Range of Motion (ROM) and Neutral Zone (NZ)

Intersegmental range of motion (ROM) and neutral zone (NZ) between L3 and L4 were calculated about the primary axis of motion, neglecting coupled motion, based on the extracted Euler angles. For flexion-extension, this resulted in rotations about the local (anatomic) x -axis, about the z -axis in lateral bending, and about the y -axis in axial rotation.

First, the NZ and neutral position (NP) were determined. The NZ was calculated by searching within a ± 0.2 Nm range for the largest difference between the loading and unloading curves. This is the point where laxity in the specimen was the greatest. The rotation difference between the two curves represented twice the NZ, with the NP being the rotation at the midpoint of this difference. The ROM was calculated separately for both directions of rotation. The positive ROM was the difference between the maximum rotation and the NP and the negative ROM was the difference between the NP and the minimum rotation. Hence, the NP was the distinction between the positive and negative ROM.

The ROM was normalized based on the intact ROM. In lateral bending and axial rotation the ROM was reported for one side only, as an average of the right and left ROM; since motion is fairly symmetrical in these two loading directions (an average difference of 24% between right and left lateral bending) [104, 110, 151].

2.4.6 Helical Axis of Motion (HAM)

The helical axes of motion (HAM) were derived using a routine developed in LabVIEW (Zhu and Cripton, 2004) based on an algorithm by Kinzel et al. [60, 101, 131], of which an overview is presented in the following subsections. The HAM was calculated for the third loading cycle over the full range of motion, from maximum to minimum rotation, as well as from the unloaded state to maximum rotation, and from the unloaded state to minimum rotation. The position

of the HAM was reported as a penetration point with a specified plane and its orientation by two angles.

After processing the HAM, the local coordinate system was altered slightly from that used to generate the rotations and translations of the preceding kinematic analysis to a system that was more specific and useful for describing the HAM. The origin was translated superiorly from the point on the anterior aspect of the vertebral body, as determined previously, by shifting the point superiorly to the level of the pedicle-vertebral body junction (based on the average of digitized points three and five). The local coordinate system was then rotated in the sagittal plane so that the z -axis was in plane with the superior endplate of L4 (based on radiograph). The penetration point of the HAM, therefore, was with the yz -plane for flexion-extension, the xy -plane for lateral bending, and the xz -plane for axial rotation (Figure 2.19). The slight adjustment of the local coordinate system for the HAM analysis allowed for a consistent comparison of the HAM between specimens. The location of the HAM was normalized by expressing it as a percentage of the height, width, and anterior-posterior diameter of the L4 vertebral body.

A description of intersegmental motion can be broken down into the orientation of the HAM, the rotation about the HAM, the translation along the HAM, and the location of the HAM. Each one of these quantities will be described separately. The emphasis is on the orientation and location of the HAM since that was reported in this study.

Orientation of the HAM

The rotation of a point in space can be expressed as

$$\mathbf{u}_2 = R\mathbf{u}_1 \quad (2.11)$$

where \mathbf{u}_1 and \mathbf{u}_2 represent the coordinates before and after a pure rotation about an axis, and R is the rotation of the body.

If one considers a vector \mathbf{n} of magnitude unity that points along the positive direction of the

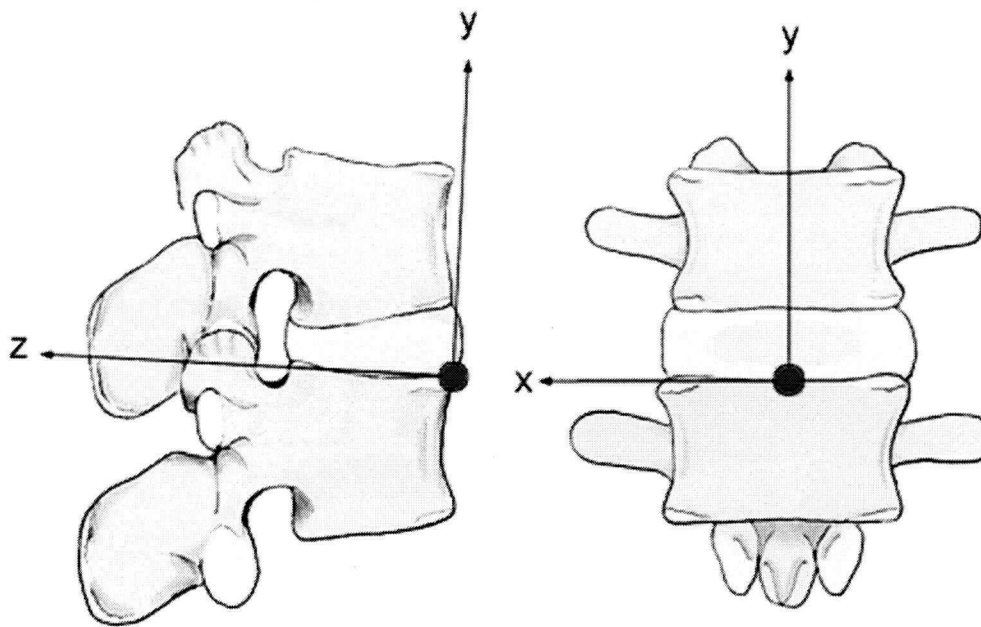


Figure 2.19: *HAM coordinate system and penetration planes. In flexion, the penetration point was in the yz -plane, the xy -plane in lateral bending, and the xz -plane in axial rotation. Figure derived from Bogduk, 1997.*

HAM, then the same relationship as that in Equation 2.11 above can be written

$$\mathbf{n}_2 = R\mathbf{n}_1 \quad (2.12)$$

but since the unit vector lies along the HAM, \mathbf{n} will remain unchanged after rotation about the HAM.

$$\mathbf{n} = R\mathbf{n} \quad (2.13)$$

Equation 2.13 can be rewritten as the eigenvalue problem

$$(R - I)\mathbf{n} = \mathbf{0} \quad (2.14)$$

where I is the identity matrix and $\mathbf{0}$ is the null vector. This can be expanded as

$$\begin{bmatrix} R_{11} - 1 & R_{12} & R_{13} \\ R_{21} & R_{22} - 1 & R_{23} \\ R_{31} & R_{32} & R_{33} - 1 \end{bmatrix} \begin{bmatrix} n_x \\ n_y \\ n_z \end{bmatrix} = \begin{bmatrix} 0 \\ 0 \\ 0 \end{bmatrix} \quad (2.15)$$

The vector \mathbf{n} cannot be solved for directly, but direction cosines of the HAM can be found from Equation 2.15

$$\begin{aligned} (R_{11} - 1)n_x + R_{12}n_y + R_{13}n_z &= 0 \\ R_{21}n_x + (R_{22} - 1)n_y + R_{23}n_z &= 0 \end{aligned} \quad (2.16)$$

incorporating the fact that \mathbf{n} is a unit vector and therefore,

$$n_x^2 + n_y^2 + n_z^2 = 1 \quad (2.17)$$

Solving for the direction cosines completely defines the orientation of the HAM.

Rotation About the HAM

The rotation angle is found once the direction cosines are known, using the rotation matrix for pure rotation about an axis, R , as given in the previous section by Equation 2.9. This matrix can also be expressed as a function of the direction cosines and rotation angle as [60]

$$Q = \begin{bmatrix} n_x^2 \text{vers} \phi + \cos \phi & n_x n_y \text{vers} \phi - n_z \sin \phi & n_x n_z \text{vers} \phi + n_y \sin \phi \\ n_x n_y \text{vers} \phi + n_z \sin \phi & n_y^2 \text{vers} \phi + \cos \phi & n_y n_z \text{vers} \phi - n_x \sin \phi \\ n_x n_z \text{vers} \phi - n_y \sin \phi & n_y n_z \text{vers} \phi + n_x \sin \phi & n_z^2 \text{vers} \phi + \cos \phi \end{bmatrix} \quad (2.18)$$

where ϕ is the rotation angle of a point on the body about the HAM and

$$\text{vers} \phi = 1 - \cos \phi$$

Equating elements of the two matrices, R and Q , one can solve for the rotation angle, ϕ .

Translation Along the HAM

The translation of the body along the HAM is calculated by assuming P is a point that lies on both the body and the HAM. As the body moves from position 1 to 2, the point P will

translate only along the HAM by an amount k . If the vector \mathbf{p} represents the location of P , then the displacement of point P can be expressed as

$$\mathbf{p}'_2 - \mathbf{p}'_1 = k\mathbf{n}' \quad (2.19)$$

where \mathbf{n}' is the augmented unit vector along the HAM and \mathbf{p}' indicates the augmented vector \mathbf{p} . The magnitude of k can be determined along with the location of the HAM and is described in the following section.

2.4.7 Location of the HAM

The simplest way to represent the location of the HAM is by specifying the intersection of the HAM with the three orthogonal planes through the origin [60, 101]. To do this, Equation 2.19 is solved to obtain both the translation along the HAM and the location of the HAM. Continuing from the previous section, \mathbf{p}'_2 can be expressed by transforming \mathbf{p}'_1 using the transformation matrix derived in Equation 2.7. This generates

$$[T_{A1, A2} - I]\mathbf{p}'_1 = k\mathbf{n}' \quad (2.20)$$

Rearranging Equation 2.20, the matrix equation can be written as

$$\begin{bmatrix} R_{11} - 1 & R_{12} & R_{13} \\ R_{21} & R_{22} - 1 & R_{23} \\ R_{31} & R_{32} & R_{33} - 1 \end{bmatrix} \begin{bmatrix} p_x \\ p_y \\ p_z \end{bmatrix} = \begin{bmatrix} kn_x - t_x \\ kn_y - t_y \\ kn_z - t_z \end{bmatrix} \quad (2.21)$$

where t_x , t_y , and t_z are the components of the translation vector from the transformation matrix.

Knowing that the translation along the HAM, k , will be the same for every point on the rigid body and by setting one of p_x , p_y , or p_z to be zero, one can solve Equation 2.21 for k and for the coordinates of intersection between the HAM and either the xy , yz , or xz planes.

2.5 Facet Load Analysis

The Tekscan sensors were used to dynamically record the loading within the facet joints during flexibility testing. I-Scan software converted the output resistance of each sensing element into

a measurement of force based on the linear calibration. A force matrix was recorded for the two sensors, based on the forces measured by each of the 121 elements.

The maximum force measured by each of the two sensors was plotted against time. The general loading profile within each facet joint was qualitatively examined for the different test conditions, taking note of any interesting and important characteristics, including force magnitude, direction of loading and unloading in the facet joints, shape of the curves, and intersection between the right and left force measurements.

Quantitative analysis was performed using the peak force from each sensor, selected from the maximum force versus time data. This was the peak force over the entire loading cycle, not specifically from the third loading cycle, as was done in the kinematic analysis. In some cases, the cyclic motion tended to cause extrusion of the sensor from the joint and therefore the force in the third cycle was not always the highest force recorded (this was most common in flexion-extension).

2.6 Intradiscal Pressure Analysis

The intradiscal pressures were compared for the L3-L4 intervertebral disc for the intact condition and with the Dynesys system implanted in the intact specimen, before destabilization (intact with Dynesys). These were the only two conditions analyzed in detail because the pressure transducer from L3-L4 was removed prior to the nucleotomy. The scope of this study did not include the effect of the Dynesys system on loading at adjacent levels, so the intradiscal pressures at levels other than L3-L4 were disregarded. The analysis included only flexibility tests with the follower preload present. Without a follower preload, the intradiscal pressure was small and not representative of physiologic loading.

Both the pattern of the intradiscal pressure as a function of applied moment as well as the intradiscal pressure magnitude at the neutral position and the maximum and minimum applied moments were evaluated. The absolute and relative magnitudes were each studied. The pattern provided a qualitative assessment of the overall effect of the Dynesys system on anterior column

loading, whereas looking at the magnitude of the pressure enabled quantitative comparison between the two specimen conditions.

2.7 Facet Joint Imaging

A stand-alone exploratory study was conducted to evaluate the feasibility of using imaging to further investigate the loading at the facet joints. This was a three-dimensional analysis of the lumbar spine using magnetic resonance imaging (MRI) and if successful, would be a valuable technique to gain a more comprehensive understanding of the changes in mechanisms and magnitude of contact within the facet joints that occur under loading. Contact area, although not directly related, can provide an indication of loads and stresses in the joint. In this case, facet loads resulting from motion in the sagittal plane were examined. There was an attempt to measure degeneration in posterior spinal structures using MRI almost two decades ago [46]. That study determined that MRI was useful in assessing degeneration of the posterior elements, but cartilage thickness could not be measured accurately. MRI has not previously been used to quantify contact area within the facet joints of the lumbar spine.

MRI has, however, been fairly widely used to calculate contact area in the knee [11, 19, 106, 107, 117, 149]. It has been found to provide accurate measurements of cartilage topography, thickness, contact areas, and surface curvatures of the knee [19], as well as comparable contact areas to pressure sensitive film [11].

Compared to the facet joints, the knee (patellofemoral and tibiofemoral) joints are of a greater size, the cartilage is thicker (2.0 mm thick on average, up to a maximum of 5.3 mm [31] as opposed to 1.5 – 1.9 mm thick in the facet joints [25]), and the articulating surfaces are less conforming. All of these factors make it more difficult to transfer this technique to the facet joints and obtain accurate measurements of contact area.

In the spine, the benefits of a method of this nature include complete three-dimensional representation of the contact within the facet joint and information depicting the changes in contact area that result from normal motion. There is much variation in the results of previous studies

measuring both facet load magnitude and contact area in vitro or via mathematical modeling. Hence, an alternative method would be advantageous. In addition, the potential use for a completely non-invasive technique to study loading patterns within the facet joints is vast. MRI is already popular for assessing the degree of degeneration of intervertebral discs [111]. It could be employed as a tool to analyze or track the progression of degeneration within the facet joints. A thorough understanding of the normal load transfer through the posterior elements could also be extremely useful in the advancement and development of joint arthroplasty.

2.7.1 Specimen Preparation

A human cadaveric lumbar spine segment (L1-L2) was prepared as in Section 2.1. Non-metallic cable ties were used in place of wires and screws to enhance the mechanical fixation of the specimen in the dental stone mounts. Care was taken in selection of the specimen for this component of the testing. A specimen that was young was chosen (male, 41 years of age) because elderly specimens often display degeneration of the facet joint cartilage. Since this was a pilot study to investigate the contact mechanism, as well as to evaluate the feasibility of a new technique for measurement of contact area in the facet joints, the healthiest cartilage attainable was desired. Caution was used to remove as little soft tissue as possible because the MR signal depends on the signal from the protons, which in the body, is largely derived from water molecules.

2.7.2 Loading Apparatus

A custom loading device was designed and constructed to apply a flexion and extension moment of approximately 7.5 Nm to the superior vertebra of the segment (Figure 2.20). The loading was simply a static load that was held in place for the short duration of the test. The required load was applied to the specimen and then the displacement of the loading jig remained fixed throughout the test. The jig was fabricated of materials compatible for use in MRI. The loading device consisted of two parallel high density polyethylene (HDPE) plates and a support base. Short threaded nylon rods were attached to the two ends of each of the plates and connected using a polyethylene fiber cable. Tightening the rods using nylon nuts reduced the distance

separating the two ends of the plates, thus applying a moment (and some inherent compressive forces) to the specimen (Figure 2.21).

A six-axis load cell (MC3-6-1000, AMTI, Newton, MA, USA) was utilized to “calibrate” the loading jig for the specimen, since the load cell could not be used in the MR suite. Prior to MR imaging, the specimen was loaded to ± 7.5 Nm in the sagittal plane while the distance of separation between the plates was measured at each end. The six-axis load cell was then removed from the apparatus and the required separation distance adjusted to account for the height of the load cell. The repeatability of this technique was investigated by loading the specimen to the pre-determined plate separation while recording the applied load using the six-axis load cell. This procedure was repeated ten times, with the same individual applying the load, while blind to the load measurements. The repeatability of the load application in flexion

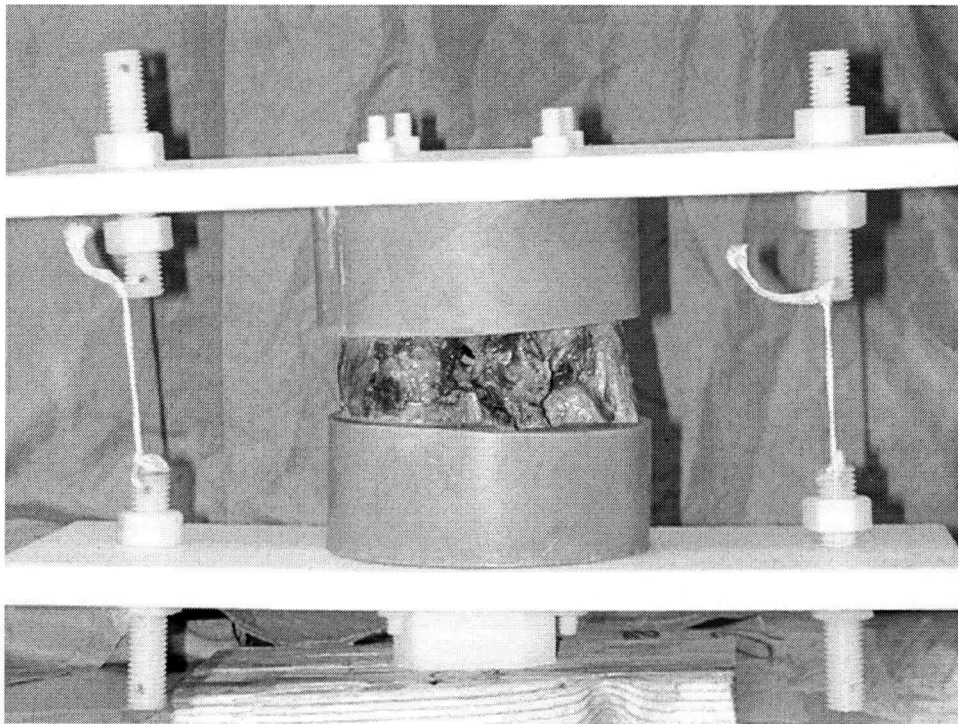


Figure 2.20: *Specimen in loading jig. The specimen is loaded with an eccentric compressive force by reducing the distance between the two plates at the anterior end to produce flexion. Viewing specimen laterally from the left side.*

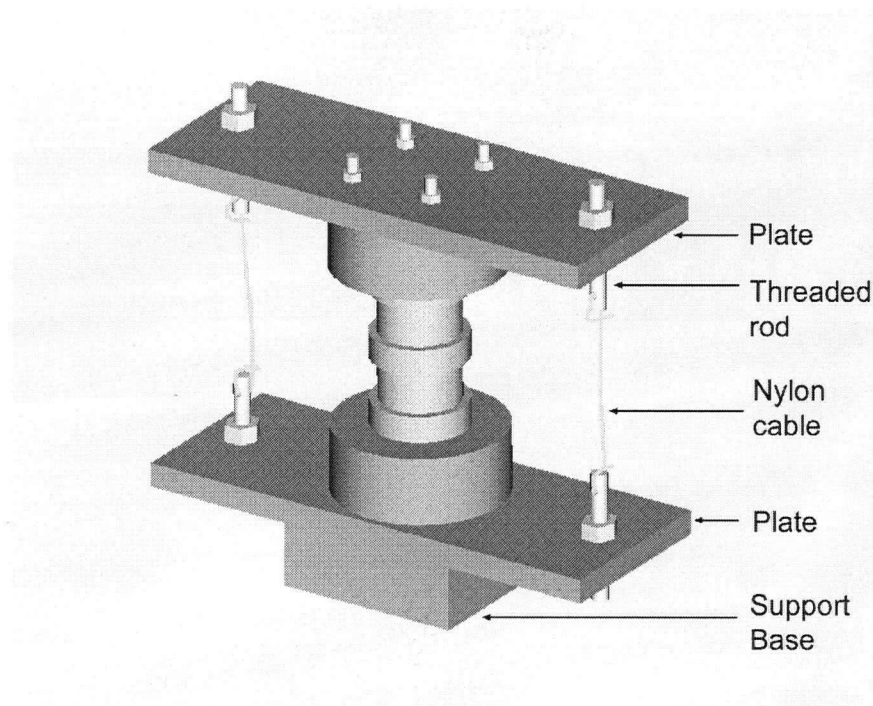


Figure 2.21: MRI Facet joint loading jig

was 2%, expressed as the standard deviation as a percentage of the mean, and was regarded as acceptable for this study.

Due to the viscoelastic nature of the spine, some relaxation of the specimen occurred. In an attempt to minimize the relaxation, three conditioning cycles were performed immediately prior to testing by loading the specimen to 100% of the load for a 30 second duration before being released. There was a 30 second relaxation time between the three preconditioning cycles. In addition, the MR scans were done on a static specimen and it was expected that the non-linear relaxation behaviour would equilibrate so that changes in load were minimal during the actual scan. This was the same procedure used in both the flexion and extension loading conditions.

2.7.3 Test Conditions

The testing was performed on the specimen in an intact condition only because of the exploratory nature of this study. The first step was to investigate if differences in contact area

between flexion and extension loading could be identified.

2.7.4 Imaging

Images were acquired in a 3 T MR scanner (Philips Gyroscan Intera, Philips Medical Systems, Bothell, WA, USA) in a neutral position, and with the specimen in flexion and extension. The specimen was loaded and the position was held constant as an MR image was generated.

The specimen was oriented with the anterior aspect entering the bore first and the L1 vertebral body located superiorly. Receiver coils (Synergy FLEX-M, Philips Medical Systems, Bothell, WA, USA) were placed on the top plate of the loading jig and against the lateral (right) aspect of the specimen. Slices were acquired in the transverse plane of the specimen since the articulating surfaces are typically perpendicular to this plane [10].

The MRI sequence used was a 3-D spoiled gradient echo sequence (T1FFE) and was one that was optimized for cartilage visualization. This was a sequence that was established for high resolution cartilage enhanced scanning in the knee (TR = 19.0 ms, TE = 6.5 ms, flip angle = 15°) (modified from Glaser et al. [39]). The in-plane resolution was 0.31 mm × 0.31 mm with a slice thickness of 1.5 mm (512 × 512 matrix with a 160 mm field of view). Forty slices were acquired over a scan time of 16:22 minutes. The number of signal acquisitions (NSA) was 2. Images were stored in DICOM format.

2.7.5 Analysis

Images were transferred to a workstation and analysis was conducted using Analyze software (Version 5.0, Mayo Foundation, Rochester, MN, USA). Contact was measured at the left and right facet joints (covered 10 – 12 slices) in flexion, extension, and in a unloaded position, using two different methods. In both cases, the process was carried out 4 – 5 times for each facet to evaluate the repeatability and to generate an average measurement based on a series of trials.

In the first method, the cartilage was segmented from the bone using a semi-automated trace on each transverse image without distinguishing between the two layers of articular cartilage (Figure 2.22A). The area on each slice was calculated, using the software, based upon the

number of pixels within the identified region. As an initial approximation, the volume of the joint space was determined by multiplying each area by the slice thickness. This method was based on the underlying assumption that loading of the facet joint would cause compression of the cartilage, thus altering the volume in the joint.

The second method measured contact area by creating B-splines on each transverse image along the line of contact (Figure 2.22B). Contact was defined as the inability to differentiate between the borders of the two cartilage layers. The length of the line in each slice was calculated and multiplied by slice thickness to generate contact area.

The magnitude of contact (as depicted by both joint volume and contact area) was averaged over the trials and compared for the three loading conditions, within each of the two methods of quantification.

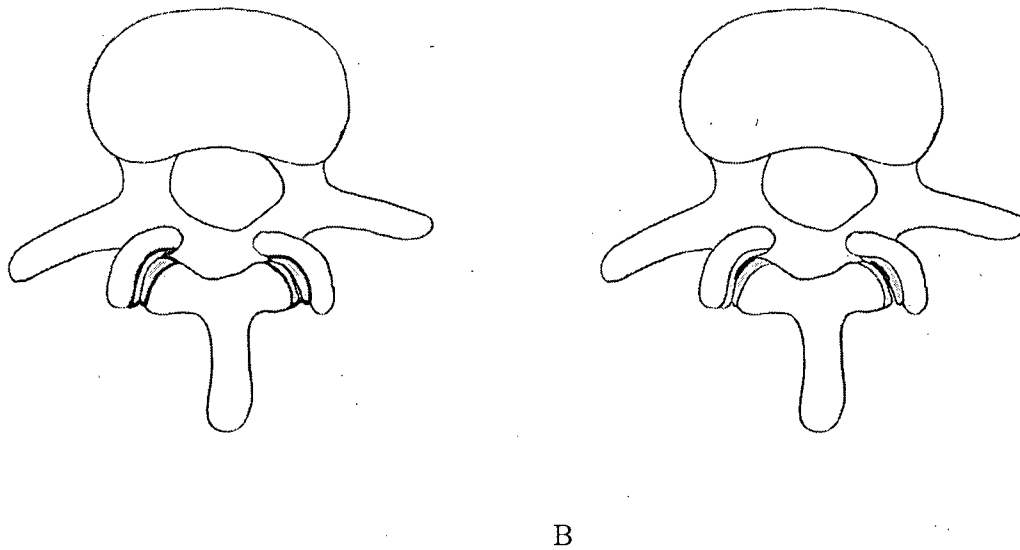


Figure 2.22: Schematic of facet contact measurement techniques. A) Measurement of joint volume using a semi-automated trace to segment the cartilage from the bone. B) Measurement of contact area using a B-spline along the line of contact between the two facet surfaces. In both cases, the measurement in each slice was multiplied by slice thickness to produce the respective joint volume or area measurements.

2.7.6 Validation

The contact measurements determined using the latter method were compared to contact areas recorded with Tekscan sensors (Tekscan 6900 Quad Sensor, Tekscan Inc., South Boston, MA, USA). The sensors were conditioned using the method described previously (Section 2.3.2). After MR imaging was completed, the articular capsules were sectioned and one finger of the sensor was placed within the right and left facet joints (Figure 2.23). The same loading scenarios as those used for the MR imaging were recreated in the laboratory. The contact area was measured at 5 Hz and the maximum area recorded under loading was used for the comparison.

2.8 Statistical Analysis

The biomechanical evaluation of the Dynesys system involved a series of flexibility tests on each specimen under multiple conditions. The effect of the specimen condition on kinematic

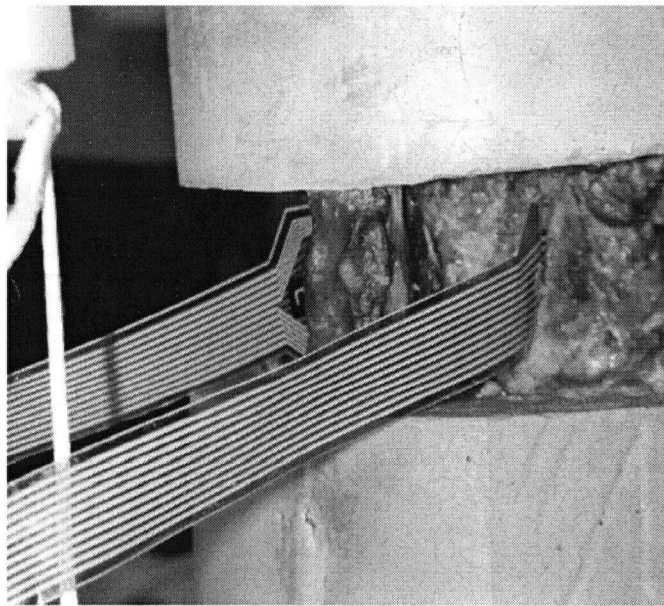


Figure 2.23: *Tekscan validation of contact area measured using MRI. Viewing specimen from the right postero-lateral aspect. One finger of the sensor was inserted into each of the right and left facet joints.*

behaviour or facet loads was measured repeatedly in the same specimens. For this reason, the individual variability between subjects must be taken into account. To analyze differences within each subject due to the specimen condition, a repeated measures multivariate analysis of variance (MANOVA) was used. In all cases, a 95% level of significance was assumed. When statistically significant differences were found for the main effect, Student-Newman-Keuls (SNK) post-hoc analyses were performed to investigate the specific differences between conditions.

All statistical analyses were performed using a commercial software package (Statistica Release 5.5, StatSoft Inc., Tulsa, OK, USA). The design of the statistical tests varied slightly between parameters and is defined in the following sections.

2.8.1 Kinematic Behaviour

The effect of the Dynesys system and specimen condition on kinematic behaviour was determined using a one-way repeated measures MANOVA. Two sets of statistical tests were performed. The first analysis looked at the effect of specimen condition (Intact, Intact with Dynesys, Capsule, Injury, Dynesys, and Rigid) on the kinematics. The comparisons that were primarily of interest were between the Intact and Intact-Dynesys, between the Intact and Capsule, Intact and Injury, Intact and Dynesys (standard), Intact and Rigid, Injury and Dynesys, Injury and Rigid, Injury and Post, and Dynesys and Rigid. The second analysis focused on the differences between the three spacer lengths (Dynesys short, Dynesys standard, and Dynesys long), but the results were first normalized to those seen in the intact condition.

For the ROM, an analysis was done in flexion, extension, lateral bending, and axial rotation. The NZ was analyzed in flexion-extension, lateral bending, and axial rotation. Each of the two coordinates describing the position of the HAM and the two angles describing the orientation were analyzed individually for flexion-extension, lateral bending, and axial rotation. All kinematic comparisons were repeated with and without a follower preload.

2.8.2 Facet Loads

Statistical differences in peak facet load were determined using a two-way repeated measures MANOVA. Again, this was done using two separate analyses; the first looking at the effect of specimen condition on facet loads and the second looking at the effect of spacer length on facet loads. The first factor was specimen condition ({Intact, Intact with Dynesys, Capsule, Injury, Dynesys standard, Rigid}{Dynesys short, Dynesys standard, Dynesys long}) and the second factor was side (left, right). The analysis was done in flexion, extension, lateral bending, and axial rotation and was repeated with and without a follower preload. The interaction between factors was also investigated when significant using SNK post-hoc analysis.

2.8.3 Intradiscal Pressures

The intradiscal pressures were compared for only two cases and thus, a one-way repeated measures ANOVA (identical to a paired t-test since only two variables) analysis was employed. Differences in intradiscal pressure were quantitatively evaluated by first comparing the magnitudes at the neutral position. To compare the increase or decrease in pressure under an applied load, the relative magnitudes of the pressures (pressure minus pressure at neutral position) were analyzed. This provided an indication of the change in pressure resulting from the applied load and whether the change was significantly greater in one condition or the other. To assess the differences in the absolute magnitude, the analysis was repeated using absolute values. While some of the difference in absolute magnitude may be evident by the difference in neutral position, changes in the shape of the pressure-moment curve are not necessarily obvious using simply a comparison of the relative magnitudes. The combination of the two led to a quantitative analysis of the overall difference (magnitude and pattern) in intradiscal pressures between the two cases.

Chapter 3

Results

3.1 Kinematic Behaviour

3.1.1 Effect of Specimen Condition

Range of Motion (ROM)

The intact specimens displayed an average intersegmental ROM at L3–L4 of 3.7° in flexion, 3.3° in extension, 3.8° in lateral bending (one side), and 2.1° in axial rotation (one side) without a follower preload. Application of the follower preload caused an increase in ROM in flexion to 4.4° and a decrease in all other directions; 2.4°, 2.4°, and 1.2° in extension, lateral bending, and axial rotation, respectively (Tables 3.1 and 3.2). A summary of the kinematic results for each specimen and the details of the statistical analysis are included in Appendices A and B, respectively.

The motion vs. applied moment curves for a typical specimen are shown in Figures 3.1 to 3.3. The condition of the specimen caused large significant differences in all loading directions, with and without a follower preload. Typically, the order from the least to most flexible was Intact–Dynesys, Rigid, Dynesys Standard, Intact, Capsule, Injury, and Post. The stiffness of the segment with the Dynesys and with rigid fixation was similar, with one sometimes more stiff than the other. The injury and post conditions in lateral bending with the follower preload were exceptions to this generalization.

Post-hoc analysis revealed that there were no significant differences in ROM between the intact and capsule conditions in any of the loading directions, with or without a follower preload

Table 3.1: Absolute average range of motion without follower load. Values (in degrees) are the average and standard deviation for ten specimens. Lateral bending and axial rotation ROM are reported as an average of one side only.

Without Follower Load				
Condition	Flexion	Extension	Lateral Bending	Axial Rotation
Intact	3.7 ± 1.5	3.3 ± 1.5	3.8 ± 1.4	2.1 ± 0.9
Intact-Dynesys	0.3 ± 0.2	0.3 ± 0.4	0.7 ± 0.3	1.0 ± 0.7
Capsule	4.3 ± 1.7	3.5 ± 0.9	4.1 ± 1.5	2.3 ± 1.1
Injury	6.1 ± 1.4	4.4 ± 1.2	5.0 ± 1.8	2.8 ± 1.2
Dynesys Standard	1.0 ± 0.6	1.1 ± 0.7	1.0 ± 0.5	1.6 ± 1.0
Rigid	1.0 ± 0.4	1.3 ± 0.9	0.9 ± 0.6	0.9 ± 0.7
Post	6.5 ± 2.2	5.0 ± 1.6	5.4 ± 1.8	2.7 ± 0.9

Table 3.2: Absolute average range of motion with follower load. Values (in degrees) are the average and standard deviation for ten specimens. Lateral bending and axial rotation ROM are reported as an average of one side only.

With Follower Load				
Condition	Flexion	Extension	Lateral Bending	Axial Rotation
Intact	4.4 ± 2.0	2.4 ± 0.9	2.4 ± 1.2	1.2 ± 0.5
Intact-Dynesys	0.4 ± 0.3	0.3 ± 0.2	0.6 ± 0.2	0.7 ± 0.4
Capsule	5.0 ± 2.1	2.3 ± 0.8	2.4 ± 1.3	1.2 ± 0.6
Injury	5.8 ± 2.5	2.7 ± 1.7	1.4 ± 0.9	1.3 ± 0.6
Dynesys Standard	0.5 ± 0.3	0.5 ± 0.3	0.5 ± 0.2	1.0 ± 0.5
Rigid	0.5 ± 0.3	0.5 ± 0.3	0.5 ± 0.2	0.7 ± 0.5
Post	6.4 ± 2.6	2.4 ± 1.1	1.8 ± 1.5	1.2 ± 0.5

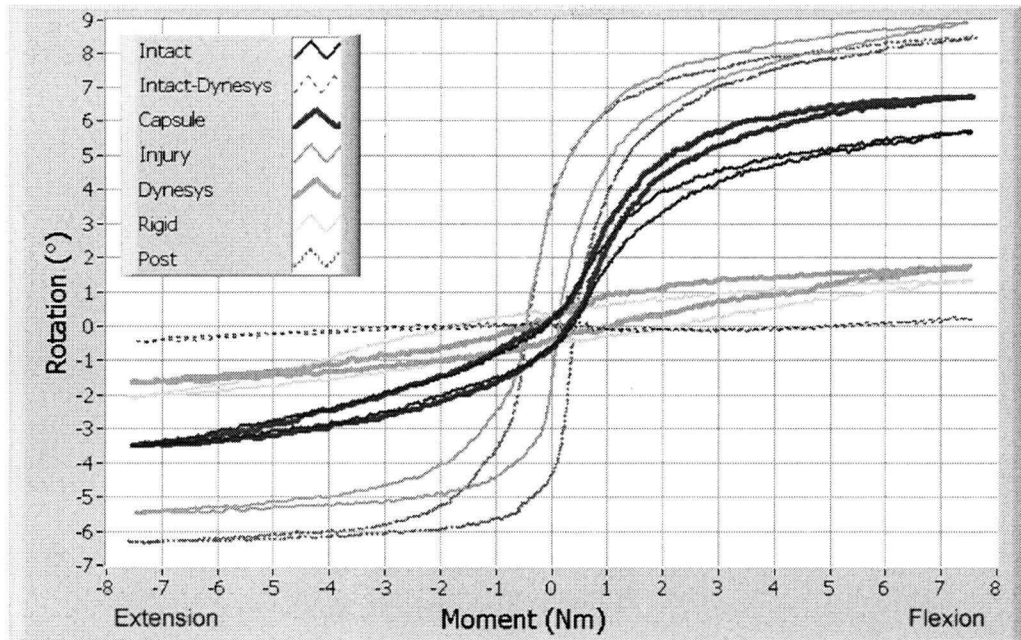


Figure 3.1: Motion vs. applied moment of a typical specimen in flexion-extension. Shown for seven specimen conditions without a follower preload.

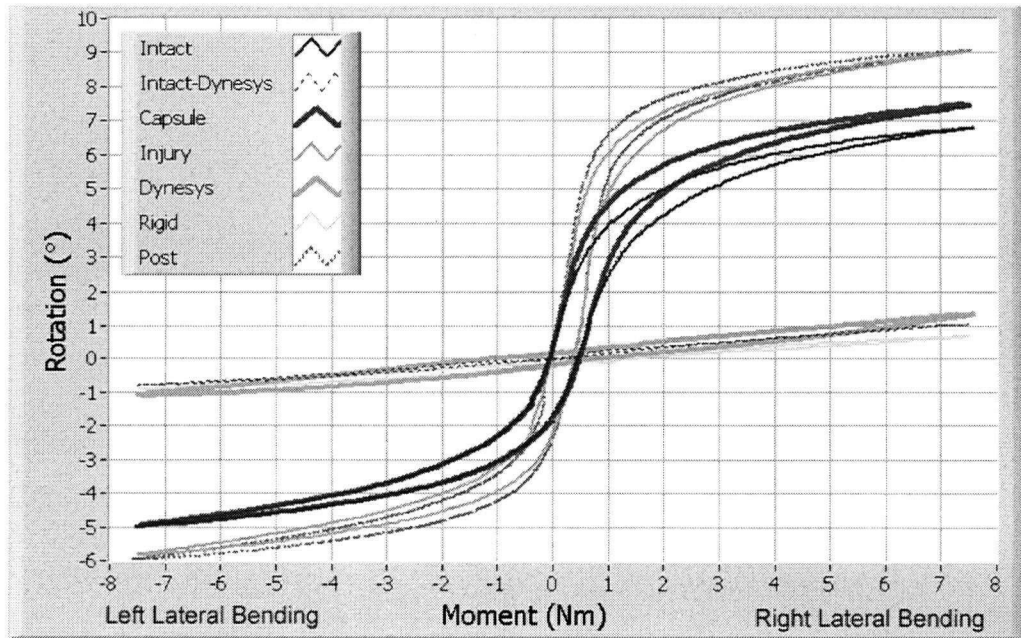


Figure 3.2: Motion vs. applied moment of a typical specimen in lateral bending. Shown for seven specimen conditions without a follower preload.

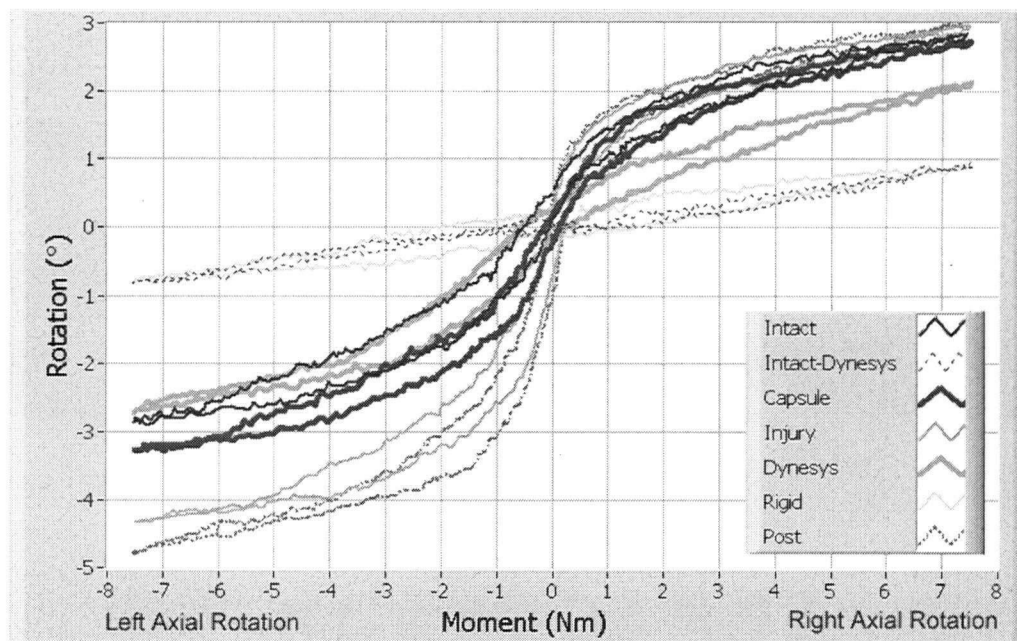


Figure 3.3: Motion vs. applied moment of a typical specimen in axial rotation. Shown for seven specimen conditions without a follower preload.

($p > 0.26$) (Figures 3.4 to 3.7). Injury, however, resulted in significantly greater motion than the intact condition in flexion ($p < 0.05$), lateral bending ($p < 0.04$), and axial rotation ($p = 0.01$) (only axial rotation without a follower preload). There was no significant difference between the intact and injury conditions in extension ($p > 0.05$). Rigid fixation always produced significantly smaller motion than that of the intact condition ($p < 0.006$). There was no significant difference in ROM when comparing the injury and post conditions ($p > 0.07$).

Implantation of the Dynesys system created a significantly smaller ROM than the intact condition in all directions ($p < 0.003$), except in axial rotation with a follower preload ($p = 0.36$). ROM with the Dynesys was 16%, 30%, 25%, and 88% of Intact ROM in flexion, extension, lateral bending, and axial rotation, respectively (with a follower preload). The motion with the Dynesys implanted was actually relatively similar to that of the rigid system, with no significant differences between the two devices ($p > 0.57$), except in axial rotation where the motion with the Dynesys was significantly greater ($p < 0.04$). Compared to the injury condition, the Dynesys resulted in significantly less motion ($p < 0.05$), except in axial rotation with a follower

preload ($p = 0.14$).

Neutral Zone (NZ)

For the intact condition, the average NZ was 0.4° , 0.7° , and 0.3° in flexion-extension, lateral bending, and axial rotation, respectively. Application of a follower preload increased the NZ in flexion-extension to 0.6° and in lateral bending to 1.1° , and decreased the NZ in axial rotation to 0.1° (Tables 3.3 and 3.4).

Injury of the specimens resulted in a significantly greater NZ in flexion-extension without a follower preload ($p = 0.02$). In all other directions, differences in NZ were not significant between the intact and injury conditions ($p > 0.10$). Typically, there was an increase in NZ following injury, except in lateral bending with a follower preload, in which NZ actually decreased once the specimen was injured. (Figures 3.8 to 3.10).

After implantation of the Dynesys, there was a significant reduction in NZ compared to that

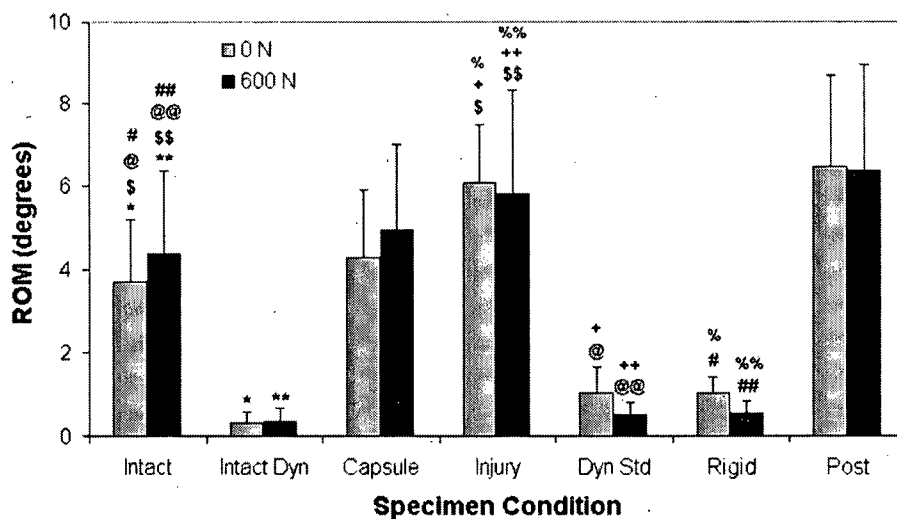


Figure 3.4: Average ROM in flexion. Shown for seven specimen conditions, with and without a compressive follower preload. @, @@, #, ##, %, %%: $p = 0.0001$; *, **, \$, +, ++: $p = 0.0002$; \$\$: $p = 0.05$.

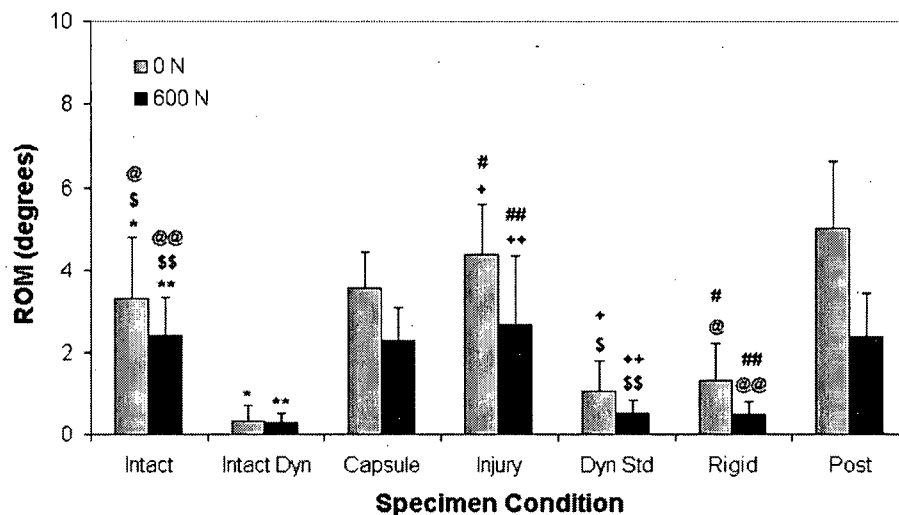


Figure 3.5: Average ROM in extension. Shown for seven specimen conditions, with and without a compressive follower preload. \$, @, @@, +, ++, ##: $p = 0.0001$; *, **, \$\$, #: $p < 0.0002$.

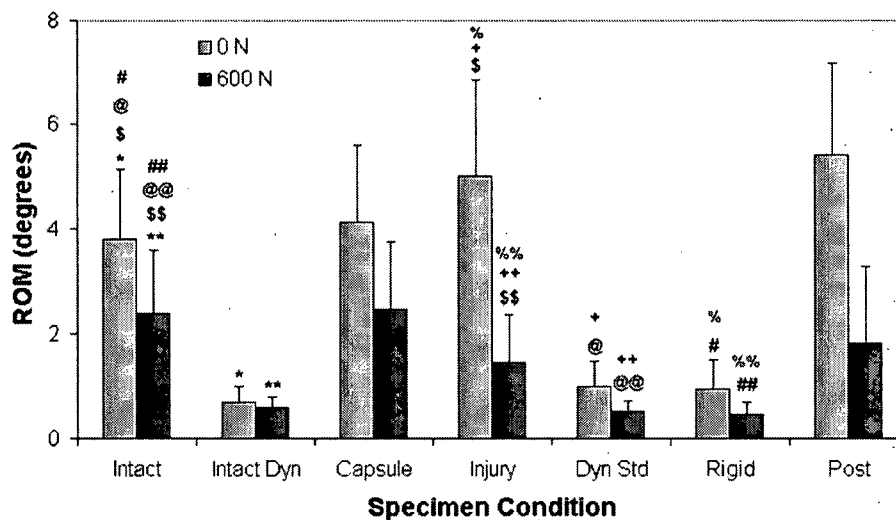


Figure 3.6: Average ROM in lateral bending. Shown for seven specimen conditions, with and without a compressive follower preload. @, #, %: $p = 0.0001$; *, **, @@, ##, +: $p = 0.0002$; \$: $p = 0.02$; \$\$, ++: $p = 0.04$.

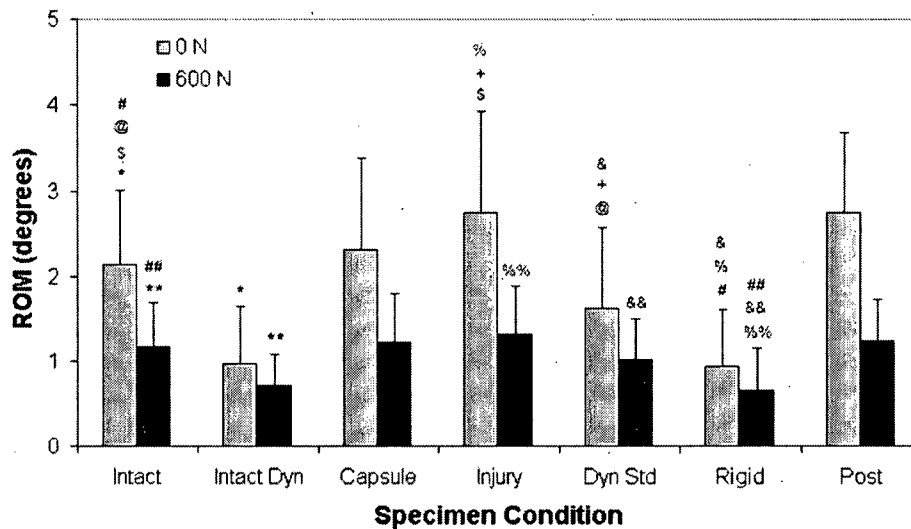


Figure 3.7: Average ROM in axial rotation. Shown for seven specimen conditions, with and without a compressive follower preload. *, %: $p = 0.0001$; #, +: $p = 0.0002$; %%: $p = 0.0004$; @, ℰ: $p = 0.002$; **: $p = 0.004$; ##: $p = 0.006$; \$: $p = 0.01$; *, ℰℰ: $p = 0.04$.

in the injury condition in all loading directions without a follower preload ($p < 0.05$) and in flexion-extension with a follower preload ($p = 0.02$). Compared to an intact specimen, the NZ with the Dynesys was only significantly different (smaller) in lateral bending ($p < 0.03$). There was no significant difference in NZ between the Dynesys and rigid conditions ($p > 0.62$). The NZ in the injury and post conditions was statistically equivalent ($p > 0.05$), except in lateral bending with a follower preload ($p = 0.03$). There was also no significant difference in NZ between the intact and capsule conditions ($p > 0.24$).

Helical Axis of Motion (HAM)

The primary HAM analysis was focused on the HAM over the entire motion. Where differences were observed between the half motions, the results were also included (refer to Appendix C for the complete results of the HAM for the unloaded to maximum rotation and unloaded to minimum rotation). The HAM for flexion and extension, individually, were not incorporated because for a large number of specimens the HAM was ill-defined (again results are in Ap-

Table 3.3: Absolute average NZ without follower load. Values (in degrees) are the average and standard deviation for ten specimens.

Condition	Without Follower Load		
	Flex-Ext	Lateral Bending	Axial Rotation
Intact	0.4 ± 0.5	0.7 ± 0.4	0.3 ± 0.3
Intact-Dynesys	0.1 ± 0.0	0.1 ± 0.1	0.2 ± 0.2
Capsule	0.8 ± 0.7	0.9 ± 0.5	0.3 ± 0.4
Injury	1.3 ± 1.0	1.1 ± 0.7	0.5 ± 0.5
Dynesys Standard	0.2 ± 0.1	0.1 ± 0.1	0.3 ± 0.3
Rigid	0.2 ± 0.2	0.2 ± 0.2	0.3 ± 0.5
Post	1.8 ± 1.7	1.3 ± 0.8	0.4 ± 0.3

Table 3.4: Absolute average NZ with follower load. Values (in degrees) are the average and standard deviation for ten specimens.

Condition	With Follower Load		
	Flex-Ext	Lateral Bending	Axial Rotation
Intact	0.6 ± 0.5	1.1 ± 0.6	0.1 ± 0.1
Intact-Dynesys	0.1 ± 0.1	0.3 ± 0.2	0.1 ± 0.1
Capsule	0.6 ± 0.4	1.0 ± 0.6	0.1 ± 0.1
Injury	0.8 ± 0.8	0.5 ± 0.3	0.2 ± 0.2
Dynesys Standard	0.1 ± 0.1	0.1 ± 0.1	0.2 ± 0.2
Rigid	0.2 ± 0.1	0.2 ± 0.2	0.1 ± 0.2
Post	0.5 ± 0.3	1.1 ± 1.3	0.1 ± 0.1

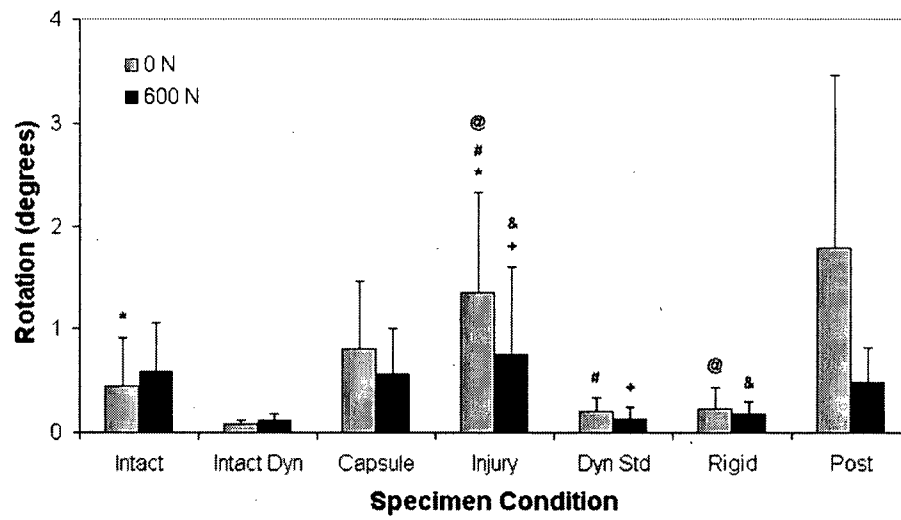


Figure 3.8: Average NZ in flexion-extension. Shown for seven specimen conditions, with and without a compressive follower preload. *, #, +, &: $p = 0.02$; @: $p = 0.03$.

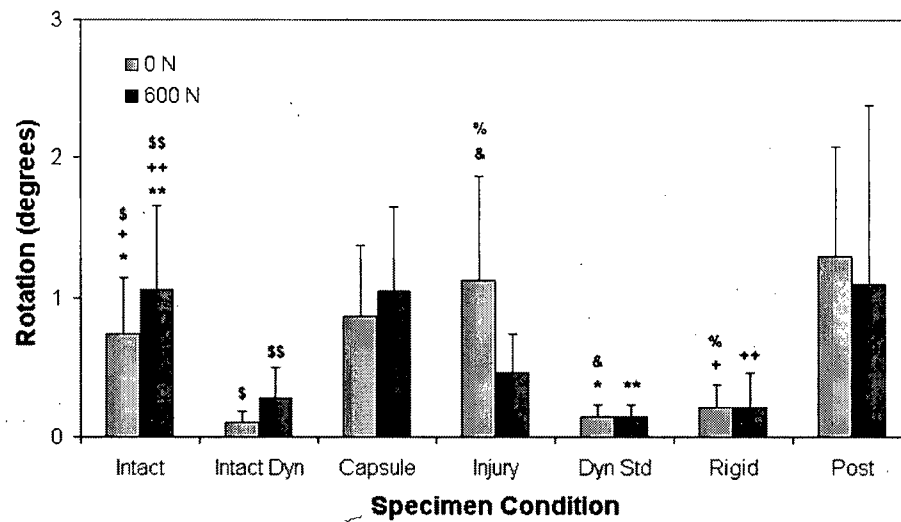


Figure 3.9: Average NZ in lateral bending. Shown for seven specimen conditions, with and without a compressive follower preload. &, %: $p = 0.0002$; *, +: $p = 0.002$; \$: $p = 0.003$; \$\$, **, ++: $p = 0.02$.

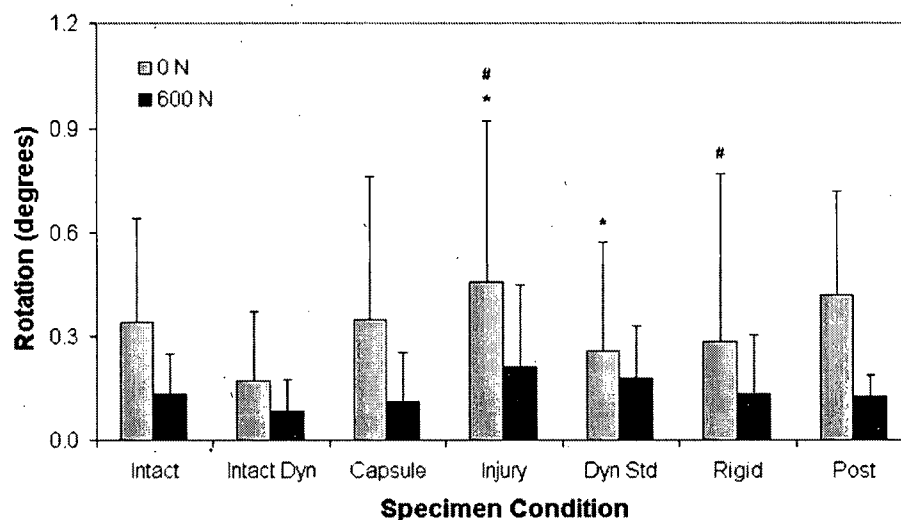


Figure 3.10: Average NZ in axial rotation. Shown for seven specimen conditions, with and without a compressive follower preload. #: $p = 0.02$; *: $p = 0.04$.

pendix C, but should be interpreted cautiously). Unless specifically noted, the HAM from here on in refers to the HAM over the entire motion.

The average HAM of the intact specimen in flexion-extension was located approximately at the centre of the L3-L4 intervertebral disc in the mid-sagittal plane and passed in a relatively straight fashion through the xz (endplate) and xy (coronal) planes (Figure 3.11). In lateral bending, the HAM of the intact specimen was located centrally and laid between the inferior edge of the L3 vertebral body and the superior aspect of the intervertebral disc (Figure 3.12). This was similar to the position of the HAM in both left and right lateral bending. The HAM was angled slightly superiorly in the mid-sagittal plane and with no inclination in the xz (endplate) plane. In left lateral bending, however, the HAM was angled towards the right side of the specimen and the opposite was observed in right lateral bending, in that the HAM was angled to the left of the specimen, indicating a degree of coupled flexion-extension motion (Figure 3.13). In axial rotation, the HAM of the intact specimen was again located centrally near the posterior wall of the L4 vertebral body, with a small inclination to the left in the

xy (coronal) plane and angled anteriorly in the mid-sagittal plane (Figure 3.14). In left and right axial rotation separately, however, the HAM was located to the right and left of the mid-sagittal plane, respectively (Figure 3.15). The HAM was angled largely to the left in the coronal plane in left axial rotation and angled a very small degree to the right in right axial rotation (Figure 3.16).

There were no significant differences in the HAM after the facet joint capsules were sectioned or after the severe injury was performed, as compared to the intact condition ($p > 0.05$). Implantation of the Dynesys resulted in a significant posterior shift in the HAM in flexion-extension ($p < 0.03$) (Figure 3.11) and axial rotation ($p < 0.05$) (Figure 3.14) (only without a follower preload in axial rotation). A non-significant asymmetric rotation in the xz (endplate) plane was evident in flexion-extension when the Dynesys was implanted. There was a slight, though non-significant, shift of the HAM laterally to the right in axial rotation with implantation of the Dynesys ($p > 0.05$). In the mid-sagittal plane for axial rotation, the orientation of the HAM rotated clockwise with implantation of the Dynesys so that the axis was directed posteriorly instead of anteriorly as in the intact condition. This indicated a change in the coupled motion. The difference was significant without a follower preload ($p < 0.004$), but not with a follower preload ($p > 0.05$). In the xy (coronal) plane, the orientation of the Dynesys switched very slightly from inclination to the right in left axial rotation to the left in right axial rotation. This change in coupling was of a similar pattern as that observed in the intact specimen between left and right axial rotation, however the angle tended to be greater, but not significantly different, in the intact specimen (Figure 3.16). There were no significant changes in lateral bending with the Dynesys as compared to the intact, capsule, and injury conditions (Figure 3.12). However, the Dynesys tended to cause an inferior and lateral shift to the right in the position of the HAM ($p > 0.05$) as well as a non-significant clockwise rotation in the xz (endplate) plane ($p > 0.05$). It was interesting to note that while the HAM in the intact, capsule, injury, and post conditions all possessed opposite angulations in the endplate plane for right and left lateral bending, for specimens stabilized with the Dynesys and rigid fixation, the orientation of the HAM did not change when looking at the entire motion or each of the half motions (Figure 3.13).

Comparing the Dynesys and rigid conditions, there were no significant differences in either position or orientation of the HAM. Looking in the xy (coronal) plane, in the rigid condition, there was not a substantial difference in the orientation of the HAM between right and left axial rotation, but with the Dynesys, the HAM alternated between inclination to the right and left. The HAM for the injury and post conditions were not statistically different.

3.1.2 Effect of Spacer Length

Range of Motion (ROM)

In all loading directions, there was generally an increase in ROM with the long spacer and a reduction in ROM with the short spacer, as compared to the kinematics of the standard length spacer. Motion vs. applied moment curves for a typical specimen are shown in Figures 3.17 to 3.19. Without a compressive follower preload, the spacer length did significantly affect ROM with $p < 0.006$ (Table 3.5, Figures 3.20 to 3.23). Post-hoc analysis revealed that the differences were significant between all three spacer lengths ($p < 0.02$), except between the long and standard spacers in flexion and extension ($p > 0.47$).

While the same trend was seen with a follower preload, the changes in ROM were only significant in axial rotation and were between all three spacer lengths ($p < 0.03$) (Table 3.6, Figures 3.20 to 3.23). The length of the spacer did not lead to significant differences in ROM in lateral bending ($p = 0.05$), extension ($p = 0.08$), or flexion ($p = 0.17$) with a follower preload.

Table 3.5: Absolute ROM without follower load for three Dynesys spacer lengths (short, standard, and long). Numbers (in degrees) are the average and standard deviation for ten specimens. Lateral bending and axial rotation ROM are reported as an average of one side only.

Condition	Without Follower Load			
	Flexion	Extension	Lateral Bending	Axial Rotation
Short	0.5 ± 0.4	0.5 ± 0.3	0.8 ± 0.5	1.3 ± 0.9
Standard	1.0 ± 0.6	1.1 ± 0.7	1.0 ± 0.5	1.6 ± 1.0
Long	1.0 ± 0.5	1.3 ± 0.9	1.2 ± 0.5	1.9 ± 0.9

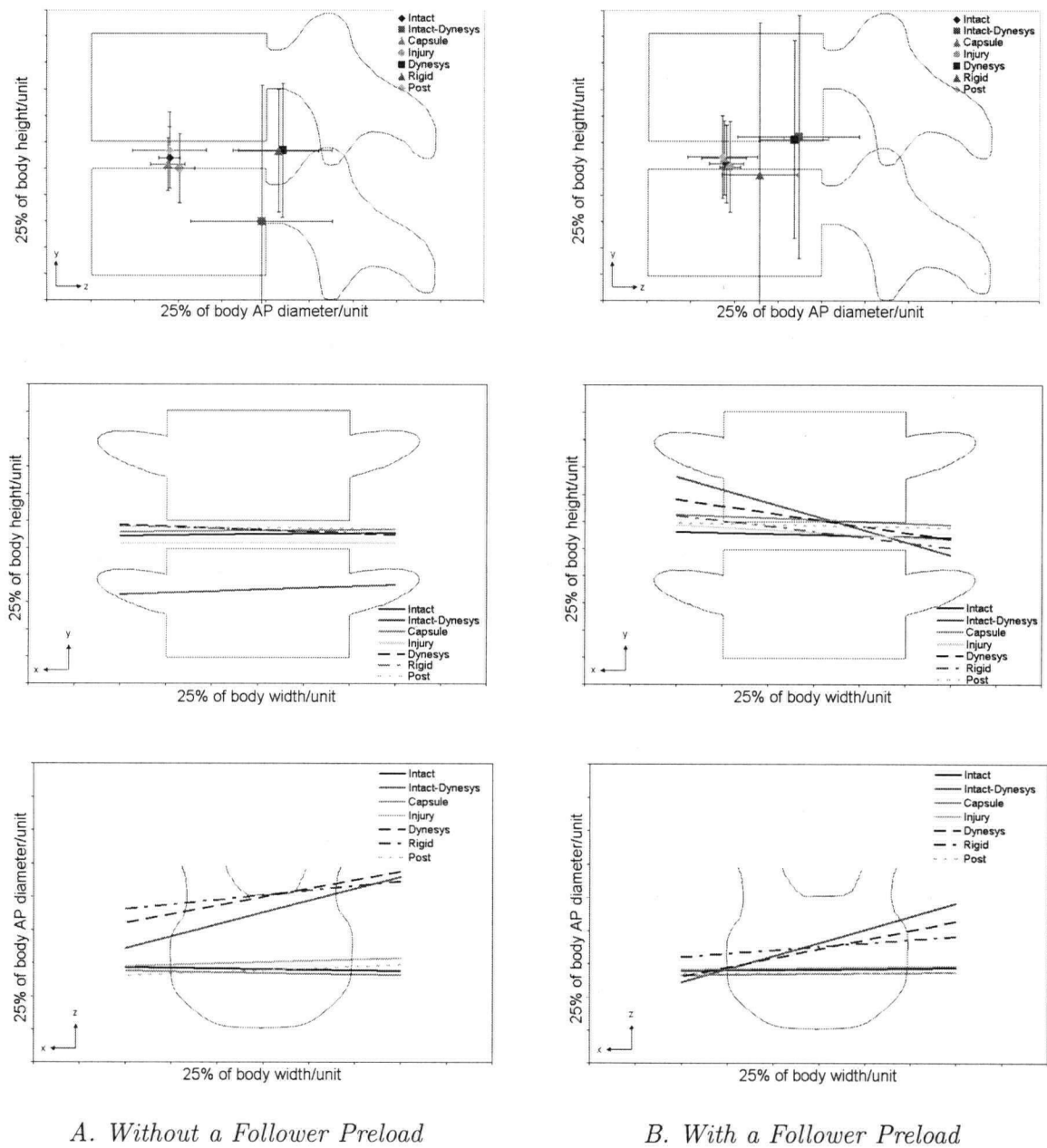
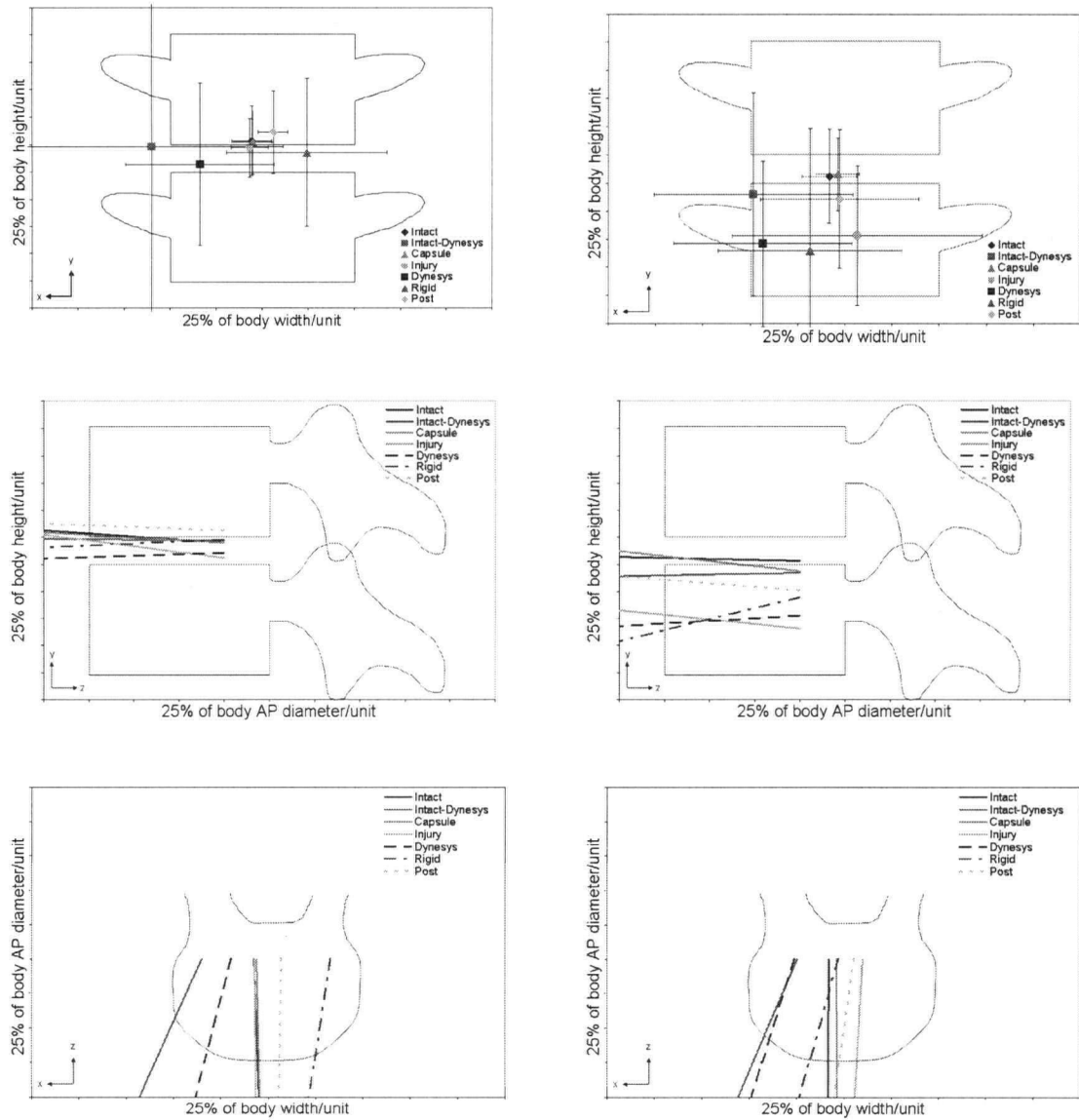


Figure 3.11: Average position (with one standard deviation) and orientation of HAM in flexion-extension. Shown with and without a compressive follower preload for seven specimen conditions. Values were normalized by the width, AP diameter, and height of the L4 vertebral body. Of interest were statistically significant differences that existed in the AP position between Intact and Dynesys ($p < 0.03$), Intact and Rigid ($p = 0.0001$ at 0 N), Injury and Dynesys ($p < 0.03$), Injury and Rigid ($p = 0.0002$ at 0 N), Intact and Intact-Dynesys ($p < 0.005$).



A. Without a Follower Preload

B. With a Follower Preload

Figure 3.12: Average position (with one standard deviation) and orientation of HAM in lateral bending. Shown with and without a compressive follower preload for seven specimen conditions. Values were normalized by the width, AP diameter, and height of the L4 vertebral body. Of interest were statistically significant differences that existed without a follower preload between Intact and Intact-Dynesys in the medial-lateral position ($p = 0.002$) and in the xz (endplate) plane ($p = 0.03$). No statistical differences were seen in position or orientation of the HAM with a follower preload ($p > 0.05$).

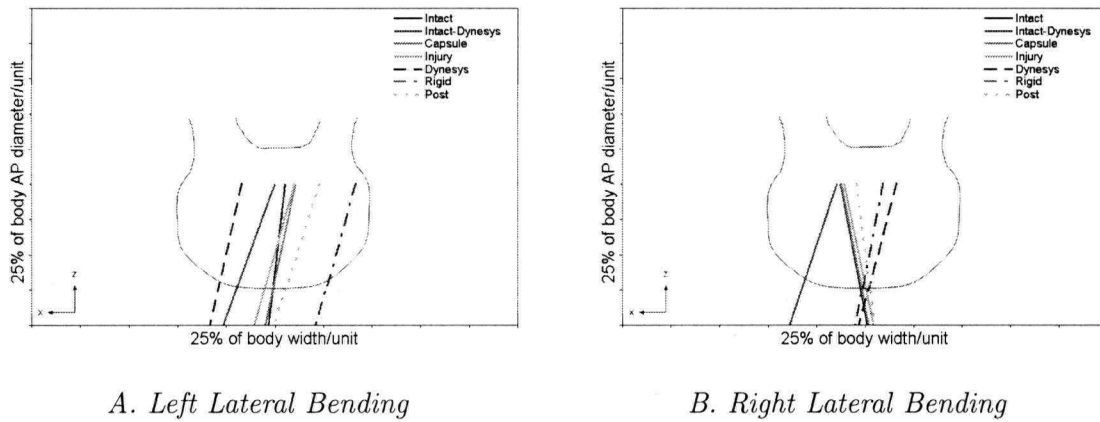


Figure 3.13: Average orientation of the HAM in left and right lateral bending. Shown without a compressive follower preload for seven specimen conditions. Values were normalized by the width, AP diameter, and height of the L4 vertebral body. Differences between conditions were not statistically significant ($p > 0.05$).

Table 3.6: Absolute ROM with follower load for three Dynesys spacer lengths (short, standard, and long). Numbers (in degrees) are the average and standard deviation for ten specimens. Lateral bending and axial rotation ROM are reported as an average of one side only.

Condition	With Follower Load			
	Flexion	Extension	Lateral Bending	Axial Rotation
Short	0.4 ± 0.3	0.3 ± 0.2	0.5 ± 0.3	0.9 ± 0.4
Standard	0.5 ± 0.3	0.5 ± 0.3	0.5 ± 0.2	1.0 ± 0.5
Long	0.5 ± 0.3	0.6 ± 0.2	0.6 ± 0.3	1.2 ± 0.5

Neutral Zone (NZ)

The average NZ was typically greatest with the long spacer, followed by the standard and short spacers. The long spacer resulted in a significantly larger NZ compared to the short spacer without a follower preload in flexion-extension ($p = 0.04$), lateral bending ($p = 0.03$), and axial rotation ($p = 0.02$) (Table 3.7 and Figures 3.24 to 3.26). Differences in NZ were also significant without a follower preload between the standard and short spacers in flexion-extension ($p = 0.03$) and between the standard and long spacers in axial rotation ($p = 0.03$).

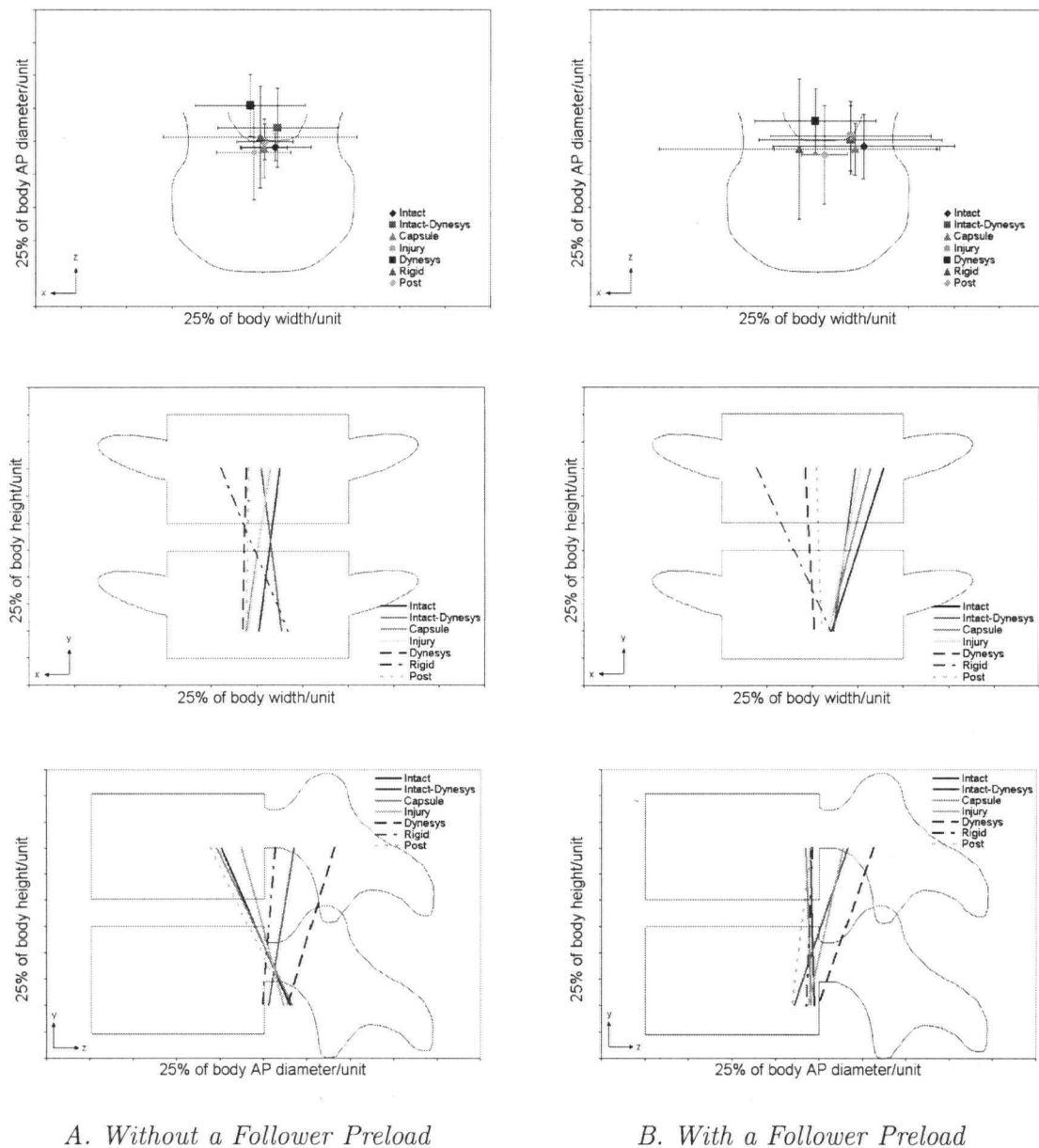
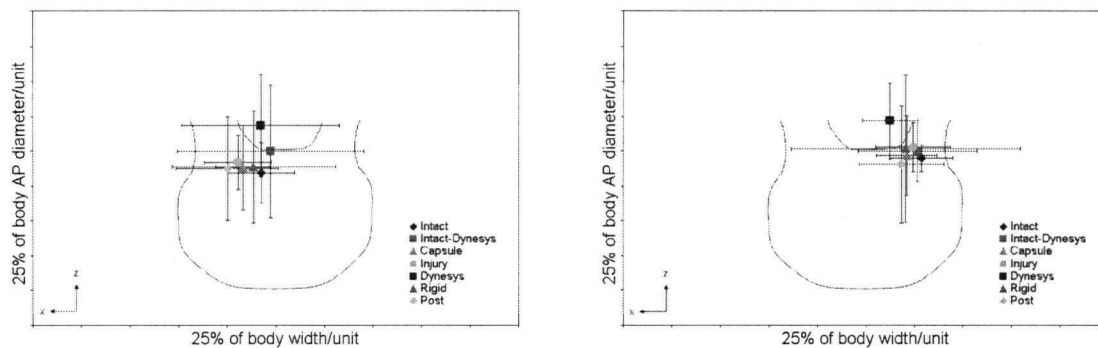


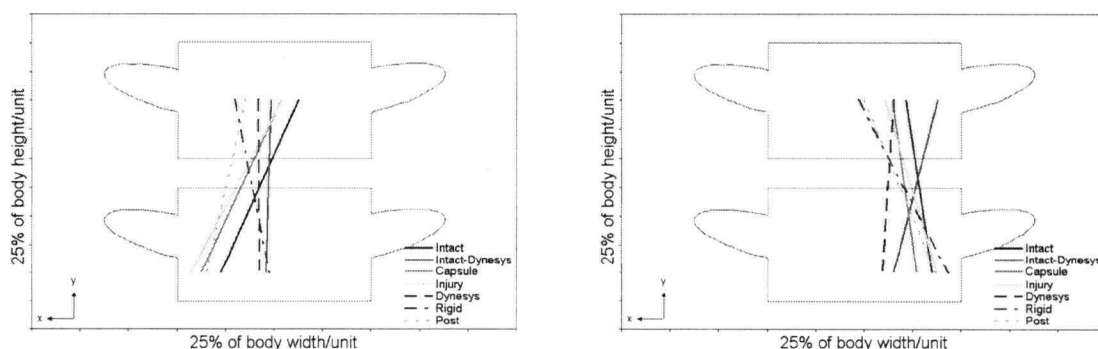
Figure 3.14: Average position (with one standard deviation) and orientation of HAM in axial rotation. Shown with and without a compressive follower preload for seven specimen conditions. Values were normalized by the width, AP diameter, and height of the L4 vertebral body. Of interest were statistically significant differences that existed without a follower preload in the AP direction between Intact and Dynesys ($p = 0.04$) and in the mid-sagittal plane between Intact and Intact-Dynesys ($p = 0.02$), Intact and Dynesys ($p = 0.003$), Intact and Rigid ($p = 0.03$), and Injury and Dynesys ($p = 0.03$). With a follower preload, of interest was a statistical difference in orientation in the xy (coronal) plane between Intact and Rigid ($p = 0.03$) Injury and Rigid ($p = 0.05$).



A. Left Axial Rotation

B. Right Axial Rotation

Figure 3.15: Average and standard deviation in position of the HAM in left and right axial rotation. Shown without a compressive follower preload for seven specimen conditions. Values were normalized by the width, AP diameter, and height of the L4 vertebral body. Differences between conditions were not statistically significant ($p > 0.05$).



A. Left Axial Rotation

B. Right Axial Rotation

Figure 3.16: Average orientation of the HAM in left and right axial rotation. Shown without a compressive follower preload for seven specimen conditions. Values were normalized by the width, AP diameter, and height of the L4 vertebral body. Differences between conditions were not statistically significant ($p > 0.05$).

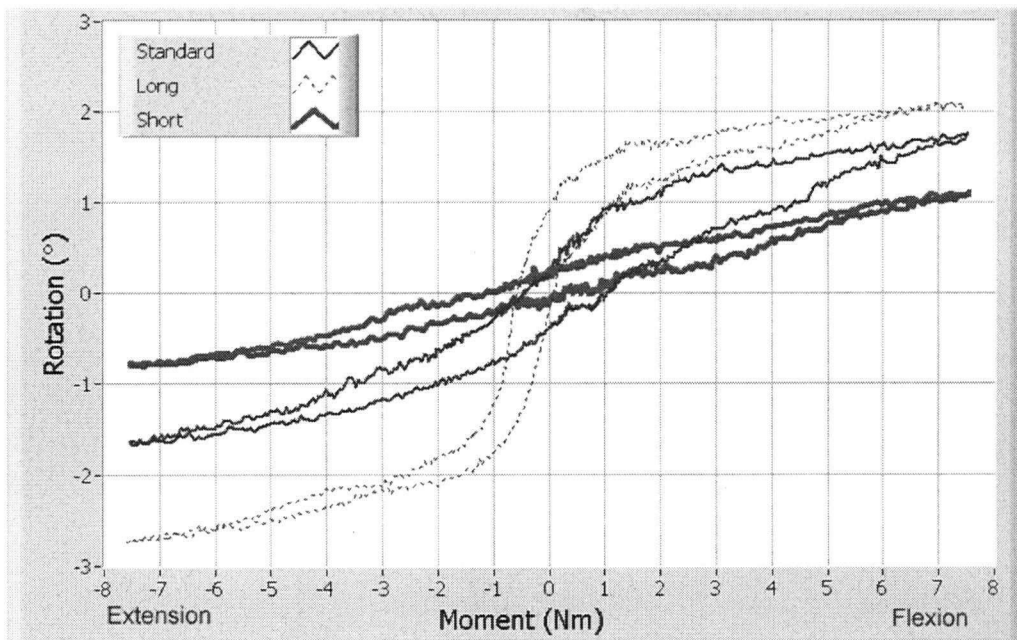


Figure 3.17: Motion vs. applied moment of a typical specimen in flexion-extension for three Dynesys spacer lengths (short, standard, long) without a follower preload.

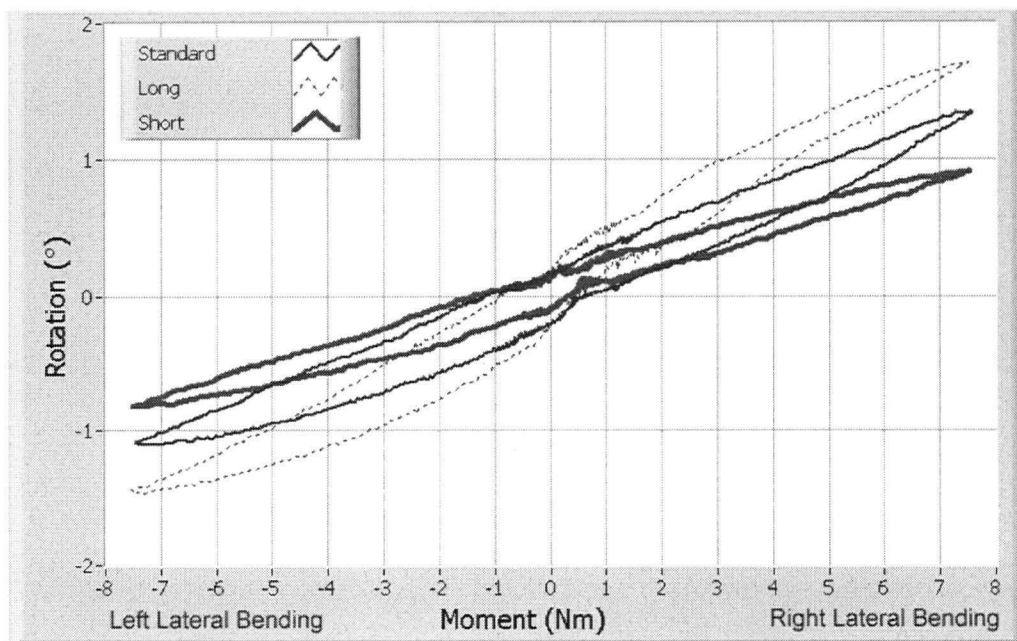


Figure 3.18: Motion vs. applied moment of a typical specimen in lateral bending for three Dynesys spacer lengths (short, standard, long) without a follower preload.

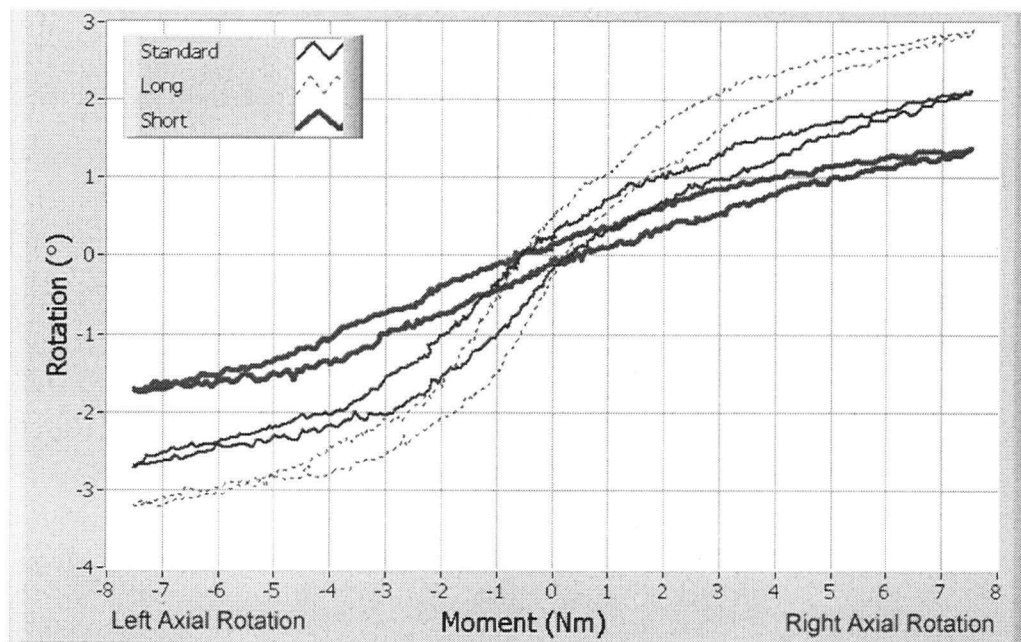


Figure 3.19: Motion vs. applied moment of a typical specimen in axial rotation for three Dynesys spacer lengths (short, standard, long) without a follower preload.

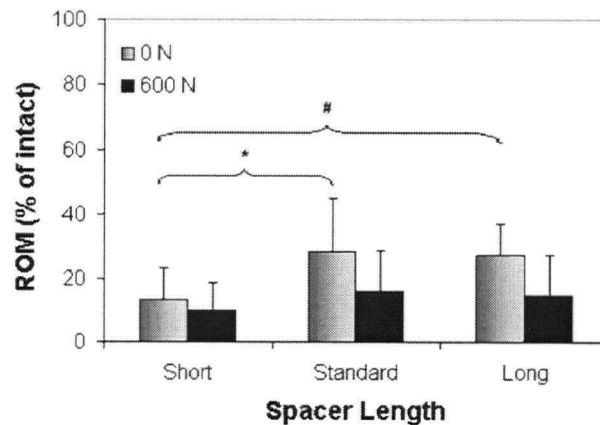


Figure 3.20: Average ROM in flexion for three spacer lengths (short, standard, long). Shown with and without a compressive follower preload. Values were normalized to ROM of the corresponding intact specimen. * $p = 0.008$; # $p = 0.005$. No significant differences existed between spacer lengths with a follower preload ($p > 0.17$).

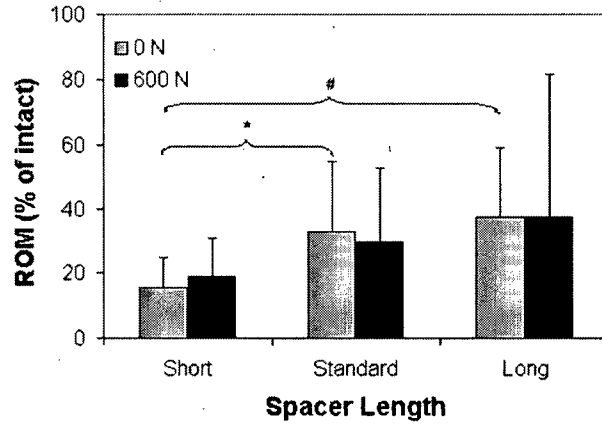


Figure 3.21: Average ROM in extension for three spacer lengths (short, standard, long). Shown with and without a compressive follower preload. Values were normalized to ROM of the corresponding intact specimen. * $p = 0.01$; # $p = 0.006$. No significant differences between spacer lengths with a follower preload ($p > 0.08$).

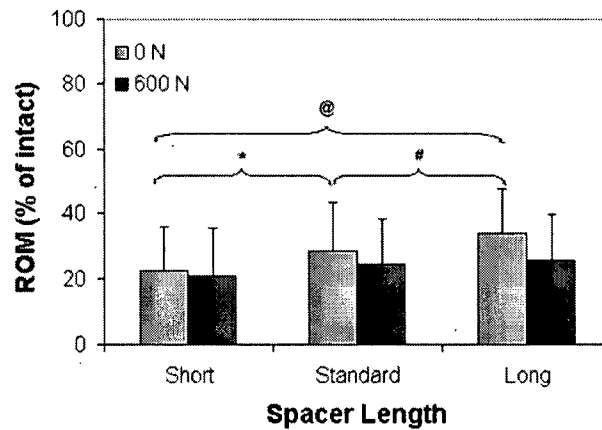


Figure 3.22: Average ROM in lateral bending for three spacer lengths (short, standard, long). Shown with and without a compressive follower preload. Values were normalized to ROM of the corresponding intact specimen. *, #: $p = 0.01$; @: $p = 0.0002$. No significant differences between spacer lengths with a follower preload ($p > 0.05$).

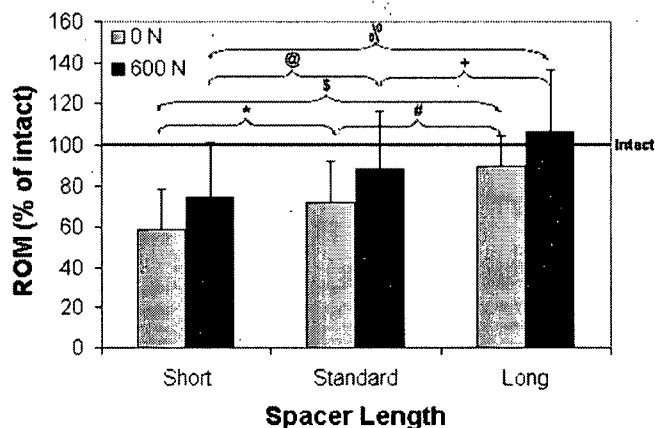


Figure 3.23: Average ROM in axial rotation for three spacer lengths (short, standard, long). Shown with and without a compressive follower preload. Values were normalized to ROM of the corresponding intact specimen. \$, %: $p = 0.0002$; # $p = 0.003$; + $p = 0.006$; * $p = 0.02$, @ $p = 0.03$.

With a follower load, spacer length only had a significant effect on NZ in lateral bending. The long spacer produced a significantly larger NZ than both the standard ($p = 0.03$) and short ($p = 0.03$) spacers in lateral bending. No significant differences were seen in flexion-extension ($p = 0.07$) or axial rotation ($p = 0.07$).

Table 3.7: Absolute NZ without follower load for three spacer lengths (short, standard, and long). Numbers (in degrees) are the average and standard deviation for ten specimens.

Without Follower Load			
Condition	Flex-Ext	Lateral Bending	Axial Rotation
Short	0.1 ± 0.0	0.1 ± 0.1	0.2 ± 0.2
Standard	0.2 ± 0.1	0.1 ± 0.1	0.3 ± 0.3
Long	0.2 ± 0.2	0.2 ± 0.1	0.3 ± 0.2

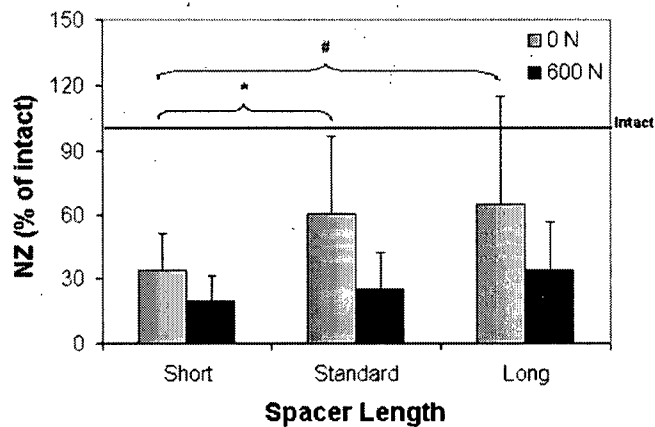


Figure 3.24: Average NZ in flexion-extension for three spacer lengths (short, standard, long). Shown with and without a compressive follower preload. Values were normalized to NZ of the corresponding intact specimen. * $p = 0.03$; # $p = 0.04$. No significant differences between spacer lengths with a follower preload ($p > 0.07$).

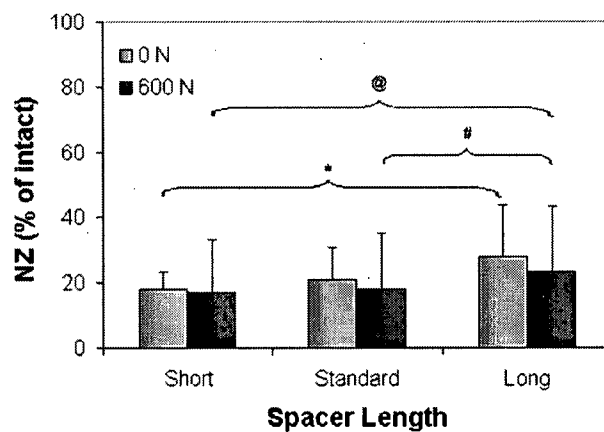


Figure 3.25: Average NZ in lateral bending for three spacer lengths (short, standard, long). Shown with and without a compressive follower preload. Values were normalized to NZ of the corresponding intact specimen. *, #, @: $p = 0.03$.

Table 3.8: Absolute NZ with follower load for three spacer lengths (short, standard, and long). Numbers (in degrees) are the average and standard deviation for ten specimens.

With Follower Load			
Condition	Flex-Ext	Lateral Bending	Axial Rotation
Short	0.1 ± 0.0	0.1 ± 0.1	0.2 ± 0.1
Standard	0.1 ± 0.1	0.1 ± 0.1	0.2 ± 0.2
Long	0.1 ± 0.0	0.2 ± 0.1	0.2 ± 0.2

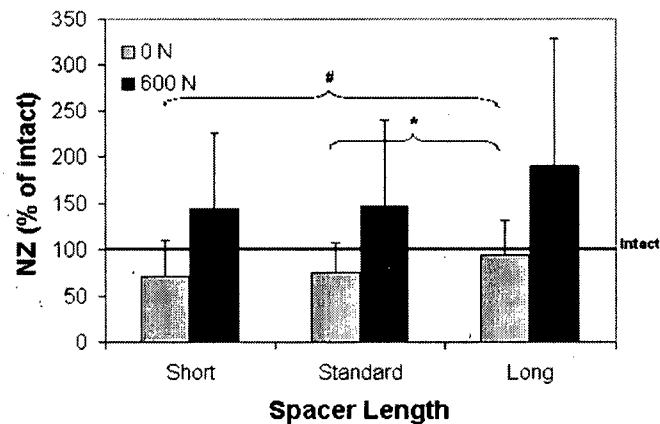


Figure 3.26: Average NZ in axial rotation for three spacer lengths (short, standard, long). Shown with and without a compressive follower preload. Values were normalized to NZ of the corresponding intact specimen. # $p = 0.02$; * $p = 0.03$. No significant differences between spacer lengths with a follower preload ($p > 0.07$).

Translation

The y -component of the translation vector between L3 and L4 at the neutral position was used as an indication of the degree of compression or distraction of the anterior annulus that was created by the three different Dynesys spacer lengths. Translation in the y -direction represented the inferior-superior displacement between the origins of the L3 and L4 anatomical coordinate systems. The average initial inferior-superior separation distance was 39.3 ± 6.6 mm,

38.6 \pm 7.3 mm, and 38.4 \pm 7.9 mm for the short, standard, and long spacers, respectively (Table 3.9). The difference in separation distance created by the three spacer lengths was not significant in the y -direction ($p = 0.35$).

Helical Axis of Motion (HAM)

Overall, the length of the spacer did not contribute to large differences in the position or orientation of the HAM. Typically the short spacer resulted in a greater shift of the HAM from that of the standard spacer and the long spacer produced lesser changes. Without a follower preload the only significant difference in HAM was a greater counter-clockwise rotation in the xz (endplate) plane in flexion-extension with the short spacer as compared to the long spacer

Table 3.9: Initial separation distance between L3 and L4 anterior points with the three Dynesys spacer lengths (short, standard, and long). For each specimen, the separation distance was represented as a single value along the y -axis. This was the average distance calculated from the initial separation distance in each loading direction (3 cases) and each preload condition (2 cases). Distances are shown in mm. There was no statistically significant difference between the y -separation distances ($p = 0.35$).

Specimen	y -Distance		
	Short	Standard	Long
H1092	28.4	22.8	20.8
H1062	36.3	38.1	37.8
H1113	35.6	36.4	36.4
H1107	49.2	48.8	50.5
H1005	49.3	47.3	46.0
H1094	36.2	36.0	35.7
H1109	37.1	36.2	37.2
H1106	35.7	36.0	35.5
H1112	41.7	41.5	41.3
H1111	43.9	43.4	42.9
Mean	39.3	38.6	38.4
St Dev	6.6	7.3	7.9

($p = 0.03$) (Figure 3.27). With a follower preload, however, a significant difference in position and orientation of the HAM existed in axial rotation. The HAM was located significantly more posteriorly and with a greater clockwise rotation in the mid-sagittal plane with the long spacer than with the short spacer ($p < 0.04$) (Figure 3.28). There was a tendency for the position of the HAM to move more posteriorly in flexion-extension and axial rotation as spacer length decreased. There was also a non-significant lateral shift to the right as spacer length was decreased in axial rotation and lateral bending (Figures 3.28 and 3.29).

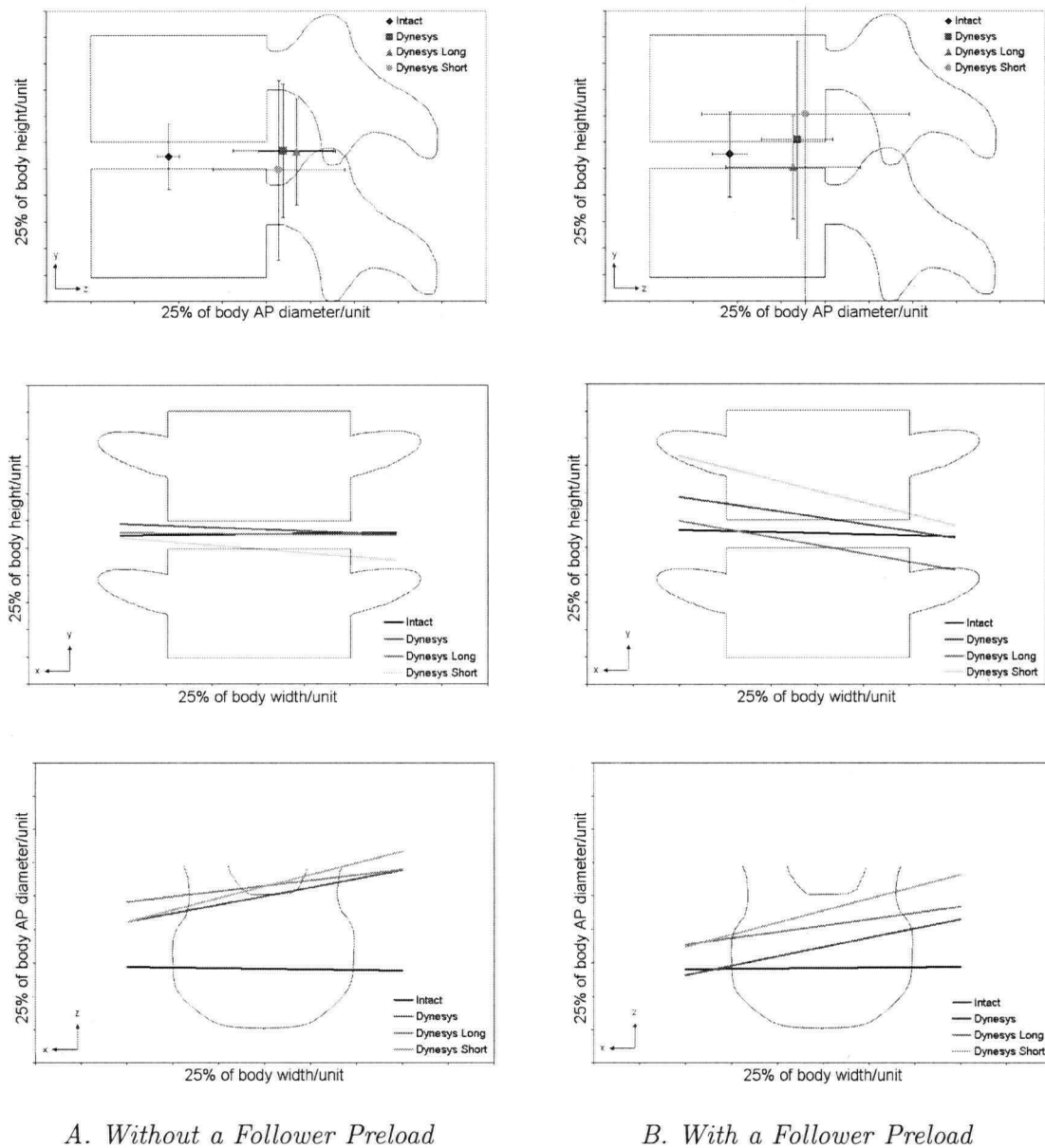


Figure 3.27: Average position (with one standard deviation) and orientation of HAM in flexion-extension (spacer length). The HAM are shown with and without a compressive follower preload for the intact condition, and short, standard, and long Dynesys spacers. Values were normalized by the width, AP diameter, and height of the L4 vertebral body. Differences were statistically significant between the long and short spacers in the xz (endplate) plane without a follower preload ($p = 0.03$). None of the other differences between spacer lengths in flexion-extension were of statistical significance ($p > 0.05$). Note that the intact condition was provided as reference only and not included in these comparisons.

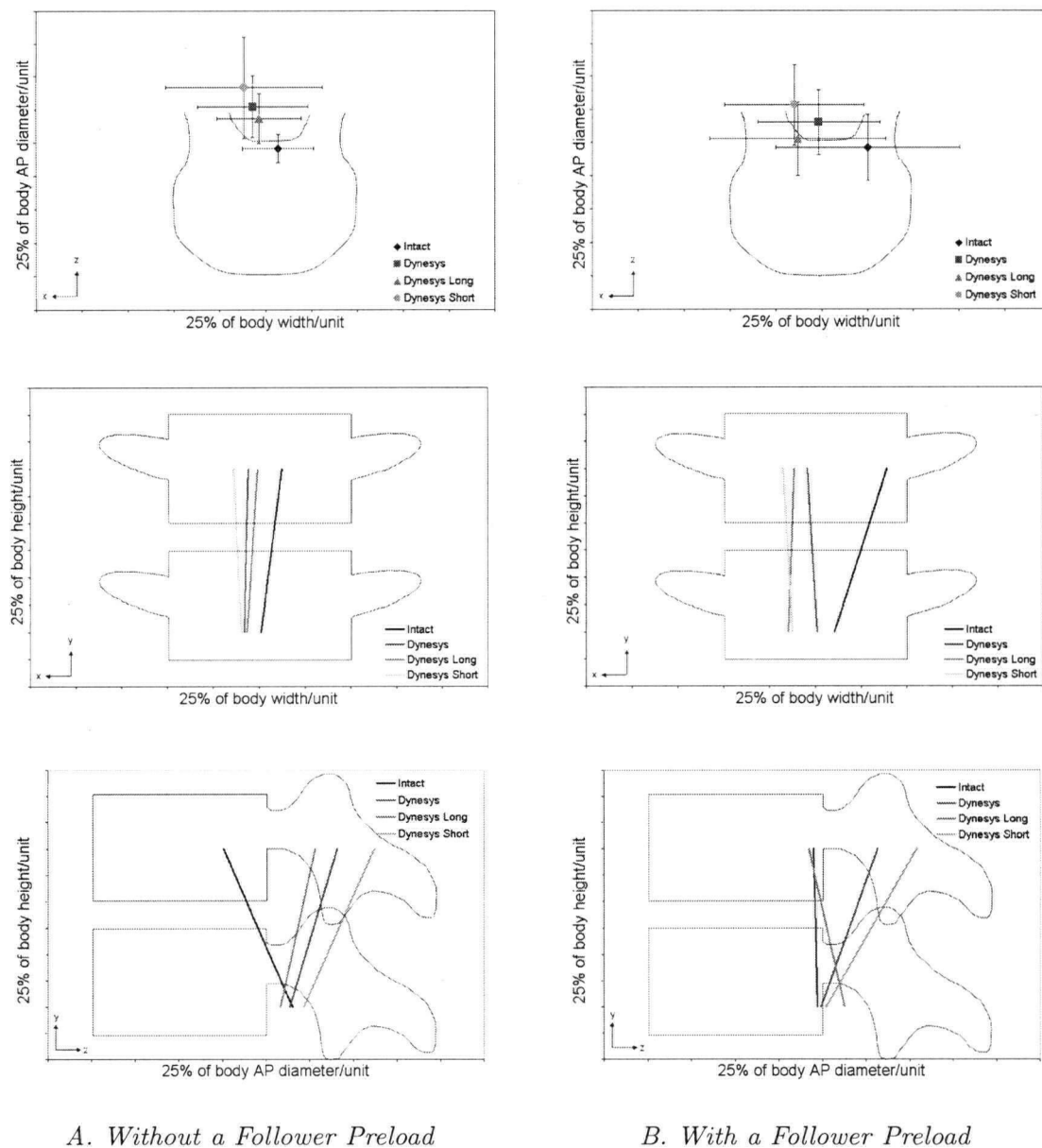


Figure 3.28: Average position (with one standard deviation) and orientation of HAM in axial rotation (spacer length). The HAM are shown with and without a compressive follower preload for the intact condition, and short, standard, and long Dynesys spacers. Values were normalized by the width, AP diameter, and height of the L4 vertebral body. There was a significant difference in position of the HAM in the anterior-posterior direction with a follower preload ($p = 0.03$) and in the orientation in the mid-sagittal plane with a follower preload ($p = 0.03$) between the short and long spacers. None of the other differences between spacer lengths in axial rotation were of statistical significance. Note that the intact condition was provided as reference only and not included in these comparisons.

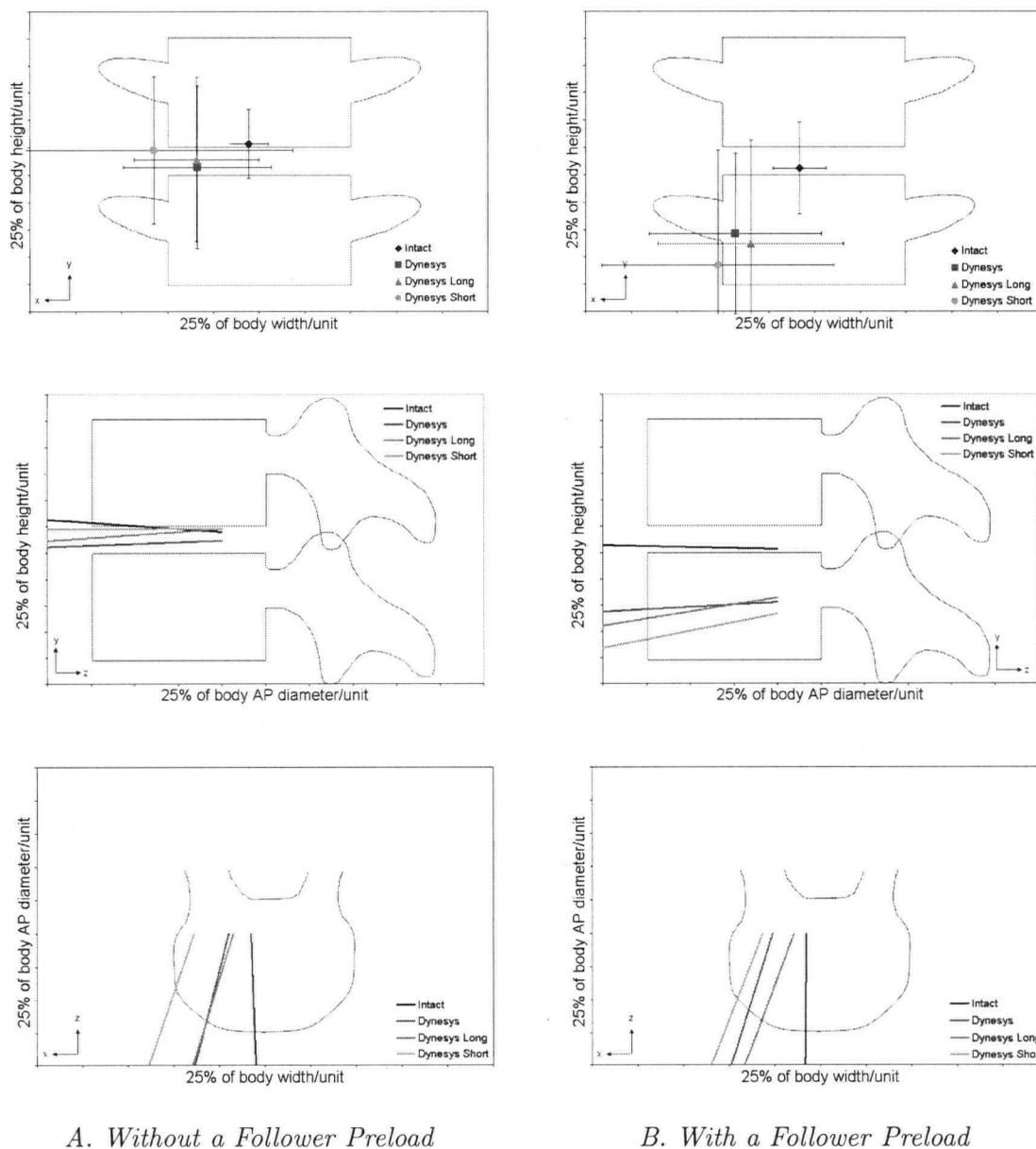


Figure 3.29: Average position (with one standard deviation) and orientation of HAM in lateral bending (spacer length). The HAM are shown with and without a compressive follower preload for the intact condition, and short, standard, and long Dynesys spacers. Values were normalized by the width, AP diameter, and height of the L4 vertebral body. None of the differences between spacer lengths in lateral bending were of statistical significance ($p > 0.15$). Note that the intact condition was provided as reference only and not included in these comparisons.

3.2 Facet Loads

3.2.1 Effect of Specimen Condition

The average total peak facet loads (sum of left and right for flexion and extension, average of maximum left and right forces for lateral bending and axial rotation) in the capsule condition without a follower preload were greatest in axial rotation (56 N), followed by extension (27 N), lateral bending (13 N), and finally flexion (7 N) (Table 3.10). Application of a follower preload did not result in significant differences in facet load compared to testing performed without a follower preload ($p > 0.16$). Facet loads for each specimen can be found in Appendix A and details of the statistical analysis in Appendix B.

Before the Dynesys was implanted, the contact load was minimal in flexion and increased with an extension moment (Figures 3.30 and 3.31). Both facets were loaded simultaneously. In

Table 3.10: Average facet contact load without and with a follower preload. Loads are the average and standard deviation for capsule-sectioned specimens and for injured specimens stabilized with the standard length Dynesys spacer. Contact loads are in all directions of applied loading and are in Newtons (N).

Loading Direction	Follower	Capsule		Dynesys	
		Left	Right	Left	Right
	(N)	(N)	(N)	(N)	(N)
Flexion	0	2 ± 5	4 ± 4	16 ± 16	27 ± 22
Extension	0	13 ± 14	14 ± 10	9 ± 11	21 ± 18
Lateral Bending	0	11 ± 11	16 ± 14	16 ± 13	31 ± 21
Axial Rotation	0	56 ± 17	55 ± 18	50 ± 24	63 ± 20
Flexion	600	1 ± 2	5 ± 6	13 ± 17	32 ± 23
Extension	600	18 ± 14	18 ± 13	9 ± 14	21 ± 17
Lateral Bending	600	11 ± 11	19 ± 18	15 ± 19	30 ± 23
Axial Rotation	600	50 ± 15	45 ± 12	40 ± 24	62 ± 29

lateral bending, the contact load pattern was less consistent among specimens, but typically shifted between sides for left and right applied moments. In axial rotation, the contact loads alternated between sides with a compressive load exerted on the contralateral facet joint, so for example, right axial rotation created a compressive force in the left facet joint (Figures 3.32 and 3.33). The peak magnitude was typically comparable between the right and left facet joints.

Implantation of the Dynesys system created an initial load on the facet joints due to inherent compression of the posterior elements of the bridged segments (Figures 3.30 and 3.32). The standard length Dynesys spacer resulted in an initial load of 13 ± 13 N and 18 ± 18 N at the

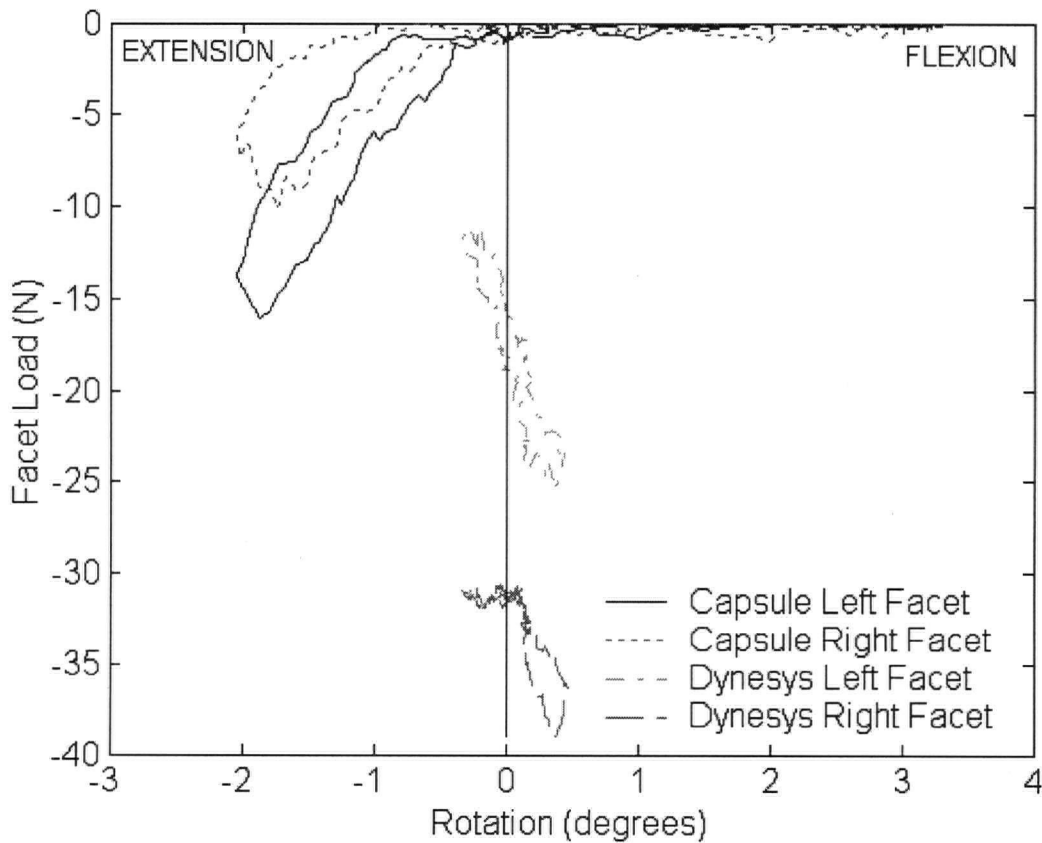


Figure 3.30: Sample contact load (in Newtons) vs. rotation (in degrees) for left and right facet joints in flexion-extension without a follower preload. Shown for the capsule condition and with the standard Dynesys spacer for Specimen H1107. Negative facet load indicates compression.

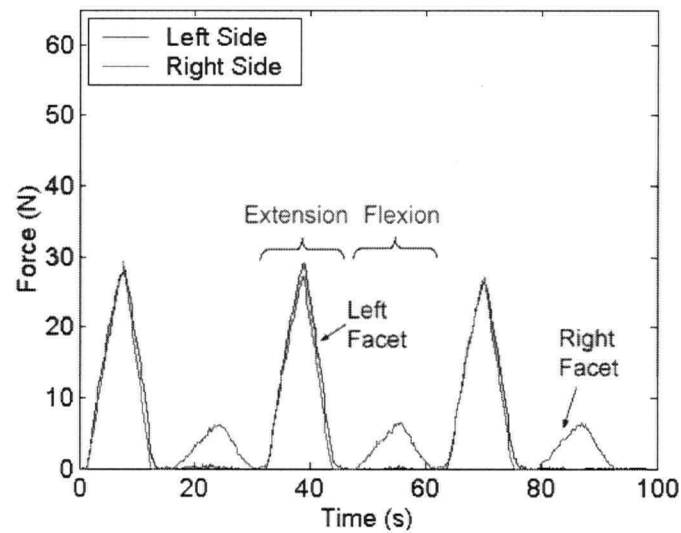


Figure 3.31: Sample contact load vs. time in flexion-extension without a follower preload for capsule condition. Facet loads are in Newtons and are shown for three cycles of loading for Specimen H1109.

left and right sides, respectively.

In an injured specimen stabilized with the Dynesys, the load profile was dramatically different from that in the capsule condition in flexion-extension (Figure 3.34) and notably different in axial rotation (Figure 3.35). Typically one facet experienced a much higher contact load than the other. In flexion-extension, the load pattern was reversed (compared to the capsule condition) with the Dynesys so that the facet loads were increasing during flexion and decreasing in extension.

With the standard length Dynesys implanted, there were significantly increased facet loads at both the left and right sides in flexion ($p < 0.03$) with and without a compressive follower preload (Table 3.10 and Figures 3.30, 3.36, and 3.37). The largest changes in facet load were observed in flexion where the Dynesys increased facet loads compared to the capsule condition from an average peak load of 2 N and 4 N for the left and right sides to 16 N and 27 N for the left and right sides without a follower preload. Although not significantly different, the facet loads tended to increase in lateral bending with implantation of the Dynesys compared to

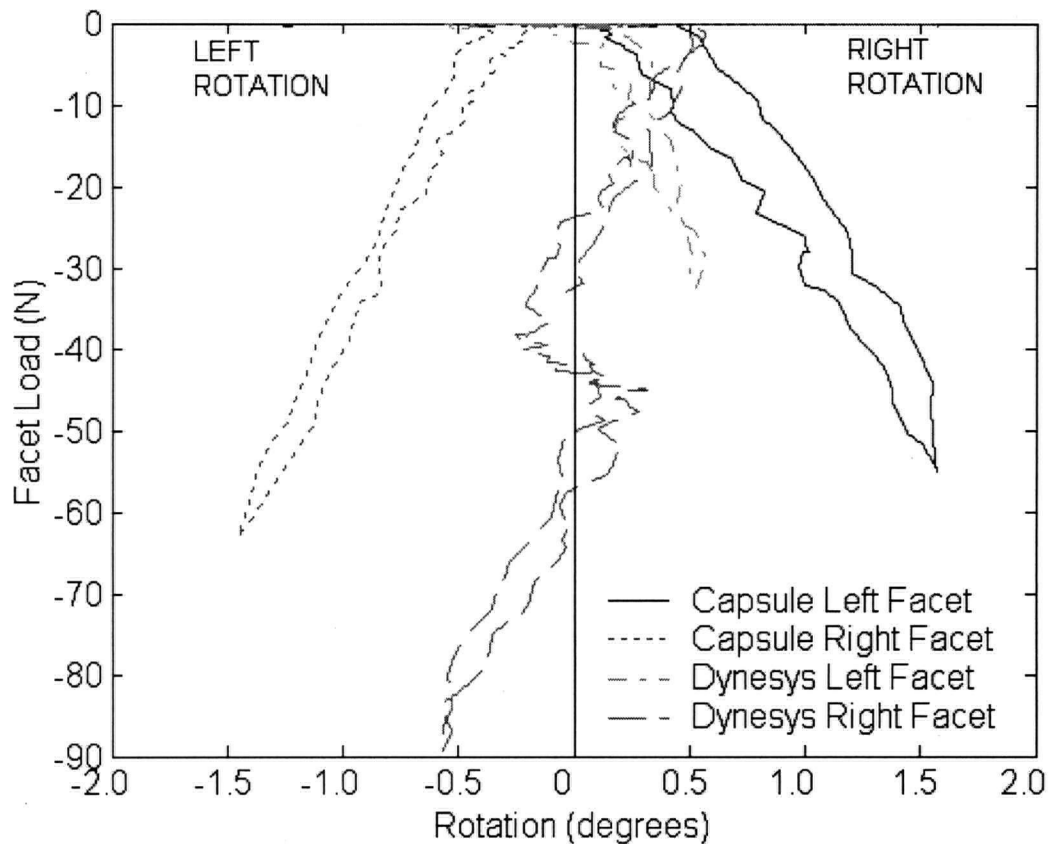


Figure 3.32: Sample contact load (in Newtons) vs. rotation (in degrees) for left and right facet in axial rotation without a follower preload. Shown for the capsule condition and with the standard Dynesys spacer for Specimen H1005. The contralateral facet joint was loaded in compression during flexion and extension. Negative facet load indicates compression.

the capsule condition (Figures 3.38 and 3.39). In extension (Figures 3.40 and 3.41) and axial rotation (Figures 3.42 and 3.43), the Dynesys typically decreased the magnitude of the average peak contact loads on the left side and increased them on the right side, but the differences were not significant.

Asymmetry in the peak contact load between the two facet joints during flexibility tests tended to increase with the Dynesys. There were significantly greater facet loads observed at the right facet compared to the left in flexion when the Dynesys was implanted ($p < 0.0007$). The same trend was observed between the right and left facets for all specimen conditions in lateral

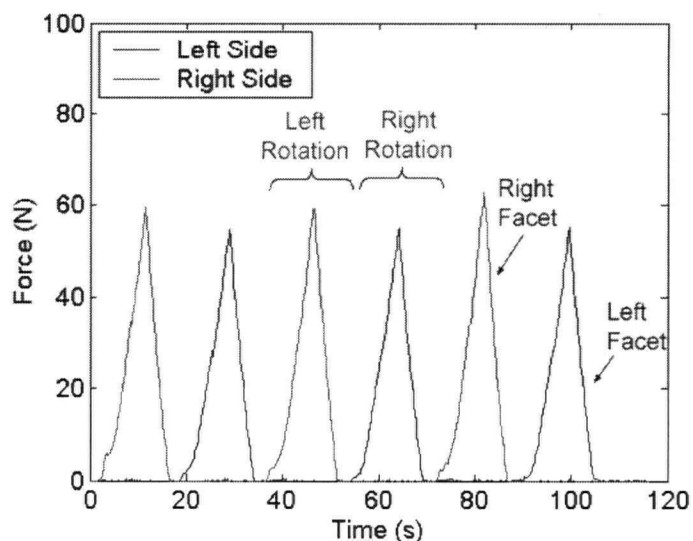


Figure 3.33: Sample contact load vs. time in axial rotation without a follower preload for capsule condition. Facet loads are in Newtons and are shown for three cycles of loading for Specimen H1005.

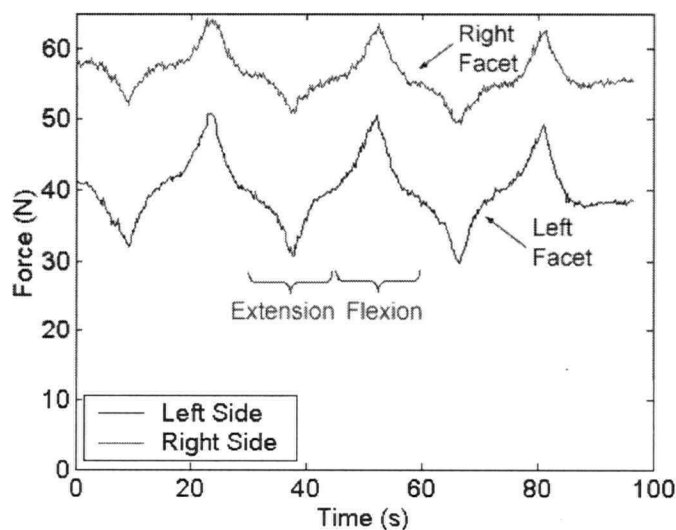


Figure 3.34: Sample contact load vs. time in flexion-extension without a follower preload for an injured specimen stabilized with Dynesys. Facet loads are in Newtons and are shown for three cycles of loading for Specimen H1109.

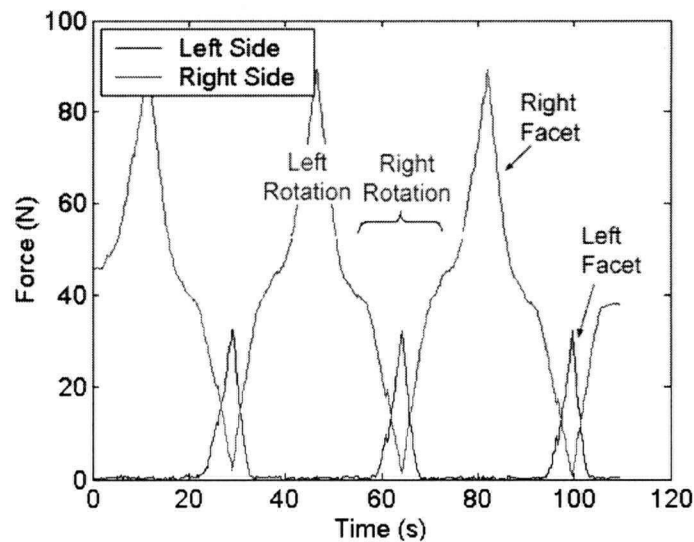


Figure 3.35: Sample contact load vs. time in axial rotation without a follower preload for an injured specimen stabilized with Dynesys. Facet loads are in Newtons and are shown for three cycles of loading for Specimen H1005.

bending without a follower preload ($p < 0.003$). Although not significant, this same pattern was also observed in extension and axial rotation ($p > 0.05$).

Facet loads with the Dynesys were significantly greater in flexion than those for the injury ($p < 0.005$) and rigid ($p < 0.002$) conditions for the left and right sides without a follower preload and right side with a follower preload. The Dynesys also resulted in significantly greater facet loads than in the rigid condition in lateral bending with a follower preload ($p < 0.03$) (Figures 3.38 and 3.39) and in axial rotation without ($p < 0.03$) and with ($p < 0.01$) a follower preload (Figures 3.42 and 3.43).

Both left and right facet loads were significantly smaller in the rigid condition than in the capsule ($p = 0.03$) and injury ($p = 0.006$) conditions in extension with a follower preload (Figures 3.40 and 3.41). In axial rotation, the rigid system produced significantly smaller left facet loads than in the Capsule ($p < 0.0002$) and Injury ($p < 0.0002$) and smaller right facet loads than in the Injury ($p < 0.02$) (Figures 3.42 and 3.43). Facet loads were asymmetric in axial rotation with the rigid device; the load at the right facet was significantly greater than

that at the left ($p < 0.0009$).

3.2.2 Effect of Spacer Length

As mentioned in Section 3.2.1, the initial facet contact loads that were created by implantation of the standard length Dynesys were 13 ± 13 N and 18 ± 18 N at the left and right sides, respectively. The length of the spacer had an effect on the magnitude of the initial contact load. The long spacer decreased the average initial load to 4 ± 8 N and 11 ± 10 N for the left and right sides, while the short spacer increased the load to 16 ± 12 N and 27 ± 27 N for the left and right sides (Figure 3.44). The differences were significant between the long and short spacers on both the left ($p = 0.004$) and right ($p = 0.02$) sides. There was no significant difference between the right and left sides, however.

Variation of the Dynesys spacer length affected the facet loads during flexibility testing. Generally, the magnitude of the contact load was greatest with the short spacer and least with the long spacer in all directions of loading (Figures 3.45 to 3.52). There was a significant difference

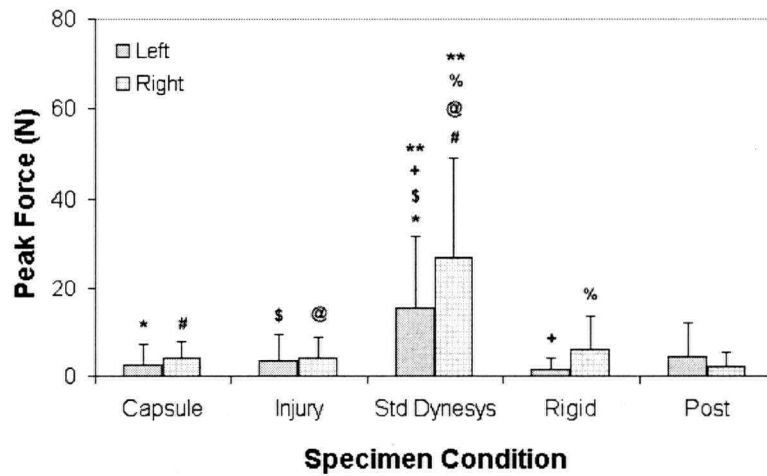


Figure 3.36: Average peak facet loads in flexion without a follower preload. Shown are contact forces within the left and right facet joints for five specimen conditions (Capsule, Injury, Standard Dynesys, Rigid, and Post). #, @, %: $p = 0.0001$; **: $p = 0.0007$; \$: $p = 0.005$; *, +: $p = 0.002$.

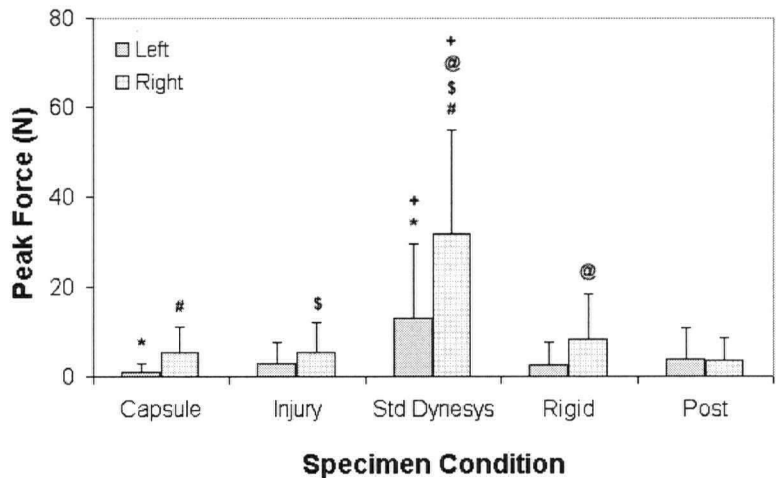


Figure 3.37: Average peak facet loads in flexion with a follower preload. Shown are contact forces within the left and right facet joints for five specimen conditions (Capsule, Injury, Standard Dynesys, Rigid, and Post). #, @, +: $p = 0.0001$; \$: $p = 0.0002$; *: $p = 0.02$.

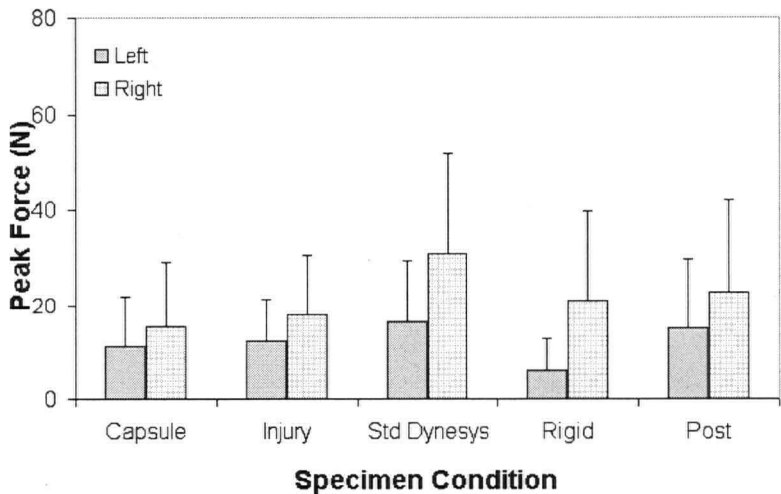


Figure 3.38: Average peak facet loads in lateral bending without a follower preload. Shown are contact forces within the left and right facet joints for five specimen conditions (Capsule, Injury, Standard Dynesys, Rigid, and Post). There was a significant difference in facet load between sides ($p = 0.003$), but not between specimen condition ($p = 0.07$).

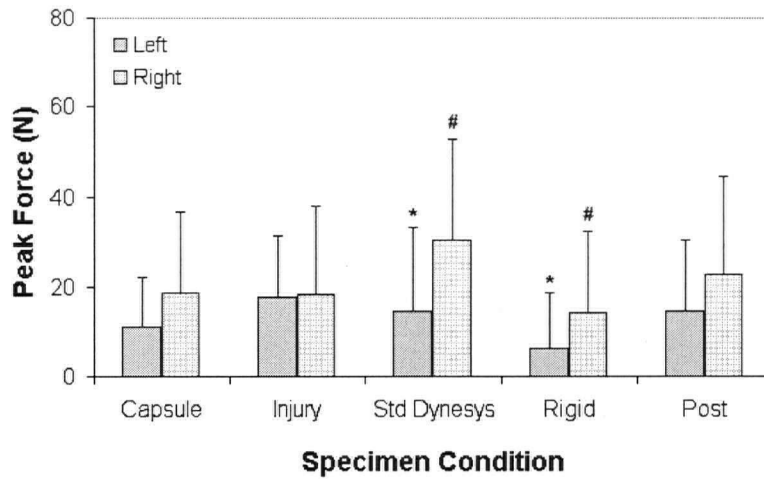


Figure 3.39: Average peak facet loads in lateral bending with a follower preload. Shown are contact forces within the left and right facet joints for five specimen conditions (Capsule, Injury, Standard Dynesys, Rigid, and Post). There was a significant difference in facet load between the Dynesys and rigid conditions (*, #: $p = 0.03$).

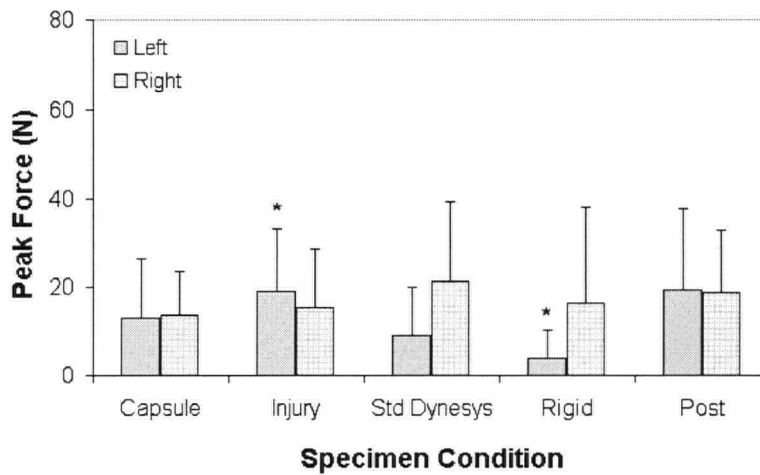


Figure 3.40: Average peak facet loads in extension without a follower preload. Shown are contact forces within the left and right facet joints for five specimen conditions (Capsule, Injury, Standard Dynesys, Rigid, and Post). * $p = 0.02$.

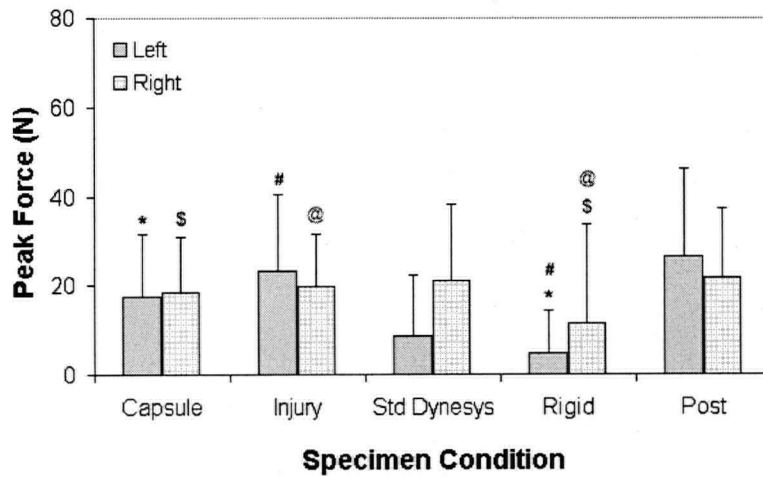


Figure 3.41: Average peak facet loads in extension with a follower preload. Shown are contact forces within the left and right facet joints for five specimen conditions (Capsule, Injury, Standard Dynesys, Rigid, and Post). There was a significant difference in facet loads between the Capsule and Rigid (*, \$: $p = 0.03$) and between Injury and Rigid (#, @: $p = 0.006$).

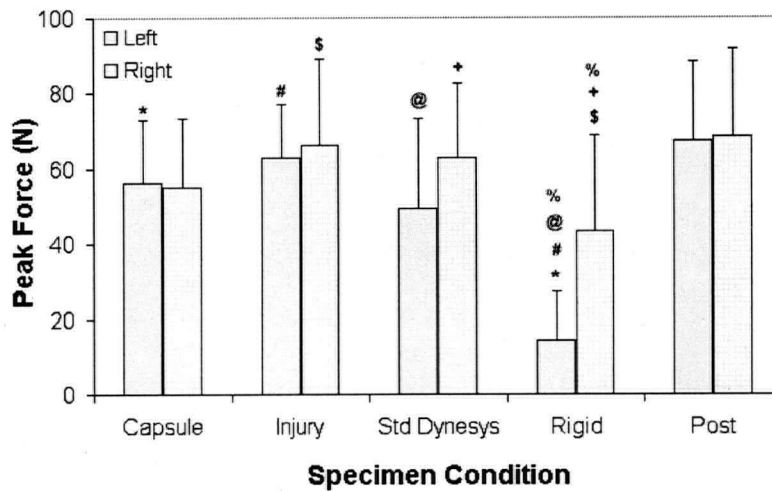


Figure 3.42: Average peak facet loads in axial rotation without a follower preload. Shown are contact forces within the left and right facet joints for five specimen conditions (Capsule, Injury, Standard Dynesys, Rigid, and Post). *, #, @, %: $p = 0.0001$; \$: $p = 0.01$; +: $p = 0.03$.

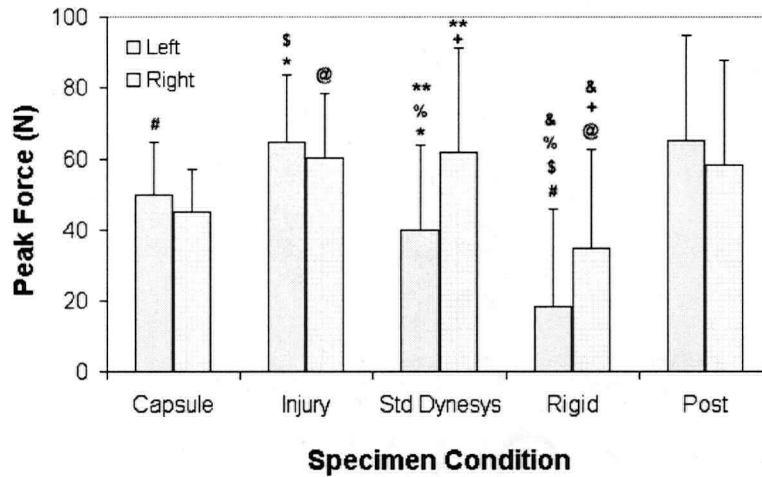


Figure 3.43: Average peak facet loads in axial rotation with a follower preload. Shown are contact forces within the left and right facet joints for five specimen conditions (Capsule, Injury, Standard Dynesys, Rigid, and Post). # $p = 0.0001$; \$ $p = 0.0002$; % $p = 0.0004$; & $p = 0.0009$; + $p = 0.01$; @ $p = 0.02$; * $p = 0.03$; ** $p = 0.04$.

in contact load between the long and short spacers in flexion ($p < 0.01$) and lateral bending ($p < 0.02$). In addition, the difference in facet loads between the long and standard spacers was significant in flexion ($p = 0.03$) and lateral bending ($p = 0.04$) with a follower preload. In extension with a follower preload, there was a significant difference in facet loads between the right and left sides ($p = 0.04$). In all other cases, the length of the spacer did not contribute to significant differences in facet loads.

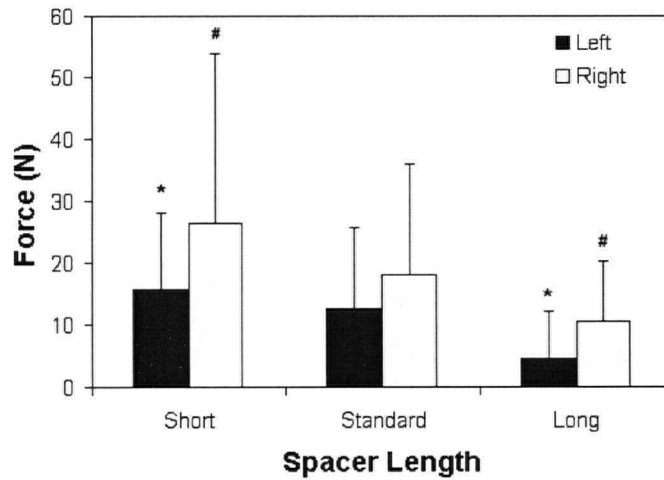


Figure 3.44: Average initial facet loads created by implantation of the three different Dynesys spacers (short, standard, and long). Shown for the left and right sides. Loads are recorded prior to commencement of dynamic flexibility testing. * $p = 0.004$ and # $p = 0.01$

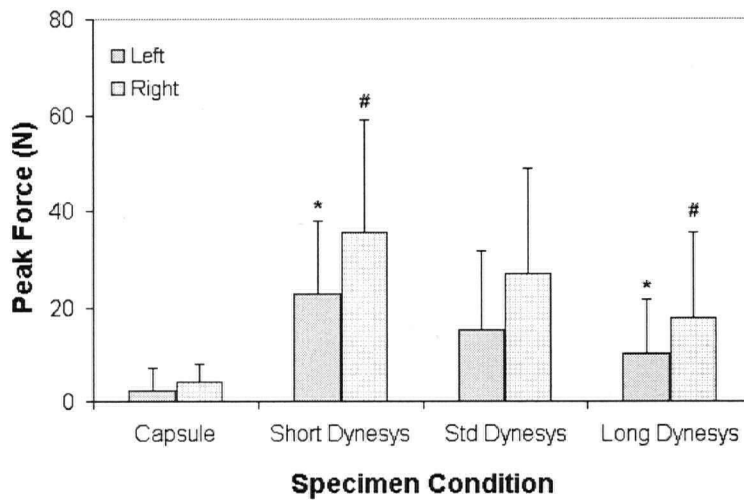


Figure 3.45: Average peak facet loads in flexion without a follower preload (spacer length). Shown are contact forces within the left and right facet joints for the capsule condition and varying spacer lengths (short, standard, and long). Note that the capsule condition was provided as reference only and not included in these comparisons. *, #: $p = 0.01$

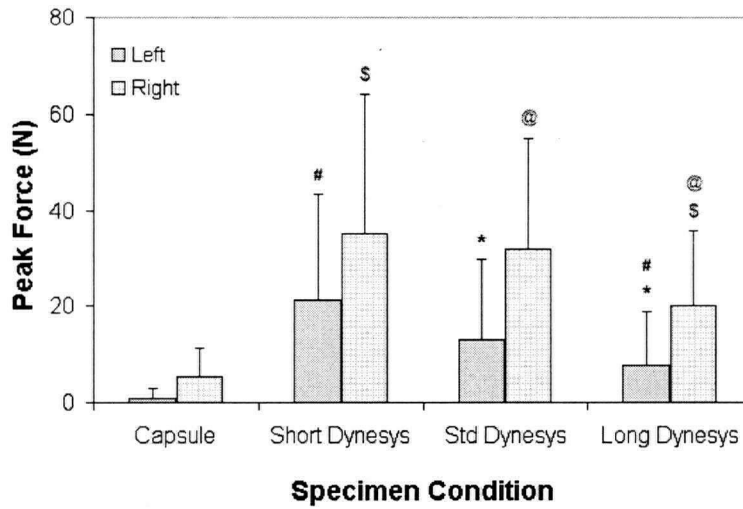


Figure 3.46: Average peak facet loads in flexion with a follower preload (spacer length). Shown are contact forces within the left and right facet joints for the capsule condition and varying spacer lengths (short, standard, and long). Note that the capsule condition was provided as reference only and not included in these comparisons. *, @: $p = 0.03$ and #, \$: $p = 0.003$

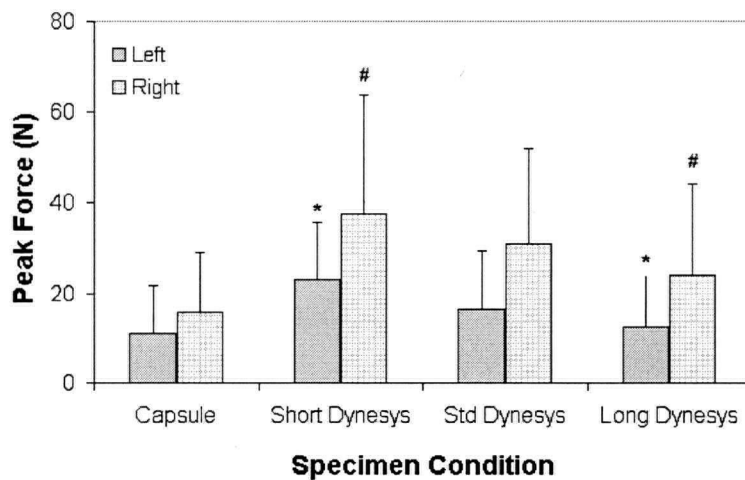


Figure 3.47: Average peak facet loads in lateral bending without a follower preload (spacer length). Shown are contact forces within the left and right facet joints for the capsule condition and varying spacer lengths (short, standard, and long). Note that the capsule condition was provided as reference only and not included in these comparisons. *, #: $p = 0.01$

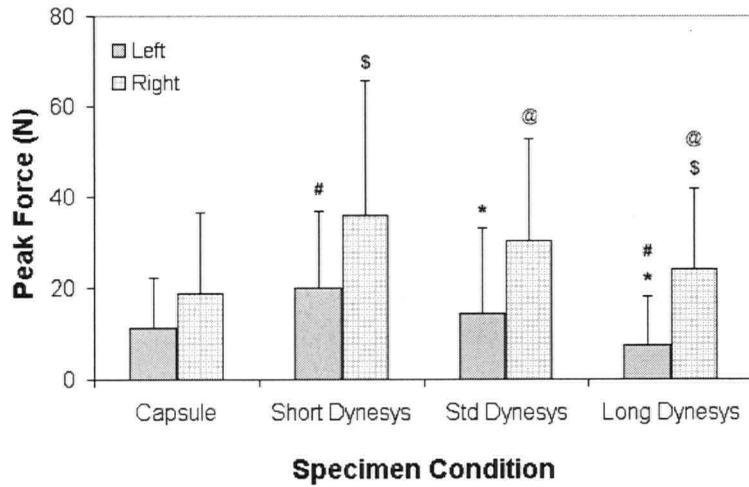


Figure 3.48: Average peak facet loads in lateral bending with a follower preload (spacer length). Shown are contact forces within the left and right facet joints for the capsule condition and varying spacer lengths (short, standard, and long). Note that the capsule condition was provided as reference only and not included in these comparisons. *, @: $p = 0.04$ and #, \$ $p = 0.002$

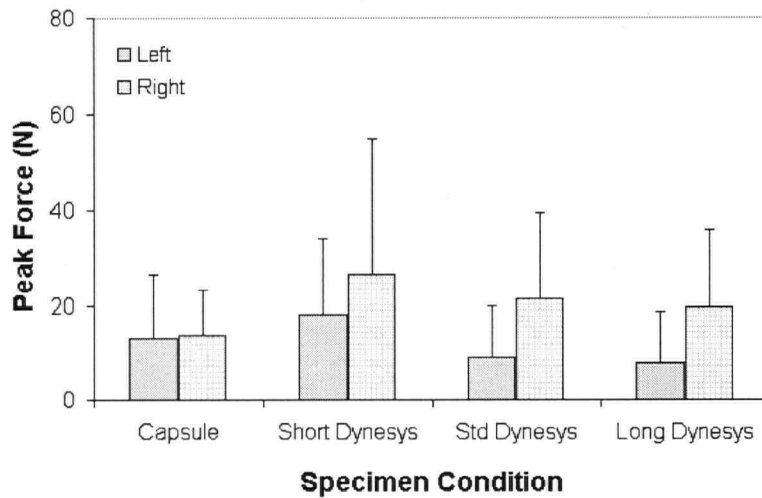


Figure 3.49: Average peak facet loads in extension without a follower preload (spacer length). Shown are contact forces within the left and right facet joints for the capsule condition and varying spacer lengths (short, standard, and long). No significant difference between spacer lengths or side ($p > 0.07$). Note that the capsule condition was provided as reference only.

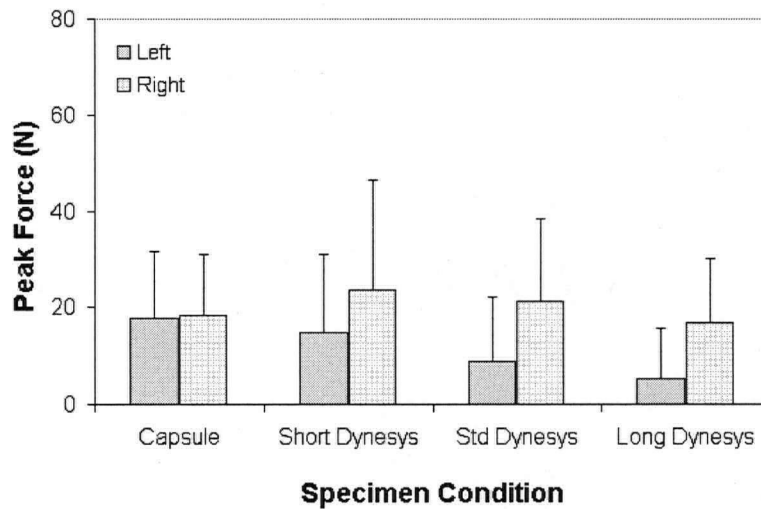


Figure 3.50: Average peak facet loads in extension with a follower preload (spacer length). Shown are forces within the left and right facet for the capsule condition and varying spacer lengths. Facet loads on the right side were significantly greater than those on the left side ($p < 0.04$). Differences between spacer lengths were not significant ($p > 0.08$).

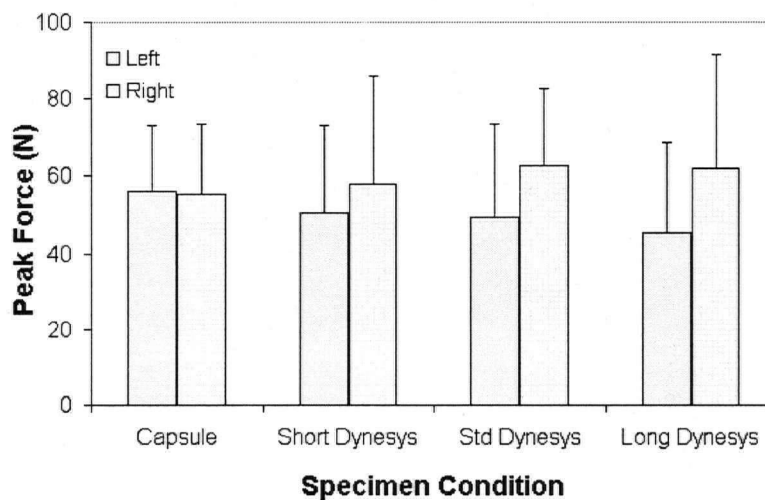


Figure 3.51: Average peak facet loads in axial rotation without a follower preload (spacer length). Shown are contact forces within the left and right facet joints for the capsule condition and varying spacer lengths (short, standard, and long). Differences between spacer lengths or side were not significant ($p > 0.14$). Note that the capsule condition was provided as reference only.

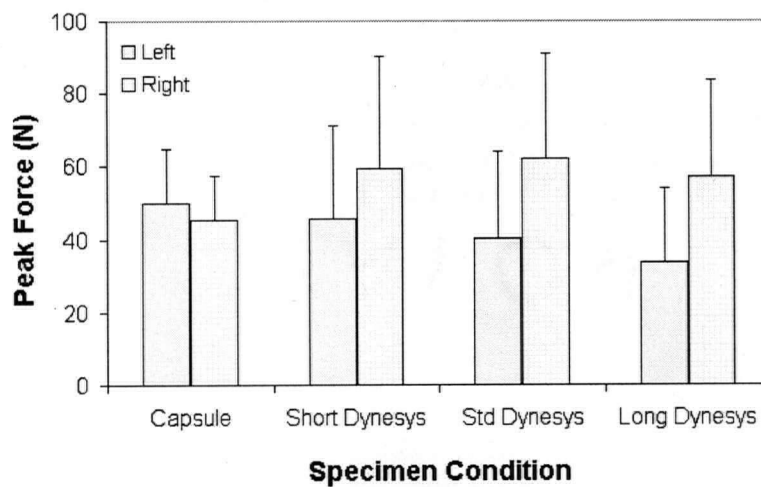


Figure 3.52: Average peak facet loads in axial rotation with a follower preload (spacer length). Shown are contact forces within the left and right facet joints for the capsule condition and varying spacer lengths (short, standard, and long). Differences between spacer lengths or side were not significant ($p > 0.09$). Note that the capsule condition was provided as reference only.

3.3 Intradiscal Pressures

The mean intradiscal pressures measured at L3–L4 during flexibility testing with a compressive follower preload are reported in Tables 3.11 and 3.12. The compressive preload alone, equivalent to the pressure at the neutral point, created an average disc pressure of 0.43 MPa in the intact condition, which was significantly ($p = 0.002$) greater than the 0.37 MPa seen in the Intact-Dynesys condition. The average intradiscal pressure magnitude was greatest in flexion and least in right lateral bending. The other loading directions were fairly similar and fell between the two extremes. A summary of the intradiscal pressures for each specimen is included in Appendix A and details of the statistical analysis in Appendix B.

In flexion-extension, the shape of the pressure-moment curve for the intact specimen typically fit one of three classification patterns (refer to sample curves from three specimens in Figure 3.53). Two specimens displayed curves of Type 1, two of Type 2, and six of Type 3. In spines stabilized

Table 3.11: Mean and standard deviation of absolute intradiscal pressure at L3–L4. Shown with a follower preload for all three directions of loading.

Loading Direction	Intact (MPa)	Intact–Dynesys (MPa)
Extension	0.44 ± 0.16	0.30 ± 0.05
Neutral	0.44 ± 0.08	0.38 ± 0.06
Flexion	0.50 ± 0.16	0.50 ± 0.09
Left Lateral Bending	0.47 ± 0.23	0.41 ± 0.20
Neutral	0.42 ± 0.11	0.34 ± 0.13
Right Lateral Bending	0.27 ± 0.13	0.29 ± 0.15
Left Axial Rotation	0.46 ± 0.08	0.40 ± 0.07
Neutral	0.42 ± 0.11	0.37 ± 0.06
Right Axial Rotation	0.45 ± 0.08	0.40 ± 0.07
Average Neutral	0.43 ± 0.10	0.37 ± 0.09

Table 3.12: Mean and standard deviation of relative intradiscal pressure at L3–L4. Shown with a follower preload for all three directions of loading calculated as the difference in pressure between maximum or minimum rotation and the neutral position. A negative number means that the pressure was lower than the pressure in the neutral position.

Loading Direction	Intact	Intact–Dynesys
	(MPa)	(MPa)
Extension	0.00 ± 0.09	−0.08 ± 0.05
Flexion	0.06 ± 0.12	0.12 ± 0.04
Left Lateral Bending	0.05 ± 0.28	0.07 ± 0.14
Right Lateral Bending	−0.15 ± 0.08	−0.05 ± 0.08
Left Axial Rotation	0.04 ± 0.06	0.03 ± 0.04
Right Axial Rotation	0.02 ± 0.06	0.03 ± 0.02

with the Dynesys there was consistently a linear variation in pressure with applied moment, with a larger intradiscal pressure magnitude in flexion than extension. The Dynesys reduced the variance in pressure magnitude between specimens. In extension, there was a significantly ($p = 0.005$) larger pressure decrease from that in the neutral position with the Dynesys implanted than in the intact condition. There was no difference seen in flexion (Figure 3.54).

The shape of the pressure-moment curve in lateral bending did not display any obvious patterns. However, in right lateral bending, the pressure magnitude was always the same or lower than that in the neutral position. In left lateral bending, there were mixed results. With the Dynesys implanted, the curve became more horizontal compared to the intact condition (Figure 3.55). There was a significantly ($p = 0.01$) smaller decrease in pressure in right lateral bending from that in the neutral position with the Dynesys implanted compared to without the implant. There was no significant difference in absolute magnitudes in either right or left lateral bending between the two conditions (Figure 3.56).

For the intact specimen in axial rotation, there was not a large change in the magnitude of the intradiscal pressure throughout the motion. With the Dynesys, the shape of the curve tended

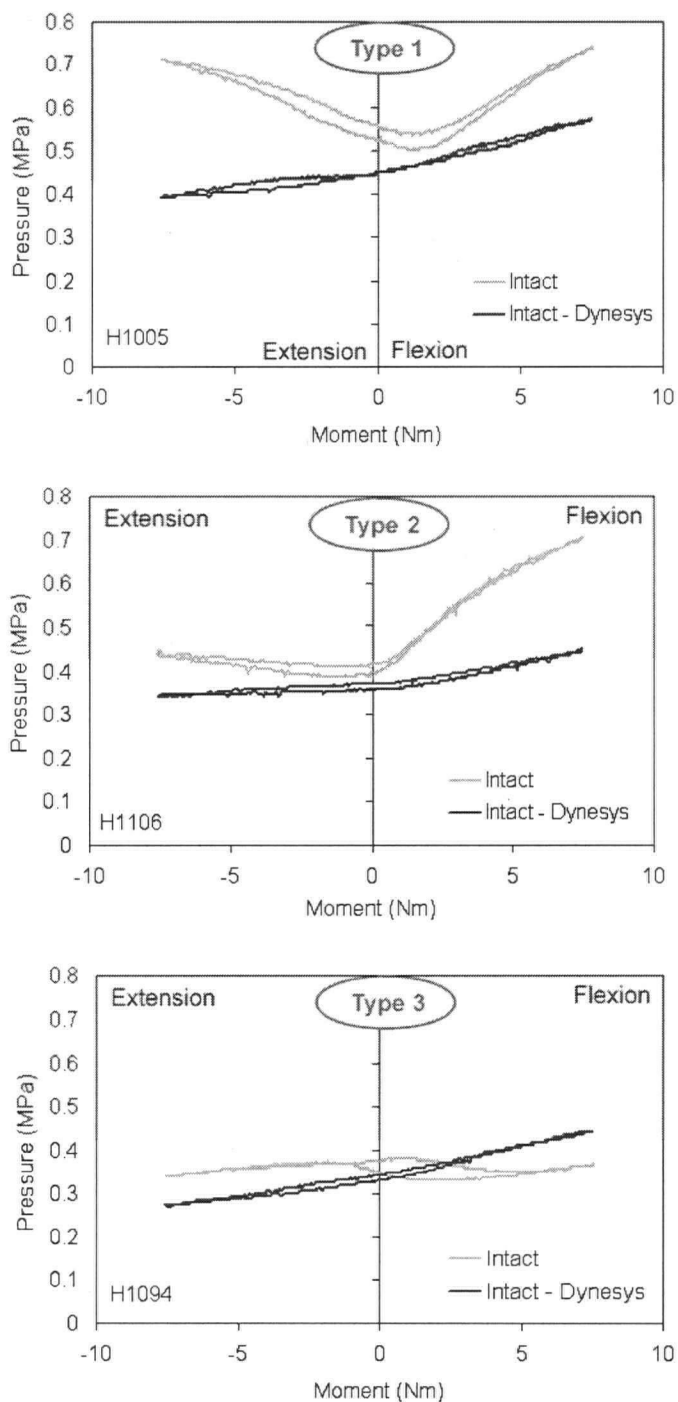


Figure 3.53: Intradiscal pressure vs. applied moment in flexion-extension. Shown for both Intact and Intact-Dynesys conditions from three specimens. These curves demonstrate the three typical shapes that were observed in the specimens.

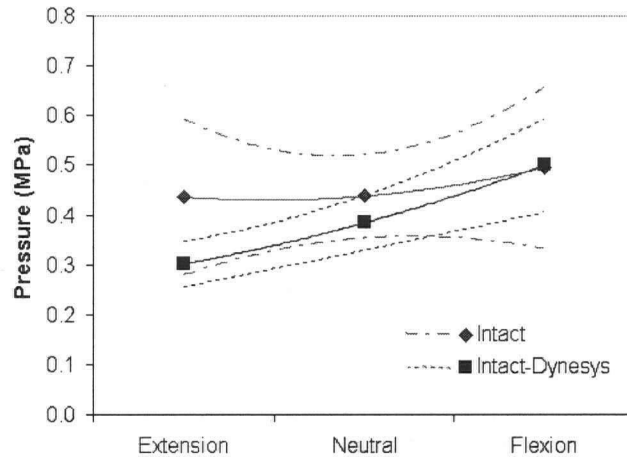


Figure 3.54: Average intradiscal pressure in flexion-extension. Shown for Intact and Intact-Dynesys at maximum extension, the neutral position, and maximum flexion. The mean for 10 specimens is represented by the solid lines and the broken lines are the standard deviation.

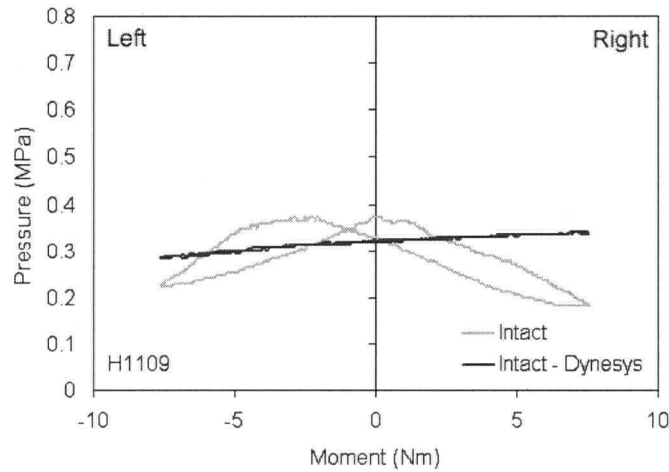


Figure 3.55: Intradiscal pressure vs. applied moment in lateral bending. Shown for both the Intact and Intact-Dynesys conditions from one specimen.

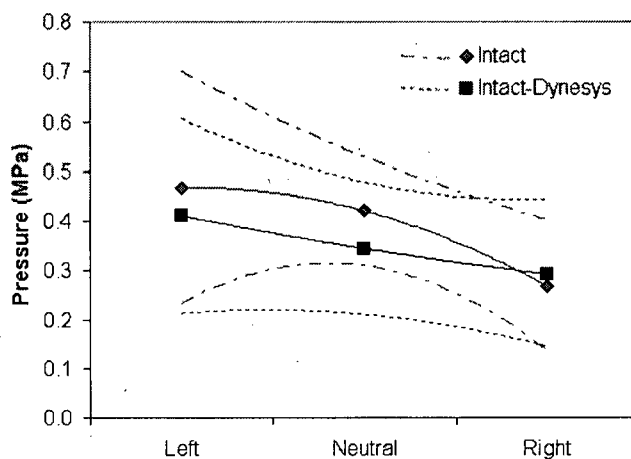


Figure 3.56: Average intradiscal pressure in lateral bending. Shown for Intact and Intact-Dynesys at maximum left bending, the neutral position, and right bending. The mean for 10 specimens is represented by the solid lines and the broken lines are the standard deviation.

to remain similar, but the magnitude decreased (Figure 3.57). Thus, there was no significant difference in change of pressure from the neutral position in right ($p = 0.94$) or left ($p = 0.25$) axial rotation, but significantly lower absolute intradiscal pressure in both right ($p = 0.02$) and left ($p = 0.007$) axial rotation for Intact-Dynesys as compared to Intact (Figure 3.58).

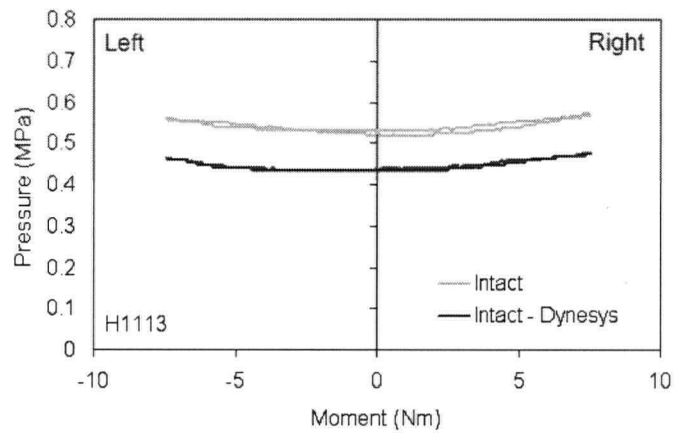


Figure 3.57: *Intradiscal pressure vs. applied moment in axial rotation. Shown for both Intact and Intact-Dynesys conditions from one specimen.*

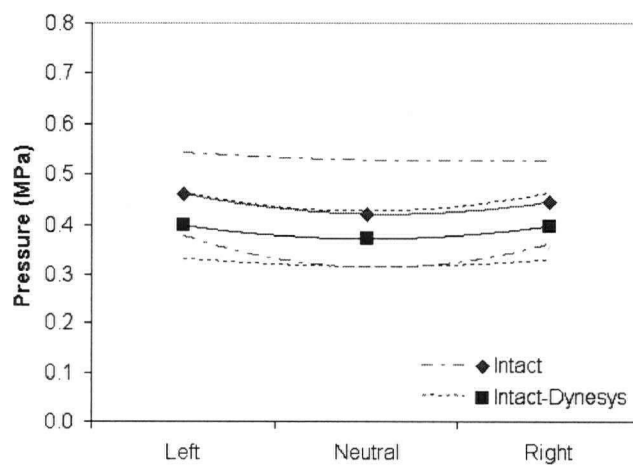


Figure 3.58: *Average intradiscal pressure in axial rotation. Shown for Intact and Intact-Dynesys at maximum left rotation, the neutral position, and right rotation. The mean for 10 specimens is represented by the solid lines and the broken lines are the standard deviation.*

3.4 Facet Joint Imaging

The load applied to the specimen was approximately 7.5 Nm, as determined prior to testing using a six-axis load cell. An eccentric axial compressive force with an average magnitude of 176 N and 331 N was applied to produce a flexion and extension moment, respectively. Forces and moments in the other directions were small in both flexion and extension (Table 3.13).

Images of the facet joints and articular cartilage could be clearly identified in each of the 10–12 slices that the facet joints spanned (Figure 3.59).

3.4.1 Contact Area

The contact between the two facet surfaces was assessed at each of the right and left facet joints using two different techniques.

Contact Measured by Volume

Semi-automated traces were used to segment the cartilage-bone boundary within the joint (Figure 3.60). Segmentation was repeated on two consecutive days. Generally, the repeatability of the individual improved slightly on the second day (from an average of 3.2% to 1.5% standard deviation as a percentage of the mean). The average volume measured was greater in the right facet than in the left in all three loading conditions. The smallest volume was observed in

Table 3.13: Forces and moments applied to specimen for MR imaging.

	Flexion		Extension	
F _x (N)	-0.6	± 2.5	-0.6	± 2.6
F _y (N)	-4.9	± 1.5	-9.5	± 4.9
F _z (N)	176.1	± 8.9	331.0	± 9.9
M _x (Nm)	0.4	± 0.2	1.9	± 0.8
M _y (Nm)	7.5	± 0.2	-7.4	± 0.4
M _z (Nm)	-0.0	± 0.2	-1.0	± 0.8



Figure 3.59: MR image of specimen in unloaded state. Cartilage within the right and left facet joints can be clearly identified in the transverse plane (arrows).

flexion and was an average of 3.0% smaller than the volume measured in an unloaded position. The volume in extension was also smaller than that in the unloaded specimen, but only by a 1.6% difference (Table 3.14).

Contact Measured by Area

In each slice, a B-spline was drawn at the midpoint of the cartilage when no distinction between the borders of the two cartilage layers could be made (Figure 3.61). This was defined as contact of the two articular surfaces. The length of this line was calculated and multiplied by slice thickness to produce a measure of contact surface area. This technique was less repeatable than the previous one where joint volume was measured (average repeatability of 9.2% compared to 3.4% standard deviation as a percentage of the mean). The average contact area at the left facet was greatest in extension, followed by the neutral position, and finally flexion. In the right facet joint, the largest contact area was also in extension, but it was the least in the unloaded position (Table 3.15).



Figure 3.60: *Segmentation of cartilage area in each slice to generate a volume within the joint. Shown is a sample image of the left facet (slice 22) from the specimen loaded in extension. Method 1.*

3.4.2 Validation

Different trends were observed in the contact area measured with Tekscan sensors between the left and right facet joints. On the left side, the contact area was greatest in extension, followed by the neutral (unloaded) position, and finally flexion (Table 3.16). In the right facet joint, the contact was greatest in the neutral position and least in extension.

Measurements with Tekscan were considered the “gold standard” with which to compare the contact area calculated using MRI combined with the second analysis method. The contact area resulting from the MR images was lower in all cases, except in left flexion, than that recorded with Tekscan. The differences ranged from 8 – 65% and an extreme 594% for the left facet joint in flexion.

Table 3.14: Summary of measured joint volume. Repeatability is expressed as the standard deviation as a percentage of the mean. Method 1.

Day	Trial	Left			Right		
		Extension mm ³	Neutral mm ³	Flexion mm ³	Extension mm ³	Neutral mm ³	Flexion mm ³
1	1	162.5	147.7	156.7	247.3	236.6	245.2
1	2	159.5	162.5	153.1	236.1	246.8	255.3
2	3	165.5	167.1	154.4	246.7	257.8	248.0
2	4	167.7	167.4	152.5	247.2	261.0	236.0
Average	Day 1	161.0	155.1	154.9	241.7	241.7	250.3
StDev	Day 1	2.1	10.5	2.6	7.9	7.3	7.1
Repeat	Day 1	1.3	6.8	1.7	3.3	3.0	2.8
Average	Day 2	166.6	167.3	153.4	252.0	259.4	242.0
StDev	Day 2	1.6	0.2	1.3	7.5	2.3	8.5
Repeat	Day 2	1.0	0.1	0.8	3.0	0.9	3.5
Average	Overall	163.8	161.2	154.2	246.8	250.6	246.1
StDev	Overall	3.6	9.3	1.9	8.6	11.1	8.0
Repeat	Overall	2.2	5.8	1.2	3.5	4.4	3.3

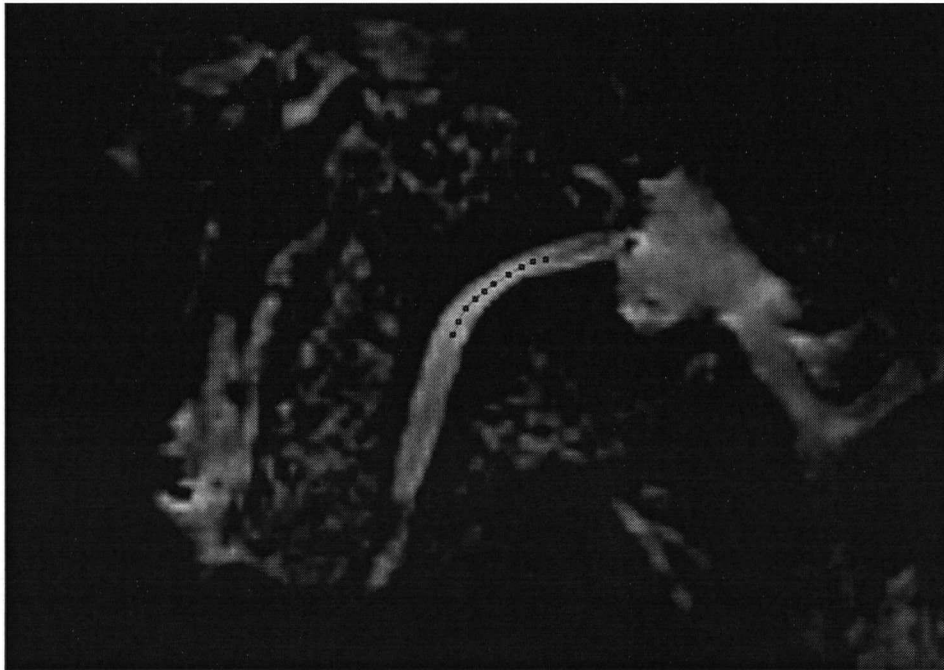


Figure 3.61: *Line of contact between cartilage layers in each slice was identified if the two layers could not be distinguished. Shown is a sample image of the left facet (slice 22) from the specimen loaded in extension. Method 2.*

Table 3.15: Summary of measured contact area. Repeatability is expressed as the standard deviation as a percentage of the mean. Method 2.

Day	Trial	Left			Right		
		Extension mm ²	Neutral mm ²	Flexion mm ²	Extension mm ²	Neutral mm ²	Flexion mm ²
1	1	38.1	25.1	20.8	33.7	23.4	31.7
1	2	37.2	24.2	23.2	34.8	22.5	35.8
2	3	29.7	23.8	20.0	34.4	27.9	30.6
2	4	28.3	19.7	24.6	31.9	24.2	28.8
Average	Day 1	33.7	24.6	22.0	34.2	22.9	33.8
StDev	Day 1	5.1	0.7	1.7	0.7	0.7	2.9
Repeat	Day 1	15.1	2.8	737	2.0	3.1	8.6
Average	Day 2	29.0	21.8	22.3	33.2	26.1	29.7
StDev	Day 2	1.0	2.9	3.2	1.7	2.6	1.3
Repeat	Day 2	3.4	13.3	14.3	5.1	10.0	4.4
Average	Overall	31.4	23.2	22.2	33.7	24.5	31.7
StDev	Overall	4.0	2.4	2.1	1.3	2.4	2.9
Repeat	Overall	12.7	10.3	9.5	3.9	9.8	9.1

Table 3.16: Comparison of contact area measured using Tekscan and imaging.

	Left			Right		
	Extension mm ²	Neutral mm ²	Flexion mm ²	Extension mm ²	Neutral mm ²	Flexion mm ²
Tekscan	36.5	27.5	3.2	36.8	70.9	51.4
MRI (method 2)	31.4	23.2	22.2	33.7	24.5	31.7
Difference	14.0%	15.6%	594%	8.4%	65.4%	38.3%

Chapter 4

Discussion

Dynamic stabilization is an alternative to fusion for the treatment of degenerative problems in the lumbar spine. The Dynesys, a posterior dynamic stabilization system, is one such device that aims to preserve kinematic behaviour and alleviate loading through the facet joints. It is becoming clinically more prevalent, but the biomechanical evaluations in the literature remain sparse. While there has been some investigation looking at the effect of the Dynesys on kinematic behaviour [33, 120], its effect on the pattern of motion has not been examined. In contrast to rigid devices where an analysis of the motion magnitude is sufficient to evaluate effectiveness, it is important to also consider the motion pattern when dealing with dynamic stabilization systems. Previous work has not investigated the effect of the Dynesys system on load transfer through the bridged segment although it is necessary given the goals of the device. Furthermore, there has been no prior evaluation of the effect of the length of the Dynesys spacer on biomechanical behaviour.

An increasing emergence of dynamic stabilization systems has forged the need for establishment of a systematic protocol for biomechanical testing of such devices. It is important to adequately evaluate efficacy, to ensure that the systems successfully meet the intended objectives, and to allow comparison of different devices across studies. This study was meant to be a step in that direction.

The principal objective of this *in vitro* study was to conduct a comprehensive biomechanical evaluation to determine how the Dynesys system affects kinematic behaviour and load transfer through the spinal column and to examine the effect of variation in the length of the spacer on

the biomechanics of the system. Ten human cadaveric lumbar spine specimens were subjected to flexibility testing in flexion-extension, lateral bending, and axial rotation, with and without a compressive follower preload. Analysis included range of motion (ROM), neutral zone (NZ), helical axis of motion (HAM), facet contact loads, and intradiscal pressures.

The results of this study show that the Dynesys affected the kinematic behaviour at the level of interest. Implantation of the Dynesys resulted in a significant reduction in ROM to a level below that seen in an intact spine in all directions of loading (except in axial rotation with a follower preload), with the least significant differences seen in axial rotation. Compared to the ROM of a severely injured specimen, the Dynesys stabilized the segment, but resulted in ROM that was more similar to that of a rigid fixation system in flexion, extension, and lateral bending. The Dynesys tended to reduce the larger NZ of the injured specimen to a magnitude that was below that of the intact specimen. The difference in NZ between the Dynesys and injured conditions was significant, but typically not significant between the Dynesys and intact specimen (except in lateral bending). Implantation of the Dynesys caused a significant posterior shift in the position of the HAM in flexion-extension and axial rotation as well as a significant shift in the orientation of the HAM.

There was an initial load created within the facet joints simply by installation of the Dynesys. Loading at the facet joints tended to remain similar or increase once the Dynesys was implanted compared to those loads observed in the intact spine. Increases in facet load were especially evident in flexion and lateral bending, although not significant in the latter case. In extension and axial rotation, the Dynesys had a tendency to decrease the contact loads on the left side and increase them on the right side, but the differences were not significant.

Stabilization with the Dynesys generated a linear variation in intradiscal pressure with applied moment in flexion-extension, with the higher pressure observed in flexion. In lateral bending and axial rotation, however the Dynesys created a relatively constant pressure throughout the motion cycle. The absolute magnitude was reduced in axial rotation with the Dynesys implanted.

In all three loading directions there was an increase in ROM with the long spacer and a reduction in ROM with the short spacer compared to the standard spacer. The differences in ROM observed with the various spacer lengths were significant in all directions of loading without a follower preload, but the most significant change was seen in axial rotation. There were not large significant differences in NZ between the different spacer lengths. Only in axial rotation were there significant differences in location of the HAM between spacer lengths. Generally, the shorter the spacer, the more posteriorly the HAM was located.

The long spacer typically decreased facet loads, while the short spacer increased facet loads when compared to the standard length spacer. The differences in magnitude of peak facet load were significant between the long and short spacers only in flexion and lateral bending.

4.1 Limitations and Assumptions

The results of this study must be interpreted in light of the various limitations and assumptions made in its design and execution.

4.1.1 Clinical Representation

The pedicle screws were cemented in place using PMMA to eliminate loosening at the bone-screw interface since that was not the focus of this study. This is typically not done as part of the surgical procedure so it may not be clinically relevant. In a multi-centre clinical study in which the Dynesys was implanted in 83 patients, follow-up at a mean time of 38.1 months revealed radiological evidence of screw loosening in seven cases [132]. Thus the integrity of the bone-screw interface may be an important factor in the function of this particular system. The stiffness of the bone-screw interface may potentially influence the function of the implant with respect to the kinematic and loading behaviour of the segment.

Due to the *in vitro* nature of this study, the results are limited to reflecting only immediate post-operative behaviour of the device. Time is a critical factor in adequately evaluating the outcome of a surgical procedure. Short and long term biomechanical function can be affected by a wide variety of *in vivo* conditions, including the body's response to the implant.

The stiffness of the spacers was modified for testing in a room temperature environment. The device was implanted using the manufacturer's recommended operative procedure with 300 N of tension applied to the PET cord. This pre-tension was equivalent to that which is imposed on the system in vivo. In hindsight, the softer material of the spacer likely led to a greater degree of compression in this study, as compared to the intra-operative situation. Thus, the long spacer may provide a better representation of the in vivo situation than the standard length spacer.

4.1.2 Specimen Loading

The magnitude of the applied rate of rotation in this study was only approximate. After the study concluded, some undesirable slippage along the joints of the spine machine arm was discovered, which led to a rotation rate that was proportional to the stiffness of the specimen. The variability in rotation rate was less than $0.4^\circ/\text{s}$ in flexion-extension. Slight reductions in rotation rate with the Dynesys implants were due to a small increase in stiffness once the device was implanted. However, if this did affect the results, the tendency would be towards more conservative measurements. An increase in stiffness would cause a decrease in the applied rotation rate, and due to the viscoelastic properties of the spine, this would lead to an increase in ROM. Therefore, in this study, the ROM resulting from testing with the Dynesys implanted may in fact be even smaller than what was measured.

With any sort of complicated and time-consuming in vitro testing protocol, degradation of the specimen becomes a concern as a result of ambient temperature, air exposure, loading rate, and duration. The loads applied to the specimen in this study were as recommended in the literature [144] to produce motion of physiological magnitude, but not cause permanent deformation of the tissues. Specimens were kept moist by periodic application of water. One study showed that the mean value of the maximum displacement did not differ significantly when testing was performed over 13 consecutive days [100]. In that study, specimens were stored at 4°C between testing days, however only two tests were conducted each day. During relatively continuous testing, the properties of a specimen were estimated to change less than

10% if testing was contained within a 20 hour period at room temperature [144, 140]. The test duration in the present study was below this time limit. A final test condition (Post) was included at the end of the test period for comparison to the results from the injured specimen to ascertain that specimen properties were not in fact altered over the course of testing. A significant increase in NZ was discovered in the post condition compared to the injury condition in lateral bending with a follower preload ($p = 0.03$). In all other cases, the ROM, NZ, HAM, and facet load measurements were not significantly different between the injury and post conditions. Therefore there is validity in the assumption that the specimen properties were unchanged over the test day.

In vitro flexibility testing to investigate the natural behaviour of the spine is limited due to very complicated true loading conditions. This is particularly evident by the lack of musculature and trunk weight in the cadaveric spine segment. A compressive follower preload has been gaining popularity in in vitro biomechanical testing to simulate the weight of the trunk and local muscle forces. A follower preload allows the in vitro spine to withstand physiologic compressive loads without buckling [109] and does affect the flexibility of the cadaveric spine with a reduction in motion [108, 116]. However, the technique used to apply a follower preload can induce artefact moments and forces into the system [20]. To best achieve isolated compressive forces and moments, a constrained-type method of preload application was advisable in flexion-extension and lateral bending, while a relatively unconstrained technique was determined best for axial rotation [20]. In the present study, the follower load technique remained constant for the three loading directions. A relatively constrained technique was employed, which was expected to generate low artefact moments, but higher artefact shear forces. The inclusion of a follower preload was a strength of this study, however, its application was not perfect. In lateral bending, there was a larger degree of hysteresis with the follower preload than in other loading directions (Figure 4.1). This can likely be attributed to friction within the system and the lateral fixation of the follower preload. An interesting phenomenon was also observed in lateral bending; the injured specimen subjected to a follower preload experienced a reduction in ROM by 42% compared to that seen in the intact spine. This was opposite to what was seen without a

follower preload, where the injury increased ROM by 32%. It remains unknown whether this is an issue with the follower load technique or if the alteration in mechanics is also present in vivo. In addition, the position of the follower load cables were optimized for the intact specimen in the neutral position to create minimal rotation in the sagittal plane upon application. The follower load was placed along the centre of rotation of each of the segments. This corresponded to the AP position of the HAM in flexion-extension. The HAM was different for the various directions of loading and ideally, a follower preload should reflect this. The condition of the specimen also had an effect on the position of the HAM. Application of the follower preload was optimized based on the intact condition, so with the Dynesys, for example, the HAM moved posteriorly while the position of the follower load remained unchanged.

Furthermore, global muscle forces have a large effect on spinal stability and influence load through the column [22, 94, 114, 143]. Global muscles, such as erector spinae and rectus abdo-

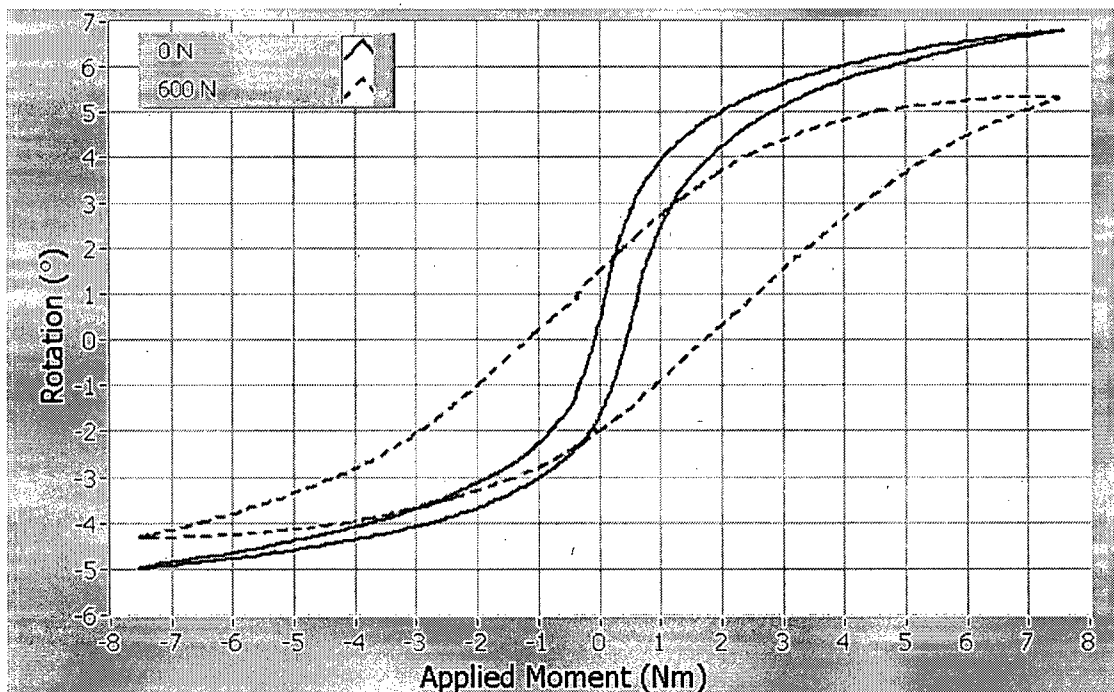


Figure 4.1: Motion with follower load in lateral bending. Shown is rotation vs. applied moment for a typical intact specimen. There was a larger degree of hysteresis during the flexibility test with a follower preload than without.

minis, have been simulated in vitro and optimized with measured in vivo intradiscal pressures and internal fixator loads [144]. Muscle forces have been found to greatly influence spinal implant loads [116], yet very few in vitro studies implement muscle forces during flexibility testing. Some groups also argue that loads exerted on the bony aspects of the spinal column would be transferred to the intervertebral disc as a compressive load, which can be simulated by a follower preload [1, 108]. The present study did not include muscle forces other than those that are incorporated into the follower preload.

4.1.3 Kinematics

It is well-known that the accuracy of the HAM is lower under small rotations. The standard deviation of the HAM with the Dynesys implanted was relatively large. The position and direction errors are inversely proportional to the rotation magnitude [147]. With the Dynesys implanted, the motion was small, hence, in some cases the calculated HAM was ill-defined and excluded from the analysis. No more than two specimens were excluded concurrently. Furthermore, the direction and rotation magnitude errors of the HAM are inversely proportional to the marker distribution radius and to minimize the error, the marker distribution radius should be sufficiently large. Errors in the position of the HAM are minimal if the HAM coincides with the centre of the marker distribution [147]. Attempts were made to ensure that each marker carrier was rigidly attached close to the body that it represented so that the markers were near the HAM. Calculation of the HAM was validated in this study for motion about a fixed, known axis with a similar marker configuration and optoelectronic camera set-up. The position of the HAM was within 1.5 mm and its attitude within 0.2° of the known axis of rotation for motions ranging from about 10° to 34° . The accuracy of the HAM was also investigated at small rotations (Figure 4.2). The calculated HAM orientation became greater than 5° from the known orientation for rotations below 0.6° . The HAM position became marginally (less than 20 mm) different between 0.6° and 2.2° and greater than 20 mm for rotations less than 0.6° .

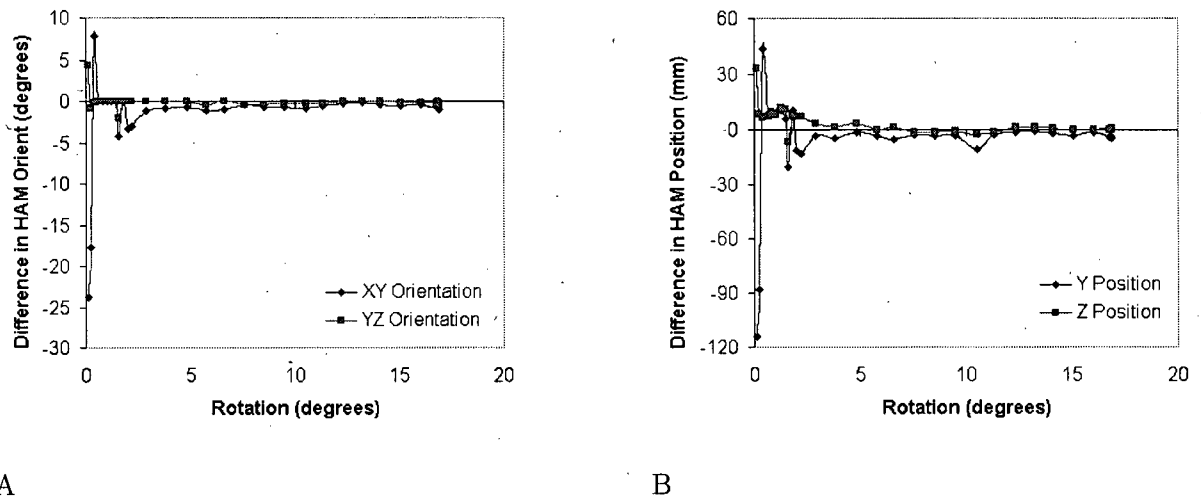


Figure 4.2: *HAM validation. Accuracy in A) orientation and B) position of the calculated HAM compared to the known axis. HAM is adequate for rotations greater than 0.6° .*

4.1.4 Facet Loads

The accuracy and repeatability of the use of Tekscan sensors to directly measure facet loads in the lumbar spine has been evaluated [146]. Accuracy was determined by applying a known compressive load to the natural facet joint in a materials testing machine. Repeatability of the sensors was assessed in the natural facet joint under flexibility testing in axial rotation and flexion-extension. That study found that the Tekscan 6900 sensors overestimated an applied load by $18\% \pm 9\%$, $35\% \pm 7\%$, and $50\% \pm 9\%$ for compressive forces of 100 N, 50 N, and 25 N, respectively. The repeatability for force and area measurements, as the standard deviation as a percentage of the mean, was 4% and 5%, respectively, in axial rotation and 7% and 10% respectively, in extension. The repeatability found using the sensor in the spine was similar to that observed using a sensor of different geometry in the patellofemoral joint [145]. One explanation for the lower accuracy found at 25 N was that the measured loads were at the very low end (5%) of the operating range of the sensor. The loads in the current study were of a similar magnitude and thus often fell in this lower accuracy zone. A sensor with a lower measurement range would be ideal, but is not currently offered by the manufacturer for this sensor geometry. Despite the low accuracy for measurement of small forces, relative differences

in loading can still be assessed.

In addition, the calibration protocol for the sensors greatly influenced the measured results. A linear calibration was found more reliable and produced a higher accuracy than a two-point power law calibration for the range of loads observed [146]. The results of the Tekscan validation also show that there would be no effect on repeatability if the sensors were calibrated once for each series of flexibility tests (six tests total: 3 loading directions, 2 preload conditions) or prior to each and every test [146]. Calibration of these sensors has not been addressed frequently in the literature, but use of a similar sensor in the knee was done using linear [51] or two-point [145] calibrations. Recently, a group using similar sensors for measurement of load in the ankle, albeit a much more abusive use of the sensors due to high compressive and shear stresses and articular incongruities, reported significant variation amongst the individual sensing elements on the array [9]. They also saw an increase in variability due to functionally induced changes. The group developed a novel device to apply a known load, and along with a finite element model of the loading, assigned a calibration parameter to each sensing element. The calibration could also be adjusted over the course of an experiment to account for degradation of individual sensing elements. In the present study, a single calibration curve was used for the entire sensor.

The accuracy of the sensor is akin to other methods of facet load measurement. In canine lumbar spines, the accuracy of both the strain gauge method and Fuji Film were assessed [12]. The strain gauges overestimated a known applied load by 3 – 10%, whereas the pressure film underestimated the load by 10 – 47%. The accuracy of load measurement using the pressure film was lower at smaller loads.

Direct facet load measurement required sectioning of the joint capsule, which was assumed to be equivalent to the intact case. Studies using canine lumbar spines have reported that the effect of capsule transection on facet loads was minimal and inconsistent [58]. Kinematically, there were no significant differences ($p > 0.05$) found in this study between the intact specimens and once the joint capsules were sectioned, for ROM, NZ, and HAM. In addition, insertion of a film into an articular joint may have an effect on the contact mechanics. A study using Fuji

Film and finite element analysis found that the film would change the maximum true contact pressure by 10 – 26% depending on the loading, geometry of the joints, and properties of the cartilage [150]. The effective thickness of the Fuji Film was 0.3 mm while the thickness of the Tekscan sensors used in this study was 0.1 mm. The thinner Tekscan sensor would be expected to have a smaller effect than that which was determined with the Fuji Film.

In this study, facet loads were compared at identical magnitudes of applied moment. Comparison of facet loads at identical rotations, as in a displacement controlled investigation, would clearly describe the effect of the implant on posterior element loading since facet load is dependent on the degree of rotation. However, it was felt that a load controlled study was more applicable and demonstrated greater clinical relevance since the motion with these devices is not the same as in an intact condition. Even so, the loads with the Dynesys implanted were much higher than those for an intact specimen at the same rotation. Because the load magnitude did depend on rotation and the ROM was smaller with the Dynesys, it would be difficult to argue that a reduction of facet loads was solely a result of the implant. Comparing the Dynesys and injury conditions, there was generally not a reduction in facet load, so this was not an issue. In addition, the long spacer typically caused an increase in motion, yet a decrease in facet load compared to the standard length spacer. Since ROM increased with the long spacer, the reduction in facet load can be attributed entirely to the implant.

4.1.5 Assessment of Facet Contact

A limitation of this exploratory part of the study was the use of a cadaveric specimen, as opposed to in vivo imaging. The condition of the specimen can affect the results since the signal detected by MR is largely due to the nuclear magnetic moment of hydrogen, which is very prevalent in the body, as 75% of the body is composed of water. Chemically, changes occur in the tissue after death and while the effect of death and freezing does not affect the kinematic behaviour produced by the bone and disc, the intensity of the MR signal may be affected. For this reason, as little soft tissue as possible was dissected from the specimen and every effort was made to keep the specimen moist. In addition, saline bottles were placed alongside the

specimen in the scanner to improve the signal attenuation.

A drawback of minimizing the soft tissue dissected from the specimen was that the bone surface was not directly exposed and visible. After the imaging was completed, soft tissue was removed in order to section the joint capsules for insertion of the Tekscan. The right facet joint was found to be very hypertrophied and not representative of a normal healthy joint. This likely had an effect on the contact within the joint and the techniques utilized to measure contact. Some of the bone had to be removed on the right side in order to insert the Tekscan. The effect of this on the contact area measurement remains unknown and the results for assessment of the contact within the right facet should be interpreted taking this into consideration. The left facet, however, did not display any obvious abnormalities and therefore likely provided a better representation of the techniques for contact area measurement.

Image Artefacts

As with any imaging modality, MRI suffers from artefacts. The basic assumption of MRI is that the frequency of precession of a spin is only dependent on the magnitude of the applied magnetic field gradient at that point [18]. There are two main artefacts that affect this assumption and are important to consider in this particular application.

Chemical shift artefacts occur due to the differences in electron environments between fat and water. This causes shielding that leads to slight differences in the Larmor frequency between the two substances and emerges during frequency encoding where the Larmor frequency is used to determine spatial position. The net result is a chemical shift artefact at the interface between fat and water. It occurs at interfaces which run perpendicular to the frequency encoding direction and appears as a dark line on the edge of one side of the structure (image void) and a bright line on the other side (image superposition) [7]. In this application, the main concern is chemical shift artefact occurring at the cartilage-bone interface [73]. The frequency encoding direction in this study was parallel to the main direction of the facet surface to minimize chemical shift artefacts. However, the curved nature of the facets means that at some locations, the facet surface was perpendicular to the frequency encoding direction likely leading

to the production of some artefacts. The effect was assumed to be fairly negligible in this case, but was acknowledged as a potential source of error because of a misrepresentation of either the cartilage or bone surface. Looking at the set-up scan in the sagittal plane (perpendicular to the frequency encoding direction), visually there did not appear to be significant dark and bright areas on the surfaces of the vertebra, indicating that chemical shift artefacts were minimal.

Susceptibility artefacts occur as a result of inhomogeneities in the static magnetic field. Differences in magnetic susceptibility between bone, tissue, and air means that the local field may not be homogeneous [18]. The magnitude of the artefacts increases proportionally with the external magnetic field strength and is proportional to the difference in susceptibility between two regions. At an interface, the susceptibility artefact depends on the size and shape of the regions with different susceptibility and the direction of the external magnetic field with respect to the object [7]. It is commonly seen at bone-air interfaces. Gradient echo pulse sequences do not rephase the phase shift induced by the magnetic inhomogeneity at the centre of the pulse, so are affected more by the differences in magnetic susceptibility. The longer the echo time, the greater the signal loss due to susceptibility [7]. This artefact is presented in images as dark and white disturbances of the tissue. In this study, it is anticipated that the presence of air in the joint could have led to the occurrence of susceptibility artefacts, which could affect the representation of the bone surface in the image. The echo time was relatively short, however, which would tend to minimize susceptibility artefacts.

Image Analysis

The individual responsible for segmentation of the cartilage was newly exposed to this field and did not have vast experience in tissue identification on MR images. Also, in many cases, it was difficult to identify whether a distinction between the two layers of cartilage was present. Both of these were subjective and were a limitation of the study.

The accuracy of the volume or area calculations could be further improved by interpolating the measurement between slices, as opposed to multiplying by the slice thickness.

Validation of Results using Thin Film Sensors

A precise value depicting the accuracy of the Tekscan for measurement of contact area is not known. It can be assumed that the accuracy is better than its accuracy for measuring force magnitudes. Since no calibration was required, a sensel was either loaded or unloaded. However, the accuracy would likely be affected by a partial volume effect that depends on the area of an individual sensing element. The maximum error due to partial volume effects would be one sensel (sensel area = 1.62 mm²) around the entire border of the true area. Therefore, as the contact area increases, measurement accuracy improves. Contact area measured using the sensors also would be affected by the geometry and contour of the articulating surfaces and the degree with which the film conforms to the joint surface. In this study, the Tekscan provided an alternative method of contact area measurement with which to compare the proposed imaging technique.

4.1.6 Statistical Analysis

The underlying assumptions of the statistical analysis were that there was equal variance between the conditions and that the data were normally distributed [38, 54, 153]. A MANOVA analysis was advantageous compared to ANOVA because the assumption of sphericity was not required [54, 153]. Sphericity is satisfied if correlations between all dependent data groups are equal and variances of the different data groups are equal.

Shapiro-Wilks test was used to analyze the normality of the data. Approximately 25% of data groups showed a significant result from the Shapiro-Wilks test ($p < 0.05$), implying that a non-normal distribution existed. A group of data was defined as the corresponding measurement for the ten specimens under one loading condition (eg. axial rotation with a follower preload). Fortunately, analysis of variance is robust and handles both heterogeneity of variances and deviations from normality very well if the number of specimens in each data group are equal or nearly equal [153], which was the case in this study.

Repeated measures designs can also be affected if there are effects of the treatment order [153].

In this study, the order of four of the conditions (standard, long, and short Dynesys spacers, and rigid fixation) was randomized to minimize differences arising due to test sequence.

4.2 Comparison with Literature

4.2.1 Kinematic Behaviour in the Literature

Intact ROM at the L3–L4 level determined in this study was comparable to the range of values reported in the literature in all directions of loading [36, 81, 104, 120, 151] (Table 4.1). Small discrepancies between studies is likely a result of different magnitudes of applied moments, techniques of load application, loading rate, and the presence and magnitude of a compressive follower preload, as well as the method used for creating the preload.

The centre of rotation (COR) for an intact lumbar segment has been described by White and Panjabi [139]. In flexion, the COR was located in the anterior portion of the disc, whereas in extension, the COR was located just posterior to the vertebral bodies at the level of the disc (Figure 4.3). The COR was reported to lie in the right side of the disc in left lateral bending and in the left side of the disc in right lateral bending. In axial rotation, the COR was located

Table 4.1: Range of motion comparison for intact specimen. Values represent ROM in degrees for an intact specimen *in vitro*. Applied moment for each study is also provided. In lateral bending and axial rotation, the motion is shown as right/left or total. Numbers in parentheses are the standard deviations, where available.

Study	Load	Flexion	Extension	Lateral Bending	Axial Rotation
Panjabi [104]	7.5 Nm	6.5	2.0	5.0/4.5	1.8/2.0
Fujiwara [36]	6.6 Nm	3.0	2.4	7.3	2.3
Mimura [81]	10 Nm		12.8	11.0(2.5)	2.5(2.0)
Schmoelz [120]	10 Nm	4.5	4.0	4.0/5.0	1.0/1.0
Yamamoto [151]	10 Nm	7.5(0.8)	3.7(0.3)	5.8(0.5)/5.7(0.3)	2.7(0.4)/2.5(0.4)
Freudiger [33]	18.3 Nm	9.6(1.7)	2.1(1.0)		
Present study	7.5 Nm	3.7(1.5)	3.3(1.5)	3.5(1.4)/4.1(1.5)	2.2(0.9)/1.2(0.6)

in the posterior nucleus and annulus. These positions were similar to the positions of the HAM found in the current study (Figure 4.3), except in lateral bending where the HAM in both left and right lateral bending were found to be located centrally across the width of the vertebral body. Differences between the two sets of results in flexion-extension occurred largely because in this study, the HAM was reported over the entire range of motion, not from the neutral position to maximum rotation. Small discrepancies in lateral bending and axial rotation may be attributed to differences in specimen loading, magnitude of motion, initial orientation of the specimen, and the fact that the former was a two-dimensional analysis.

Other studies have also reported a HAM in axial rotation that was located slightly anterior to the posterior wall of the vertebral body with superior-inferior and anterior-posterior components to its orientation [49, 93]. This was consistent with the results of the current study. In lateral bending, the HAM was previously reported to be oriented in the anterior-posterior direction [93]. In flexion, the HAM was found to be oriented to the left of the specimen and located about 13 mm anterior to the posterior vertebral wall in the mid-sagittal plane [93]. That same study

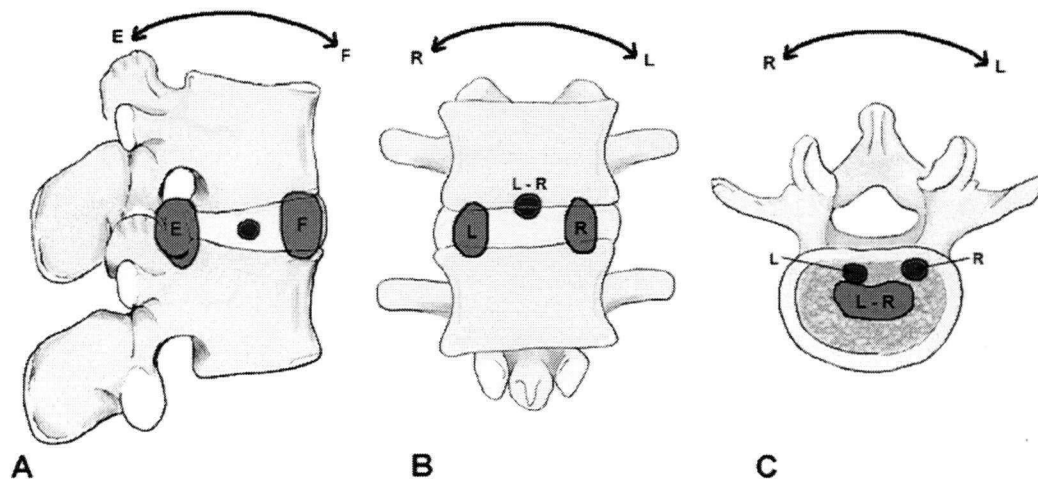


Figure 4.3: Helical axis of motion comparison for intact specimen. A) flexion-extension (F-E), B) lateral bending, and C) axial rotation. The larger areas are the approximate locations of the centre of rotation reported by White and Panjabi [139] and the smaller dark areas provide qualitative results from the present study. L and R indicate right and left motions. Figure modified from White and Panjabi, 1990.

reported the HAM orientation to be to the right of the specimen in extension, with a position about 11 mm anterior to the posterior wall. These findings were also comparable to the results of the present study.

Intersegmental ROM observed at the implanted level with the Dynesys was similar to that obtained by Schmoelz et al. [120] in all loading directions except extension (Table 4.2). In general, the ROM was only slightly greater in the Schmoelz study which may be explained by their larger applied moment (± 10 Nm). In extension, however, the difference in ROM between the two studies was more considerable. Schmoelz et al. observed a ROM with the Dynesys that was in the range of the intact specimen, whereas we saw a decrease in the motion by an average of 67%. The ROM reported by Freudiger et al. [33] in flexion-extension was much greater than the values observed in the present study. This might be due to a substantially larger applied moment and a different mechanism for application of the load. However in that study, the model did not include a simulated destabilization so motions may have been even greater had an injury been created. Freudiger et al. did notice a significant decrease in ROM of nearly 50% in both flexion and extension with the Dynesys compared to an intact specimen, which was consistent with the results of the current study.

Table 4.2: Range of motion comparison with Dynesys system. Values represent ROM in degrees for a specimen with the Dynesys system implanted (standard length). Applied moment for each study is also provided. In lateral bending and axial rotation, the motion is shown as right/left.

Study	Load	Flexion	Extension	Lateral Bending	Axial Rotation
Freudiger [33]	18.3 Nm	4.3	1.1		
Schmoelz [120]	10 Nm	1.0	4.0	1.8/1.1	2.0/1.7
Present study	7.5 Nm	1.0	1.1	0.9/1.1	1.7/1.5

4.2.2 Facet Loads in the Literature

Comparison of the measured facet loads in this study to work by other groups was limited strictly to the intact case since there have been no previously published biomechanical studies examining the facet loads with the Dynesys implanted. In flexion, the facet joints have been found to support very minimal or no load [118, 125, 152]. This was consistent with the findings of the present study. Under varying degrees of extension, previous work has found that the facet joints support about 10 – 40% of the applied load [28, 68, 125, 152] or between 52 N and 130 N [42, 118] for an applied moment comparable to the one in this study (Table 4.3). A rough conversion of the results of the current study based on average three-dimensional quantitative lumbar anatomy [99] showed an average facet load of approximately 13% of the applied load or 27 N. This was within the range of most of the literature, although at the lower end of the spectrum. In lateral bending and axial rotation, the loads measured in this study were smaller than most of the values in the literature (Table 4.3). Discrepancies between these results and the work of others are likely due in part to differences in facet load measurement technique. The studies by Goel et al. [42] and Shirazi-Adl et al. [127] were finite element analyses and Schendel et al. [118] measured facet loads indirectly using strain gauges, in contrast to the direct measurement technique used in this study.

It is also interesting to note, however, that there is considerable variation in facet loads amongst the previous studies themselves, not only in magnitude of contact load, but also in the relative load compared across different motions. Goel et al. [42] observed facet loads of greater magnitude in lateral bending than in extension, whereas Schendel et al. [118] reported the largest facet loads in extension, followed by lateral bending, and finally axial rotation. In the current study, the highest facet load magnitudes were seen in axial rotation, followed by extension, and lastly in lateral bending, in which the contact loads were of a relatively small magnitude. These results appear somewhat contradictory and highlight some of the ambiguity in the precise function of the facet joints and the need to further clarify the contact mechanism within the joint.

Table 4.3: Comparison of intact (or capsule cut) facet loads in extension, lateral bending, and axial rotation. Values are either a force in Newtons (with applied load in brackets) or as a percentage of the applied load.

	Extension	Lateral Bending	Axial Rotation
Goel [42]	52 N (7 Nm)	90 N (7 Nm)	
Schendel [118]	130 N (8 Nm)	104 N (3 Nm)	30 N (7.5 Nm)
Sharma [125]	26%		
Dunlop [28]	10–40%		
Yang and King [152]	12–19%		
Lorenz [68]	13–30%		
Shirazi-Adl [127]		8.3 N (10 Nm)	67 N (10 Nm)
Present study	27 N/13% (7.5 Nm)	13 N (7.5 Nm)	56 N (7.5 Nm)

4.2.3 Intradiscal Pressure in the Literature

In an early study by Nachemson and Morris [86], the loads on the third and fourth lumbar discs measured in vivo with subjects in a standing position were an average of 7.6 kg/cm². This is equivalent to a pressure of about 0.75 MPa. Another study found that for an individual standing in 20° of flexion, the load on the third lumbar disc of a 70 kg subject was 148 kg or approximately 1.13 MPa [84]. In addition, Wilke et al. [142] found pressures in the fourth lumbar disc in vivo of 0.50 MPa and 1.10 MPa in relaxed standing and standing bent forward, respectively. In vitro experiments have recorded disc pressures of 0.87 MPa, 0.79 MPa, and 0.84 MPa in extension, a neutral position, and flexion, respectively, under a 7.5 Nm applied moment and a 700 N superimposed compressive load [134]. In an intact specimen, intradiscal pressures were found to increase from that in a neutral position in both flexion and extension, with the greatest pressure in extension [115]. Pressures in lateral bending and axial rotation both increased from that seen in the neutral position. In that same study, the pressures were greatest in extension, followed by right and left lateral bending, flexion, and right and left axial rotation. There was, however, a lot of variation seen among individual specimens. The

results of the present study are comparable to previous work found in the literature. In this study, intradiscal pressures of 0.44 ± 0.16 MPa, 0.44 ± 0.08 MPa, and 0.50 ± 0.16 MPa were measured in extension, a neutral position, and flexion, respectively. Pressures were greatest in flexion, followed by lateral bending and axial rotation, and finally extension. The magnitude of intradiscal pressure in a degenerated disc has been found to be reduced compared to in a normal, healthy disc [77, 152]. This may account for some discrepancies between this study and disc pressures found in the literature. Degeneration of the spine is a prevalent problem that generally advances with age and since the average age of specimens in this work was 77 years, some disc degeneration was expected.

In a specimen stabilized with the Dynesys, there was a linear variation in pressure during flexion-extension, which was also observed in the literature [123, 124]. However, details of that study are scarce. With the Dynesys implanted in an intact specimen, there was a reduction in intradiscal pressure in the neutral position by an average of 15% in the present study. In a study using an interspinous implant under similar loading conditions, there was a 20% decrease in pressure in the neutral position resulting from the implant [134]. Another group observed a significant decrease in intradiscal pressure of approximately 40% and 50% with implantation of hook and screw constructs, respectively, under an axial compressive load of 600 N compared to an intact condition [23]. In the current study, there was no change in the intradiscal pressure in flexion with the Dynesys implanted and a 32% decrease in pressure in extension compared to in the intact specimen. Swanson et al. observed a 4% and 41% decrease in pressure in flexion and extension, respectively after installation of an interspinous spacer [134], which is very consistent with this study. Rohlmann et al. looked at the disc pressures with an internal fixator and found a decrease in relative disc pressure in extension, lateral bending, and axial rotation, and an increase in relative disc pressure in flexion, where relative pressure was measured as the change from the pressure in a neutral position [115]. The results in flexion are opposite to what was seen in the current study, but may be due to no application of a compressive follower preload in the other study and the nature of the implant itself. In that study, the device was rigid as opposed to the dynamic implant examined in this study.

4.3 Facet Loading Patterns

When the Dynesys system was implanted, the greatest change in facet load was observed in flexion. The load at the facet joints increased significantly in flexion compared to the intact specimen and became larger than those in extension. It has been commonly accepted that in flexion, the facet joints are distracted and therefore the contact load is very minimal [3, 12, 125], which was seen in the capsule cut condition in the current study. However in this study, the device appeared to reverse the loading pattern compared to that seen in the intact specimen, such that the contact load increased with greater degree of flexion (Figure 4.4). This observation can be attributed to the significant posterior shift in the location of the HAM in flexion-extension that occurred with implantation of the Dynesys from its central position in the intact specimen. The Dynesys compressed the posterior elements, which was largely responsible for the changes in HAM and may have also led to alteration of the natural contact mechanism between the articulating surfaces, resulting in increased facet loads in flexion.

The facets were typically loaded independently in axial rotation, with the contralateral facet joint experiencing the compressive force. For example, while a moment was applied to produce right axial rotation, the right facet joint was virtually unloaded. Implantation of the Dynesys

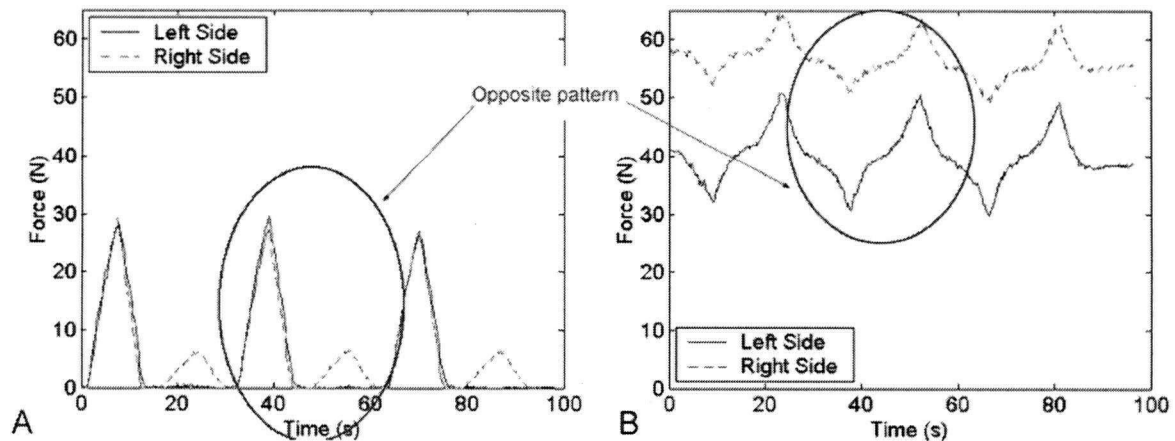


Figure 4.4: Comparison of facet load pattern in flexion-extension. For specimen H1109 for A) capsule condition and B) standard Dynesys.

introduced some load sharing between the two facets. While the contralateral joint still experienced the entire compressive load at the maximum rotation, there was a transition period where one facet was being loaded at the same time that the other side was being unloaded. This was evident by an intersection between the two forces when plotted against time and can likely be explained by the initial device-induced preload that was produced at the joints. Both facets were not always unloaded in the neutral position, as was the situation in the intact specimen. In addition, the time period in which the facet was unloaded with the Dynesys was often reduced to simply an instant in time (Figure 4.5).

4.4 Intradiscal Pressure Patterns

Amongst the intact specimens, a lot of variation in the shape of the measured intradiscal pressure vs. applied moment curve existed in flexion-extension and lateral bending. In flexion-extension, some specimens demonstrated an increase in pressure at maximum flexion and extension, as compared to the neutral position. In other specimens, the pressure was higher in extension than in flexion, or vice versa. Implantation of the Dynesys consistently created a linear variation in intradiscal pressure with applied load in flexion-extension in all specimens, regardless of the intradiscal pressure pattern prior to the device. In all instances, disc pressure

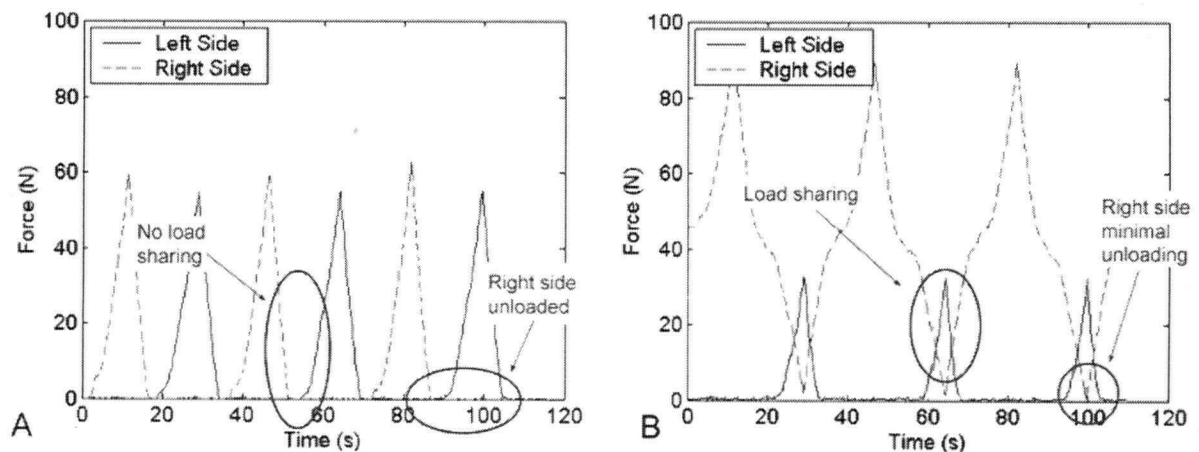


Figure 4.5: Comparison of facet load pattern in axial rotation. For specimen H1005 for A) capsule condition and B) standard Dynesys.

was greatest in flexion and least in extension. This was as expected because the intersegmental motion was essentially controlled by the device. The Dynesys became a load bearing structure of the spinal segment in extension, as well as shifting a portion of the compressive load from the anterior column to the posterior elements, thus reducing the load in the anterior column during extension. In lateral bending, the Dynesys typically resulted in a constant intradiscal pressure throughout the motion, despite varying curves for the intact specimens. The intradiscal pressure pattern remained relatively unchanged in axial rotation once the Dynesys was implanted, however, the absolute pressure magnitude decreased significantly.

The intradiscal pressure provided an indication of load transfer through the anterior column. Implanting the Dynesys reduced the load through the intervertebral disc in the neutral position, as well as in axial rotation, extension, and somewhat in lateral bending. This is likely a desirable effect since the disc has been identified as a common site of low back pain, so lessening the force at this location could reduce the degree of pain experienced by an individual.

4.5 Compression of the Posterior Elements

Implantation of the Dynesys created an inherent compression of the posterior elements due to pre-tensioning of the cord. This was apparent by the presence of a static load at the facet joints immediately after the device was installed and prior to flexibility testing. An average force of 15 N was produced at each facet joint by the standard length spacer. To put this magnitude into perspective, the average peak dynamic load in the intact facet ranged from 13 N in lateral bending and extension to 56 N in axial rotation.

In compressing the posterior elements, because the vertebrae are fairly rigid, it was only natural that the anterior column experienced some distraction. Generally the distance between the anterior points of the vertebral body increased as the length of the Dynesys spacer was decreased, although the difference was not significant. There was however, a significant reduction in intradiscal pressure of approximately 15% in the neutral position with the Dynesys compared to in an intact specimen without the implant. This further confirmed that the Dynesys compressed

the posterior elements. Combined compression of the posterior elements and distraction of the anterior annulus may restore a portion of the disc height and clinically, this may be beneficial in possibly decelerating further disc degeneration. In cases of disc bulge, distraction could result in indirect decompression eliminating the disc bulge and thus surgical intrusion into the canal would not be required. However, a potential outcome resulting from compression of the posterior elements is an increase in facet loads, as was seen in some instances in this study. This would not be desirable clinically since increased loads at the facet joints would likely produce degeneration at the joint and possibly emerge as pain. Ideally, the implant would provide an additional path for load transfer through the segment, thus reducing the loads through both the anterior column and posterior elements.

As the posterior elements were compressed, a significant shift in the posterior direction of the HAM in flexion-extension and axial rotation was produced with the Dynesys implanted. The position of the HAM moved from the centre of the disc space in flexion-extension and anterior to the posterior wall of the vertebral body in axial rotation for an intact specimen to within the vertebral canal with the Dynesys. The shift in HAM led to changes in load transfer through the column. Generally there was a reduction in load through the anterior column and a change in load through the facet joints (increase in flexion and lateral bending, no significant effect in extension and axial rotation).

4.5.1 Effect of Spacer Length on Segmental Compression

Constraint to segmental motion was created not only by the Dynesys configuration, such as a pre-tensioned cord, but also by the compression of the segment that was produced by the device. Compression of the posterior elements was dependent on the spacer length, which largely affected intersegmental ROM, most notably in axial rotation. The results of this study show that a 4 mm increase in spacer length led to an average intersegmental motion increase of 30% in axial rotation, 23% in extension, 14% in flexion, and 11% in lateral bending. The average initial contact load in the facet joints created by implantation of the device decreased from 42 N with the short spacer to 15 N with the long spacer. There was also a significant

decrease in peak facet load in flexion and lateral bending with the long spacer compared to the short spacer, further emphasizing the increased compression of posterior elements that occurred with the shorter spacer.

Lund et al. [70] observed similar results when looking at the effects of variations in compression of posterior instrumentation on motion. In that study, distraction of the posterior elements resulted in greater motion along the anterior column when loaded in axial compression. Although Lund et al. examined the effects only in axial loading, their results were consistent with the findings of this study in determining that the stiffness of the segment was affected by compression or distraction of the posterior elements due to the length of the spacer, which resulted in kinematic changes, specifically in the ROM.

4.6 Asymmetry

The bilateral nature of the Dynesys implant introduced an asymmetric stiffness to the segment. This was evident by the lateral shift in the HAM in axial rotation and lateral bending that occurred with its implantation. In addition, there was a non-significant rotation in the orientation of the HAM in the coronal and endplate planes. Accompanying the change in HAM after implantation of the device was a significantly higher contact load at the right facet joint than the left in flexion and lateral bending. A similar trend was seen in extension and axial rotation, but the differences were not significant.

The order of implantation was performed randomly between the right and left sides and the asymmetry appeared independent of which side was installed first. For some specimens, the right and left spacers were of different lengths due to anatomical variations, but there was no obvious correlation between the side with the shorter spacer and higher facet loads. Reasons for the asymmetry could include small variation in pre-tension that was applied to the cord. The cord was pre-tensioned using an identical surgical tool to that which would be used in the operating room. To achieve the correct level of tension, two arrows on the handle of the tool were aligned (Figure 4.6). A quick calibration of the tool in a materials testing machine

showed that the slightest variation in alignment led to a relatively large difference in tension. In this application, it is anticipated that the tension present in the cord plays a role in the biomechanical behaviour of the device. A mismatch in tension between the right and left sides would therefore likely cause asymmetrical biomechanical behaviour. In addition, variability in sizing of the standard spacer length may have contributed to the asymmetrical behaviour. The spacers were sized by a spine surgeon, but the method of determining the appropriate length is clearly subjective. These are both common occurrences that would be encountered in a clinical situation, so their presence in this study was not considered a limitation.

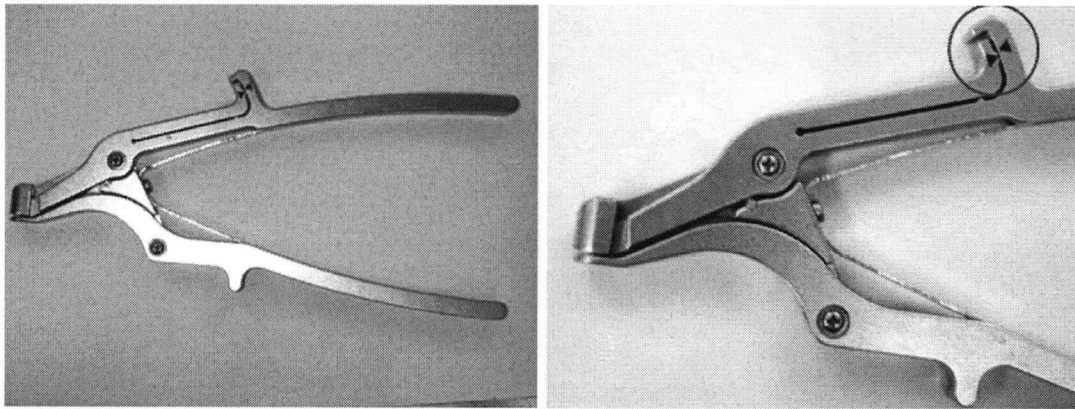


Figure 4.6: *Surgical tensioning tool for tightening the implant (Zimmer GmbH). There is 300 N generated when the two arrows on the handle are aligned.*

The asymmetric stiffness may have important implications clinically. For instance, it would likely have an effect on the loading mechanism through the facet joints, possibly asymmetric wear, alteration of the process of natural degeneration in the joint, or even emerge as pain.

4.7 Changes in Motion Coupling

There was evidence that in an intact specimen, right axial rotation was coupled with left lateral bending and flexion and left axial rotation was accompanied by right lateral bending and flexion. Right and left lateral bending were both coupled with flexion and a slight degree of left and right axial rotation, respectively. These are similar to HAM results reported in the literature [96] and coupled motion found in previous studies [95, 104, 110, 112, 139].

The rotational shifts in the orientation of the HAM that were observed in this study with implantation of the Dynesys led to alterations in the coupled behaviour of the segment. Over the full motion, the differences were significant in axial rotation in the mid-sagittal plane. In a specimen stabilized with the Dynesys, right axial rotation was coupled with left lateral bending and left axial rotation was accompanied by right lateral bending. This coupling pattern was opposite that seen in the intact specimen. In the endplate plane, the Dynesys introduced a significant lateral bending motion that accompanied the primary flexion-extension movement, whereas without the Dynesys, there was virtually no obvious coupled motion. Finally, in right lateral bending implantation of the Dynesys created a coupled extension motion, which was significantly different from the flexion movement that resulted in the intact specimen.

Previously, it has been found that chronic low back pain is associated with abnormal motion patterns, specifically in coupled axial rotation during lateral bending, in the symmetry between flexion and extension, and in the symmetry between right and left lateral bending [44, 47, 48, 69]. When comparing in vivo motions of a low back pain sufferer to motion measured in vitro, one must also consider compounding factors, like pain, that would exist and affect motion in vivo.

4.8 Feasibility of Quantifying Contact in Facet Joints Using Imaging

The results of this study suggest that quantification of cartilage contact within the facet joints is difficult even with an MRI sequence that has been optimized for cartilage visualization. The cartilage is quite thin, the joint is relatively small, and the articular surfaces are very conforming, all of which contribute to the challenging task.

Given the difficulty in distinguishing between the two layers of cartilage, the contact area measured with the imaging technique corresponded with the Tekscan measurements better than was expected. This was encouraging.

The potential for successful implementation of imaging in this application still exists, but may benefit from the use of a contrast agent to intensify the superficial region of the cartilage. This

would lead to easier visualization of contact within the joint. Based on this study, it appears that the technique in which a line of contact is created when no distinction can be made between cartilage layers would be more appropriate provided that the superficial border of the cartilage could be enhanced. With the protocol of this study, it was not possible to accurately detect a line of contact within the joint. Attempting to quantify contact based on joint volume assumes that the cartilage compression would be quantifiable, but given the thickness of the cartilage and in-plane resolution of the scan, this would likely not be possible.

4.9 Comparison of Dynesys to Rigid, Intact, and Injured Conditions

A severe injury was utilized to simulate degenerative instability in the specimens. As a result, there was a significant increase in ROM in all directions, except extension, and typically an increase in NZ (only significantly greater in flexion without a follower preload) compared to an intact specimen. Implantation of the Dynesys significantly reduced the ROM and NZ compared to those in the injured segment, but the reduction was to magnitudes below those observed in the intact specimen. The NZ was only significantly lower with the Dynesys compared to the intact condition in lateral bending. In axial rotation, the changes were least significant and the ROM was 72% and 86% of intact ROM. In flexion, extension, and lateral bending, however, motion was a lot more constrained.

Controlling and guiding the rotation has implications on the HAM and on the loading through the segment. The Dynesys caused significant changes in the motion pattern compared to an intact specimen. Typically, the aim with dynamic devices is to replicate the HAM of the intact specimen. The loading generally decreased through the anterior column when the Dynesys was implanted. A reduction in load through the intervertebral disc could reduce pain generated by the disc and provide an environment that may stimulate regeneration of the disc [123, 130]. The Dynesys increased compression at the posterior elements and increased facet loads in flexion and lateral bending. This increase may have negative implications in vivo.

One of the problems associated with a rigid device is the acceleration of degeneration at adjacent

levels due to elimination of motion at the operated level [29, 64, 119]. Advantages of a dynamic system would be a preservation of motion that would theoretically reduce adjacent level damage. Compared to fusion, what some consider the most effective surgical treatment for degenerative problems in the lumbar spine [34], the Dynesys did not result in a significant difference in NZ. There was significantly greater intersegmental motion in axial rotation with the Dynesys, but no significant differences in the other loading directions.

4.10 Dynesys Spacer Length

The length of the Dynesys spacer had the largest effect on ROM, with the long spacer resulting in significantly greater motion than that with the short spacer in all directions without a follower preload and in axial rotation with a follower preload. In all loading directions, the general trend was identical. The ROM decreased in all three loading directions with a follower load, and since the motion with the Dynesys was already small, differences between the spacers became less pronounced.

There was a significantly smaller posterior shift in the HAM in axial rotation with the long spacer as compared to the HAM with the short spacer. The spacer length also had a significant effect on the orientation of the HAM in the endplate plane in flexion-extension and in the mid-sagittal plane in axial rotation. The short spacer generated a HAM position and orientation that was generally of greater difference from the intact HAM than the long spacer.

Initial compression of the posterior elements was significantly less with the long spacer. Typically, facet loads during motion were smaller with the long spacer, but the differences between spacers were only significant in flexion and lateral bending. One can also speculate that due to the increased compression at the facet joints with the short spacer, the short spacer would likely reduce the pressure in the disc, and thus reduce anterior column loading compared to the long spacer.

Considering the kinematic and load-bearing behaviour of the segment, the long spacer resulted in biomechanical behaviour that was more similar to that of an intact specimen.

4.11 Clinical Implications

Even though ROM was substantially reduced with the Dynesys implanted, the long spacer length produced motion that was more similar to that in an intact spine and resulted in lower facet loads compared to the other spacer lengths tested. However, a balance between desirable kinematics and neutral position of the spine must be found. By increasing the length of the spacer too much, the spine may potentially become kyphotic, which could lead to adverse changes in loading patterns and additional clinical problems not predictable with in vitro testing.

The Dynesys was relatively stiff in flexion, extension, and lateral bending, but provided the same or more motion than rigid fixation. The Dynesys appeared to improve biomechanical behaviour compared to a rigid system, specifically in axial rotation. However, the dynamic system is of a greater complexity than a rigid device and therefore, the motion pattern and load transfer must also be considered.

There is a partial restoration of disc height and reduction of anterior column load with implantation of the Dynesys, which some claim could create an environment that would stimulate regeneration of a partially degenerated disc. The Dynesys may also result in indirect decompression of bulging discs, thus possibly eliminating the need for surgical intrusion of the spinal canal. However, if the decrease in anterior column load is compensated for by an increase in load through the posterior elements, this may accelerate facet joint degeneration as well as cause low back pain.

4.12 Goals for Biomechanical Testing

The results of this work demonstrate the importance of including an evaluation of all aspects of kinematic behaviour when biomechanically assessing the efficacy of dynamic stabilization systems. An analysis of the HAM provides insight into changes in the centre of rotation and coupling of motion that may result from implantation of a dynamic system.

Since a degree of motion is preserved with these devices, it is also critical to examine the effect of the device on load transfer through the segment. Ideally, a device would either alleviate or maintain load through the anterior column, posterior elements, or both. An increase in load may have adverse effects with respect to pain, degeneration, osteoarthritis, and other pathologies.

The spine is a complicated structure, one in which the kinematic behaviour and loading patterns are highly intertwined. Alterations of one aspect will affect the other. It is not sufficient, therefore, to draw conclusions regarding the functionality of a dynamic stabilization system based solely on one aspect of the biomechanical behaviour.

The biomechanical testing of dynamic stabilization systems needs to be standardized to allow comparison of devices across studies and with a sufficient test protocol to clearly evaluate that the device performs as intended.

Chapter 5

Conclusions

The Dynesys affected the kinematic behaviour at the implanted level. There was a significant reduction in ROM in all directions of loading (except axial rotation with a follower preload) that occurred with the Dynesys, with the least significant differences seen in axial rotation. The Dynesys resulted in a ROM that was 16%, 30%, 25%, and 88% of intact ROM in flexion, extension, lateral bending, and axial rotation, respectively. Compared to the ROM of a severely injured segment, the Dynesys did have a stabilizing effect, but to the extent that the magnitude of motion was more comparable to that of the rigid system in flexion, extension, and lateral bending. Implantation of the Dynesys also tended to reduce the larger NZ of an injured specimen to a level that was below, but not significantly lower, than the intact NZ. There was a significant posterior shift in the position of the HAM in flexion-extension and axial rotation with the Dynesys, as well as a significant rotation in the orientation of the HAM.

Implantation of the Dynesys created an initial load at the facet joints. As a result, the dynamic loading within the facet joints generally either increased or remained relatively unchanged with the Dynesys. The largest difference was seen in flexion where the device caused a significant increase in facet load, followed by a non-significant increase in load during lateral bending. The bilateral nature of the device introduced an asymmetric stiffness in the specimen, which manifested not only as kinematic differences in the HAM, but also as significant differences between right and left facet loads in flexion and lateral bending. Anterior column loading was also affected by the Dynesys. The intradiscal pressure decreased significantly with implantation of the Dynesys and the device produced a linear relationship between pressure and applied

moment in flexion-extension.

The largest effect created by varying the length of the Dynesys spacer was on ROM. The long spacer generated a significantly greater motion than the short spacer in all loading directions (without a follower preload), most predominantly in axial rotation. There were not large significant differences in NZ that occurred between the three spacer lengths. The HAM, however, was generally located more posteriorly with the long spacer compared to that with the short spacer and there was a smaller degree of rotation in the mid-sagittal plane with the long spacer.

Typically, the long spacer resulted in lesser facet loads than the short spacer, which can be attributed to the greater degree of posterior compression that occurred with the short spacer. Differences in facet load magnitude were significant in flexion and lateral bending between the short and long spacer lengths.

MR imaging may have the potential to be a useful tool in improving the understanding of facet joint loading and the role of the facet joints in kinematic behaviour. The protocol investigated in this study was only mildly successful in monitoring facet contact in vitro. It will be challenging to incorporate the imaging modality to achieve quantifiable results of the contact within the joints and may require the use of a contrast agent to enhance the superficial zone of the articular cartilage.

The objectives of the emerging dynamic stabilization systems have changed in contrast to the well-established fusion devices where the goal was elimination of motion in order to relieve low back pain. With this change in functional goals, it is necessary for the biomechanical test protocol to evolve and include evaluation of all aspects of kinematic and load-bearing behaviour, more than simply just the range of motion, to adequately examine the efficacy of dynamic stabilization systems.

5.1 Future Directions

Improvements to the Dynesys system based on the results of this study would lead to a more viable treatment alternative from a biomechanical perspective. It may also be worthwhile to investigate additional parameters of the Dynesys system on the biomechanics of the device.

Load transfer through the facet joints is an important part of the function of the spinal column. There remains large inconsistencies, however, in the function and mechanism of load transfer through the facet joints. Further study in this area to enhance the knowledge of the loading patterns in the posterior elements would be useful in understanding specific spinal pathologies, as well as in the development of treatments and implants for use in the spine. Three-dimensional imaging may still have potential value in this application, but would require additional work to generate a methodology that would yield accurate and useful results. It could then be used for quantification of contact area within the joints, which would provide an indication of the stress in the joint. The centroid of the contact area could also be measured and monitored over various specimen conditions. This would be a valuable tool in evaluating the effects of spinal devices on loading patterns through the posterior elements. Ultimately, it would be a technique that could be used to study facet loads in vivo, to monitor progressive degeneration, and potentially be used to select the most promising treatment option.

In the broader picture, a test protocol needs to be established to standardize the biomechanical evaluation of dynamic stabilization systems. In addition to providing a thorough and solid indication of the behaviour of a particular device, a standardized procedure would facilitate comparisons of devices across studies.

5.2 Contributions

It is expected that this work will provide valuable information for further improvements to the Dynesys system, as well as for other dynamic stabilization devices.

This research supports the need to establish a standardized test protocol for biomechanical

Chapter 5. Conclusions

evaluation of dynamic stabilization systems to allow appropriate assessment of whether the device satisfies the intended objectives and to allow comparison of devices across different studies.

In the long term, the results of this study could guide future research and development activities in the area of dynamic stabilization of the lumbar spine.

Bibliography

- [1] Adams MA. Mechanical testing of the spine. an appraisal of methodology, results, and conclusions. *Spine*, 20(19):2151-6., 1995.
- [2] Adams MA, Dolan P, and Hutton WC. The lumbar spine in backward bending. *Spine*, 13(9):1019-26, 1988.
- [3] Adams MA and Hutton WC. The effect of posture on the role of the apophysial joints in resisting intervertebral compressive forces. *J Bone Joint Surg Br*, 62(3):358-62, 1980.
- [4] Adams MA and Hutton WC. The relevance of torsion to the mechanical derangement of the lumbar spine. *Spine*, 6(3):241-8, 1981. Journal Article.
- [5] Adams MA and Hutton WC. The mechanical function of the lumbar apophyseal joints. *Spine*, 8(3):327-30, 1983.
- [6] Adams MA, McNally DS, and Dolan P. Stress distributions inside intervertebral discs. the effects of age and degeneration. *J Bone Joint Surg Br*, 78(6):965-72, 1996.
- [7] Amershamhealth. *The Encyclopaedia of Medical Imaging*, volume 1 of *Physics, Techniques, and Procedures*. www.amershamhealth.com, 2001.
- [8] Andersson GB. Epidemiological features of chronic low-back pain. *Lancet*, 354(9178):581-5., 1999.
- [9] Baer T, Pedersen D, Rudert M, Vos N, Grosland N, and Brown T. Calibrating and monitoring sheet array pressure sensors for intra-articular load measurement. In *5th Combined Meeting of the Orthopaedic Research Societies of Canada, USA, Japan, and Europe.*, Banff, Canada, 2004.
- [10] Bogduk N. *Clinical Anatomy of the Lumbar Spine and Sacrum*. Churchill Livingstone, Philadelphia, 3rd edition, 1997.
- [11] Brechter J, Powers CM, Terk MR, Ward SR, and Lee T. Quantification of patellofemoral joint contact area using magnetic resonance imaging. *Magnetic Resonance Imaging*, 21:955-959, 2003.
- [12] Buttermann GR, Kahmann RD, Lewis JL, and Bradford DS. An experimental method for measuring force on the spinal facet joint: description and application of the method. *J Biomech Eng*, 113(4):375-86, 1991.
- [13] Buttner-Janzen K, Schellnack K, and Zippel H. Biomechanics of the sb charite lumbar intervertebral disc endoprosthesis. *Int Orthop*, 13(3):173-6., 1989.
- [14] Caserta S, La Maida GA, Misaggi B, Peroni D, Pietrabissa R, Raimondi MT, and Redaelli A. Elastic stabilization alone or combined with rigid fusion in spinal surgery: a biomechanical study and clinical experience based on 82 cases. *Eur Spine J*, 11(Suppl 2):S192-7, 2002.

Bibliography

- [15] Cats-Baril W and Frymoyer JW. The economics of spinal disorders. In Frymoyer JW, editor, *The Adult Spine: Principles and Practice*, volume 1, pages 85–106. Raven Press, New York, 1991.
- [16] Chadwick P. *Continuum Mechanics, Concise Theory and Problems*. George Allen and Unwin, London, 1976.
- [17] Cherkin DC, Deyo RA, Loeser JD, Bush T, and Waddell G. An international comparison of back surgery rates. *Spine*, 19(11):1201–6., 1994.
- [18] Clare S. *Functional MRI: Methods and Applications*. Phd, University of Nottingham, 1997.
- [19] Cohen ZA, McCarthy DM, Kwak SD, Legrand P, Fogarasi F, Ciaccio EJ, and Ateshian GA. Knee cartilage topography, thickness, and contact areas from mri: in-vitro calibration and in-vivo measurements. *Osteoarthritis Cartilage*, 7(1):95–109., 1999.
- [20] Cripton PA, Bruehlmann SB, Orr TE, Oxland TR, and Nolte LP. In vitro axial preload application during spine flexibility testing: towards reduced apparatus-related artefacts. *J Biomech*, 33(12):1559–68, 2000.
- [21] Crisco J, Panjabi M, Yamamoto I, and Oxland T. Euler stability of the human ligamentous lumbar spine. part ii: Experiment. *Clinical Biomechanics*, 7:27–32, 1992.
- [22] Crisco J and Panjabi M. Euler stability of the human ligamentous lumbar spine. part i: Theory. *Clinical Biomechanics*, 7:19–26, 1992.
- [23] Cunningham BW, Kotani Y, McNulty PS, Cappuccino A, and McAfee PC. The effect of spinal destabilization and instrumentation on lumbar intradiscal pressure: an in vitro biomechanical analysis. *Spine*, 22(22):2655–63., 1997.
- [24] Cunningham BW, Lowery GL, Serhan HA, Dmitriev AE, Orbegoso CM, McAfee PC, Fraser RD, Ross RE, and Kulkarni SS. Total disc replacement arthroplasty using the acroflex lumbar disc: a non-human primate model. *Eur Spine J*, 11 Suppl 2:S115–23, 2002.
- [25] Delmas A, Ndjaga-Mba M, Vannareth T, Monson NL, Haughton VM, Modl JM, Sether LA, and Ho KC. [articular cartilage of l4-l5 and l5-s1] normal and degenerating articular cartilage: in vitro correlation of mr imaging and histologic findings. *C R Assoc Anat*, 147(1):230–4., 1970.
- [26] Dooris AP, Goel VK, Grosland NM, Gilbertson LG, and Wilder DG. Load-sharing between anterior and posterior elements in a lumbar motion segment implanted with an artificial disc. *Spine*, 26(6):E122–9, 2001.
- [27] Dubois G, de Gernay B, Schaerer N, and Fennema P. Dynamic neutralization: a new concept for restabilization of the spine. In Szpalski M, Gunzburg R, and Pope MH, editors, *Lumbar Segmental Instability*, pages 233–240. Lippincott Williams and Wilkins, Philadelphia, 1999.

Bibliography

- [28] Dunlop RB, Adams MA, and Hutton WC. Disc space narrowing and the lumbar facet joints. *J Bone Joint Surg Br*, 66(5):706-10, 1984.
- [29] Eck JC, Humphreys SC, and Hodges SD. Adjacent-segment degeneration after lumbar fusion: a review of clinical, biomechanical, and radiologic studies. *Am J Orthop*, 28(6):336-40, 1999.
- [30] Eysel P, Rompe J, Schoenmayr R, and Zoellner J. Biomechanical behaviour of a prosthetic lumbar nucleus. *Acta Neurochir (Wien)*, 141(10):1083-7., 1999.
- [31] Faber SC, Eckstein F, Lukasz S, Muhlbauer R, Hohe J, Englmeier KH, and Reiser M. Gender differences in knee joint cartilage thickness, volume and articular surface areas: assessment with quantitative three-dimensional mr imaging. *Skeletal Radiol*, 30(3):144-50., 2001.
- [32] Frei H, Oxland TR, Rathonyi GC, and Nolte LP. The effect of nucleotomy on lumbar spine mechanics in compression and shear loading. *Spine*, 26(19):2080-9, 2001.
- [33] Freudiger S, Dubois G, and Lorrain M. Dynamic neutralisation of the lumbar spine confirmed on a new lumbar spine simulator in vitro. *Arch Orthop Trauma Surg*, 119(3-4):127-32, 1999.
- [34] Fritzell P, Hagg O, Wessberg P, and Nordwall A. 2001 volvo award winner in clinical studies: Lumbar fusion versus nonsurgical treatment for chronic low back pain: a multicenter randomized controlled trial from the swedish lumbar spine study group. *Spine*, 26(23):2521-32; discussion 2532-4., 2001.
- [35] Frymoyer JW and Nachemson A. Natural history of low back disorders. In Frymoyer JW, editor, *The Adult Spine: Principles and Practice*, volume 1, pages 1537-1550. Raven Press, New York, 1991.
- [36] Fujiwara A, Lim TH, An HS, Tanaka N, Jeon CH, Andersson GB, and Haughton VM. The effect of disc degeneration and facet joint osteoarthritis on the segmental flexibility of the lumbar spine. *Spine*, 25(23):3036-44, 2000.
- [37] Gentleman J, Vayda E, Parsons G, and Walsh M. Surgical rates in subprovincial areas across canada: rankings of 39 procedures in order of variation. *Canadian Journal of Surgery*, 39(5):361-7, 1996.
- [38] Glantz S. *Primer of Biostatistics*. McGraw-Hill Companies, Inc., USA, 5th edition, 2002.
- [39] Glaser C, Faber S, Eckstein F, Fischer H, Springer V, Heudorfer L, Stammberger T, Englmeier KH, and Reiser M. Optimization and validation of a rapid high-resolution t1-w 3d flash water excitation mri sequence for the quantitative assessment of articular cartilage volume and thickness. *Magn Reson Imaging*, 19(2):177-85., 2001.
- [40] Goel VK, Goyal S, Clark C, Nishiyama K, and Nye T. Kinematics of the whole lumbar spine. effect of discectomy. *Spine*, 10(6):543-54, 1985.
- [41] Goel VK, Wilder DG, Pope MH, and Edwards WT. Biomechanical testing of the spine. load-controlled versus displacement-controlled analysis. *Spine*, 20(21):2354-7, 1995.

Bibliography

- [42] Goel VK, Winterbottom JM, Weinstein JN, and Kim YE. Load sharing among spinal elements of a motion segment in extension and lateral bending. *J Biomech Eng*, 109(4):291-7, 1987.
- [43] Goertzen DJ, Lane C, and Oxland TR. Neutral zone and range of motion in the spine are greater with stepwise loading than with a continuous loading protocol. an in vitro porcine investigation. *J Biomech*, 37(2):257-61, 2004.
- [44] Gomez TT. Symmetry of lumbar rotation and lateral flexion range of motion and isometric strength in subjects with and without low back pain. *J Orthop Sports Phys Ther*, 19(1):42-8., 1994.
- [45] Grassmann S, Oxland TR, Gerich U, and Nolte LP. Constrained testing conditions affect the axial rotation response of lumbar functional spinal units. *Spine*, 23(10):1155-62, 1998.
- [46] Grenier N, Kressel HY, Schiebler ML, Grossman RI, and Dalinka MK. Normal and degenerative posterior spinal structures: Mr imaging. *Radiology*, 165(2):517-25, 1987.
- [47] Haas M and Nyiendo J. Lumbar motion trends and correlation with low back pain. part ii. a roentgenological evaluation of quantitative segmental motion in lateral bending. *J Manipulative Physiol Ther*, 15(4):224-34., 1992.
- [48] Haas M, Nyiendo J, Peterson C, Thiel H, Sellers T, Dal Mas E, Kirton C, and Cassidy D. Lumbar motion trends and correlation with low back pain. part i. a roentgenological evaluation of coupled lumbar motion in lateral bending. *J Manipulative Physiol Ther*, 15(3):145-58., 1992.
- [49] Haberl H, Crompton PA, Orr TE, Beutler T, Frei H, Lanksch WR, and Nolte LP. Kinematic response of lumbar functional spinal units to axial torsion with and without superimposed compression and flexion/extension. *Eur Spine J*, 7:7, 2004.
- [50] Hamming J, Goertzen DJ, and Oxland T. The effect of marker configuration and placement on kinematic accuracy. In *54th Annual Meeting of the Canadian Orthopaedic Association*, page 59, St. Johns, Newfoundland, Canada, 1999.
- [51] Harris ML, Morberg P, Bruce WJ, and Walsh WR. An improved method for measuring tibiofemoral contact areas in total knee arthroplasty: a comparison of k-scan sensor and fuji film. *J Biomech*, 32(9):951-8., 1999.
- [52] Hedman TP. A new transducer for facet force measurement in the lumbar spine: benchmark and in vitro test results. *J Biomech*, 25(1):69-80, 1992.
- [53] Horst M and Brinckmann P. 1980 volvo award in biomechanics. measurement of the distribution of axial stress on the end-plate of the vertebral body. *Spine*, 6(3):217-32, 1981.
- [54] Howell D. *Statistical Methods for Psychology*. Duxbury, Thompson Learning Inc., California, USA, 5th edition, 2002.
- [55] Janevic J, Ashton-Miller JA, and Schultz AB. Large compressive preloads decrease lumbar motion segment flexibility. *J Orthop Res*, 9(2):228-36., 1991.

Bibliography

- [56] Joubert S. Review of 140 cases over 2 years with special emphasis on active sportsmen. In *Sulzer Orthopedics Joint, Fracture, Spine Care 3rd Dynesos Meeting*, Lyon, France, 2002.
- [57] Kadoya K, Kotani Y, Abumi K, Takada T, Shimamoto N, Shikinami Y, Kadosawa T, and Kaneda K. Biomechanical and morphologic evaluation of a three-dimensional fabric sheep artificial intervertebral disc: in vitro and in vivo analysis. *Spine*, 26(14):1562-9., 2001.
- [58] Kahmann RD, Buttermann GR, Lewis JL, and Bradford DS. Facet loads in the canine lumbar spine before and after disc alteration. *Spine*, 15(9):971-8, 1990.
- [59] Kettler A, Wilke HJ, Haid C, and Claes L. Effects of specimen length on the monosegmental motion behavior of the lumbar spine. *Spine*, 25(5):543-50., 2000.
- [60] Kinzel GL, Hall J, A. S., and Hillberry BM. Measurement of the total motion between two body segments. i. analytical development. *J Biomech*, 5(1):93-105, 1972.
- [61] Kotani Y, Abumi K, Shikinami Y, Takada T, Kadoya K, Shimamoto N, Ito M, Kadosawa T, Fujinaga T, and Kaneda K. Artificial intervertebral disc replacement using bioactive three-dimensional fabric: design, development, and preliminary animal study. *Spine*, 27(9):929-35; discussion 935-6., 2002.
- [62] Langrana NA, Lee CK, and Yang SW. Finite-element modeling of the synthetic intervertebral disc. *Spine*, 16(6 Suppl):S245-52., 1991.
- [63] Leahy JC, Mathias KJ, Hukins DW, Shepherd DE, and Deans WF. Mechanical testing of a flexible fixation device for the lumbar spine. *Proc Inst Mech Eng [H]*, 214(5):489-95., 2000.
- [64] Lee CK. Accelerated degeneration of the segment adjacent to a lumbar fusion. *Spine*, 13(3):375-7, 1988.
- [65] Lemaire JP, Skalli W, Lavaste F, Templier A, Mendes F, Diop A, Sauty V, and Laloux E. Intervertebral disc prosthesis. results and prospects for the year 2000. *Clin Orthop*, (337):64-76., 1997.
- [66] Link HD. History, design and biomechanics of the link sb charite artificial disc. *Eur Spine J*, 11 Suppl 2:S98-S105, 2002.
- [67] Lipman J, Campbell D, Girardi FP, Cammisa J, F. P., Myers E, and Wright T. Mechanical behaviour of the prodisc ii intervertebral disc prosthesis in human cadaveric spines. In *Orthopaedic Research Society, 49th Annual*, 2003.
- [68] Lorenz M, Patwardhan A, and Vanderby J, R. Load-bearing characteristics of lumbar facets in normal and surgically altered spinal segments. *Spine*, 8(2):122-30, 1983.
- [69] Lund T, Nydegger T, Schlenzka D, and Oxland TR. Three-dimensional motion patterns during active bending in patients with chronic low back pain. *Spine*, 27(17):1865-74, 2002.

Bibliography

- [70] Lund T, Rathonyi G, Schlenzka D, and Oxland TR. The external spinal fixator does not reduce anterior column motion under axial compressive loads. a mechanical in vitro study. *Acta Orthop Scand*, 70(1):37-41, 1999.
- [71] Luo ZP, Buttermann GR, and Lewis JL. Determination of spinal facet joint loads from extra articular strains—a theoretical validation. *J Biomech*, 29(6):785-90, 1996.
- [72] Mansour M, Spiering S, Lee C, Dathe H, Kalscheuer AK, Kubein-Meesenburg D, and Nagerl H. Evidence for iha migration during axial rotation of a lumbar spine segment by using a novel high-resolution 6d kinematic tracking system. *J Biomech*, 37(4):583-92, 2004.
- [73] McGibbon CA, Bencardino J, and Palmer WE. Subchondral bone and cartilage thickness from mri: effects of chemical-shift artifact. *Magma*, 16(1):1-9., 2003.
- [74] McKinnon ME, Vickers MR, Ruddock VM, Townsend J, and Meade TW. Community studies of the health service implications of low back pain. *Spine*, 22(18):2161-6., 1997.
- [75] McNally DS. The objectives for the mechanical evaluation of spinal instrumentation have changed. *Eur Spine J*, 11 Suppl 2:S179-85, 2002.
- [76] McNally DS and Adams MA. Internal intervertebral disc mechanics as revealed by stress profilometry. *Spine*, 17(1):66-73., 1992.
- [77] McNally DS, Shackelford IM, Goodship AE, and Mulholland RC. In vivo stress measurement can predict pain on discography. *Spine*, 21(22):2580-7, 1996.
- [78] Meakin JR, Reid JE, and Hukins DW. Replacing the nucleus pulposus of the intervertebral disc. *Clin Biomech (Bristol, Avon)*, 16(7):560-5., 2001.
- [79] Metaxas N. Indications and contraindications for patient selection for dynesys. In *Sulzer Orthopedics Joint, Fracture, Spine Care 3rd Dynesos Meeting*, Lyon, France, 2002.
- [80] Miles M and Sullivan W. Lateral bending at the lumbar and lumbosacral joints. *The Anatomical Record*, 139:387-398, 1961.
- [81] Mimura M, Panjabi MM, Oxland TR, Crisco JJ, Yamamoto I, and Vasavada A. Disc degeneration affects the multidirectional flexibility of the lumbar spine. *Spine*, 19(12):1371-80, 1994.
- [82] Minns RJ and Walsh WK. Preliminary design and experimental studies of a novel soft implant for correcting sagittal plane instability in the lumbar spine. *Spine*, 22(16):1819-25; discussion 1826-7, 1997.
- [83] Nachemson A. Measurement of intradiscal pressure. *Acta Orthop Scand*, 28:269-89, 1959.
- [84] Nachemson A. The load on lumbar disks in different positions of the body. *Clin Orthop*, 45:107-22, 1966.
- [85] Nachemson A. The role of spine fusion. *Spine*, (May/June):306-7, 1981.

Bibliography

- [86] Nachemson A and Morris JM. In vivo measurements of intradiscal pressure. discometry, a method for the determination of pressure in the lower lumbar discs. *J Bone Joint Surg Am*, 46:1077-92., 1964.
- [87] Nachemson A, Zdeblick TA, and O'Brien JP. Lumbar disc disease with discogenic pain. what surgical treatment is most effective? *Spine*, 21(15):1835-8., 1996.
- [88] Nachemson AL. Advances in low-back pain. *Clin Orthop*, (200):266-78., 1985.
- [89] Nachemson AL. Evaluation of results in lumbar spine surgery. *Acta Orthop Scand Suppl*, 251:130-3., 1993.
- [90] Nagi S, Riley L, and Newby L. A social epidemiology of back pain in a general population. *Journal of Chronic Diseases*, 26:769-779, 1973.
- [91] Nohara H and Kanaya F. Biomechanical study of adjacent intervertebral motion after lumbar spinal fusion and flexible stabilization using polyethylene-terephthalate bands. *J Spinal Disord Tech*, 17(3):215-9., 2004.
- [92] Nydegger T. Personal communication, October 6 2004.
- [93] Oxland TR, Panjabi MM, and Lin RM. Axes of motion of thoracolumbar burst fractures. *J Spinal Disord*, 7(2):130-8., 1994.
- [94] Panjabi M, Abumi K, Duranceau J, and Oxland T. Spinal stability and intersegmental muscle forces. a biomechanical model. *Spine*, 14(2):194-200, 1989.
- [95] Panjabi M, Yamamoto I, Oxland T, and Crisco J. How does posture affect coupling in the lumbar spine? *Spine*, 14(9):1002-11, 1989.
- [96] Panjabi M, Yamamoto I, Oxland T, and Crisco J. Helical axes of motion change with lumbar vertebral level. *37th Annual Meeting, Orthopaedic Research Society, March 4-7, 1991, Anaheim, California*, 1991.
- [97] Panjabi MM. Biomechanical evaluation of spinal fixation devices: I. a conceptual framework. *Spine*, 13(10):1129-34., 1988.
- [98] Panjabi MM, Abumi K, Duranceau J, and Crisco JJ. Biomechanical evaluation of spinal fixation devices: II. stability provided by eight internal fixation devices. *Spine*, 13(10):1135-40., 1988.
- [99] Panjabi MM, Goel V, Oxland T, Takata K, Duranceau J, Krag M, and Price M. Human lumbar vertebrae. quantitative three-dimensional anatomy. *Spine*, 17(3):299-306., 1992.
- [100] Panjabi MM, Krag M, Summers D, and Videman T. Biomechanical time-tolerance of fresh cadaveric human spine specimens. *J Orthop Res*, 3(3):292-300., 1985.
- [101] Panjabi MM, Krag MH, and Goel VK. A technique for measurement and description of three-dimensional six degree-of-freedom motion of a body joint with an application to the human spine. *J Biomech*, 14(7):447-60, 1981.

Bibliography

- [102] Panjabi MM, Krag MH, White r, A. A., and Southwick WO. Effects of preload on load displacement curves of the lumbar spine. *Orthop Clin North Am*, 8(1):181-92, 1977.
- [103] Panjabi MM, Oxland T, Takata K, Goel V, Duranceau J, and Krag M. Articular facets of the human spine. quantitative three-dimensional anatomy. *Spine*, 18(10):1298-310, 1993.
- [104] Panjabi MM, Oxland TR, Yamamoto I, and Crisco JJ. Mechanical behavior of the human lumbar and lumbosacral spine as shown by three-dimensional load-displacement curves. *J Bone Joint Surg Am*, 76(3):413-24, 1994.
- [105] Papp T, Porter RW, Aspden RM, and Shepperd JA. An in vitro study of the biomechanical effects of flexible stabilization on the lumbar spine. *Spine*, 22(2):151-5, 1997.
- [106] Patel VV, Hall K, Ries M, Lindsey C, Ozhinsky E, Lu Y, and Majumdar S. Magnetic resonance imaging of patellofemoral kinematics with weight-bearing. *J Bone Joint Surg Am*, 85-A(12):2419-24., 2003.
- [107] Patel VV, Hall K, Ries M, Lotz J, Ozhinsky E, Lindsey C, Lu Y, and Majumdar S. A three-dimensional mri analysis of knee kinematics. *J Orthop Res*, 22(2):283-92., 2004.
- [108] Patwardhan AG, Havey RM, Carandang G, Simonds J, Voronov LI, Ghanayem AJ, Meade KP, Gavin TM, and Paxinos O. Effect of compressive follower preload on the flexion-extension response of the human lumbar spine. *J Orthop Res*, 21(3):540-6, 2003.
- [109] Patwardhan AG, Havey RM, Meade KP, Lee B, and Dunlap B. A follower load increases the load-carrying capacity of the lumbar spine in compression. *Spine*, 24(10):1003-9, 1999.
- [110] Pearcy MJ and Tibrewal SB. Axial rotation and lateral bending in the normal lumbar spine measured by three-dimensional radiography. *Spine*, 9(6):582-7, 1984.
- [111] Pfirrmann CW, Metzdorf A, Zanetti M, Hodler J, and Boos N. Magnetic resonance classification of lumbar intervertebral disc degeneration. *Spine*, 26(17):1873-8, 2001.
- [112] Plamondon A, Gagnon M, and Maurais G. Application of a stereoradiographic method for the study of intervertebral motion. *Spine*, 13(9):1027-32, 1988.
- [113] Prasad P, King A, and Ewing C. The role of articular facets during +gz acceleration. *J Appl Mech*, 41:321-326, 1974.
- [114] Rohlmann A, Bergmann G, Graichen F, and Mayer HM. Influence of muscle forces on loads in internal spinal fixation devices. *Spine*, 23(5):537-42., 1998.
- [115] Rohlmann A, Neller S, Bergmann G, Graichen F, Claes L, and Wilke HJ. Effect of an internal fixator and a bone graft on intersegmental spinal motion and intradiscal pressure in the adjacent regions. *Eur Spine J*, 10(4):301-8., 2001.
- [116] Rohlmann A, Neller S, Claes L, Bergmann G, and Wilke HJ. Influence of a follower load on intradiscal pressure and intersegmental rotation of the lumbar spine. *Spine*, 26(24):E557-61, 2001.

Bibliography

- [117] Salsich GB, Ward SR, Terk MR, and Powers CM. In vivo assessment of patellofemoral joint contact area in individuals who are pain free. *Clin Orthop*, (417):277-84., 2003.
- [118] Schendel MJ, Wood KB, Buttermann GR, Lewis JL, and Ogilvie JW. Experimental measurement of ligament force, facet force, and segment motion in the human lumbar spine. *J Biomech*, 26(4-5):427-38, 1993.
- [119] Schlegel JD, Smith JA, and Schleusener RL. Lumbar motion segment pathology adjacent to thoracolumbar, lumbar, and lumbosacral fusions. *Spine*, 21(8):970-81, 1996.
- [120] Schmoelz W, Huber JF, Nydegger T, Dipl I, Claes L, and Wilke HJ. Dynamic stabilization of the lumbar spine and its effects on adjacent segments: an in vitro experiment. *J Spinal Disord Tech*, 16(4):418-23, 2003.
- [121] Schultz AB. Loads on the lumbar spine. In Jayson M, editor, *The Lumbar Spine and Back Pain*, pages 204-14. Churchill Livingstone, Edinburgh, 1987.
- [122] Sciavicco L and Siciliano B. *Modeling and Control of Robot Manipulators*. McGraw-Hill Companies, Inc., 1996.
- [123] Sengupta DK. Dynamic stabilization devices in the treatment of low back pain. *Orthop Clin North Am*, 35(1):43-56., 2004.
- [124] Sengupta D, Herkowitz HN, Hochschuler SH, and Mulholland RC. Load sharing characteristics of two novel soft stabilization devices in the lumbar motion segments - a biomechanical study in cadaver spine. In *Spine Arthroplasty Society Annual Conference*, Scottsdale, AZ, 2003.
- [125] Sharma M, Langrana NA, and Rodriguez J. Role of ligaments and facets in lumbar spinal stability. *Spine*, 20(8):887-900, 1995.
- [126] Sharma M, Langrana NA, and Rodriguez J. Modeling of facet articulation as a nonlinear moving contact problem: sensitivity study on lumbar facet response. *J Biomech Eng*, 120(1):118-25, 1998.
- [127] Shirazi-Adl A. Finite-element evaluation of contact loads on facets of an l2-l3 lumbar segment in complex loads. *Spine*, 16(5):533-41, 1991.
- [128] Shirazi-Adl A, Ahmed AM, and Shrivastava SC. A finite element study of a lumbar motion segment subjected to pure sagittal plane moments. *J Biomech*, 19(4):331-50, 1986.
- [129] Shirazi-Adl A and Drouin G. Load-bearing role of facets in a lumbar segment under sagittal plane loadings. *J Biomech*, 20(6):601-13, 1987.
- [130] Specchia N. Can dynamic stabilization help disc repair? In *Sulzer Orthopedics Joint, Fracture, Spine Care 3rd Dynesos Meeting*, Lyon, France, 2002.
- [131] Spoor CW and Veldpaus FE. Rigid body motion calculated from spatial co-ordinates of markers. *J Biomech*, 13(4):391-3., 1980.

Bibliography

- [132] Stoll TM, Dubois G, and Schwarzenbach O. The dynamic neutralization system for the spine: a multi-center study of a novel non-fusion system. *Eur Spine J*, 11 Suppl 2:S170-8, 2002.
- [133] Strauss PJ, Novotny JE, Wilder DG, Grobler LJ, and Pope MH. Multidirectional stability of the graf system. *Spine*, 19(8):965-72, 1994.
- [134] Swanson KE, Lindsey DP, Hsu KY, Zucherman JF, and Yerby SA. The effects of an interspinous implant on intervertebral disc pressures. *Spine*, 28(1):26-32., 2003.
- [135] Tekscan. I-scan user's manual, 2001.
- [136] Veldpaus FE, Woltring HJ, and Dortmans LJ. A least-squares algorithm for the equiform transformation from spatial marker co-ordinates. *J Biomech*, 21(1):45-54, 1988.
- [137] Volinn E. The epidemiology of low back pain in the rest of the world. a review of surveys in low- and middle-income countries. *Spine*, 22(15):1747-54., 1997.
- [138] Vuono-Hawkins M, Zimmerman MC, Lee CK, Carter FM, Parsons JR, and Langrana NA. Mechanical evaluation of a canine intervertebral disc spacer: in situ and in vivo studies. *J Orthop Res*, 12(1):119-27., 1994.
- [139] White AA and Panjabi M. *Clinical Biomechanics of the Lumbar Spine*. J.B. Lippincott Company, Philadelphia, second edition, 1990.
- [140] Wilke HJ, Jungkunz B, Wenger K, and Claes LE. Spinal segment range of motion as a function of in vitro test conditions: effects of exposure period, accumulated cycles, angular-deformation rate, and moisture condition. *Anat Rec*, 251(1):15-9., 1998.
- [141] Wilke HJ, Krischak S, and Claes L. Biomechanical comparison of calf and human spines. *J Orthop Res*, 14(3):500-3., 1996.
- [142] Wilke HJ, Neef P, Caimi M, Hoogland T, and Claes LE. New in vivo measurements of pressures in the intervertebral disc in daily life. *Spine*, 24(8):755-62., 1999.
- [143] Wilke HJ, Rohlmann A, Neller S, Graichen F, Claes L, and Bergmann G. Issls prize winner: A novel approach to determine trunk muscle forces during flexion and extension: a comparison of data from an in vitro experiment and in vivo measurements. *Spine*, 28(23):2585-93, 2003.
- [144] Wilke HJ, Wenger K, and Claes L. Testing criteria for spinal implants: recommendations for the standardization of in vitro stability testing of spinal implants. *Eur Spine J*, 7(2):148-54., 1998.
- [145] Wilson DR, Apreleva MV, Eichler MJ, and Harrold FR. Accuracy and repeatability of a pressure measurement system in the patellofemoral joint. *J Biomech*, 36(12):1909-15., 2003.
- [146] Wilson D, Niosi C, Zhu Q, Oxland T, and Wilson DR. Validation of a new method for measuring facet loads in the lumbar spine. *Submitted to Journal of Biomechanics*, 2004.

Bibliography

- [147] Woltring HJ, Huiskes R, de Lange A, and Veldpaus FE. Finite centroid and helical axis estimation from noisy landmark measurements in the study of human joint kinematics. *J Biomech*, 18(5):379-89, 1985.
- [148] Woltring HJ. Representation and calculation of 3-d joint movement. *Human Movement Science*, 10:603-616, 1991.
- [149] Wretenberg P, Ramsey DK, and Nemeth G. Tibiofemoral contact points relative to flexion angle measured with mri. *Clin Biomech (Bristol, Avon)*, 17(6):477-85., 2002.
- [150] Wu JZ, Herzog W, and Epstein M. Effects of inserting a pressensor film into articular joints on the actual contact mechanics. *J Biomech Eng*, 120(5):655-9., 1998.
- [151] Yamamoto I, Panjabi MM, Crisco T, and Oxland T. Three-dimensional movements of the whole lumbar spine and lumbosacral joint. *Spine*, 14(11):1256-60, 1989.
- [152] Yang KH and King AI. Mechanism of facet load transmission as a hypothesis for low-back pain. *Spine*, 9(6):557-65, 1984.
- [153] Zar J. *Biostatistical Analysis*. Prentice Hall, New Jersey, USA, 4th edition, 1999.
- [154] Zucherman J, Hsu K, Picetti r, G., White A, Wynne G, and Taylor L. Clinical efficacy of spinal instrumentation in lumbar degenerative disc disease. *Spine*, 17(7):834-7., 1992.

Appendix A
Summary of Results by Specimen

Table A.1: Kinematic summary for specimens 1-10. Values are rotations in degrees.

Specimen	ROM in flexion												ROM in extension												ROM in flexion-extension												RZ in flexion-extension											
	Intact	Injured	Dyn	Capsule	Injury	Dyn Std	Dyn Long	Dyn Short	Rigid	Post	Intact	Injured	Dyn	Capsule	Injury	Dyn Std	Dyn Long	Dyn Short	Rigid	Post	Intact	Injured	Dyn	Capsule	Injury	Dyn Std	Dyn Long	Dyn Short	Rigid	Post	Intact	Injured	Dyn	Capsule	Injury	Dyn Std	Dyn Long	Dyn Short	Rigid	Post								
H1092	3.9	0.6	4.7	7.1	0.9	0.8	0.7	1.5		4.0	1.0	4.3	5.5	2.5	2.8	0.9	2.8			7.9	1.6	9.0	12.5	3.4	3.6	1.7	4.3			1.7	0.2	1.9	2.7	0.3	0.3	0.1	0.1	0.7										
H1062	2.7	-0.1	4.5	8.1	0.7	1.1	-0.1	0.5	5.7	7.1	-0.5	5.4	6.4	0.7	1.2	0.6	0.8	5.4			9.8	-0.5	9.9	12.5	1.4	2.3	0.6	1.3	11.1		0.3	0.1	1.8	2.6	0.2	0.2	0.2	0.1	3.3									
H1113	5.8	0.1	6.8	8.9	1.6	2.0	1.0	1.3	8.4	3.5	0.5	3.4	5.4	1.7	2.7	0.8	2.1	8.4			8.1	0.8	10.2	14.2	3.3	4.8	1.9	3.4	14.7		0.4	0.1	0.5	2.9	0.3	0.7	0.2	0.5	4.0									
H1107	2.6	0.3	4.4	5.9	0.3	0.4	0.1	0.6	5.4	1.8	0.4	3.2	3.0	0.4	0.5	0.4	0.3	3.0			4.4	0.5	5.2	8.1	0.7	0.9	0.3	1.4	8.4		0.1	0.1	0.3	0.7	0.1	0.1	0.1	0.1	0.7									
H1005	3.8	0.3	4.4	6.8	0.6	0.9	0.5	0.8	7.5	3.9	0.3	3.3	5.8	0.5	1.3	0.2	0.8	6.1			7.1	0.6	7.7	12.5	1.1	2.2	0.7	1.7	13.7		0.5	0.1	0.5	1.3	0.1	0.1	0.1	0.1	1.5									
H1094	1.9	0.1	2.2	4.2	0.5	0.3	0.1	0.5	3.8	2.4	0.2	2.8	3.4	0.6	0.5	0.3	0.6	4.8			4.3	0.3	4.9	7.6	1.1	0.8	0.4	1.1	8.4		0.4	0.1	0.8	0.9	0.1	0.1	0.0	0.1	0.6									
H1109	3.4	0.5	4.1	5.9	2.4	1.1	0.6	1.2	4.8	2.4	0.2	3.8	3.7	1.7	0.6	0.1	0.4	5.4			5.9	0.7	7.9	9.6	4.2	1.7	0.7	1.6	10.2		0.4	0.1	1.4	0.8	0.4	0.1	0.2	0.2	0.8									
H1106	3.8	0.6	3.7	5.5	0.8	1.0	0.8	1.1	6.5	2.2	0.1	2.2	3.2	0.1	0.4	0.1	0.5	2.9			6.0	0.8	5.9	8.7	0.9	1.4	0.8	1.6	9.4		0.2	0.0	0.1	0.6	0.1	0.1	0.1	0.1	0.6									
H1112	6.9	0.6	7.1	8.8	1.3	1.3	1.2	1.4	11.1	3.6	0.4	4.1	3.8	1.4	1.4	0.9	2.6	7.7			10.5	0.4	11.2	10.6	2.7	2.8	2.1	3.9	10.8		0.3	0.0	0.7	0.6	0.3	0.3	0.1	0.2	4.5									
H1111	2.5	0.4	3.2	4.2	1.0	1.1	0.6	1.3	4.9	2.9	0.7	3.1	3.7	0.9	1.1	0.8	1.8	3.7			5.4	1.0	6.3	7.9	1.9	2.1	1.4	3.2	8.6		0.2	0.0	0.2	0.4	0.1	0.2	0.1	0.3	0.6									
mean	3.7	0.3	4.3	6.1	1.0	1.0	0.5	1.0	6.5	3.3	0.3	3.5	4.4	1.1	1.3	0.5	1.3	5.0			7.8	1.0	8.6	10.4	2.1	2.3	1.1	2.3	11.5		0.4	0.1	0.6	1.3	0.2	0.2	0.1	0.2	1.8									
sd	1.5	0.2	1.7	1.4	0.6	0.5	0.4	0.4	2.2	1.5	0.4	0.9	1.2	0.7	0.9	0.3	0.9	1.6			2.2	0.5	2.2	2.4	1.2	1.2	0.7	1.2	3.6		0.5	0.0	0.7	1.0	0.1	0.2	0.0	0.2	1.7									

Appendix A. Summary of Results by Specimen

Appendix A. Summary of Results by Specimen

Table A.2: Helical axis of motion summary for specimens 1-10 with the position presented as a penetration point with a specified plane and with the orientation presented as two angles. Values were normalized to the width, AP diameter, and height of the L4 vertebral body.

Specimen		Flexion to Extension (based on PA orientation)														Flexion to Extension (based on PA orientation)																																																									
		Intact							600N follower load							Intact							600N follower load																																																		
		Intact	Intact-Dyn	Capsule	Injury	Dynesis	Dynesis L	Dynesis S	Rigid	Post	Intact	Intact-Dyn	Capsule	Injury	Dynesis	Dynesis L	Dynesis S	Rigid	Post	Intact	Intact-Dyn	Capsule	Injury	Dynesis	Dynesis L	Dynesis S	Rigid	Post	Intact	Intact-Dyn	Capsule	Injury	Dynesis	Dynesis L	Dynesis S	Rigid	Post																																				
H1113	PA	-38	49	-230	126	33	55	45	59	86	112	79	128	35	123	52	127	68	53	-39	47	-219	123	-26	57	-46	45	-178	71	-250	73	-272	68	-254	32	-51	55	19	46	71	80	25	47	7	48	6	63	59	83	62	104	111	69	3	42	73	49	48	49	72	48	78	46	41	66	63	39	37	49	45	35	71	42
H1111	PA	20	48	75	67	20	47	6	46	30	113	62	114	30	86	49	105	17	30	19	46	71	80	25	47	7	48	6	63	59	83	62	104	111	69	3	42	73	49	48	49	72	48	78	46	41	66	63	39	37	49	45	35	71	42																		
H1109	PA	69	50	47	108	52	48	53	47	3	106	45	97	-5	104	96	98	43	43	30	50	-74	34	89	27	66	50	1774	91	15	57	69	53	117	2	48	37	50	50	-74	34	89	27	66	50	1774	91	15	57	69	53	117	2	48	37																		
H1107	PA	2	51	125	83	2	48	7	47	89	50	41	57	523	581	7	92	-8	41	-24	51	36	91	2	52	-10	52	9	63	43	43	-177	236	26	75	-26	50	28	51	36	91	2	52	-10	52	9	63	43	43	-177	236	26	75	-26	50																		
H1106	PA	24	50	-13	36	6	51	30	54	53	88	47	90	35	59	32	89	36	51	28	51	0	48	30	55	32	55	56	74	10	79	55	63	34	49	29	69	18	40	152	90	26	36	26	43	57	85	-10	50	162	85	201	64	19	44																		
H1094	PA	13	37	-23	45	13	31	16	41	42	98	5	83	-101	103	84	82	24	42	18	40	152	90	26	36	26	43	57	85	-10	50	162	85	201	64	19	44	18	40	152	90	26	36	26	43	57	85	-10	50	162	85	201	64	19	44																		
H1092	PA	-10	47	-26	136	-14	25	-26	56	32	147	13	146	49	119	-54	136	0	0	25	27	8	90	-32	18	-49	37	90	130	4	169	230	126	-94	66	0	0	25	27	8	90	-32	18	-49	37	90	130	4	169	230	126	-94	66	0	0																		
H1002	PA	0	40	-278	126	-13	49	-42	89	-53	149	30	137	-76	184	-44	144	35	78	11	43	145	145	-15	41	-23	53	172	33	8	66	-1319	567	-118	93	47	45	11	43	145	145	-15	41	-23	53	172	33	8	66	-1319	567	-118	93	47	45																		
H1005	PA	14	35	39	159	15	46	8	42	116	82	76	133	143	76	73	104	67	47	67	46	556	73	94	45	69	41	139	82	99	107	297	10	86	115	73	47	67	46	556	73	94	45	69	41	139	82	99	107	297	10	86	115	73	47																		
mean		13	45	-39	66	16	42	4	51	72	100	69	150	17	101	19	49	45	13	45	-39	66	16	42	4	51	72	100	69	150	17	101	19	49	45	13	45	-39	66	16	42	4	51	72	100	69	150	17	101	19	49	45																					
sd		29	6	127	49	45	10	34	8	166	32	49	29	180	156	65	29	34	20	29	6	127	49	45	10	34	8	166	32	49	29	180	156	65	29	34	20	29	6	127	49	45	10	34	8	166	32	49	29	180	156	65	29	34	20																		

Appendix A. Summary of Results by Specimen

Table A.3: Facet load summary for specimens 1-10. Values are facet loads in Newtons.

Specimen	Left Side Axial Rotation - No Load							Right Side Axial Rotation - No Load						
	Capsule	Injury	Std Dyns	Long Dyns	Short Dyns	Rigid	Post	Injury-Capsule	Full Injury	Standard Dyns	Long Dyns	Short Dyns	Rigid Flexion	Post Injury
1092	47.475	45.075	31.125	45.6	31.575	43		55.25	59.4	55.875	54.275	47.925	28.875	89.25
1093	54.875	57.3	85.6	71.7	73.25	62.65	65.25	62.925	67.275	69.825	54.45	62	41.4	81.5
1113	79.5	75.1	57.7	65.9	34.1	84		66.1	107.3	90.3	132.5	56.9	81.5	82.3
1107	35.5	42.1	57	63.4	74.6	0	22.8	11	14.8	51.3	29	64.6	5.3	10.4
1005	55	70.5	32.2	17.4	44.3	13.1	75.5	63.1	67.9	91.3	78.1	102.1	13.1	24.9
1004	70.6	79.5	61.1	39.4	45.4	0	61.3	54.3	73.9	61.6	52.6	5.6	13.9	7.5
1100	63.6	50.4	41.9	31.4	42	7.2	63	84.4	62	65	62.3	63	60.4	79.2
1106	64.6	80.5	77.2	60.2	54	19.7	67	70.3	82.3	24.6	69	64.7	68.8	79.1
1112	23.5	69.4	0	0	3	0	55.8	36.8	67.9	47.1	26.7	30.1	76.1	60.7
1111	68.3	78.6	62.6	66.6	67.8	26.9	63.5	54.5	56.6	71	70.8	94.2	42.8	71.9
Mean	58.1	63.1	45.5	45.6	59.6	14.2	67.5	55.2	65.1	62.8	61.9	57.9	43.4	68.7
St. Dev	16.9	14.2	23.8	23.4	22.5	13.3	20.9	18.3	23.0	19.9	29.8	27.9	26.7	23.3

Specimen	Left Side Axial Rotation - With Load							Right Side Axial Rotation - With Load						
	Capsule	Injury	Std Dyns	Long Dyns	Short Dyns	Rigid	Post	Injury-Capsule	Full Injury	Standard Dyns	Long Dyns	Short Dyns	Rigid Flexion	Post Injury
1092	25.425	53.925	15.725	32.475	70.35	79.65	0	39.475	57.075	51.425	34.55	39.6	10.725	22.875
1093	42.225	26.475	15.725	32.475	24.6	0.375	0	58.775	73.875	78.45	64.35	63.75	41.475	22.875
1113	53.4	53.5	39.4	20.8	45.9	19.9	58.5	42.6	89.3	109.5	-119.2	97.4	90.6	119.3
1107	88.2	82.1	60.3	43.7	67.7	0	67.5	55.6	68.8	88.1	65.4	106.8	11.9	49.6
1005	51.9	71.2	37	19.3	40.1	9.1	73.9	42.3	49.2	37	60.9	89	17.6	57.9
1004	53.9	60.9	40	43.4	41	1.3	59.6	49.8	69.1	60.1	47.9	7.2	16.8	67.4
1100	49.2	61.3	40	30.5	31	1.3	73.2	59.4	57.7	57	70	44	27.2	71.7
1106	56.1	90.1	68.3	37.6	30.9	17.4	79	51.1	58.8	11.2	43.6	57.2	46.7	56.2
1112	30.9	62.6	0	0	7.4	0	63.9	21.6	60.9	49.1	40.3	38	73.2	62.9
1111	71.4	94.7	77.4	78.5	77.9	56.4	112.2	33.5	19.9	36.9	24.1	51	10.4	19
Mean	50.2	64.7	40.2	33.6	45.8	18.5	65.3	45.3	60.3	62.2	57.2	65.5	34.7	66.4
St. Dev	14.5	18.9	0.13	20.4	25.4	27.6	29.3	12.0	18.0	28.8	26.5	30.6	28.2	28.3

Specimen	Left Side Extension - No Load							Right Side Extension - No Load						
	Capsule	Injury	Std Dyns	Long Dyns	Short Dyns	Rigid	Post	Injury-Capsule	Full Injury	Standard Dyns	Long Dyns	Short Dyns	Rigid Flexion	Post Injury
1092	0	2.25	0	0	0.45	0	2.025	7.2	13.65	21.825	28.5	33.075	7.475	32.175
1093	5.1	3.025	10.95	25.5	29.7	0	0	12.675	9.325	0	0	3.75	15.225	0
1113	30.5	29	2.1	0	13.6	19.7	38.1	23.4	8.2	28	28.4	0	45.7	21
1107	16.1	27.3	11.2	6.7	40.5	0	20.4	11.2	11.8	31.3	9.1	57.4	0	15.5
1005	8.2	25.2	0	0.3	3.9	0.7	18.3	10.4	18.1	29	42.7	39.9	3.5	16.3
1004	7	21.3	0	0	30.5	0	24.1	2.7	5.2	2.9	0	0	0	0
1100	29.6	24.1	29.9	21.2	9.1	9.4	27.3	29.4	38.1	49.2	42	32	46	32.9
1106	3.2	5.8	7.3	0.6	5.2	0	5	8.5	6	7.3	6.4	22.5	5.8	4.5
1112	1	4.9	0.5	0	2.6	0	0.9	11.2	2.5	0	10.1	0	9.6	1.9
1111	35	46.2	25.8	23	42.2	7.1	52.1	27.9	40.3	43.3	38.7	81.4	0.1	45.2
Mean	13.1	18.9	6.8	7.7	19.2	3.7	19.3	13.6	15.2	21.3	19.6	26.7	16.1	18.7
St. Dev	13.7	14.4	11.1	10.9	16.0	6.6	18.5	9.9	13.7	18.0	16.1	28.2	22.0	14.5

Specimen	Left Side Extension - With Load							Right Side Extension - With Load						
	Capsule	Injury	Std Dyns	Long Dyns	Short Dyns	Rigid	Post	Injury-Capsule	Full Injury	Standard Dyns	Long Dyns	Short Dyns	Rigid Flexion	Post Injury
1092	0.375	0	0	2.25	19.725	20.1	17.7	36.925	36.525	21.75	13.95	17.25	1.125	13.2
1093	5.7	0	0	0	0	0	0	18.725	15.075	19.275	15.9	18.75	1.675	6.225
1113	31.4	26.2	0	0	3	0	39.2	19.9	30.2	34.3	29.8	10.0	53.4	50.5
1107	36.3	47.3	17.9	18.1	50.2	0	48.9	42.6	38.2	58.8	38.7	81.4	0	44.8
1005	15.4	29.4	0	0	6.2	1.2	28.4	10.9	27.9	8.3	6.2	24.1	0	18.6
1004	4.4	21.2	0	0	16.2	0	20.4	4.8	3.3	5.7	0	0.5	0	2.1
1100	23.8	15.3	22.1	0	5	0	22.8	22.1	16.6	36.7	32.2	23.3	0	17.5
1106	10.4	14.8	8.2	4.1	13	0	14.1	11.3	13.8	9.4	10.6	26	3.1	12.3
1112	9.9	24.3	0	0	1.2	0	6.1	7.6	9.7	7	20.1	2.8	54.5	26.8
1111	39.4	52.3	39.2	29.6	34.1	26.8	65.6	18.2	10.3	11.3	0	33.7	0	25.2
Mean	17.6	23.2	8.7	5.4	14.8	4.7	26.3	18.4	18.7	21.2	16.7	23.8	11.4	21.7
St. Dev	13.9	17.4	13.5	10.2	16.2	9.7	20.0	12.5	11.9	17.1	13.4	22.7	22.5	15.7

Specimen	Left Side Flexion - No Load							Right Side Flexion - No Load						
	Capsule	Injury	Std Dyns	Long Dyns	Short Dyns	Rigid	Post	Injury-Capsule	Full Injury	Standard Dyns	Long Dyns	Short Dyns	Rigid Flexion	Post Injury
1092	0	0	1.975	5.95	24	7.725	0	11.625	15.875	13.975	12.15	5.625	0	0.45
1093	10.875	12.825	13.8	28.8	28.95	12	6.7	0	2.775	16.8	0	15.2	0.975	5.7
1113	0.6	12.4	26.1	1.6	34.6	5.1	21.7	5.8	0	51.6	14.1	61.5	1.2	0
1107	0	0	25.5	19.9	48.7	0	0	0	0	39.1	14.9	59.3	0	3.9
1005	0	0	0	0	0.7	0.8	0	0	0	48.9	42.7	51.2	0.6	3.9
1004	0.5	0	0	0.6	10	1.2	0	0.5	4	14.7	0.5	6.2	13.4	4.9
1100	0	0	49.2	25.7	20.8	0	0	6.2	5.5	62.7	51.8	42.7	14.5	2.1
1106	11.8	11.1	23.2	17	23	0	12.4	6	7.1	22	29.2	40.4	6.3	9.5
1112	0.5	0	0	0	1.9	0	0	11.2	4.5	0	2.5	8	21.1	0
1111	0	0	8.6	0	34.5	0	0	4.3	5.4	9.9	4	20.9	3.9	0
Mean	2.4	3.8	15.5	9.9	22.7	1.5	4.3	4.3	4.0	27.0	17.7	35.6	6.0	2.1
St. Dev	4.7	5.8	16.2	11.7	15.2	2.7	7.5	3.7	4.9	21.9	17.0	23.5	7.6	3.2

Specimen	Left Side Flexion - With Load							Right Side Flexion - With Load						
	Capsule	Injury	Std Dyns	Long Dyns	Short Dyns	Rigid	Post	Injury-Capsule	Full Injury	Standard Dyns	Long Dyns	Short Dyns	Rigid Flexion	Post Injury
1092	4.425	7.575	0	2.025	45.525	13.725	3.925	14.775	16.5	10.2	14.7	6.15	1.425	0
1093	0	0	0	0	0.15	0	0	0	13.5	29.4	2.55	17.7	2.325	5.7
1113	0	0	5.5	0.5	16.8	0.5	0.5	5	3.9	61.3	23.4	72.3	17.4	0
1107	0	0	34.3	33.3	61.8	0	0	15	13.4	73.4	49	89.9	2.6	15.2
1005	0	0	0	0	0.3	0	0	0	0	31.1	28.4	44.5	0	0
1004	0	0	0	0	2.4	1.1	0	4.1	0	14.4	0	8.5	13.3	3.8
1100	0	0	40.3	7.7	15.6	0	0.3	8.3	1.9	50	24.4	33.4	4.8	0
1106	4.5	17.7	20.8	13.7	25	0	31.6	5.5	4.6	29.8	29.4	42.5	6.6	9.1
1112	0	0	0	0	1.1	0.5	0	0	0	24.2	28.3	31.5	32.0	0
1111	0.7	12.9	30.4	18.8	43	10.7	20.4	0	0	1.4	0.1	5	0	0
Mean	1.0	2.9	13.1	7.6	21.2	2.6	3.9	5.3	5.4	31.8	20.0	36.2	8.1	3.4
St. Dev	1.9	4.7	16.5	11.2	22.2	5.0	7.1	5.8	6.5	23.0	15.7	28.7	10.4	5.2

Specimen	Left Side Lateral Bending - No Load							Right Side Lateral Bending - No Load						
	Capsule	Injury	Std Dyns	Long Dyns	Short Dyns	Rigid	Post	Injury-Capsule	Full Injury	Standard Dyns	Long Dyns	Short Dyns	Rigid Flexion	Post Injury
1092	20.475	20.175	7.05	12.825	15.525	18.875	25.05	39.75	33	12.525	18.975	26.25	8.025	57.45
1093	6.625	3.45	21.225	36.025	31.95	3	0.15	9.775	20.95	17.325	0.3	-11.175	17.95	25.05
1113	33.1	21.5	25.5	19.1	19.8	16.5	41.9	28	37.4	38.5	45.7	47.4	37	50.1
1107	3.1	2.6	26.9	11.8	44	0	2	12.5	11.3	50.3	16	71.8	0.8	10.5
1005	0.1	0.6	0.6	0.5	12.1	6.9	1.5	8.8	6.8	61.2	59.7	72.7	14	8.2
1004	2.5	19.8	1.7	0.4	22.4	3.9	15.6	2.1	7.1	18	3.4	5	12.8	12
1100	20.9	24.6	35.5	28.4	27.5	3.8	31.6	31.7	32.7	63.4	46.7	43.3	53.3	36.9
1106	10.5	11	26	11.7	17.6	3.7	13.6	1.8	4.7	21.4	19.3	30	15	1.4
1112	0.1	1.8	0	0.1	2.8	0.4	1.6	2.7	5.7	0.6	6	3.1	48.9	7.4
1111	12.1	15.4	16	9.2	36.1	1.3	18.3	18.5	18.3	28.3	23.5	62.8	3	18.8
Mean	11.0	12.1	16.3	12.6	23.2	5.8	15.2	15.5	17.8	30.9</				

Appendix A. Summary of Results by Specimen

Table A.4: Intradiscal pressure summary for specimens 1-10. Values are absolute intradiscal pressures in MPa.

Follower load = 600N			
Flexion			
Specimen	Intact	Intact-Dyn	Capsule
H1092	0.33	0.63	0.22
H1062	0.37	0.56	0.36
H1113	0.63	0.58	0.69
H1107	0.37	0.32	0.39
H1005	0.74	0.57	0.68
H1094	0.37	0.44	0.43
H1109	0.34	0.41	0.32
H1106	0.70	0.45	0.69
H1112	0.64	0.51	0.61
H1111	0.46	0.52	0.42
mean	0.50	0.50	0.48
stdev	0.16	0.09	0.17

Follower load = 600N			
Right Lateral Bending			
Specimen	Intact	Intact-Dyn	Capsule
H1092	0.01	0.06	0.03
H1062	0.13	0.41	0.10
H1113	0.40	0.43	0.44
H1107	0.40	0.28	0.37
H1005	0.31	0.42	0.31
H1094	0.31	0.00	0.31
H1109	0.23	0.29	0.20
H1106	0.21	0.32	0.20
H1112	0.45	0.41	0.43
H1111	0.23	0.32	0.24
mean	0.27	0.29	0.26
stdev	0.13	0.15	0.14

Follower load = 600N			
Right Axial Rotation			
Specimen	Intact	Intact-Dyn	Capsule
H1092	0.35	0.34	0.37
H1062	0.42	0.44	0.40
H1113	0.57	0.48	0.57
H1107	0.40	0.29	0.41
H1005	0.56	0.48	0.58
H1094	0.42	0.38	0.41
H1109	0.37	0.32	0.38
H1106	0.41	0.36	0.41
H1112	0.55	0.44	0.54
H1111	0.41	0.45	0.44
mean	0.45	0.40	0.45
stdev	0.08	0.07	0.08

Follower load = 600N			
Extension			
Specimen	Intact	Intact-Dyn	Capsule
H1092	0.13	0.25	0.10
H1062	0.45	0.32	0.44
H1113	0.58	0.32	0.61
H1107	0.47	0.26	0.50
H1005	0.71	0.39	0.76
H1094	0.34	0.27	0.36
H1109	0.34	0.25	0.35
H1106	0.44	0.34	0.45
H1112	0.53	0.32	0.54
H1111	0.36	0.29	0.41
mean	0.44	0.30	0.45
stdev	0.16	0.05	0.18

Follower load = 600N			
Left Lateral Bending			
Specimen	Intact	Intact-Dyn	Capsule
H1092	0.83	0.76	0.78
H1062	0.17	0.48	0.17
H1113	0.39	0.42	0.40
H1107	0.41	0.31	0.38
H1005	0.73	0.53	0.68
H1094	0.23	0.00	0.23
H1109	0.16	0.34	0.17
H1106	0.48	0.31	0.48
H1112	0.62	0.43	0.61
H1111	0.63	0.51	0.63
mean	0.47	0.41	0.45
stdev	0.23	0.20	0.22

Follower load = 600N			
Left Axial Rotation			
Specimen	Intact	Intact-Dyn	Capsule
H1092	0.38	0.45	0.41
H1062	0.52	0.41	0.53
H1113	0.56	0.46	0.56
H1107	0.40	0.28	0.39
H1005	0.59	0.49	0.59
H1094	0.40	0.34	0.38
H1109	0.35	0.34	0.35
H1106	0.44	0.39	0.44
H1112	0.52	0.43	0.52
H1111	0.45	0.39	0.42
mean	0.46	0.40	0.46
stdev	0.08	0.07	0.08

Follower load = 600N			
Neutral			
Specimen	Intact	Intact-Dyn	Capsule
H1092	0.30	0.43	0.25
H1062	0.52	0.41	0.47
H1113	0.51	0.43	0.56
H1107	0.38	0.29	0.40
H1005	0.55	0.45	0.58
H1094	0.38	0.33	0.38
H1109	0.38	0.32	0.37
H1106	0.42	0.37	0.42
H1112	0.52	0.41	0.53
H1111	0.43	0.40	0.44
mean	0.44	0.38	0.44
stdev	0.08	0.06	0.10

Follower load = 600N			
Neutral			
Specimen	Intact	Intact-Dyn	Capsule
H1092	0.19	0.32	0.18
H1062	0.43	0.43	0.46
H1113	0.59	0.43	0.40
H1107	0.40	0.29	0.37
H1005	0.52	0.46	0.54
H1094	0.40	0.00	0.41
H1109	0.37	0.32	0.36
H1106	0.38	0.37	0.37
H1112	0.52	0.43	0.51
H1111	0.39	0.40	0.39
mean	0.42	0.34	0.40
stdev	0.11	0.13	0.10

Follower load = 600N			
Neutral			
Specimen	Intact	Intact-Dyn	Capsule
H1092	0.18	0.33	0.19
H1062	0.47	0.38	0.46
H1113	0.52	0.43	0.52
H1107	0.39	0.28	0.39
H1005	0.55	0.45	0.57
H1094	0.39	0.34	0.38
H1109	0.36	0.32	0.36
H1106	0.40	0.36	0.40
H1112	0.51	0.40	0.51
H1111	0.44	0.42	0.44
mean	0.42	0.37	0.42
stdev	0.11	0.06	0.11

Appendix B
Results of Statistical Analysis

B.1 Effect of Specimen Condition

Table B.1: Effect of specimen condition on range of motion. Results of repeated measures MANOVA with a 95% level of significance.

Direction	Follower Load	p-value
Flexion	0 N	3.77425E-20
Intact - Intact Dyn	0 N	0.00017
Intact - Capsule	0 N	0.26588
Intact - Injury	0 N	0.00016
Intact - Dynesys	0 N	0.00012
Intact - Rigid	0 N	0.00013
Intact - Post	0 N	0.00017
Intact Dyn - Capsule	0 N	0.00013
Intact Dyn - Injury	0 N	0.00014
Intact Dyn - Dynesys	0 N	0.26292
Intact Dyn - Rigid	0 N	0.14296
Intact Dyn - Post	0 N	0.00014
Capsule - Injury	0 N	0.00063
Capsule - Dynesys	0 N	0.00013
Capsule - Rigid	0 N	0.00017
Capsule - Post	0 N	0.00017
Injury - Dynesys	0 N	0.00017
Injury - Rigid	0 N	0.00013
Injury - Post	0 N	0.29383
Dynesys - Rigid	0 N	0.92634
Dynesys - Post	0 N	0.00013
Rigid - Post	0 N	0.00014
Extension	0 N	1.57935E-16
Intact - Intact Dyn	0 N	0.00017
Intact - Capsule	0 N	0.58653
Intact - Injury	0 N	0.05128
Intact - Dynesys	0 N	0.00013
Intact - Rigid	0 N	0.00012
Intact - Post	0 N	0.00074
Intact Dyn - Capsule	0 N	0.00013
Intact Dyn - Injury	0 N	0.00014
Intact Dyn - Dynesys	0 N	0.12916
Intact Dyn - Rigid	0 N	0.09953
Intact Dyn - Post	0 N	0.00014
Capsule - Injury	0 N	0.06862
Capsule - Dynesys	0 N	0.00017
Capsule - Rigid	0 N	0.00013
Capsule - Post	0 N	0.00181
Injury - Dynesys	0 N	0.00013
Injury - Rigid	0 N	0.00017
Injury - Post	0 N	0.07664
Dynesys - Rigid	0 N	0.57804
Dynesys - Post	0 N	0.00014
Rigid - Post	0 N	0.00013

Direction	Follower Load	p-value
Flexion	600 N	1.5251E-15
Intact - Intact Dyn	600 N	0.00017
Intact - Capsule	600 N	0.33957
Intact - Injury	600 N	0.04927
Intact - Dynesys	600 N	0.00012
Intact - Rigid	600 N	0.00013
Intact - Post	600 N	0.02472
Intact Dyn - Capsule	600 N	0.00013
Intact Dyn - Injury	600 N	0.00014
Intact Dyn - Dynesys	600 N	0.93983
Intact Dyn - Rigid	600 N	0.81475
Intact Dyn - Post	600 N	0.00014
Capsule - Injury	600 N	0.15070
Capsule - Dynesys	600 N	0.00013
Capsule - Rigid	600 N	0.00017
Capsule - Post	600 N	0.12764
Injury - Dynesys	600 N	0.00017
Injury - Rigid	600 N	0.00013
Injury - Post	600 N	0.60445
Dynesys - Rigid	600 N	0.92065
Dynesys - Post	600 N	0.00013
Rigid - Post	600 N	0.00014
Extension	600 N	2.31122E-11
Intact - Intact Dyn	600 N	0.00015
Intact - Capsule	600 N	0.56449
Intact - Injury	600 N	0.47761
Intact - Dynesys	600 N	0.00017
Intact - Rigid	600 N	0.00013
Intact - Post	600 N	0.74491
Intact Dyn - Capsule	600 N	0.00015
Intact Dyn - Injury	600 N	0.00014
Intact Dyn - Dynesys	600 N	0.80694
Intact Dyn - Rigid	600 N	0.74488
Intact Dyn - Post	600 N	0.00017
Capsule - Injury	600 N	0.40423
Capsule - Dynesys	600 N	0.00014
Capsule - Rigid	600 N	0.00018
Capsule - Post	600 N	0.87893
Injury - Dynesys	600 N	0.00013
Injury - Rigid	600 N	0.00014
Injury - Post	600 N	0.47551
Dynesys - Rigid	600 N	0.76703
Dynesys - Post	600 N	0.00013
Rigid - Post	600 N	0.00014

Appendix B. Results of Statistical Analysis

Table B.2: Effect of specimen condition on range of motion (continued). Results of repeated measures MANOVA with a 95% level of significance.

Direction	Follower Load	p-value
Lateral Bending	0 N	2.48754E-18
Intact - Intact Dyn	0 N	0.00017
Intact - Capsule	0 N	0.52699
Intact - Injury	0 N	0.02304
Intact - Dynesys	0 N	0.00012
Intact - Rigid	0 N	0.00013
Intact - Post	0 N	0.00098
Intact Dyn - Capsule	0 N	0.00013
Intact Dyn - Injury	0 N	0.00014
Intact Dyn - Dynesys	0 N	0.77365
Intact Dyn - Rigid	0 N	0.53627
Intact Dyn - Post	0 N	0.00014
Capsule - Injury	0 N	0.04078
Capsule - Dynesys	0 N	0.00013
Capsule - Rigid	0 N	0.00017
Capsule - Post	0 N	0.00317
Injury - Dynesys	0 N	0.00017
Injury - Rigid	0 N	0.00013
Injury - Post	0 N	0.17631
Dynesys - Rigid	0 N	0.95134
Dynesys - Post	0 N	0.00013
Rigid - Post	0 N	0.00014
Axial Rotation	0 N	1.40419E-17
Intact - Intact Dyn	0 N	0.00013
Intact - Capsule	0 N	0.42235
Intact - Injury	0 N	0.01010
Intact - Dynesys	0 N	0.00244
Intact - Rigid	0 N	0.00017
Intact - Post	0 N	0.00030
Intact Dyn - Capsule	0 N	0.00017
Intact Dyn - Injury	0 N	0.00013
Intact Dyn - Dynesys	0 N	0.00066
Intact Dyn - Rigid	0 N	0.98902
Intact Dyn - Post	0 N	0.00014
Capsule - Injury	0 N	0.02929
Capsule - Dynesys	0 N	0.00068
Capsule - Rigid	0 N	0.00013
Capsule - Post	0 N	0.00115
Injury - Dynesys	0 N	0.00017
Injury - Rigid	0 N	0.00014
Injury - Post	0 N	0.11878
Dynesys - Rigid	0 N	0.00157
Dynesys - Post	0 N	0.00013
Rigid - Post	0 N	0.00014

Direction	Follower Load	p-value
Lateral Bending	600 N	1.09479E-07
Intact - Intact Dyn	600 N	0.00023
Intact - Capsule	600 N	0.84202
Intact - Injury	600 N	0.03453
Intact - Dynesys	600 N	0.00020
Intact - Rigid	600 N	0.00020
Intact - Post	600 N	0.09643
Intact Dyn - Capsule	600 N	0.00020
Intact Dyn - Injury	600 N	0.02793
Intact Dyn - Dynesys	600 N	0.81342
Intact Dyn - Rigid	600 N	0.94719
Intact Dyn - Post	600 N	0.00791
Capsule - Injury	600 N	0.03792
Capsule - Dynesys	600 N	0.00018
Capsule - Rigid	600 N	0.00018
Capsule - Post	600 N	0.15069
Injury - Dynesys	600 N	0.04084
Injury - Rigid	600 N	0.06024
Injury - Post	600 N	0.36332
Dynesys - Rigid	600 N	0.93925
Dynesys - Post	600 N	0.00762
Rigid - Post	600 N	0.00966
Axial Rotation	600 N	2.17664E-06
Intact - Intact Dyn	600 N	0.00382
Intact - Capsule	600 N	0.68416
Intact - Injury	600 N	0.42658
Intact - Dynesys	600 N	0.35593
Intact - Rigid	600 N	0.00604
Intact - Post	600 N	0.38250
Intact Dyn - Capsule	600 N	0.00221
Intact Dyn - Injury	600 N	0.00036
Intact Dyn - Dynesys	600 N	0.01687
Intact Dyn - Rigid	600 N	0.95421
Intact Dyn - Post	600 N	0.00024
Capsule - Injury	600 N	0.40138
Capsule - Dynesys	600 N	0.37949
Capsule - Rigid	600 N	0.00296
Capsule - Post	600 N	0.45834
Injury - Dynesys	600 N	0.14109
Injury - Rigid	600 N	0.00041
Injury - Post	600 N	0.72482
Dynesys - Rigid	600 N	0.03800
Dynesys - Post	600 N	0.09807
Rigid - Post	600 N	0.00026

Appendix B. Results of Statistical Analysis

Table B.3: Effect of specimen condition on neutral zone. Results of repeated measures MANOVA with a 95% level of significance.

Direction	Follower Load	p-value
Flexion-Extension	0 N	6.51539E-08
Intact - Intact Dyn	0 N	0.88667
Intact - Capsule	0 N	0.24297
Intact - Injury	0 N	0.02353
Intact - Dynesys	0 N	0.74579
Intact - Rigid	0 N	0.93470
Intact - Post	0 N	0.00033
Intact Dyn - Capsule	0 N	0.33004
Intact Dyn - Injury	0 N	0.01412
Intact Dyn - Dynesys	0 N	0.91826
Intact Dyn - Rigid	0 N	0.71341
Intact Dyn - Post	0 N	0.00018
Capsule - Injury	0 N	0.12776
Capsule - Dynesys	0 N	0.29604
Capsule - Rigid	0 N	0.42638
Capsule - Post	0 N	0.00375
Injury - Dynesys	0 N	0.01850
Injury - Rigid	0 N	0.02684
Injury - Post	0 N	0.05813
Dynesys - Rigid	0 N	0.98085
Dynesys - Post	0 N	0.00023
Rigid - Post	0 N	0.00026
Lateral Bending	0 N	1.65243E-10
Intact - Intact Dyn	0 N	0.00247
Intact - Capsule	0 N	0.63081
Intact - Injury	0 N	0.20173
Intact - Dynesys	0 N	0.00243
Intact - Rigid	0 N	0.00223
Intact - Post	0 N	0.00264
Intact Dyn - Capsule	0 N	0.00097
Intact Dyn - Injury	0 N	0.00016
Intact Dyn - Dynesys	0 N	0.83333
Intact Dyn - Rigid	0 N	0.85692
Intact Dyn - Post	0 N	0.00014
Capsule - Injury	0 N	0.21586
Capsule - Dynesys	0 N	0.00115
Capsule - Rigid	0 N	0.00152
Capsule - Post	0 N	0.00597
Injury - Dynesys	0 N	0.00016
Injury - Rigid	0 N	0.00021
Injury - Post	0 N	0.05166
Dynesys - Rigid	0 N	0.75152
Dynesys - Post	0 N	0.00014
Rigid - Post	0 N	0.00013
Axial Rotation	0 N	3.74894E-05
Intact - Intact Dyn	0 N	0.17447
Intact - Capsule	0 N	0.58988
Intact - Injury	0 N	0.28480
Intact - Dynesys	0 N	0.23251
Intact - Rigid	0 N	0.15322
Intact - Post	0 N	0.02766
Intact Dyn - Capsule	0 N	0.32399
Intact Dyn - Injury	0 N	0.01886
Intact Dyn - Dynesys	0 N	0.81647
Intact Dyn - Rigid	0 N	0.90705
Intact Dyn - Post	0 N	0.00033
Capsule - Injury	0 N	0.24528
Capsule - Dynesys	0 N	0.27109
Capsule - Rigid	0 N	0.25379
Capsule - Post	0 N	0.01234
Injury - Dynesys	0 N	0.04166
Injury - Rigid	0 N	0.01829
Injury - Post	0 N	0.11952
Dynesys - Rigid	0 N	0.62607
Dynesys - Post	0 N	0.00063
Rigid - Post	0 N	0.00033

Direction	Follower Load	p-value
Flexion-Extension	600 N	0.00380
Intact - Intact Dyn	600 N	0.16014
Intact - Capsule	600 N	0.88288
Intact - Injury	600 N	0.46804
Intact - Dynesys	600 N	0.14874
Intact - Rigid	600 N	0.11610
Intact - Post	600 N	0.69024
Intact Dyn - Capsule	600 N	0.15803
Intact Dyn - Injury	600 N	0.01685
Intact Dyn - Dynesys	600 N	0.88461
Intact Dyn - Rigid	600 N	0.95834
Intact Dyn - Post	600 N	0.23882
Capsule - Injury	600 N	0.30530
Capsule - Dynesys	600 N	0.15944
Capsule - Rigid	600 N	0.14411
Capsule - Post	600 N	0.84737
Injury - Dynesys	600 N	0.01884
Injury - Rigid	600 N	0.01902
Injury - Post	600 N	0.39628
Dynesys - Rigid	600 N	0.89545
Dynesys - Post	600 N	0.19371
Rigid - Post	600 N	0.11003
Lateral Bending	600 N	0.00020
Intact - Intact Dyn	600 N	0.02148
Intact - Capsule	600 N	0.95821
Intact - Injury	600 N	0.09669
Intact - Dynesys	600 N	0.01540
Intact - Rigid	600 N	0.02370
Intact - Post	600 N	0.99821
Intact Dyn - Capsule	600 N	0.01592
Intact Dyn - Injury	600 N	0.42913
Intact Dyn - Dynesys	600 N	0.93231
Intact Dyn - Rigid	600 N	0.92894
Intact Dyn - Post	600 N	0.00878
Capsule - Injury	600 N	0.06291
Capsule - Dynesys	600 N	0.01336
Capsule - Rigid	600 N	0.01935
Capsule - Post	600 N	0.99562
Injury - Dynesys	600 N	0.65789
Injury - Rigid	600 N	0.64926
Injury - Post	600 N	0.02520
Dynesys - Rigid	600 N	0.79241
Dynesys - Post	600 N	0.00955
Rigid - Post	600 N	0.01261
Axial Rotation	600 N	0.10332

Appendix B. Results of Statistical Analysis

Table B.4: Effect of specimen condition on position of helical axis of motion. Results of repeated measures MANOVA with a 95% level of significance.

Direction	Follower Load	p-value	p-value
Flexion-Extension		y	z
Overall effect	0 N	0.05325	0.00000
Intact - Intact Dyn	0 N		0.00013
Intact - Capsule	0 N		0.99448
Intact - Injury	0 N		0.55787
Intact - Dynesys	0 N		0.00017
Intact - Rigid	0 N		0.00013
Intact - Post	0 N		0.99785
Intact Dyn - Capsule	0 N		0.00015
Intact Dyn - Injury	0 N		0.00013
Intact Dyn - Dynesys	0 N		0.53679
Intact Dyn - Rigid	0 N		0.59228
Intact Dyn - Post	0 N		0.00018
Capsule - Injury	0 N		0.90003
Capsule - Dynesys	0 N		0.00015
Capsule - Rigid	0 N		0.00014
Capsule - Post	0 N		0.92238
Injury - Dynesys	0 N		0.00013
Injury - Rigid	0 N		0.00017
Injury - Post	0 N		0.82451
Dynesys - Rigid	0 N		0.72143
Dynesys - Post	0 N		0.00013
Rigid - Post	0 N		0.00014
Lateral Bending		x	y
Overall effect	0 N	0.00635	0.97394
Intact - Intact Dyn	0 N	0.00166	
Intact - Capsule	0 N	0.95836	
Intact - Injury	0 N	0.99448	
Intact - Dynesys	0 N	0.20513	
Intact - Rigid	0 N	0.48238	
Intact - Post	0 N	0.98528	
Intact Dyn - Capsule	0 N	0.00190	
Intact Dyn - Injury	0 N	0.00103	
Intact Dyn - Dynesys	0 N	0.04954	
Intact Dyn - Rigid	0 N	0.02214	
Intact Dyn - Post	0 N	0.00124	
Capsule - Injury	0 N	0.99877	
Capsule - Dynesys	0 N	0.24267	
Capsule - Rigid	0 N	0.57341	
Capsule - Post	0 N	0.99728	
Injury - Dynesys	0 N	0.10518	
Injury - Rigid	0 N	0.18755	
Injury - Post	0 N	0.93484	
Dynesys - Rigid	0 N	0.46237	
Dynesys - Post	0 N	0.14918	
Rigid - Post	0 N	0.33914	
Axial Rotation		x	z
Overall effect	0 N	0.63812	0.03145
Intact - Intact Dyn	0 N		0.66705
Intact - Capsule	0 N		0.98079
Intact - Injury	0 N		0.88426
Intact - Dynesys	0 N		0.04247
Intact - Rigid	0 N		0.84677
Intact - Post	0 N		0.82882
Intact Dyn - Capsule	0 N		0.55872
Intact Dyn - Injury	0 N		0.66287
Intact Dyn - Dynesys	0 N		0.09711
Intact Dyn - Rigid	0 N		0.60152
Intact Dyn - Post	0 N		0.62864
Capsule - Injury	0 N		0.65567
Capsule - Dynesys	0 N		0.03237
Capsule - Rigid	0 N		0.71011
Capsule - Post	0 N		0.98836
Injury - Dynesys	0 N		0.06331
Injury - Rigid	0 N		0.73352
Injury - Post	0 N		0.90021
Dynesys - Rigid	0 N		0.07827
Dynesys - Post	0 N		0.03208
Rigid - Post	0 N		0.83872

Direction	Follower Load	p-value	p-value
Flexion-Extension		y	z
Overall effect	600 N	0.91333	0.00037
Intact - Intact Dyn	600 N		0.00475
Intact - Capsule	600 N		0.90942
Intact - Injury	600 N		0.85373
Intact - Dynesys	600 N		0.02571
Intact - Rigid	600 N		0.20748
Intact - Post	600 N		0.97946
Intact Dyn - Capsule	600 N		0.00489
Intact Dyn - Injury	600 N		0.00506
Intact Dyn - Dynesys	600 N		0.42888
Intact Dyn - Rigid	600 N		0.11927
Intact Dyn - Post	600 N		0.00523
Capsule - Injury	600 N		0.95167
Capsule - Dynesys	600 N		0.02960
Capsule - Rigid	600 N		0.26908
Capsule - Post	600 N		0.93680
Injury - Dynesys	600 N		0.02260
Injury - Rigid	600 N		0.13099
Injury - Post	600 N		0.98111
Dynesys - Rigid	600 N		0.22794
Dynesys - Post	600 N		0.03384
Rigid - Post	600 N		0.32254
Lateral Bending		x	y
Overall effect	600 N	0.03698	0.03358
Intact - Intact Dyn	600 N	0.17032	0.52711
Intact - Capsule	600 N	0.81194	0.94638
Intact - Injury	600 N	0.85799	0.18032
Intact - Dynesys	600 N	0.18960	0.14720
Intact - Rigid	600 N	0.60238	0.11709
Intact - Post	600 N	0.95287	0.71012
Intact Dyn - Capsule	600 N	0.15278	0.76182
Intact Dyn - Injury	600 N	0.07966	0.33641
Intact Dyn - Dynesys	600 N	0.79734	0.32844
Intact Dyn - Rigid	600 N	0.26942	0.29962
Intact Dyn - Post	600 N	0.18085	0.87820
Capsule - Injury	600 N	0.84593	0.22457
Capsule - Dynesys	600 N	0.17658	0.17068
Capsule - Rigid	600 N	0.72676	0.12911
Capsule - Post	600 N	0.95489	0.82575
Injury - Dynesys	600 N	0.11080	0.77473
Injury - Rigid	600 N	0.68270	0.85323
Injury - Post	600 N	0.62286	0.21003
Dynesys - Rigid	600 N	0.19675	0.60394
Dynesys - Post	600 N	0.22441	0.27335
Rigid - Post	600 N	0.84433	0.28203
Axial Rotation		x	z
Overall effect	600 N	0.57678	0.45899
Intact - Intact Dyn	600 N		
Intact - Capsule	600 N		
Intact - Injury	600 N		
Intact - Dynesys	600 N		
Intact - Rigid	600 N		
Intact - Post	600 N		
Intact Dyn - Capsule	600 N		
Intact Dyn - Injury	600 N		
Intact Dyn - Dynesys	600 N		
Intact Dyn - Rigid	600 N		
Intact Dyn - Post	600 N		
Capsule - Injury	600 N		
Capsule - Dynesys	600 N		
Capsule - Rigid	600 N		
Capsule - Post	600 N		
Injury - Dynesys	600 N		
Injury - Rigid	600 N		
Injury - Post	600 N		
Dynesys - Rigid	600 N		
Dynesys - Post	600 N		
Rigid - Post	600 N		

Appendix B. Results of Statistical Analysis

Table B.5: Effect of specimen condition on orientation of helical axis of motion. Results of repeated measures MANOVA with a 95% level of significance.

Direction	Follower Load	p-value	p-value
Flexion-Extension		XY	XZ
Overall effect	0 N	0.70598	0.01243
Intact - Intact Dyn	0 N		0.10612
Intact - Capsule	0 N		0.97673
Intact - Injury	0 N		0.90688
Intact - Dynesys	0 N		0.06046
Intact - Rigid	0 N		0.90963
Intact - Post	0 N		0.95762
Intact Dyn - Capsule	0 N		0.08500
Intact Dyn - Injury	0 N		0.13465
Intact Dyn - Dynesys	0 N		0.72139
Intact Dyn - Rigid	0 N		0.08312
Intact Dyn - Post	0 N		0.08477
Capsule - Injury	0 N		0.69657
Capsule - Dynesys	0 N		0.04977
Capsule - Rigid	0 N		0.83903
Capsule - Post	0 N		0.86316
Injury - Dynesys	0 N		0.09169
Injury - Rigid	0 N		0.89910
Injury - Post	0 N		0.93399
Dynesys - Rigid	0 N		0.09436
Dynesys - Post	0 N		0.07442
Rigid - Post	0 N		0.72293
Lateral Bending		YZ	XZ
Overall effect	0 N	0.11991	0.01440
Intact - Intact Dyn	0 N		0.03069
Intact - Capsule	0 N		0.91129
Intact - Injury	0 N		0.98054
Intact - Dynesys	0 N		0.39043
Intact - Rigid	0 N		0.70470
Intact - Post	0 N		0.98622
Intact Dyn - Capsule	0 N		0.03111
Intact Dyn - Injury	0 N		0.02708
Intact Dyn - Dynesys	0 N		0.19077
Intact Dyn - Rigid	0 N		0.12593
Intact Dyn - Post	0 N		0.02599
Capsule - Injury	0 N		0.93896
Capsule - Dynesys	0 N		0.36912
Capsule - Rigid	0 N		0.64994
Capsule - Post	0 N		0.97154
Injury - Dynesys	0 N		0.30870
Injury - Rigid	0 N		0.52456
Injury - Post	0 N		0.87980
Dynesys - Rigid	0 N		0.51134
Dynesys - Post	0 N		0.25543
Rigid - Post	0 N		0.35285
Axial Rotation		XY	YZ
Overall effect	0 N	1.09E-01	8.30E-05
Intact - Intact Dyn	0 N		0.01735
Intact - Capsule	0 N		0.81925
Intact - Injury	0 N		0.38019
Intact - Dynesys	0 N		0.00349
Intact - Rigid	0 N		0.02724
Intact - Post	0 N		0.95815
Intact Dyn - Capsule	0 N		0.01445
Intact Dyn - Injury	0 N		0.08355
Intact Dyn - Dynesys	0 N		0.47245
Intact Dyn - Rigid	0 N		0.68748
Intact Dyn - Post	0 N		0.01789
Capsule - Injury	0 N		0.50926
Capsule - Dynesys	0 N		0.00250
Capsule - Rigid	0 N		0.02747
Capsule - Post	0 N		0.96111
Injury - Dynesys	0 N		0.02653
Injury - Rigid	0 N		0.08127
Injury - Post	0 N		0.65195
Dynesys - Rigid	0 N		0.50103
Dynesys - Post	0 N		0.00288
Rigid - Post	0 N		0.03720

Direction	Follower Load	p-value	p-value
Flexion-Extension		XY	XZ
Overall effect	600 N	0.19536	0.02015
Intact - Intact Dyn	600 N		0.06015
Intact - Capsule	600 N		0.96274
Intact - Injury	600 N		0.93220
Intact - Dynesys	600 N		0.21969
Intact - Rigid	600 N		0.96130
Intact - Post	600 N		0.97383
Intact Dyn - Capsule	600 N		0.04453
Intact Dyn - Injury	600 N		0.06753
Intact Dyn - Dynesys	600 N		0.42962
Intact Dyn - Rigid	600 N		0.04262
Intact Dyn - Post	600 N		0.06350
Capsule - Injury	600 N		0.99043
Capsule - Dynesys	600 N		0.14758
Capsule - Rigid	600 N		0.82612
Capsule - Post	600 N		0.99335
Injury - Dynesys	600 N		0.26318
Injury - Rigid	600 N		0.98475
Injury - Post	600 N		0.89389
Dynesys - Rigid	600 N		0.09835
Dynesys - Post	600 N		0.26852
Rigid - Post	600 N		0.98824
Lateral Bending		YZ	XZ
Overall effect	600 N	0.03698	0.34760
Intact - Intact Dyn	600 N		0.17032
Intact - Capsule	600 N		0.81194
Intact - Injury	600 N		0.85799
Intact - Dynesys	600 N		0.16960
Intact - Rigid	600 N		0.60238
Intact - Post	600 N		0.95287
Intact Dyn - Capsule	600 N		0.15278
Intact Dyn - Injury	600 N		0.07966
Intact Dyn - Dynesys	600 N		0.79734
Intact Dyn - Rigid	600 N		0.26942
Intact Dyn - Post	600 N		0.18085
Capsule - Injury	600 N		0.84593
Capsule - Dynesys	600 N		0.17658
Capsule - Rigid	600 N		0.72676
Capsule - Post	600 N		0.95489
Injury - Dynesys	600 N		0.11080
Injury - Rigid	600 N		0.66270
Injury - Post	600 N		0.62286
Dynesys - Rigid	600 N		0.19675
Dynesys - Post	600 N		0.22441
Rigid - Post	600 N		0.84433
Axial Rotation		XY	YZ
Overall effect	600 N	0.03831	0.11255
Intact - Intact Dyn	600 N		0.87036
Intact - Capsule	600 N		0.80067
Intact - Injury	600 N		0.86618
Intact - Dynesys	600 N		0.52959
Intact - Rigid	600 N		0.03236
Intact - Post	600 N		0.60046
Intact Dyn - Capsule	600 N		0.86686
Intact Dyn - Injury	600 N		0.80175
Intact Dyn - Dynesys	600 N		0.70880
Intact Dyn - Rigid	600 N		0.07686
Intact Dyn - Post	600 N		0.49741
Capsule - Injury	600 N		0.79783
Capsule - Dynesys	600 N		0.69037
Capsule - Rigid	600 N		0.04731
Capsule - Post	600 N		0.63366
Injury - Dynesys	600 N		0.72354
Injury - Rigid	600 N		0.06414
Injury - Post	600 N		0.62026
Dynesys - Rigid	600 N		0.10006
Dynesys - Post	600 N		0.91301
Rigid - Post	600 N		0.18474

Appendix B. Results of Statistical Analysis

Table B.6: Effect of specimen condition on facet loads. Results of two-way repeated measures MANOVA with a 95% level of significance.

	0 N Follower Load				600 N Follower Load			
	Ax Rot	Extension	Flexion	Lat Bend	Ax Rot	Extension	Flexion	Lat Bend
Main Effect: Condition	0.00000	0.17528	0.00004	0.06532	0.00000	0.00167	0.00001	0.04575
Main Effect: Side	0.09772	0.09500	0.08132	0.00236	0.60091	0.61114	0.06235	0.37543
Interaction	0.00115	0.01963	0.03464	0.30948	0.00132	0.12467	0.00364	0.31512
Capsule L - Capsule R	0.61707	0.90281	0.93202		0.32137		0.80080	
Capsule L - Injury L	0.38016	0.72926	0.70252		0.42408		0.83576	
Capsule L - Dynesys L	0.62698	0.31609	0.00233		0.25997		0.02492	
Capsule L - Rigid L	0.00013	0.07911	0.94665		0.00014		0.63146	
Capsule L - Post L	0.42375	0.75162	0.97310		0.38485		0.91779	
Capsule R - Injury R	0.22482	0.71375	0.94623		0.16443		0.97622	
Capsule R - Dynesys R	0.26349	0.53877	0.00013		0.10780		0.00013	
Capsule R - Rigid R	0.29760	0.61945	0.62900		0.42140		0.66239	
Capsule R - Post R	0.21286	0.62238	0.95280		0.18140		0.84449	
Injury L - Injury R	0.76835	0.80350	0.88557		0.86831		0.94948	
Injury L - Dynesys L	0.17932	0.22299	0.00497		0.02722		0.06520	
Injury L - Rigid L	0.00014	0.01786	0.89843		0.00016		0.93026	
Injury L - Post L	0.91794	0.92951	0.99613		0.93494		0.96263	
Injury R - Dynesys R	0.84361	0.69206	0.00013		0.69028		0.00016	
Injury R - Rigid R	0.01408	0.81711	0.91363		0.02042		0.42477	
Injury R - Post R	0.91123	0.67862	0.91754		0.75128		0.93590	
Dynesys L - Dynesys R	0.20370	0.10598	0.00073		0.03970		0.00012	
Dynesys L - Rigid L	0.00012	0.23173	0.00159		0.00042		0.06626	
Dynesys L - Post L	0.13915	0.22725	0.00219		0.02641		0.06690	
Dynesys R - Rigid R	0.03012	0.73707	0.00013		0.00978		0.00013	
Dynesys R - Post R	0.91123	0.92693	0.00014		0.75238		0.00013	
Rigid L - Rigid R	0.00014	0.05611	0.80599		0.00086		0.67058	
Rigid L - Post L	0.00015	0.01743	0.96741		0.00015		0.97203	
Rigid R - Post R	0.01029	0.54533	0.84948		0.03177		0.63599	
Post L - Post R	0.84322	0.98808	0.97834		0.74743		0.90187	
Capsule - Injury						0.36795		0.68369
Capsule - Dynesys						0.42424		0.20854
Capsule - Rigid						0.03264		0.24009
Capsule - Post						0.26204		0.63736
Injury - Dynesys						0.21157		0.26318
Injury - Rigid						0.00597		0.25726
Injury - Post						0.50086		0.62095
Dynesys - Rigid						0.07672		0.02541
Dynesys - Post						0.09513		0.28173
Rigid - Post						0.00150		0.17390

Table B.7: Effect of Dynesys on intradiscal pressure. Results of repeated measures ANOVA with a 95% level of significance. Shown are for p-values for comparisons using relative pressures (relative to pressure at neutral position) and p-values for comparisons using absolute pressures.

Direction	Relative p-value	Absolute p-value
Flexion	0.2123	0.9305
Extension	0.0054	0.0067
Right Lateral Bending	0.0136	0.6311
Left Lateral Bending	0.7698	0.3281
Right Axial Rotation	0.9387	0.0186
Left Axial Rotation	0.2494	0.0066
**Neutral Position		0.0024

B.2 Effect of Dynesys Spacer Length

Table B.8: Effect of Dynesys spacer length on range of motion. Results of repeated measures MANOVA with a 95% level of significance.

Direction	Follower Load	p-value
Flexion	0 N	0.00437
Standard - Long	0 N	0.82984
Standard - Short	0 N	0.00777
Long - Short	0 N	0.00480
Extension	0 N	0.00575
Standard - Long	0 N	0.47403
Standard - Short	0 N	0.01189
Long - Short	0 N	0.00646
Lateral Bending	0 N	9.8482E-05
Standard - Long	0 N	0.01289
Standard - Short	0 N	0.00959
Long - Short	0 N	0.00020
Axial Rotation	0 N	3.28115E-05
Standard - Long	0 N	0.00266
Standard - Short	0 N	0.01496
Long - Short	0 N	0.00016

Direction	Follower Load	p-value
Flexion	600 N	0.17318
Extension	600 N	0.08361
Lateral Bending	600 N	0.05274
Axial Rotation	600 N	0.00015
Standard - Long	600 N	0.00642
Standard - Short	600 N	0.03028
Long - Short	600 N	0.00023

Table B.9: Effect of Dynesys spacer length on neutral zone. Results of repeated measures MANOVA with a 95% level of significance.

Direction	Follower Load	p-value
Flexion	0 N	0.03158
Standard - Long	0 N	0.72791
Standard - Short	0 N	0.03255
Long - Short	0 N	0.03949
Lateral Bending	0 N	0.03056
Standard - Long	0 N	0.05934
Standard - Short	0 N	0.42153
Long - Short	0 N	0.02819
Axial Rotation	0 N	0.02032
Standard - Long	0 N	0.02927
Standard - Short	0 N	0.57244
Long - Short	0 N	0.02250

Direction	Follower Load	p-value
Flexion	600 N	0.07394
Lateral Bending	600 N	0.02540
Standard - Long	600 N	0.02585
Standard - Short	600 N	0.75006
Long - Short	600 N	0.03333
Axial Rotation	600 N	0.07495

Appendix B. Results of Statistical Analysis

Table B.10: Effect of Dynesys spacer length on helical axis of motion. Results of repeated measures MANOVA with a 95% level of significance.

Direction	Follower Load	p-value	p-value
Flexion-Extension			
Overall effect	0 N	y	I
		0.47122	0.50221
Standard - Long	0 N		
Standard - Short	0 N		
Long - Short	0 N		
Lateral Bending			
Overall effect	0 N	x	y
		0.15937	0.74321
Standard - Long	0 N		
Standard - Short	0 N		
Long - Short	0 N		
Axial Rotation			
Overall effect	0 N	x	z
		0.34760	0.06910
Standard - Long	0 N		
Standard - Short	0 N		
Long - Short	0 N		

Direction	Follower Load	p-value	p-value
Flexion-Extension			
Overall effect	0 N	XY	XZ
		0.27479	0.04355
Standard - Long	0 N		0.18336
Standard - Short	0 N		0.18008
Long - Short	0 N		0.03488
Lateral Bending			
Overall effect	0 N	YZ	XZ
		0.42628	0.67707
Standard - Long	0 N		
Standard - Short	0 N		
Long - Short	0 N		
Axial Rotation			
Overall effect	0 N	XY	YZ
		0.70593	0.14269
Standard - Long	0 N		
Standard - Short	0 N		
Long - Short	0 N		

Direction	Follower Load	p-value	p-value
Flexion-Extension			
Overall effect	600 N	y	I
		0.93977	0.47319
Standard - Long	600 N		
Standard - Short	600 N		
Long - Short	600 N		
Lateral Bending			
Overall effect	600 N	x	y
		0.30758	0.52129
Standard - Long	600 N		
Standard - Short	600 N		
Long - Short	600 N		
Axial Rotation			
Overall effect	600 N	x	z
		0.50634	0.04222
Standard - Long	600 N		0.18156
Standard - Short	600 N		0.18955
Long - Short	600 N		0.03340

Direction	Follower Load	p-value	p-value
Flexion-Extension			
Overall effect	600 N	XY	XZ
		0.25714	0.57493
Standard - Long	600 N		
Standard - Short	600 N		
Long - Short	600 N		
Lateral Bending			
Overall effect	600 N	YZ	XZ
		0.16889	0.64612
Standard - Long	600 N		
Standard - Short	600 N		
Long - Short	600 N		
Axial Rotation			
Overall effect	600 N	XY	YZ
		0.70593	0.03539
Standard - Long	600 N		0.06274
Standard - Short	600 N		0.45022
Long - Short	600 N		0.03319

Table B.11: Effect of Dynesys spacer length on facet loads. Results of two-way repeated measures MANOVA with a 95% level of significance.

	0 N Follower Load				600 N Follower Load			
	Ax Rot	Extension	Flexion	Lat Bend	AxRot	Extension	Flexion	Lat Bend
Main Effect: Condition	0.85529	0.12673	0.01417	0.01868	0.25733	0.08664	0.00350	0.00309
Main Effect: Side	0.13559	0.07555	0.08747	0.07149	0.09069	0.04032	0.05000	0.05907
Interaction	0.65201	0.77273	0.48574	0.74218	0.59543	0.76826	0.58942	0.99398
Standard - Long			0.12646	0.17814			0.02916	0.04349
Standard - Short			0.10729	0.09627			0.13453	0.08113
Long - Short			0.01071	0.01444			0.00273	0.00230

Appendix C

HAM Results for Unloaded Position to Max/Min Rotation

C.1 Effect of Specimen Condition

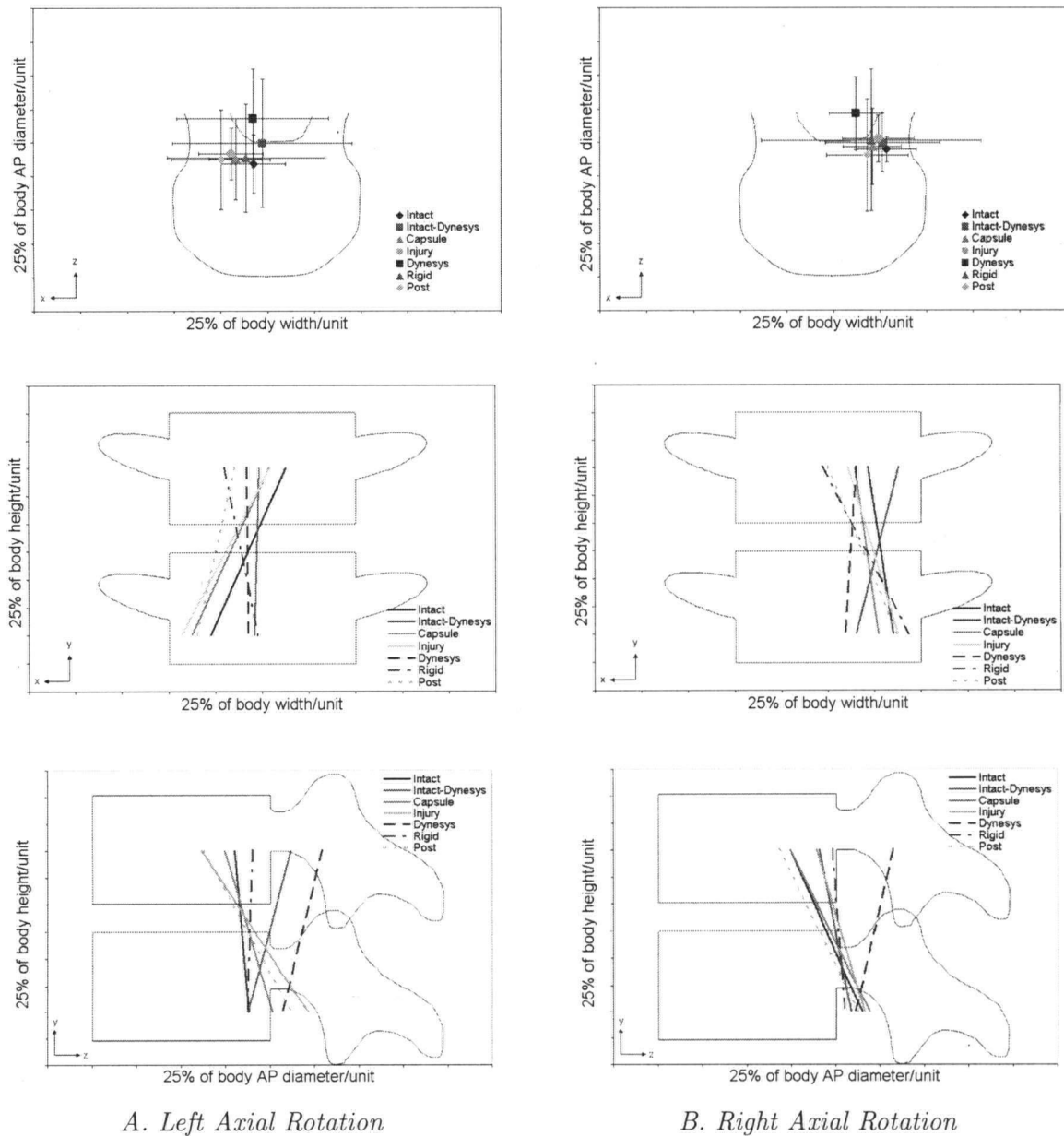


Figure C.1: Average HAM in A) left and B) right axial rotation without follower preload for seven specimen conditions.

Appendix C. HAM Results for Unloaded Position to Max/Min Rotation

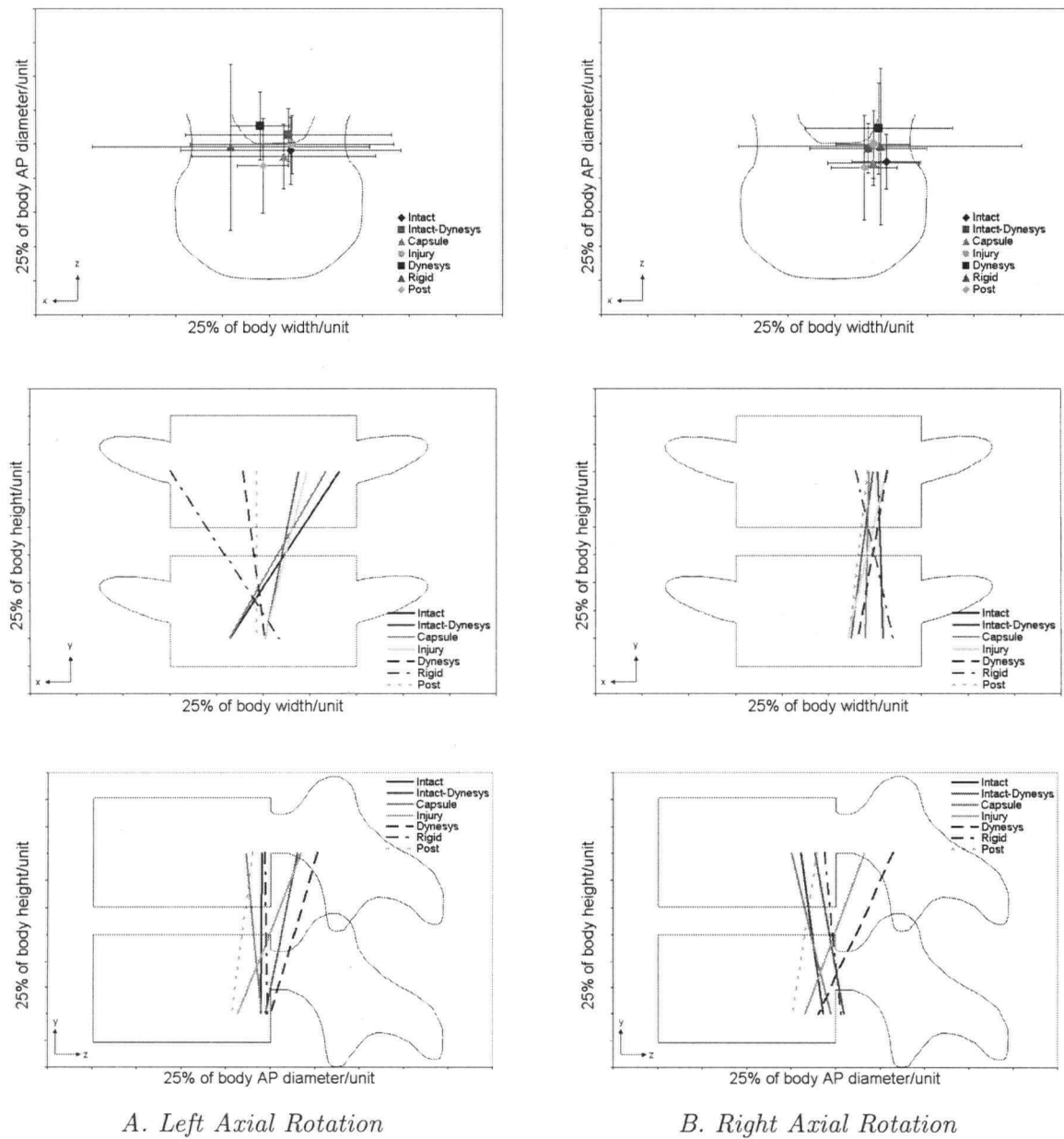


Figure C.2: Average HAM in A) left and B) right axial rotation with follower preload for seven specimen conditions.

Appendix C. HAM Results for Unloaded Position to Max/Min Rotation

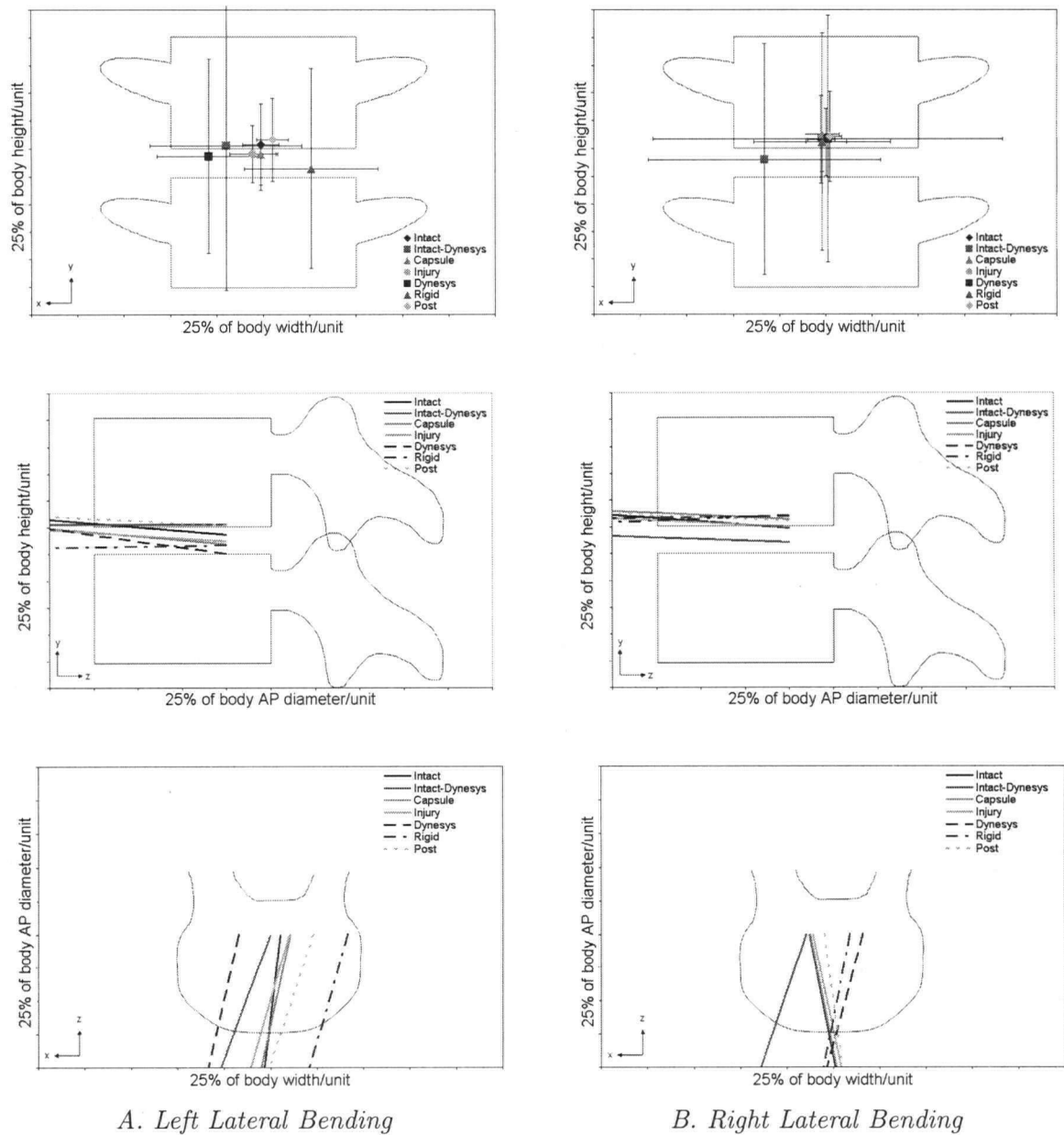


Figure C.3: Average HAM in A) left and B) right lateral bending without follower preload for seven specimen conditions.

Appendix C. HAM Results for Unloaded Position to Max/Min Rotation

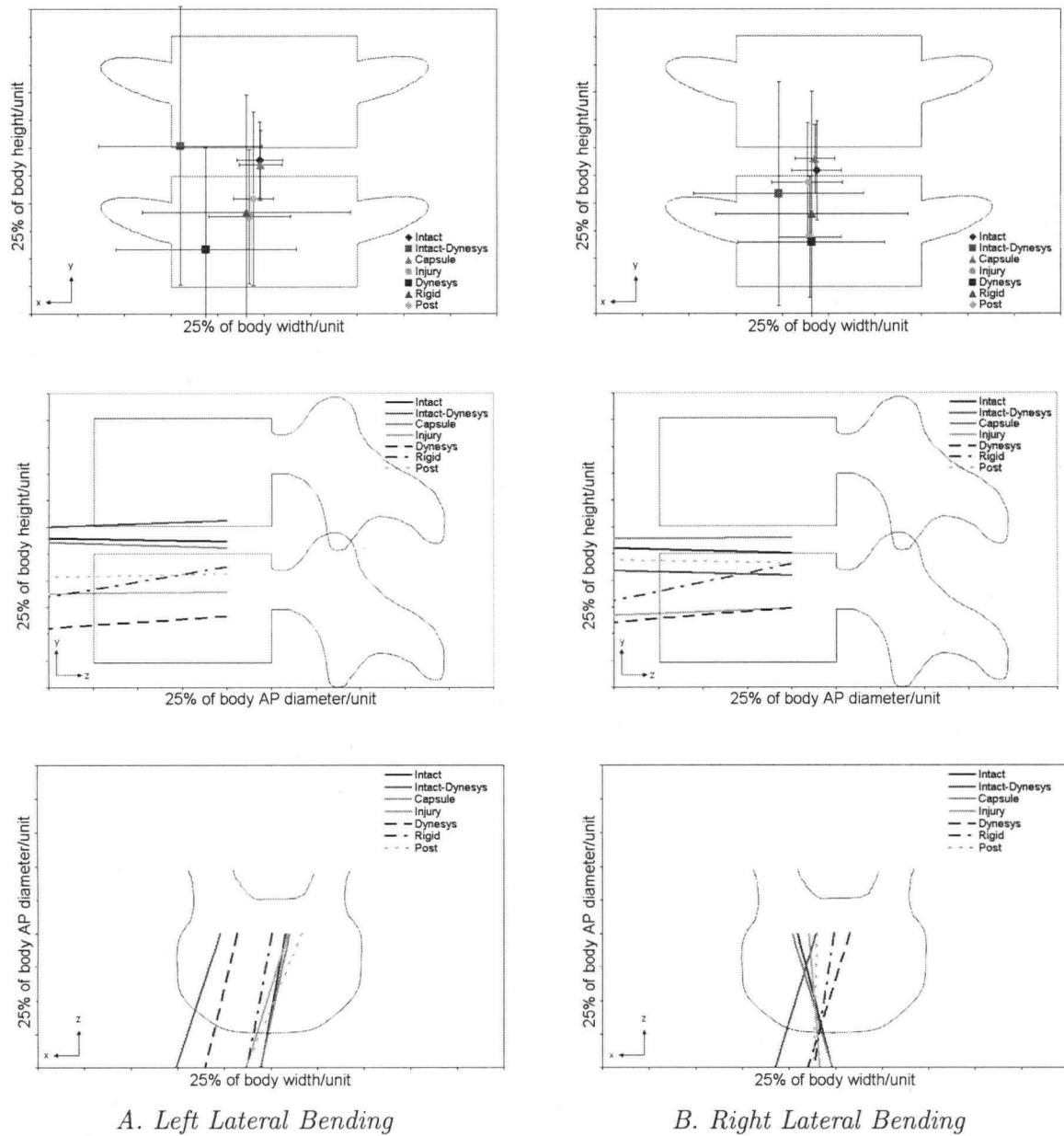


Figure C.4: Average HAM in A) left and B) right lateral bending with follower preload for seven specimen conditions.

Appendix C. HAM Results for Unloaded Position to Max/Min Rotation

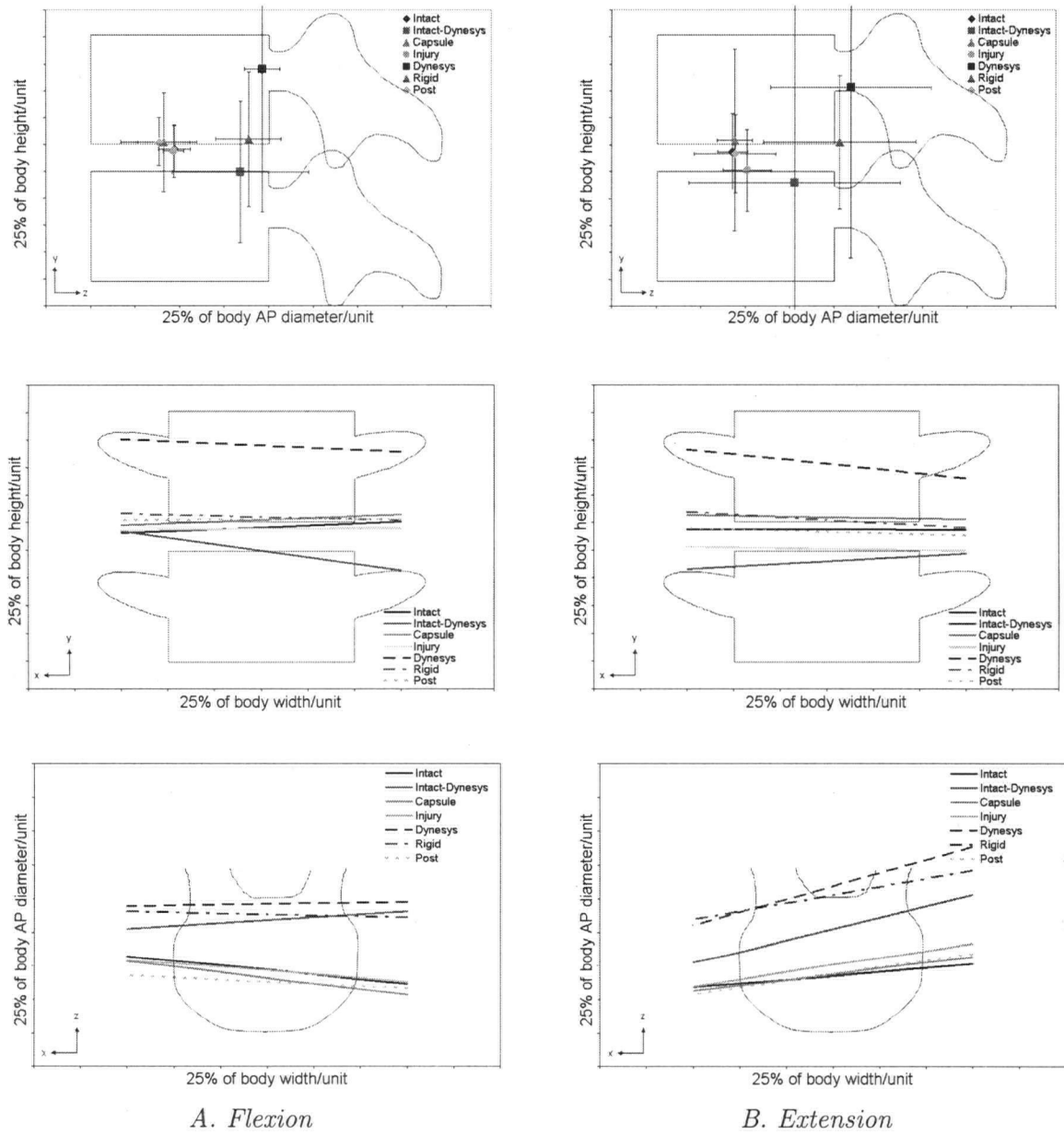


Figure C.5: Average HAM in A) flexion and B) extension without follower preload for seven specimen conditions.

Appendix C. HAM Results for Unloaded Position to Max/Min Rotation

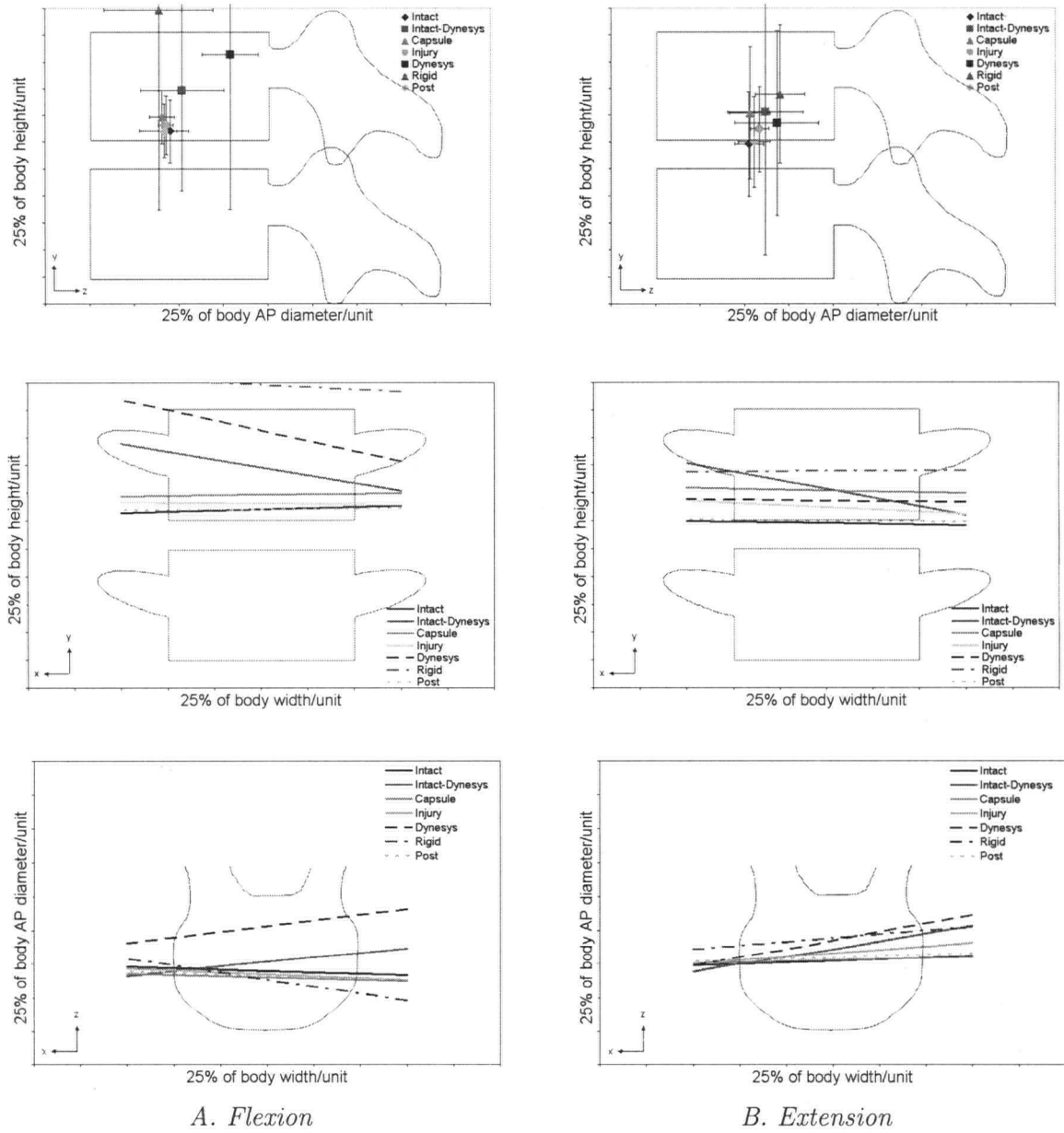


Figure C.6: Average HAM in A) flexion and B) extension with follower preload for seven specimen conditions.

C.2 Effect of Spacer Length

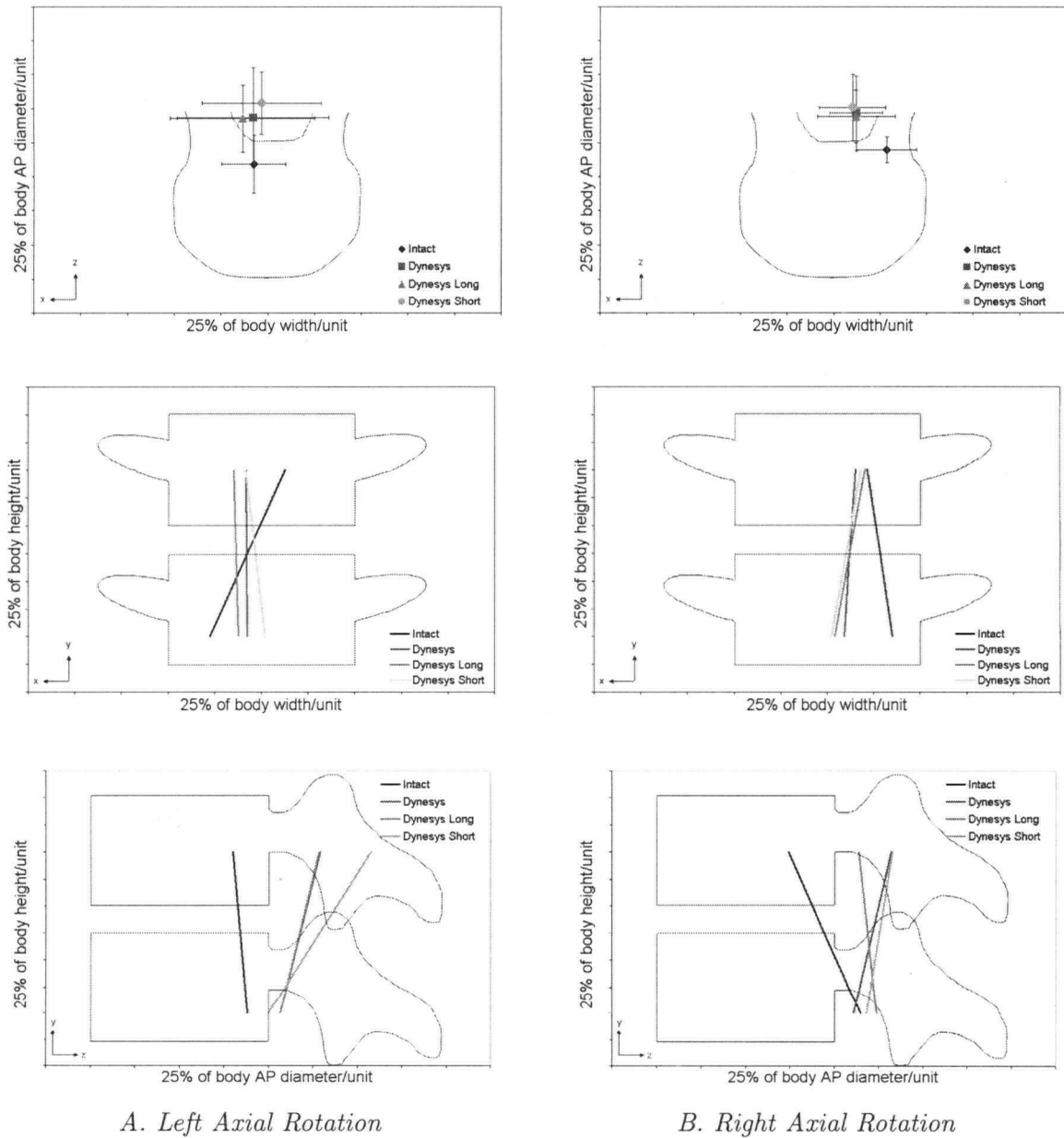
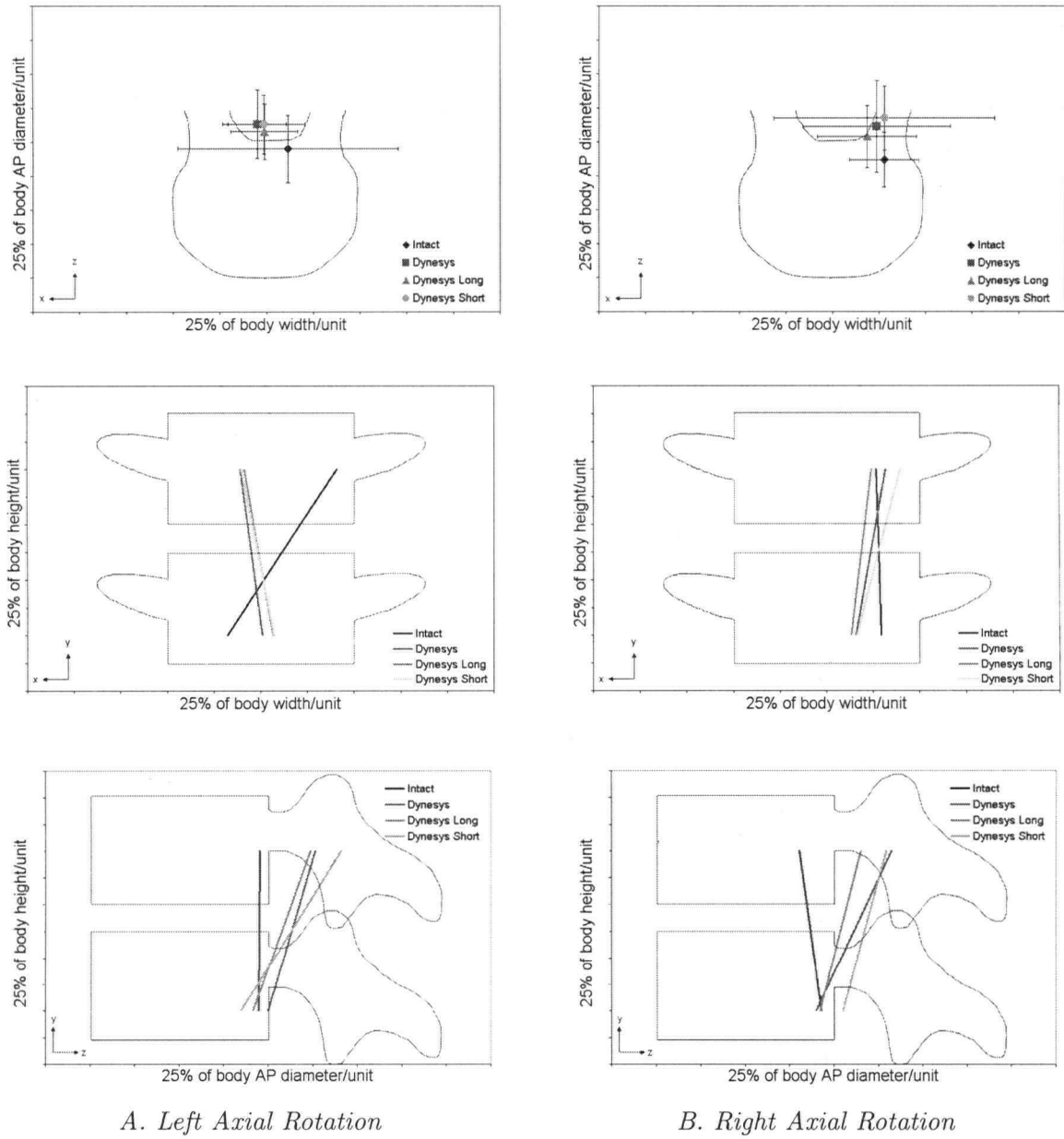


Figure C.7: Average HAM in A) left and B) right axial rotation without follower preload for three spacer lengths.

Appendix C. HAM Results for Unloaded Position to Max/Min Rotation



A. Left Axial Rotation

B. Right Axial Rotation

Figure C.8: Average HAM in A) left and B) right axial rotation with follower preload for three spacer lengths.

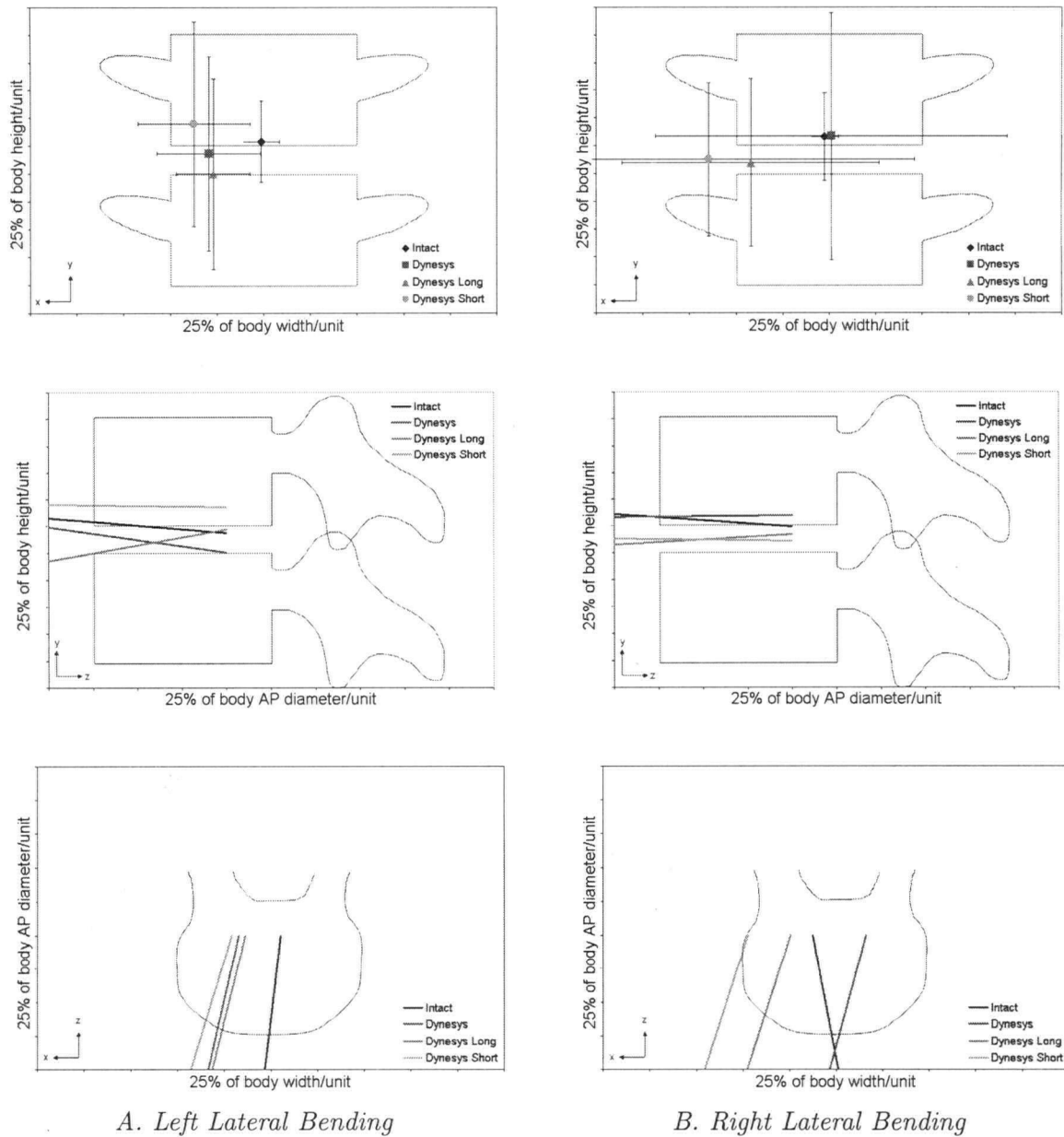


Figure C.9: Average HAM in A) left and B) right lateral bending without follower preload for three spacer lengths.

Appendix C. HAM Results for Unloaded Position to Max/Min Rotation

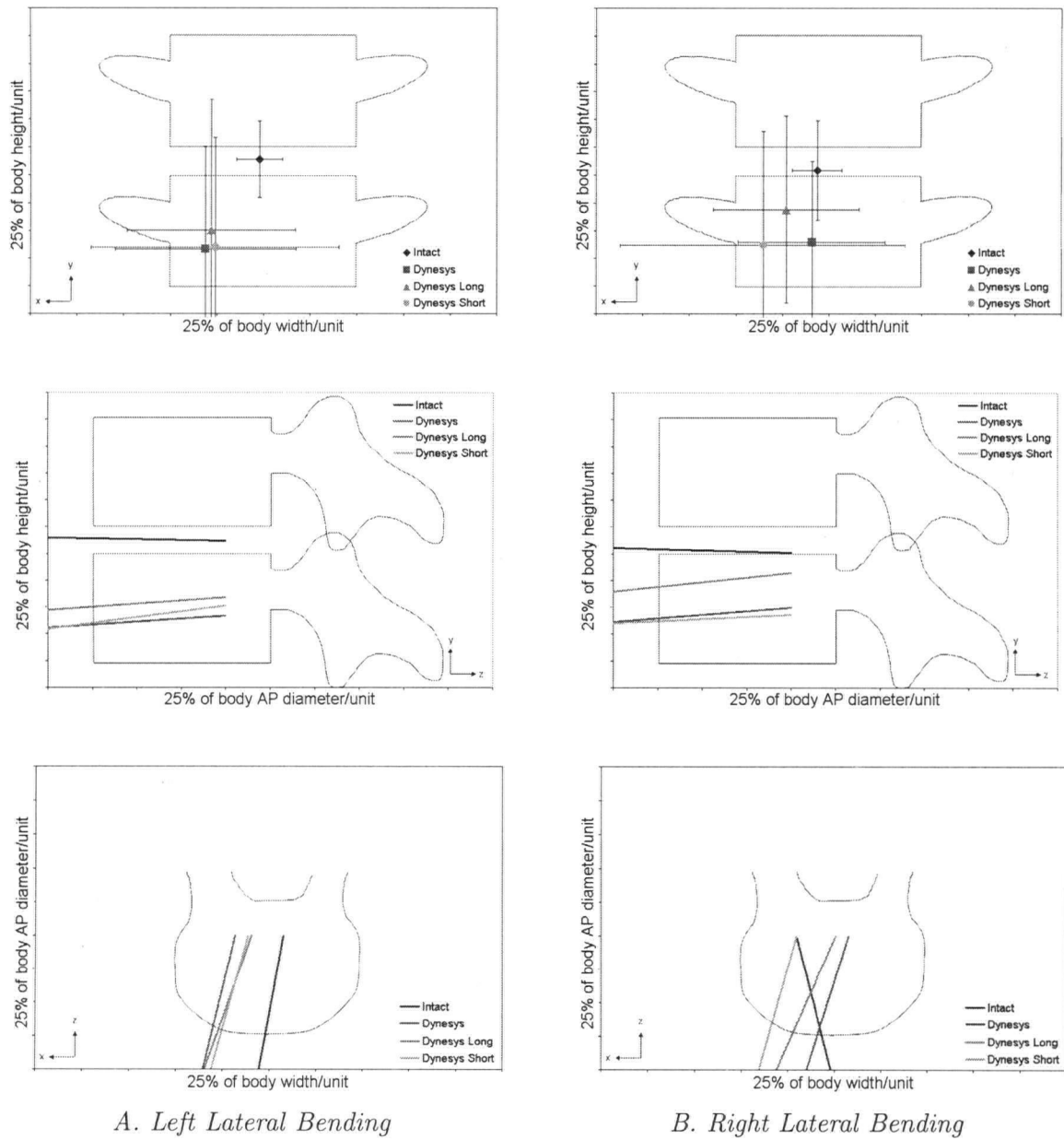


Figure C.10: Average HAM in A) left and B) right lateral bending with follower preload for three spacer lengths.

Appendix C. HAM Results for Unloaded Position to Max/Min Rotation

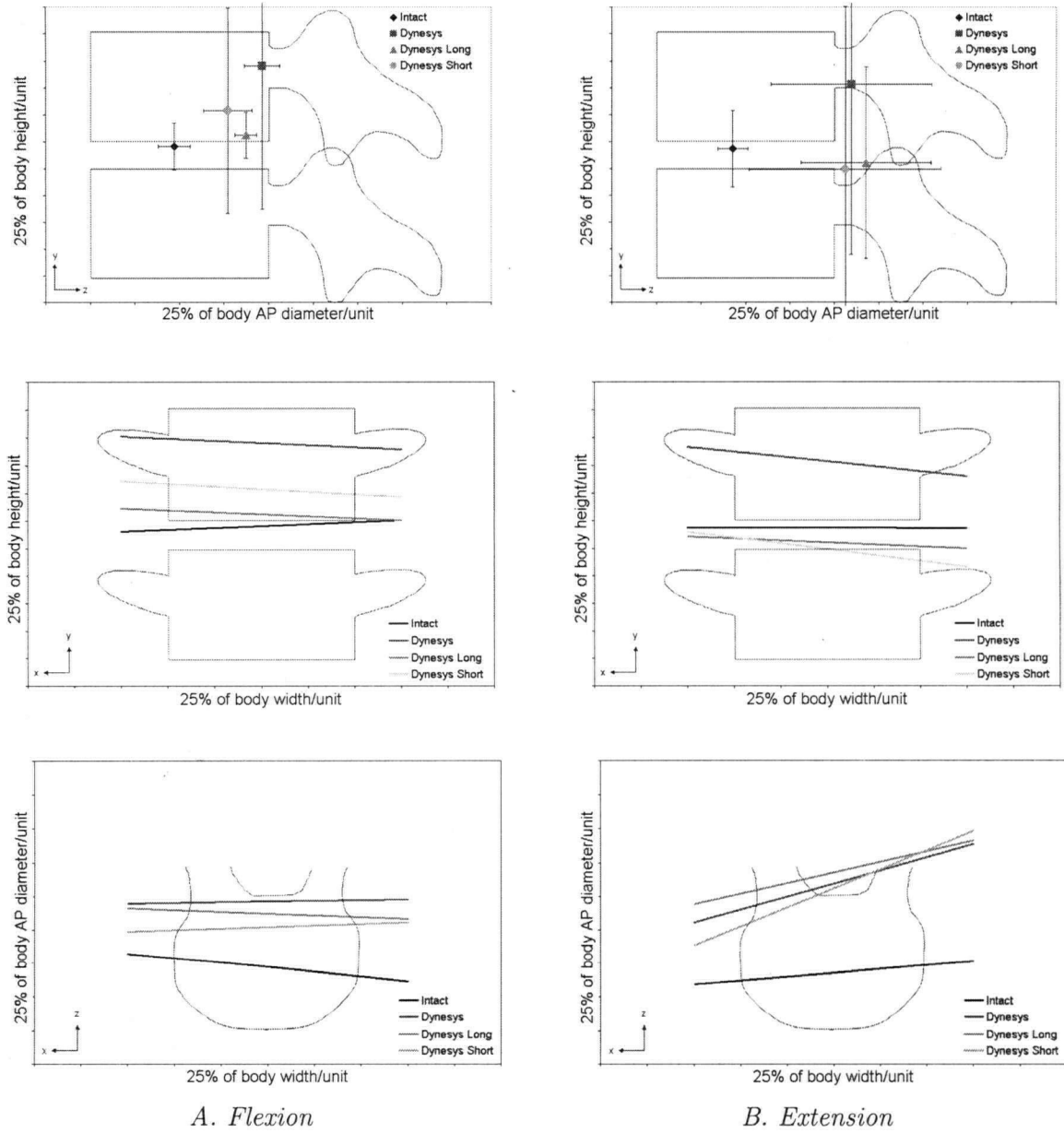


Figure C.11: Average HAM in A) flexion and B) extension without follower preload for three spacer lengths.

Appendix C. HAM Results for Unloaded Position to Max/Min Rotation

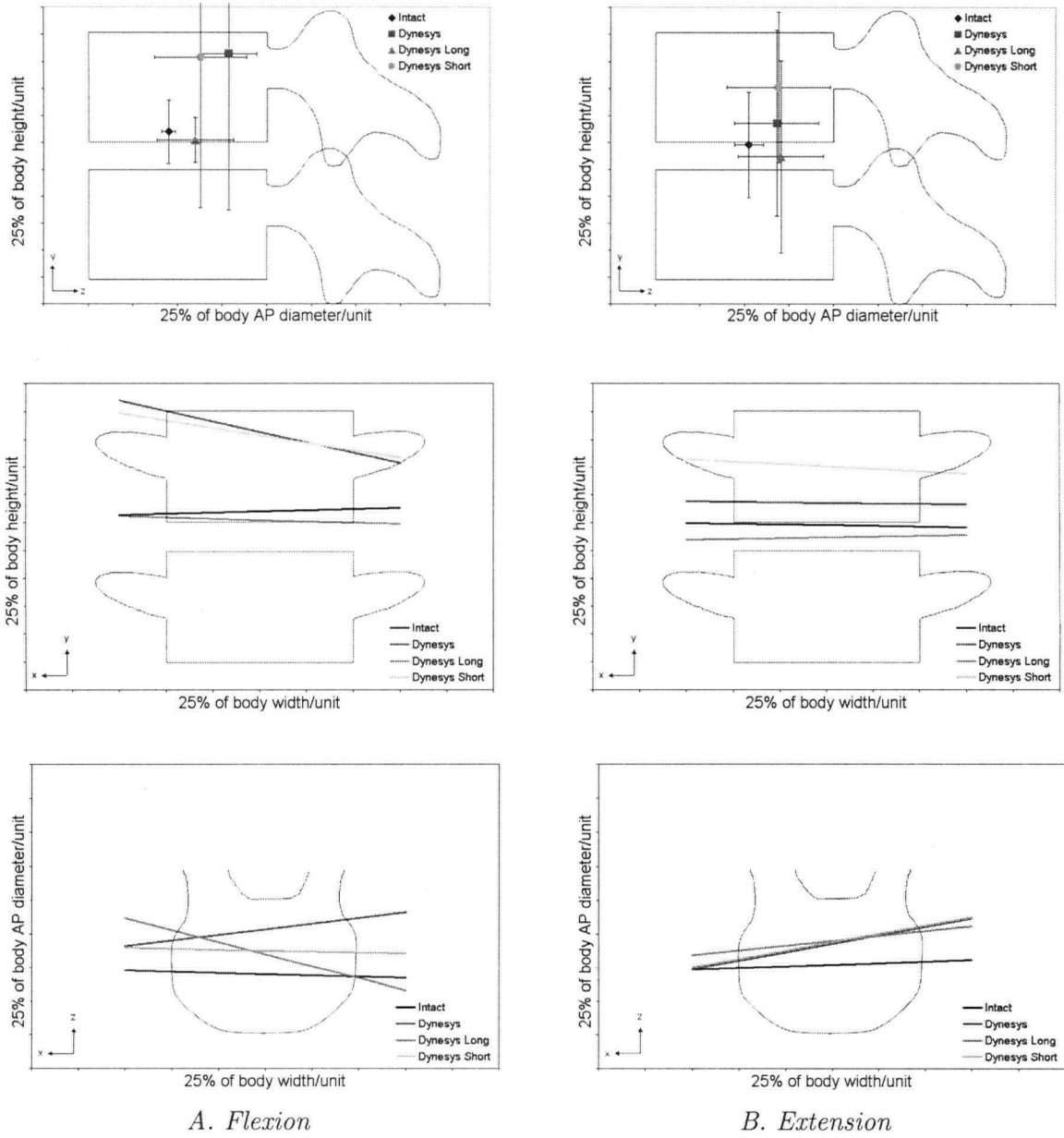


Figure C.12: Average HAM in A) flexion and B) extension with follower preload for three spacer lengths.